

DISS. ETH NO. 18230

MATTHIAS HUSS

PAST AND FUTURE CHANGES IN
GLACIER MASS BALANCE

DISS. ETH No. 18230

Past and future changes in glacier mass balance

A dissertation submitted to
ETH ZURICH

for the degree of
Doctor of Sciences

presented by

MATTHIAS HUSS

Dipl. Natw. ETH

born 9. March, 1980

citizen of Wiesendangen ZH, Switzerland

accepted on the recommendation of

Prof. Dr. M. Funk, examiner

Dr. A. Bauder, co-examiner

Prof. Dr. H. Blatter, co-examiner

Prof. Dr. C. Schär, co-examiner

Prof. Dr. G. Kaser, co-examiner

2009

*But these recede. Above me are the Alps,
The palaces of Nature, whose vast walls
Have pinnacled in clouds their snowy scalps,
And throned Eternity in icy halls
Of cold sublimity, where forms and falls
The avalanche – the thunderbolt of snow!
All that expands the spirit, yet appals,
Gather around these summits, as to show
How Earth may pierce to Heaven, yet leave vain man below.*

Lord G. Byron, Childe Harold's Pilgrimage, 1816

Contents

Abstract	v
Zusammenfassung	vii
1 Introduction	1
1.1 Glaciers in a changing climate	1
1.2 Investigating glacier changes	1
1.3 Thesis objectives and structure	6
I Long-term mass balance records	9
2 Mass balance of Alpine glaciers	11
2.1 Introduction	12
2.2 Study sites and field data	13
2.3 Methods	16
2.4 Results	21
2.5 Discussion	26
2.6 Conclusion	28
3 Long-term time series of seasonal point mass balance	31
3.1 Introduction	32
3.2 Study sites and field data	33
3.3 Methods	34
3.4 Results	37
3.5 Discussion	42
3.6 Conclusions	45

4	Homogenization of mass balance time series	47
4.1	Introduction	48
4.2	Study sites and field data	49
4.3	Methods	50
4.4	Results	54
4.5	Error analysis	59
4.6	Conclusion	61
II	Applications to glacier hydrology and Arctic regions	63
5	Glacier-dammed lake outbursts	65
5.1	Introduction	66
5.2	Field Site	67
5.3	Field Campaigns and Methods	68
5.4	Results	71
5.5	Discussion	75
5.6	Conclusions	82
6	Temporal and spatial changes of Laika Glacier	85
6.1	Introduction	86
6.2	Study site	86
6.3	Data sources and methods	88
6.4	Results and discussion	96
6.5	Conclusions	101
III	Projections of future glacier extent and runoff	103
7	Modelling the retreat of Unteraargletscher	105
7.1	Introduction	106
7.2	Study area and relevant data	107
7.3	Flowline model	109
7.4	Future climate	114
7.5	Results	116
7.6	Discussion and Conclusion	119

8	Future runoff from highly glacierized basins	123
8.1	Introduction	124
8.2	Study site and field data	125
8.3	Methods	127
8.4	Results	137
8.5	Discussion	143
8.6	Conclusion	146
9	Parameterizations of future glacier retreat	149
9.1	Introduction	149
9.2	Study site and field data	151
9.3	Methods	152
9.4	Results	156
9.5	Discussion	167
10	Conclusion	171
10.1	Synthesis	171
10.2	Concluding discussion and outlook	172
A	Mass balance of Pizolgletscher	177
A.1	Mass balance measurements on Pizolgletscher	177
A.2	Results	183
B	New evidence for strong glacier melt around 1950	191
C	Co-authored publications	197
	Bibliography	198
	Acknowledgements	215
	Curriculum Vitae	217

Abstract

The retreat of Alpine glaciers is one of the clearest indicators of climate change. Glaciers are the symbol of healthy mountain environment and represent an important touristic and economic factor in Switzerland. The objective of the present thesis is to understand the links between climate warming and the glacier mass budget. A wealth of field data acquired during the 20th century exists. This allows a study of the past which is a prerequisite for forecasts of the future glacier evolution. Climate forcing acting on glaciers is directly reflected by the mass balance at the glacier surface – this factor is, thus, central to this thesis.

A method to determine the seasonal mass balance of alpine glaciers since 1865 based on climate data and field measurements was developed. A distributed accumulation and temperature-index melt model was applied to four Swiss glaciers (Grosser Aletsch-, Rhone-, Gries- and Silvrettagletscher). The model was calibrated using ice volume changes, in-situ measurements of seasonal mass balance and discharge. It combines all available data for these glaciers in the 20th century. The investigated ice masses display significantly differing mass changes throughout the last 140 years; the year to year fluctuations, however, are similar. The glaciers gained mass in two decadal periods in the 1910s and '70s. Since 1982 an accelerated mass loss is inferred, which was, however, even faster in the 1940s. This observation could be confirmed by analyzing the longest mass balance time series worldwide. Seasonal mass balance is determined since more than 90 years at four stakes at or above the mean equilibrium line. In spite of lower air temperatures in the 1940s, significantly more energy was consumed for melt. There is evidence that the parameters of the widely used temperature-index models can vary systematically over long time periods. This indicates a substantial change in the relative magnitude of energy balance components in high mountain regions over the last century.

The homogenization of long-term mass balance time series is important in order to obtain a comparable and unbiased basis for climate change impact studies. A strategy for correcting time series of comprehensive mass balance monitoring programs for systematic errors has been developed and applied to two glaciers. The direct glaciological and the indirect geodetic method are combined and homogeneous seasonal mass balance quantities referring to the hydrological year are computed.

Several components of the developed methods were applied to related fields of research. The lake outburst events of Gornersee were analyzed over the last five decades with a melt model in high temporal and spatial resolution. A variety of field measurements acquired on Gornergletscher were included in the evaluation. Different triggering mechanisms for the glacier floods could be identified and long-periodic variations of the lake volume were inferred. In the course of an outburst event a substantial amount of lake water is temporally stored in the glacier system, inducing important alterations of the hydraulic conditions with congruent impacts on the glacier dynamics.

Satellite based remote sensing is increasingly important for glacier change studies in remote regions. To demonstrate the potential of the mass balance tested in the Alps for such studies,

it was applied to a small glacier in the Canadian Arctic. In-situ field measurements, different types of remote sensing data, weather records and climate re-analysis time series were compiled and could be combined using a glacier evolution model. The model can thus link various data types, hence considerably increasing their value. The model can be used for investigating the response of remote ice masses to climate change in high temporal and spatial resolution and to close gaps in the glacier monitoring in these regions.

The assessment of the future changes in the Alpine cryosphere is a major challenge. One must account for the considerable uncertainties in the climate projections, but also the complex response of glaciers to changing climatic conditions needs to be adequately modelled. Within the course of this thesis impact studies were performed connected with applied problems. The retreat of the tongue of Unteraargletscher was simulated using a combined ice-flow mass-balance model for the next 50 years based on different climate scenarios. It could be shown that the imbalance between mass loss due to melt and the compensating effect of ice flow will rapidly increase in the near future. Nevertheless, the heavily debris-covered tongue of Unteraargletscher will persist for several decades.

Glacier wastage most directly affects our daily life with changes in runoff from high mountain catchments. For dry alpine valleys (e.g. the Valais) melt water from glaciers represents an indispensable resource during summertime. Moreover, they play a central role in the Swiss hydropower production. In the present work a new glacio-hydrological model was developed for calculating the future runoff from highly glacierized drainage basins. Model components describe the glacier surface mass balance, evaporation and runoff routing. The change in glacier coverage is simulated using a simple, widely applicable parameterization, which is field data independent. This parameterization was validated against a three dimensional finite element ice flow model applied for Rhonegletscher. Using this parameterization, glacier retreat over the entire 21st century can be computed within the uncertainty range of the ice flow model and is thus well suited for a simplified calculation of future glacier change. The combined glacier evolution runoff model was driven by several regional climate scenarios in seasonal resolution for the period 2008-2100 and applied to several glacierized catchments. Due to intense glacier melt runoff will significantly increase in the next decades. Many Alpine glaciers will have reduced their size so drastically by 2100 that they lose their storage capacity. Thus, there will be a reduction in runoff volume in the second half of the century, as well as a shift of peak discharge to spring. Water shortage in the summer months are therefore highly probable and the management of reservoirs used for hydropower production needs to be adapted.

This thesis attempts to bridge the gap between glacier changes observed in the past and the future. The combination of long-term time series of field measurements with modelling allows the analysis of climate change impacts on glaciers in the last century. With this knowledge it is possible to face the challenge of forecasting the future of alpine glaciers.

Zusammenfassung

Der Rückzug der Alpengletscher gehört zu den deutlichsten Indikatoren des Klimawandels in der Schweiz. Gletscher sind Symbole der Hochgebirgswelt und haben einen grossen touristischen und wirtschaftlichen Wert. Das Ziel der vorliegenden Arbeit ist es die Zusammenhänge zwischen Klimaerwärmung und dem Massenhaushalt der Gletscher zu verstehen. Eine Fülle von Gletscherdaten aus dem letzten Jahrhundert steht in den Alpen zur Verfügung. Aus diesen Daten werden Erkenntnisse gewonnen und umgesetzt, um die zukünftige Entwicklung der Gletscher zu prognostizieren. Über die Massenbilanz der Gletscheroberfläche lassen sich direkte Aussagen über den Einfluss des Klimas auf die Gletscher machen – dieser Faktor ist deshalb zentral in der Arbeit.

Es wurde eine Methode entwickelt, mit der sich saisonale Gletscher-Massenbilanzen seit 1865 mit Hilfe von Klimadaten und Gletschermessungen berechnen lassen. Ein verteiltes Akkumulations- und Temperatur-Index Schmelz-Modell wurde auf vier Gletscher (Grosser Aletsch-, Rhone-, Gries- und Silvrettagletscher) angewandt. Das Modell wurde mit Eisvolumenänderungen, auf dem Gletscher bestimmten saisonalen Massenbilanzen und Abfluss-Aufzeichnungen kalibriert. Es vereinigt somit sämtliche für diese Gletscher vorhandenen Daten. Dabei zeigt sich, dass die Gletscher unterschiedlich starke Massenverluste während des 20. Jahrhundert aufweisen. Die Schwankungen von Jahr zu Jahr sind aber ähnlich. In zwei 10-Jahres Perioden in den 1910er und den 1970er Jahren konnten die Alpengletscher Massengewinne verzeichnen. Seit 1982 befinden sie sich in einer Phase mit rapidem Massenverlust, der allerdings in den 1940er Jahren noch ausgeprägter war. Diese Beobachtung konnte ebenfalls durch eine Analyse der weltweit längsten Massenbilanzreihen an vier Pegelstangen auf rund 3000 m.ü.M. bestätigt werden. Trotz tieferer Temperaturen wurde in den '40ern mehr Energie für Schmelze aufgewendet. Daraus lässt sich schliessen, dass sich die Parameter der weit verbreiteten Temperatur-Index Modelle über lange Zeiträume systematisch ändern können. Dies steht mit einer signifikanten Veränderung des relativen Anteils der Energiebilanzkomponenten im Hochgebirge während des letzten Jahrhunderts im Zusammenhang.

Die Homogenisierung von Massenbilanz-Zeitreihen ist äusserst wichtig, um Studien der Klimaänderung auf vergleichbaren und nicht verzerrten Grundlagen abzustützen. Eine Strategie zur Korrektur von systematischen Fehlern in langjährigen Datenreihen wurde entwickelt und auf zwei Gletscher angewandt. Damit werden die direkte glaziologische und die indirekte geodätische Methode miteinander kombiniert und homogenisierte, saisonale Massenbilanz-Werte, die sich auf das hydrologische Jahr beziehen, berechnet.

Verschiedene Bestandteile der erarbeiteten Methoden wurden in Exkursen auf Fragestellungen in verwandten Forschungsgebieten angewendet. Die Seeausbrüche des Gornersees während den letzten fünf Jahrzehnten wurden mit einem Schmelzmodell in hoher zeitlicher und räumlicher Auflösung analysiert. Eine Vielzahl von Feldmessungen auf dem Gornergletscher wurde in die Auswertung miteinbezogen. Dabei konnte auf verschiedene Auslösemechanismen der Gletscherfluten geschlossen, sowie langperiodische Veränderungen des am Seeausbruch

beteiligten Wasservolumens festgestellt werden. Während einer Gletscherflut wird eine grosse Menge Wasser temporär im Gletschersystem gespeichert und bewirkt dort substantielle Veränderungen der hydraulischen Bedingungen im Gletscher, mit entsprechenden Auswirkungen auf die Eisdynamik.

Satelliten basierte Fernerkundung stellt in der heutigen Zeit eine immer wichtigere Basis für Gletscherstudien in abgelegenen Regionen dar. Das in den Alpen erprobte Modell zur Massenbilanz-Bestimmung wurde auf einen kleinen Gletscher in der Kanadischen Arktis angewendet. Dabei wurden neben lokalen Messungen, verschiedene Fernerkundungsdaten, Wetter-Aufzeichnungen und Klima-Reanalysen zusammengestellt und über ein Gletscherentwicklungs-Modell kombiniert. Dieses Modell kann verschiedenste Datentypen verbinden und damit deren Wert beträchtlich steigern. Es kann daher verwendet werden, um die Reaktion von abgelegenen Eismassen auf die Klimaänderung im Detail zu erforschen und damit Lücken in der Gletscherbeobachtung schliessen.

Die Vorhersage der Zukunft der alpinen Kryosphäre ist eine Herausforderung. Dabei muss man den grossen Unsicherheiten der Klimaszenarien Rechnung tragen, aber auch die komplexe Reaktion der Gletscher auf veränderte Bedingungen im Klimasystem berücksichtigen. Zukunftsprognosen wurden im Zusammenhang mit angewandten Fragestellungen durchgeführt. Der Rückzug der Zunge des Unteraargletschers wurde mit einem kombinierten Massenbilanz-Eisfluss-Modell für die nächsten 50 Jahre mit verschiedenen Klimaszenarien berechnet. Dabei zeigt sich, dass sich das Ungleichgewicht zwischen Massenverlust durch Schmelze und dem kompensierenden Effekt des Eisflusses in Zukunft weiter verstärken wird. Trotzdem kann sich die stark schuttbedeckte Zunge des Unteraargletschers noch mehrere Jahrzehnte lang halten.

Der Gletscherrückzug betrifft unseren Alltag unmittelbar über die Veränderung des Abflusses aus Hochgebirgsregionen. Gletscher liefern im Sommer lebensnotwendiges Wasser für trockene Alpentäler (z.B. das Wallis) und spielen in der Schweiz in der Stromproduktion eine zentrale Rolle. In dieser Arbeit wurde ein neues glazio-hydrologisches Modell entwickelt, das die zukünftigen Abflüsse aus stark vergletscherten Einzugsgebieten berechnet. Das Modell beschreibt die Gletscher-Massenbilanz, die Evaporation und die Wasserspeicherung. Der Gletscherrückzug wird mit einer einfachen, breit anwendbaren Parametrisierung bestimmt, die unabhängig von Felddaten ist. Diese Parametrisierung konnte auf dem Rhonegletscher über den Vergleich mit einem dreidimensionalen finite Elemente Gletscherfliess-Modell validiert werden. Sie kann den Gletscherrückzug über das ganze 21. Jahrhundert im Unsicherheitsbereich des Eisfluss-Modells wiedergeben und ist deshalb zur vereinfachten Beschreibung der zukünftigen Gletscherveränderung sehr geeignet. Das Gletscher-Abfluss-Modell wurde mit verschiedenen regionalen Klimaszenarien in saisonaler Auflösung bis ins Jahr 2100 angetrieben und auf mehrere stark vergletscherte Einzugsgebiete angewendet. Durch die intensive Gletscherschmelze wird in den nächsten Jahrzehnten der Abfluss deutlich ansteigen. Viele Alpengletscher werden bis 2100 ihre Fläche jedoch soweit verringert haben, dass sie ihre Speicherkapazität verlieren. Damit ist neben der Verringerung des Abflusses in der zweiten Hälfte dieses Jahrhunderts mit einer Verschiebung der Abflussspitze in den Frühling zu rechnen. Im Hochsommer kann es zu Wasserknappheit kommen und die Bewirtschaftung von Wasserkraftwerken muss grundlegend angepasst werden.

Diese Arbeit versucht die Brücke zwischen den Gletscherveränderungen in der Vergangenheit und der Zukunft zu schlagen. Die Kombination von langen Datenreihen und Modellierung erlaubt es, die Auswirkung der Klimaänderung auf die Gletscher im letzten Jahrhundert zu verstehen. Ausgerüstet mit diesen Erkenntnissen kann man sich der Herausforderung stellen, den zukünftigen Gletscherrückzug zu prognostizieren.

Chapter 1

Introduction

1.1 Glaciers in a changing climate

Glaciers are the symbol of a healthy mountain environment. In the Alps, the public interest in glaciers seems to be increasing at an even faster rate than the glacier tongues receded during the last 100 years. Glaciers are important touristic factors in Switzerland. However, they sometimes also represent a threat to alpine communities: with glacier retreat mountain flanks may become instable and newly formed glacial lakes can produce destructive outburst floods. Last but not least, glaciers are an important storage component in the hydrological cycle. Ice masses store vast amounts of fresh water at high elevations and provide an indispensable water supply for dry alpine valleys during summertime and are central to hydropower production. With the glacier retreat predicted for the near future, substantial changes in alpine environments will occur. Glaciers react sensitively to climatic variations which are immediately revealed through their mass balance. An understanding of the processes determining glacier variations in the past is a prerequisite for forecasting the response of the Alpine cryosphere to the 21st century climate warming. Climate change in Switzerland is not a disaster – we have (in contrast to many mountainous countries) the financial means to adapt ourselves to changed environmental conditions. This must be done, however, as early as possible. Realistic scenarios for the impact of a warming atmosphere on glaciers in the Alps are required.

This PhD thesis attempts to bridge the gap between glacier changes in the 20th century – the past – and the 21st century – the future. A wealth of almost forgotten field measurements acquired over more than 100 years, as well as concurrent data allow a comprehensive picture of past climate forcing on Alpine glaciers to be drawn. Only by putting this knowledge into our backpack we can face the challenge of forecasting future glacier retreat.

1.2 Investigating glacier changes

Already in the early 19th century Agassiz (1840) investigated various glaciological processes on Unteraargletscher, Bernese Alps. Measurements of glacier surface mass balance were performed on many Swiss glaciers over large parts of the 20th century representing a unique data basis for the interpretation of glacier variations in response to climate change. Only in recent years the application of numerical models for calculating glacier mass balance – conveniently

sitting in the office – provides an alternative to measuring accumulation and ablation in the field. Currently, models are popular in glaciological science. Although mass balance models have a great value for extending the measurements in space and time, they can – as far as glaciers are concerned – not be reasonably applied without data measured in the field: too complex are the processes determining the mass balance of alpine glaciers to be described entirely with mathematical formulations. Field measurements are the most important link to tie glacier models to reality!

1.2.1 Glacier surface mass balance

The mass balance of the glacier surface is generally acknowledged to be one the most direct indicators of climate variations (e.g. Vincent, 2002; Kaser and others, 2006) and is therefore a central element of this thesis. The mass balance b can be separated into two components: accumulation c and ablation a . On alpine glaciers accumulation is mainly determined by the deposition of solid precipitation on the glacier surface and ablation is given by melting of snow and ice. In other climatic regimes also refreezing of melt water in the snow and firn cover and sublimation may contribute substantially to glacier surface mass balance (e.g. Dyurgerov and Meier, 2002). For Arctic glaciers and ice sheets calving of icebergs is the most important ablation process (Paterson, 1994). Calving is not a component of the glacier surface mass balance and is not relevant for alpine glaciers.

At any given point (x, y) on the glacier surface and at any time t the accumulation rate $\dot{c} = \dot{c}(x, y, t)$ is the rate of mass gain. The ablation rate $\dot{a} = \dot{a}(x, y, t)$ is the rate of mass loss. $\dot{b} = \dot{c} - \dot{a}$ yields the rate of mass balance. Usually mass balance is expressed as a specific quantity in kg m^{-2} or a local thickness change in metres water equivalent (m w.e.). The integral of \dot{b} over a given time interval can be measured in the field. The mass balance

$$b = b(x, y) = a + c = \int_{t_1}^{t_2} (\dot{c} - \dot{a}) dt \quad (1.1)$$

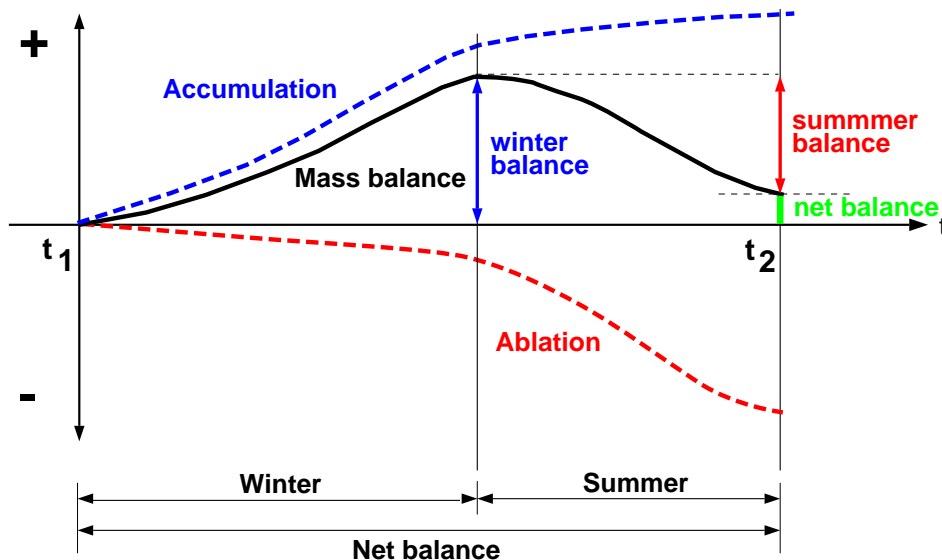


Figure 1.1: Definition of mass balance terms for a given point (x, y) on the glacier surface.

at any point (x, y) is the algebraic sum of accumulation and ablation over the period $t_1 \dots t_2$ (Fig. 1.1) and is, according to Meier (1962), termed 'specific' mass balance. The mass balance year is often divided into a winter and a summer period (Anonymous, 1969). On alpine glaciers the specific winter balance b_w is dominated by accumulation and is positive. During summer ablation prevails and the specific summer balance b_s is normally negative (Fig. 1.1). The specific net balance b_n is given by the integration of \dot{b} over an annual period or by

$$b_n = b_w + b_s. \quad (1.2)$$

Seasonal and annual mass balance quantities can be determined in a fixed-date system or a stratigraphic system (Anonymous, 1969; Mayo and others, 1972). In the fixed-date system the time interval $t_1 \dots t_2$ for the evaluation of the mass balance quantities is kept constant in every year. The hydrological year (October 1 to September 30) is often used for determining b_n . In contrast, the evaluation dates differ from year to year according to the stratigraphic system. In this system, b_n is defined as the mass balance between the absolute minima in the mass balance function (Fig. 1.1) in two consecutive years (Anonymous, 1969). In reality, field surveys rarely coincide with neither the dates t_1 and t_2 of the fixed-date system nor with those of the stratigraphic system. Thus, a third system for the evaluation of mass balance – the measurement period (Huss and others, in press) – must be considered. t_1 and t_2 in this system are defined as the actual dates of the field surveys.

Mass balance quantities can be defined – in analogy to those for a point – for the entire glacier area. These glacier-wide or area-averaged mass balances are particularly important for hydrological aspects and allow direct comparison of individual glaciers. The volumetric net balance B_n (in m^3 water equivalent) is defined as the integration of b_n at every point of the glacier over that year's glacier surface area S :

$$B_n = \int_S b_n dS. \quad (1.3)$$

The mean specific net balance $\overline{b_n}$ (Meier, 1962) is then obtained by

$$\overline{b_n} = B_n/S. \quad (1.4)$$

$\overline{b_n}$ can be regarded as the glacier-wide mean thickness change in water equivalent in that particular year.

The measurement of glacier surface mass balance can be performed using (1) the direct glaciological method and (2) the indirect geodetic method (Paterson, 1994). The glaciological method is based on one or several field surveys per year. Stakes are drilled into the ice allowing the monitoring of changes in surface elevation relative to their upper end. In the ablation area the difference in ice thickness relative to the stake is converted into water equivalent usually assuming an ice density of 900 kg m^{-3} . In the accumulation area the density of the accumulated firn is determined in a snow pit or by drilling to a marked horizon. In addition, snow probings to the last summer surface are performed for determining the spatial pattern of accumulation. The geodetic method provides ice volume changes of the entire glacier over periods of several years to decades based on comparison of repeated digital elevation models of the glacier surface.

1.2.2 Measurements of glacier mass change in Switzerland

The monitoring of glacier surface mass balance in Switzerland looks back onto a long tradition. Nowhere in the world mass balance measurements were started so early as in the Swiss Alps!

In 1885 the first stakes were installed on Rhonegletscher. The measurements at over a dozen locations were maintained for more than two decades (Mercanton, 1916). In 1914 the longest mass balance time series worldwide were started at two stakes in the accumulation area of Claridenfirn (Müller and Kappenberger, 1991). They were continued in seasonal resolution almost without disruptions until present. At the same time similar measurement series were begun at one stake on Grosser Aletschgletscher and two on Silvrettagletscher (Firnberichte, 1914–1978; Huss and Bauder, in press). In connection with hydropower production first efforts to determine the glacier-wide mass balance were undertaken in the late 1940s. An extensive stake network was set up on Limmern- and Plattalvagletscher and observed until 1984 (Glaciological reports, 1881–2008). In the 1960s comprehensive mass balance monitoring programs were started on Silvrettagletscher and Griesgletscher, both also connected to the planned construction of reservoirs for hydropower production (Aellen, 1996). These measurements of mean specific net balance are continued until today. Additional stake measurements of mass balance, partly covering the entire glacier over several decades, are available for Grosser Aletschgletscher, Glacier du Giéto, Glacier de Corbasière, four glaciers in the Mattmark region and Ghiacciaio del Basodino.

In total, several thousands of measurements exist covering a large fraction of the 20th century. Generations of glaciologists have put an immense effort into the establishment of this unique data basis. Nevertheless, this wealth of field data was never comprehensively compiled and evaluated so far.

Besides the vast number of in-situ measurements on different Swiss glaciers a comprehensive data set of ice volume changes has recently become available and covers more than 100 years (Bauder and others, 2007). For more than 30 glaciers series of up to ten digital elevation models per glacier have been established. They are based on digitized topographic maps before 1960 and later on a photogrammetrical evaluation of aerial photographs. Differencing of two successive digital elevation models allows the change in ice volume over time intervals of some years to decades to be calculated. These geodetic mass balances are assumed to be the most accurate record of long-term change in of glacier mass.

1.2.3 Mass balance modelling

The modelling of glacier mass balance is of interest for many fields of science, however, has also a practical importance, e.g. for water resource management and studies of glacier dynamics (Hock, 2005). During the last decades a wide range of glacier melt models of differing sophistication have been developed. Most of them can be categorized into the groups of (1) physically based energy balance models and (2) empirical temperature-index models. In order to simulate glacier mass balance over an annual period an accumulation model must be coupled to both types of melt models. There is a trend towards fully distributed models, which necessarily involves the extrapolation of meteorological variables.

Energy balance models compute all energy fluxes (in W m^{-2}) from and to the snow or ice surface.

$$Q_N + Q_H + Q_L + Q_M = 0, \quad (1.5)$$

where Q_N is net radiation, Q_H and Q_L is the sensible and the latent heat flux (turbulent fluxes), respectively, and Q_M is the energy consumed for melt (ground heat flux and heat supplied by rain are lower order terms). Any surplus of energy is consumed for melt over a snow or ice surface of 0° . Using the the latent heat of fusion L_f , the melt rate M can be calculated from Q_M .

Distributed models solving the energy balance at every grid cell of the glacier have been developed (e.g. Oerlemans and Fortuin, 1992; Arnold and others, 1996; Hock and Noetzli, 1997; Klok and Oerlemans, 2002; Paul and others, 2005; Gerbaux and others, 2005). The applicability of these approaches is limited by uncertainties due to extrapolating sensitive input variables in space.

Temperature-index models are based on a relationship between air temperature and melt (Hock, 2003). Air temperature is the most readily available meteorological variable and is easy to be extrapolated and forecasted. Thus, temperature-index models are widely used for the computation of snow- and icemelt (e.g. Bergström, 1995; Braun and others, 1995; Braithwaite, 1995; Hock, 1999; Vincent, 2002). Due to their empirical character temperature-index models require calibration using field data.

The melt rate M is calculated as a linear function of positive air temperature:

$$M = \begin{cases} (DDF_{\text{snow/ice}}) T & : T > 0 \\ 0 & : T \leq 0 \end{cases} \quad (1.6)$$

The two degree-day factors DDF_{snow} and DDF_{ice} account for different albedos of the surface. The good performance of simple degree-day approaches is attributed to the fact that many components of the energy balance show a strong correlation with air temperature (Ohmura, 2001). However, degree-day factors vary substantially in space and time as they implicitly include all components of the heat budget (Hock, 2003). Thus, several approaches were developed to adapt degree-day factors, e.g. with aspect (Braun and others, 1995), with albedo (Arendt and Sharp, 1999) or in a fully distributed manner with potential radiation I (Hock, 1999):

$$M = \begin{cases} (f_m + r_{\text{ice/snow}} I) T & : T > 0 \\ 0 & : T \leq 0 \end{cases} \quad (1.7)$$

With this approach the spatial variability of melt in complex terrain, as well as the subdaily variations mainly due to shortwave incoming radiation, can be captured. There is a transition from simple degree-day approaches (Eq. 1.6) to expressions resembling energy balance formulations. Often an explicit radiation term is added (e.g. Kane and Gieck, 1997; Pellicciotti and others, 2005).

Whereas the contribution of melt to glacier surface mass balance can be modelled relatively well, the accumulation term did not receive comparable attention so far. Most mass balance models simulate accumulation simply as precipitation occurring at temperatures below a certain threshold (e.g. Schaepli and others, 2005). The preferential deposition of snow determined by wind direction and velocity and the snow redistribution by wind and avalanches is often not taken into account. This is mostly because these processes are too complex and too poorly understood to be incorporated in models. Recently, attempts have been made for simulating both processes within the snow cover and the transport of snow by wind (Lehning and others, 2006, 2008). Additionally, the measurement of precipitation in high mountain regions is affected by significant biases (Sevruk, 1985). Actual precipitation is often underestimated. Snow probing provides the most accurate estimate of total winter precipitation amount. Currently, the accumulation term represents the major source of uncertainty in the state-of-the-art distributed mass balance models.

1.3 Thesis objectives and structure

1.3.1 Objectives

The goal of this thesis can be concentrated into one question:

How can we optimally combine field data and modelling in order to learn how glaciers react to climate forcing in the past and in the future?

This single question involves such a large field of different areas of research that it cannot be finalized within one PhD thesis. This study is not the first one dedicated to this topic and, thus, could build upon a thorough basis of previous research. The steps and the objectives followed in this thesis towards finding answers to this questions are:

- Compilation of all accessible data on glacier mass balance in Switzerland.
- Field measurements of mass balance on several Swiss glaciers, contributing to the continuation of long-term mass balance observations and performing additional measurements to fill gaps in the monitoring programs.
- Set up of a distributed mass balance model for alpine glaciers which can match all types of field observations available for the last century.
- Careful re-analysis and homogenization of long-term mass balance measurements in Switzerland in order to understand the climate forcing on Alpine glaciers in the past 100 years as well as the ongoing changes.
- Development of widely applicable methods for calculating future glacier retreat.
- Application of combined models of mass balance and stream-flow runoff to highly glacierized catchment basins using climate scenarios for the future.

1.3.2 Structure

The thesis consists of eight chapters written as independent papers. They are framed by an Introduction and a Synthesis. Some repetition is inevitable, especially in the introductory part and individual methodological issues of each paper. For presentation the papers are aggregated in three parts. Part I deals with the interpretation of long-term mass balance measurements during the last century by the use of models. Part II contains applications of the methods developed in the course of this dissertation to glacier hydrology and the mass balance of an Arctic glacier. Part III is focussed on future changes in glacier extent and their consequences. The Appendix includes the latest results that have not yet been published. In the following, a short outline of each chapter is provided.

Part I: Long-term mass balance records

Chapter 2:

”Determination of the seasonal mass balance of four Alpine glaciers since 1865”

This paper describes a method to compute seasonal mass balances of Alpine glaciers since the begin of the meteorological records in 1865. All available field data (ice volume changes, in-situ measurements of seasonal mass balance at stakes, annual runoff volumes) are used to calibrate a distributed mass balance model based on the temperature-index approach.

Chapter 3:

”Twentieth century climate change inferred from four long-term point observations of seasonal mass balance”

Within this chapter the longest mass balance observations worldwide are homogenized and interpreted. Since 1914 the seasonal mass balance has been measured almost continuously at four stakes located at or above the equilibrium line in the Swiss Alps. This exceptional data set allows the detection of rates and trends in the heat budget over snow and ice throughout the entire 20th century.

Chapter 4:

”Homogenization of long-term mass balance time series”

Time series of mean specific surface mass balance have been evaluated using different techniques in the past and often reveal inhomogeneities. A method for homogenizing long-term mass balance records of glacier monitoring programs is presented. The homogenization procedure is based on a daily mass balance model that is tightly constrained with field data. Indirect geodetic and direct glaciological measurements are combined. The methodology allows a reduction of mass balance quantities measured at arbitrary dates to the hydrological year.

Part II: Applications to glacier hydrology and Arctic regions

Chapter 5:

”Glacier-dammed lake outburst events of Gornersee, Switzerland”

Short-term processes of glacier hydrology are determined to a large extent by the meltwater input into the system. This paper presents an analysis of the outburst events of a glacier-dammed lake over the last five decades and in more detail for two field seasons with a wealth of field data. In order to interpret different field observations a surface melt model running in high temporal resolution is applied.

Chapter 6:

”Temporal and spatial changes of Laika Glacier, Canadian Arctic, since 1959 inferred from satellite remote sensing and mass balance modelling”

Whereas glacier retreat is known from various data sources in the Alps, the reaction of remote Arctic glaciers to climate change during the 20th century is often not documented. This chapter presents a method that combines in-situ measurements during a limited time period, different types of remote sensing data and modelling. Changes in glacier geometry and the mass balance of the small Laika Glacier are assessed over five decades.

Part III: Projections of future glacier extent and runoff

Chapter 7:

”Modelling the future retreat of Unteraargletscher”

With climate warming Alpine glaciers are expected to retreat substantially. The rate of future glacier wastage is, however, yet difficult to estimate. This paper presents a combined ice-flow mass-balance model that is applied to the debris-covered tongue of Unteraargletscher. In order to simulate future climate conditions three scenarios for the seasonal change in temperature and precipitation are defined.

Chapter 8:

”Modelling runoff from highly glacierized drainage basins in a changing climate”

Runoff from glacierized drainage basins is important for hydropower production and water supply in dry alpine valleys. With ongoing climate change and the partial or complete disappearance of glaciers the hydrological regime of high alpine catchments will change significantly. A new glacio-hydrological model is presented. The model provides runoff forecasts in daily resolution for the next century. It explicitly takes into account the dynamic retreat of the glaciers.

Chapter 9:

”Parameterizations for calculating future glacier retreat”

The assessment of glacier retreat in the 21st century requires the description of the climate forcing and the ice flow dynamics. This chapter answers the question whether complex 3D ice flow modelling is required for calculating future glacier extent. Simple parameterizations for the ice thickness change in response to glacier surface mass balance changes are proposed and validated against a 3D finite element ice flow model.

Appendix

Appendix A:

”The mass balance of Pizolgletscher”

In the course of this PhD thesis a mass balance monitoring program was started on the very small Pizolgletscher, eastern Switzerland. First results of the field campaigns in 2006 to 2008 and a reconstruction of the seasonal mass balance since 1961 are presented. The benefit of mass balance modelling for the interpretation of seasonal point measurements is illustrated.

Appendix B:

”New evidence for strong glacier melt around 1950”

This short résumé is the essence of the findings achieved by analyzing the longest mass balance records worldwide. The changes in the climatic forcing on Alpine glacier throughout the 20th century are highlighted.

Part I

Long-term mass balance records

Chapter 2

Determination of the seasonal mass balance of four Alpine glaciers since 1865

MATTHIAS HUSS¹, ANDREAS BAUDER¹,
MARTIN FUNK¹, REGINE HOCK^{2,3}

¹Versuchsanstalt für Wasserbau, Hydrologie und Glaziologie (VAW), ETH Zürich, 8092 Zürich, Switzerland

²Department of Earth Sciences, Uppsala University, 75236 Uppsala, Sweden

³Geophysical Institute, University of Alaska Fairbanks, Alaska 99775-7320

Published, Journal of Geophysical Research

Citation: Huss M., A. Bauder, M. Funk and R. Hock (2008). Determination of the seasonal mass balance of four Alpine glaciers since 1865. *Journal of Geophysical Research*, 113, F01015, doi:10.1029/2007JF000803.

ABSTRACT: Alpine glaciers have suffered major losses of ice in the last century. We compute spatially distributed seasonal mass balances of four glaciers in the Swiss Alps (Grosser Aletschgletscher, Rhonegletscher, Griesgletscher and Silvrettagletscher) for the period 1865 to 2006. The mass balance model is forced by daily air temperature and precipitation data compiled from various long-term data series. The model is calibrated using ice volume changes derived from five to nine high-resolution digital elevation models, annual discharge data and a newly compiled data set of more than 4000 in-situ measurements of mass balance covering different subperiods. The cumulative mass balances over the 142 year period vary between 35 and 97 m revealing a considerable mass loss. There is no significant trend in winter balances, whereas summer balances display important fluctuations. The rate of mass loss in the 1940s was higher than in the last decade. Our approach combines different types of field data with mass balance modeling to resolve decadal scale ice volume change observations to seasonal and spatially distributed mass balance series. The results contribute to a better understanding of the climatic forcing on Alpine glaciers in the last century.

2.1 Introduction

Temporal glacier variations are among the clearest natural indicators of ongoing climate change (e.g. IPCC, 2007; Oerlemans and Fortuin, 1992). A sound knowledge of the response of glaciers to climate change is of crucial importance for the assessment of water resources, sea level rise and natural hazards (e.g. Haeberli, 1995; Zuo and Oerlemans, 1997; Kaser and others, 2006; Huss and others, 2007b). In order to be able to predict the future reaction of alpine glaciers to climate change, we must understand their evolution in the past. Of several key parameters on glaciers, it is the mass balance which most clearly reflects climatic variation (Oerlemans, 1994; Braithwaite and Zhang, 2000; Vincent, 2002).

Mass balance of alpine glaciers is dominated by two processes not directly related to one another: Accumulation is due to deposition of solid precipitation and contributes mainly to the winter balance of the glacier surface; ablation is determined by the melting of ice and snow, and dominates the summer balance. Conventional mass balance programs often do not distinguish between the two components (Dyurgerov and Meier, 1999). However, seasonal values of mass balance provide the best insights to assess the effects of climatic forcing on glaciers. Mean specific mass balance can be biased by the dynamic response of the ice mass when the glacier shape and size is adapting to changed climatic conditions (Jóhannesson and others, 1989). Nevertheless, mean specific mass balance time series are of broad interest and have been determined in numerous glacier monitoring programs (Dyurgerov and F.Meier, 2005).

Direct measurements of mass balance are available only for a limited number of glaciers and seldom extend far back in time. Numerical mass balance models can be applied in order to expand existing time series (e.g. Torinesi and others, 2002; Vincent, 2002; Machguth and others, 2006). A variety of models relating measured climatic variables to glacier mass balance using different methods have been developed (Braithwaite, 1995; Arnold and others, 1996; Oerlemans and others, 1998; Hock, 1999; Pellicciotti and others, 2005; Gerbaux and others, 2005; Steiner and others, 2005). Vincent (2002) and Vincent and others (2004) reconstructed the mass balance of four French glaciers over the 20th century using a simple degree-day model, but without calculating the spatial distribution of the mass balance. The model was calibrated using in-situ mass balance measurements and ice volume changes. Results showed a significant increase in summer ablation during the last 20 years and a period of enhanced glacier recession in the 1940s. Schöner and Böhm (2007) calculated the mass balance evolution of glaciers in the Austrian Alps back to 1800 using regression equations and gridded data sets of meteorological variables.

The aim of this study is to determine continuous time series of mean specific seasonal mass balance as well as the spatial distribution of mass balance of four well-documented glaciers in the Swiss Alps for the last 142 years. We extend the temporally limited mass balance series to the entire period since 1865, which marked the beginning of instrumental weather observations in Switzerland, and then resolve them into spatially distributed winter and summer balances. This provides a basis for the study of climate-glacier interaction in alpine environments and for the identification of processes that govern the mass balance evolution.

We apply a numerical model as a tool for calculating seasonal glacier mass balances and merge all types of measurements which are accessible within the extensive glacier monitoring programs. The mass balance model is calibrated with ice volume changes which are known for all investigated glaciers from high-resolution digital elevation models (DEMs), a newly compiled

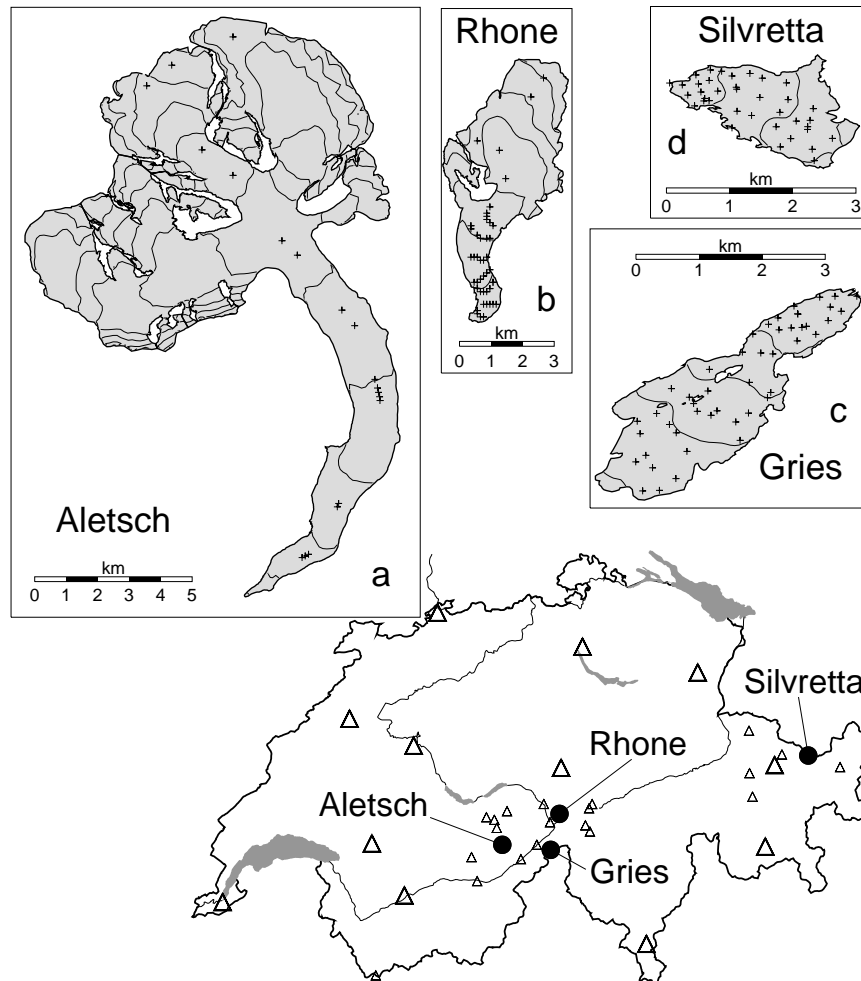


Figure 2.1: Location in Switzerland and outline of the four investigated glaciers. Triangles represent MeteoSchweiz weather stations. Large symbols indicate stations with continuous monthly air temperature and precipitation series since 1864 and small symbols refer to weather stations with shorter meteorological records of daily resolution. Note, that the scales of the glacier outlines in (a) and (b) differ from those in (c) and (d). The glacier extent is based on the latest DEM. The contour interval is 200 m, and crosses mark the position of mass balance stakes during the year 1980.

data set of point-based mass balance measurements and discharge records. Using air temperature and precipitation data we resolve the ice volume changes given at a decadal scale to a seasonal scale and calculate the spatial distribution of mass balance on a regular grid. We derive the first complete seasonal mass balance time series for four Alpine glaciers for the 1865-2006 period. The results are backed up in an optimal way with numerous independent field data.

2.2 Study sites and field data

This study focuses on four glaciers in the Swiss Alps (Grosser Aletschgletscher, Rhonegletscher, Griesgletscher and Silvrettagletscher, Fig. 2.1) for which exceptional data sets including extensive measurements of mass balance at stakes over several decades are available. The glaciers have different geometries, exposures and regional climate conditions and range in

Table 2.1: *Glacier characteristics and field data basis. The time interval of available in-situ measurements (b_n : surface net balance measured at stakes, b_w : surface winter balance) and discharge measurements (Q_a : annual runoff volume) are given.*

Glacier	Area* (km ²)	Elevation* (m a.s.l.)	Periods of field data		
			b_n	b_w	Q_a
Aletsch	83.01	1560 - 4085	1921-2006	1921-2006	1923-2006
Rhone	16.45	2197 - 3600	1885-1909,1980-82	1980-1982	1957-2006
Gries	5.26	2410 - 3327	1961-2006	1994-2006	1957-2004
Silvretta	2.89	2460 - 3073	1917-2006	1915-83,2003-06	1934-2004
	Number of DEMs		Years		
Aletsch	5		1880, 1926, 1957, 1980, 1999		
Rhone	6		1874, 1929, 1959, 1980, 1991, 2000		
Gries	9		1884, 1923, 1961, 1967, 1979, 1986, 1991, 1998, 2003		
Silvretta	7		1892, 1938, 1959, 1973, 1986, 1994, 2003		

* based on the latest DEM available

size from 3 to 80 km². Grosser Aletschgletscher is the largest ice mass in the European Alps. Whereas the local climate at the glacier terminus is relatively dry, high precipitation amounts are reported in the accumulation area owing to regional advection effects (Schwarb and others, 2001). Rhonegletscher is a south-exposed medium-sized valley glacier with a climatic setting similar to Aletsch. Griesgletscher is exposed to different meteorological conditions than the other three glaciers as it is situated south of the main Alpine crest. The small valley glacier has a north-eastern exposure. Silvrettagletscher is a small glacier in the north-eastern Swiss Alps with exposure to the west. The regional climate is characterized by relatively high precipitation amounts (Fig. 2.1 and Table 2.1). The glaciers have lost between 16% (Aletsch) and 39% (Gries) of their area during the 20th century. Mass balance monitoring programs were set up on Griesgletscher and on Silvrettagletscher in the 1960s in the context of hydropower projects. The measurements on Aletsch and Rhonegletscher were conducted mostly as part of glaciological research projects and data were usually too sparse to obtain area-averaged means.

We use the following types of data for the modeling: (i) meteorological data, (ii) digital elevation models and ice volume changes, (iii) point-based mass balance measurements, and (iv) annual runoff volumes.

We use different classes of climate data: Homogenized continuous monthly time series of temperature and precipitation since 1864 are available for 12 MeteoSchweiz stations (Begert and others, 2005). Twenty additional weather stations in the vicinity of the investigated glaciers provide information about the regional climate (Fig. 2.1). These span shorter time periods but have daily resolution. High-alpine precipitation distribution information is provided by the PRISM data set (see Section 3.3) compiled by Schwarb and others (2001).

For each glacier a set of five to nine high-resolution DEMs is available (Bauder and others, 2007). They cover the last century in decadal to semicentennial time periods (Table 2.1). DEMs for the period before 1960 are produced by the manual digitizing of topographic maps. The accuracy of the altitudinal information is estimated at ± 5 -10 m for digitized maps. The recent DEMs are based on photogrammetrical evaluation of aerial photographs. Their accuracy is ± 0.3 m in the ablation zone, where the largest elevation changes occur, and ± 1 m in the firn area (Bauder and others, 2007). The DEMs are interpolated to a regular grid of 25 m (50 m in

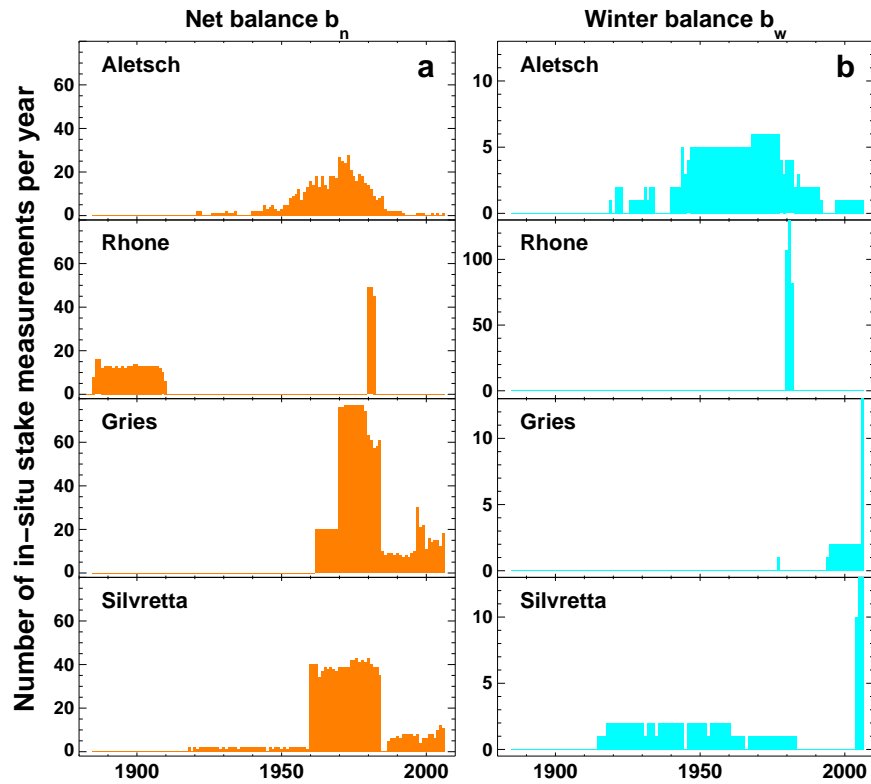


Figure 2.2: Number of in-situ stake measurements per year for each glacier of (a) net mass balance and (b) winter mass balance.

the case of Aletsch). The DEMs provide a unique data basis for assessing long-term geometrical changes, in particular enabling ice volume changes to be calculated.

During the last century mass balance measurements were conducted employing an enormous amount of manpower (e.g. Aellen, 1996). Mass balance measurements mainly used for monitoring purposes have been performed on all four glaciers with varying intensity and during different subperiods of the 142 year study period (Fig. 2.2). We evaluated all accessible data from reports and original field books and compiled a new digital data set of point-based mass balance measurements. It includes 3544 stake readings of surface net balance b_n and 773 measurements of surface winter balance b_w . Figure 2.2 shows the available data for each glacier. The uncertainty in direct measurements of net balance b_n at stakes is estimated as ± 0.1 m water equivalent (w.e.) in the ablation area and may reach up to ± 0.4 m w.e. in the accumulation area. An uncertainty of ± 0.15 m w.e. is attributed to the measurement of winter balance b_w Gerbaux and others (2005).

Discharge records for the drainage basins are available, provided by the Swiss Federal Office for the Environment (Aletsch, Rhone and Silvretta). Runoff from the Gries catchment is determined based on water balance figures from a proglacial reservoir used for hydropower production. We use annual runoff volumes Q_a (Table 2.1). Their accuracy is estimated as $\pm 5\%$ (personal communication BAFU, 2007). The catchment basins of Aletsch, Rhone and Gries are more than 50% glacierized, whereas the Silvrettagletscher catchment is only 7% ice-covered.

2.3 Methods

Determination of mass balance

We refer to two different types of mass balance: (i) point-based balance terms, and (ii) values integrated over the whole glacial area. All balance terms are specific quantities expressed in meters of water equivalent (m w.e.). \bar{b}_n is the mean specific surface net balance that corresponds to the integrated sum of accumulation and ablation over the entire glacier over one year divided by that year's glacier surface area. \bar{b}_w is the mean specific winter balance and \bar{b}_s the mean specific summer balance. In this paper, \bar{b}_n (1 Oct. – 30 Sept.), \bar{b}_w (1 Oct. – 30 April) and \bar{b}_s (1 May – 30 Sept.) are modeled quantities. b_n , b_w and b_s are the point-based specific net, winter and summer balances measured at a stake, respectively. The time interval corresponds to the effective dates of the readings. Accumulation and ablation on the glacier surface balance out at the equilibrium line. Its mean elevation is evaluated on 30th September each year and expressed in terms of the ELA (equilibrium line altitude).

We calculate 'conventional' mass balances (Elsberg and others, 2001; Harrison and others, 2005), i.e. the glacier area is updated annually. An annual time series of glacier area is obtained by linear interpolation of the glacier surface geometry between two successive DEMs. Using this technique both the annual change in glacier surface elevation and the change in glacier extent are estimated and step changes in the glacier geometry are avoided. The potential for error in this approach is low, as the measured DEMs constrain the interpolation in decadal intervals.

The method for determining mass balance time series since 1865 is based on a surface melt model (Hock, 1999) coupled with a distributed accumulation model that calculates accumulation and ablation on a regular grid in daily time steps. Temperature and precipitation are the required input variables. The model is calibrated using ice volume changes, in-situ mass balance measurements and discharge. In the following paragraphs each of the methodological steps is described in detail.

Ice volume changes

The changes in ice volume provide an important basis for this study as they supply independent benchmarks for our approach which aid in determining the seasonal mass balance time series and in constraining the course of the calculated cumulative mass balance curve. By comparing two successive DEMs an ice volume change can be calculated. The imprecision of the volume change determination is less than 5% (Bauder and others, 2007). The ice volume change is converted to water equivalent by assuming a constant ice density of 900 kg m^{-3} . For further information on this subject refer to Bauder and others (2007).

Meteorological time series

The mass balance model requires a continuous time series of daily air temperature and precipitation for the investigated period 1865-2006. As temperature and precipitation variables were not recorded at locations in immediate proximity to the glaciers, the measured data series needed to

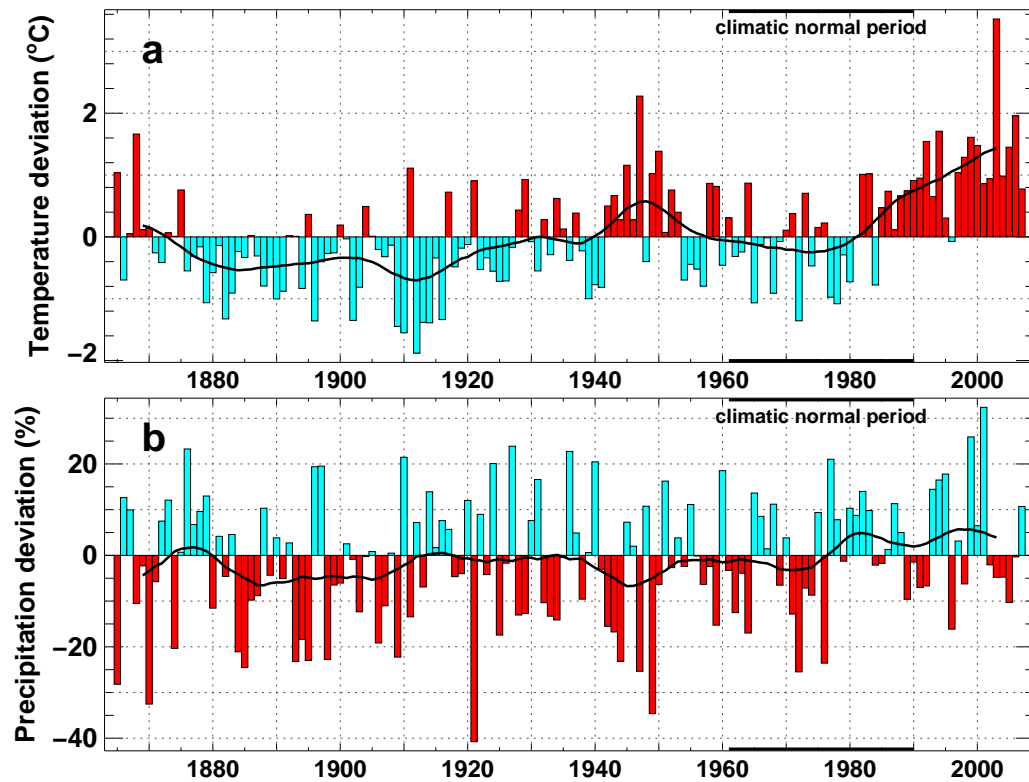


Figure 2.3: Homogenized time series of MeteoSchweiz: Mean deviations (12-station average) from the 1961-1990 climatic normal period of (a) summer temperature (May to September) and (b) annual precipitation. Solid curves indicate 10-year running means.

be scaled to the study sites. The procedures for the compilation of representative time series of temperature and precipitation are treated separately. In order to model the spatial distribution of mass balance accurately, the use of climatic data in high temporal resolution is essential. By adopting a daily time resolution, the short-term meteorological variability is taken into account, as for example, the height rise in the zero degree isotherm, albedo effects due to summer snow fall events, etc.

Air temperature is relatively well correlated over large distances (Begert and others, 2005) and can therefore be extrapolated with confidence. As temperature input we calculate a representative temperature time series for each glacier using the 12 homogenized data sets provided by MeteoSchweiz (Fig. 2.3a). The time series are corrected for systematic biases which may be due, for example, to the relocation of the weather station or changed measuring techniques (Begert and others, 2005). The monthly temperature anomalies of the weather stations are averaged weighted with their inverse distance from the glacier.

A local temperature lapse rate is determined for each month using weather stations within distances of less than 30 km to the glacier. Using these gradients, the glacier-specific homogenized temperature time series is shifted to the mean glacier elevation. The temperature data of monthly resolution thus obtained are downscaled by applying the daily fluctuations of the weather station at Bern.

The distribution of precipitation in alpine environments is complex. Regional differences in precipitation are considerable, and altitudinal gradients of precipitation are variable over short horizontal distances (Frei and Schär, 1998; Schwarb and others, 2001). Measurements of precipitation over mountainous terrain are difficult and can be significantly biased by wind, es-

pecially in winter (Sevruk, 1985). Hence, the uncertainties are large regarding high alpine precipitation amounts.

Because of the lack of precipitation data recorded close to the glaciers, we rely on a gridded precipitation map for obtaining a spatial distribution pattern of precipitation. The PRISM data set (Schwarb and others, 2001) was generated using all available precipitation data in the Alpine region. It provides the monthly mean of precipitation sums during the period 1971-1990 on a grid of about 2 km. Interpolation of precipitation is conducted based on local altitudinal gradients determined by weighted regression between surrounding precipitation records (Schwarb, 2000).

To obtain representative times series of high mountain precipitation we use daily data from the local weather station that correlate best with the winter snow water equivalent time series measured at stakes. The monthly precipitation sum recorded at this station is scaled to the values given by the PRISM data set for the glacier site. Thus, the precipitation time series is composed of the temporal fluctuations of precipitation observed at a weather station near the glacier and the spatial distribution of precipitation sums given by the PRISM data set.

Model description

We calculate mass balance using a distributed temperature-index melt model (Hock, 1999) coupled to an accumulation model. This model elaborates on classical models using degree-day factors by varying these as a function of clear-sky direct radiation in order to account for the effects of slope, aspect and shading. Temperature-index models are based on a linear relation between positive air temperature and melt rate (e.g. Braithwaite, 1995; Hock, 2003). Ohmura (2001) demonstrated that the physical base of temperature-index modeling is stronger than previously assumed. Melt is highly correlated with long-wave heat flux, for which air temperature is a good indicator. Temperature and precipitation at daily resolution are required input data which make the model applicable to centennial periods with poor spatial coverage of weather data. Daily surface melt rates M are computed for each cell of the DEM by:

$$M = \begin{cases} (f_M + r_{\text{ice/snow}} I) T & : T > 0 \\ 0 & : T \leq 0 \end{cases} \quad (2.1)$$

where f_M denotes a melt factor, $r_{\text{ice/snow}}$ are radiation factors for ice and snow surfaces and I is the potential direct solar radiation. Due to the empirical character of the temperature-index model (Hock, 1999) the site-specific parameters f_M and $r_{\text{ice/snow}}$ must be calibrated using field data.

Air temperature at every grid cell is determined by a constant lapse rate. Precipitation is assumed to increase linearly with elevation (dP/dz). A correction factor accounts for gauge undercatch errors (c_{prec}) and a threshold temperature distinguishes snow from rainfall (Hock, 1999). Discharge from the catchment basin is calculated as the sum of liquid precipitation and snow- and icemelt. It is corrected for evaporation by subtracting a constant value derived from basin characteristics (Braun and others, 1995). The spatial variation of accumulation on the glacier surface is influenced by snowdrift, avalanches and, for larger glaciers, by the regional precipitation field. The latter is evaluated based on the PRISM data set (Schwarb and others, 2001). To account for effects of avalanches and snowdrift we use slope and curvature derived from a DEM. We decrease accumulation linearly from 100 to 0% between a slope angle of 40° to

60°. Curvature is good indicator of regions with snow erosion and redeposition due to winds (Blöschl and others, 1991) and is evaluated within a range of 200 m around each grid point. We multiply solid precipitation with a factor depending on curvature which varies between 0.5 and 1.5. A precipitation matrix is generated that describes the differential deposition of snow and is able to explain some of the complex patterns of accumulation in high mountain areas. Where measurements of the snow cover in individual years are available in high spatial resolution, the distribution map of solid precipitation is refined.

Model calibration

The calibration of our model is an automated multilayer iterative procedure. It is schematized in Figure 2.4. A wide range of field data originating from various sources is included. The procedure tunes the mass balances to the ice volume changes and minimizes the misfit between modeling results and in-situ mass balance data and runoff.

In calibration Loop 1 the calculated annual ice volume change is cumulated over each subperiod given by two successive DEMs of the glacier surface. Initialized by arbitrarily chosen values

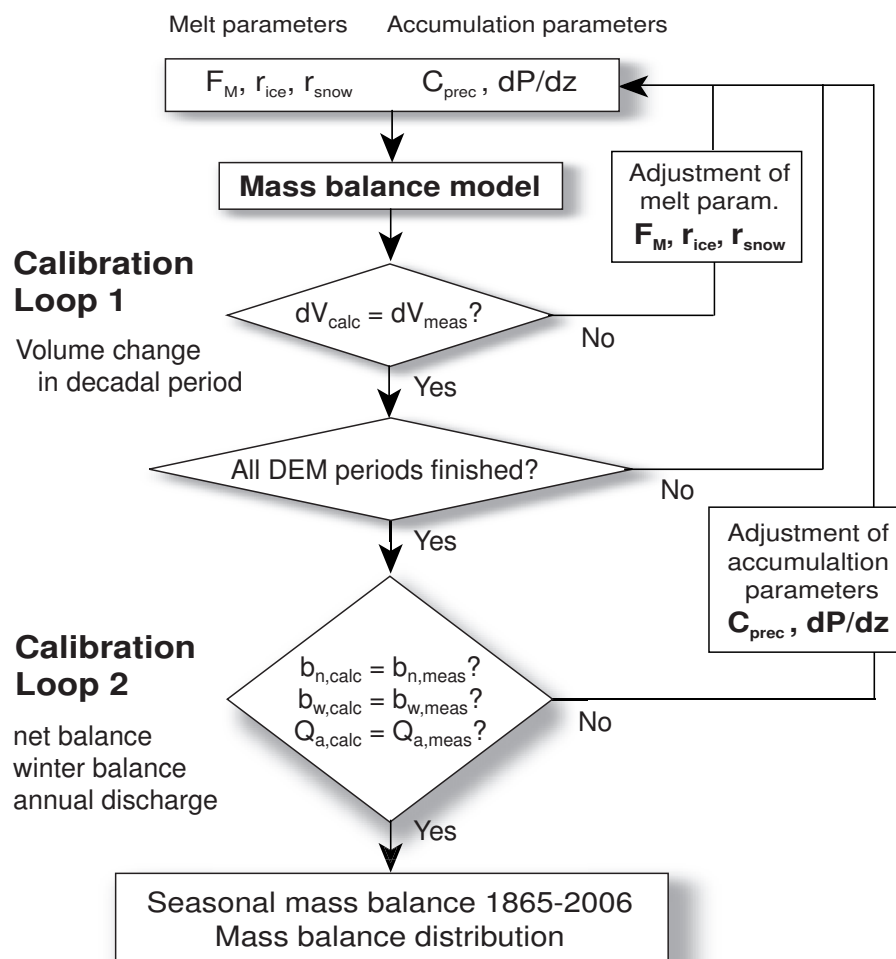


Figure 2.4: Calibration procedure. Melt parameters are calibrated for each subperiod given by two successive DEMs in Loop 1. Accumulation parameters are adjusted in Loop 2 for the entire 1865-2006 period.

of c_{prec} and dP/dz the ice volume change is adjusted by varying the melt parameters f_M and $r_{\text{ice/snow}}$ to match the corresponding value determined geodetically (Fig. 2.4). This calibration method integrates long-term overall changes of the glacier and does not depend on local effects of surface mass balance distribution. The procedure is repeated for all subperiods with available volume changes. Calibration Loop 2 adjusts the accumulation parameters (c_{prec} , dP/dz). Calibration Loop 1 and 2 are repeated until optimal agreement between both measured and modeled quantities is achieved. We minimize (1) the mean residual and (2) the standard deviation σ_d of the misfit between modeling results and independent in-situ measurements of (i) point-based net balance b_n , (ii) point-based winter balance b_w and (iii) annual discharge volume Q_a .

As precipitation parameters are atmospheric boundary conditions, they are assumed to be valid for the entire modeling period 1865-2006 (Fig. 2.4). In contrast, for the melt parameters a different optimal set of parameters is obtained for each subperiod of consecutive DEMs. The subperiodical variations of the melt parameters are in the range of $\pm 10\%$ for each glacier. We

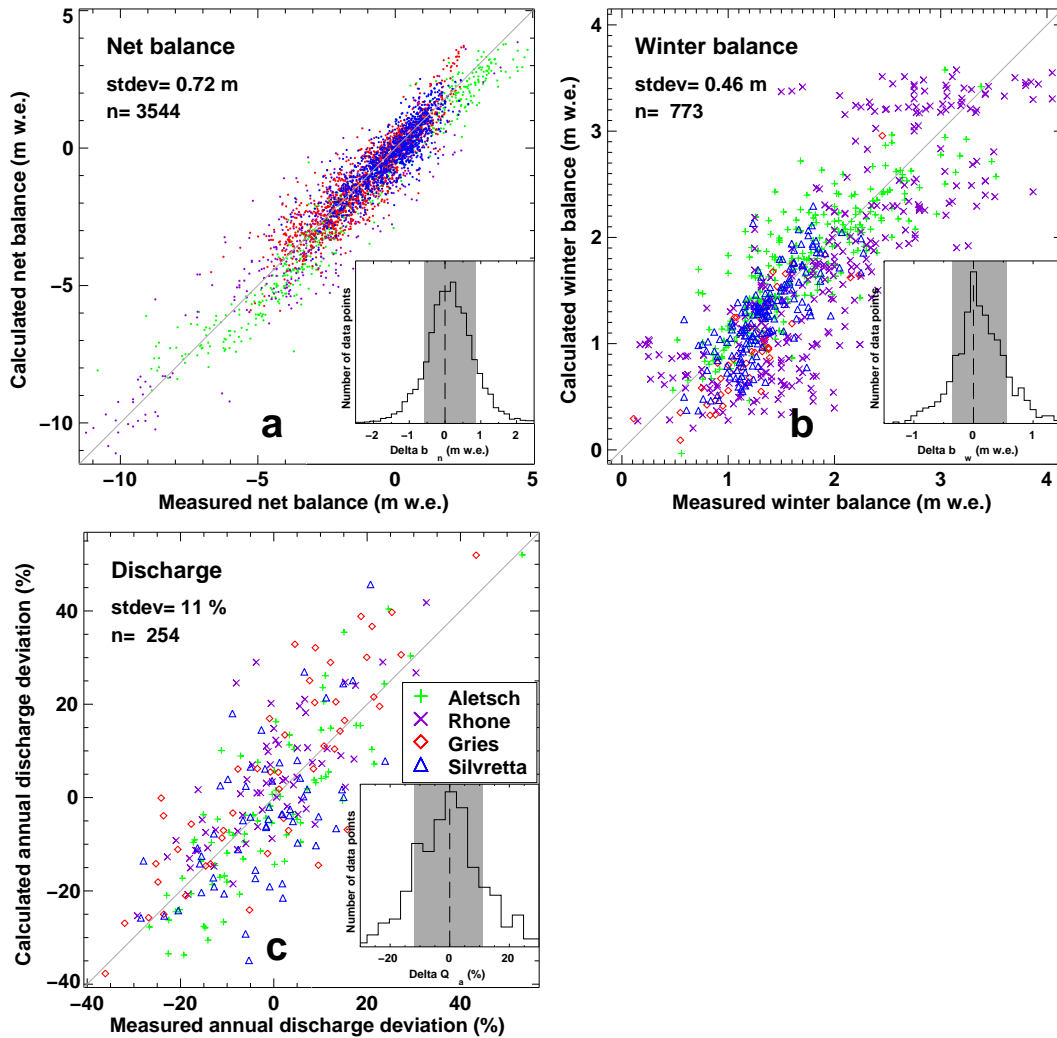


Figure 2.5: Comparison of measured and calculated (a) net mass balance b_n , (b) winter mass balance b_w at all available measurement locations, and (c) annual discharge volume Q_a normalized with the average runoff from the catchment. The standard deviation of the residuals between measured and calculated quantities, and the number of data points are stated. The distribution of the residuals is shown in the insets. The shaded bar corresponds to $\pm 1\sigma$ (containing 70% of the data points).

assume the parameter combination of the first DEM subperiod to be valid for the two decades before the initial DEM. The parameters of the last period are used to model the mass balances after the last DEM acquired between 1999 and 2003. For this case the results are not constrained by measured ice volume change but can be corrected, if necessary, using the in-situ measurements of b_n and b_w available for these years, with the exception of Rhonegletscher (Table 2.1).

The calibration of the model using different types of in-situ measurements is important. Both seasonal balance and mass balance distribution could be in error if volume changes alone were used for calibration. By using the extensive data set of different field data types for calibration and validation of the results, we are able to resolve the ice volume change series seasonally and to determine a spatial distribution of the balance terms. Our results are well founded, based on independent field data of ice volume changes, in-situ mass balance measurements and runoff volumes. The calculated and the measured quantities correspond well in most cases (Fig. 2.5 and Table 2.2). The differences cluster in a zero-centered gaussian-shaped distribution (insets in Fig. 2.5). To compare the runoff volumes of different catchment basins, the differences are normalized with the mean measured annual runoff $\overline{Q_a}$, and standard deviations $\sigma_{d,n}$ are given in percent (Fig. 2.5 and Table 2.2).

Table 2.2: Comparison of model results with field data. n is the number of data points, σ_d the standard deviation of the differences.

Glacier	net balance		winter balance		annual discharge	
	n	σ_d (m)	n	σ_d (m)	n	$\sigma_{d,n}$ (%)
Aletsch	572	0.67	250	0.34	80	9.8
Rhone	423	1.16	318	0.58	66	10.1
Gries	1401	0.64	41	0.28	48	11.3
Silvretta	1148	0.57	164	0.27	60	13.3

In the simultaneous minimization procedure to calibrate the mass balance model, an exact match of all classes of field data with the modeling results is usually not achievable (Fig. 2.5). This is due to the inability of a numerical model to describe correctly all processes involved. Essentially, the model is tuned to the ice volume changes within each subperiod and the overall misfit is minimized between in-situ measurements and model results.

2.4 Results

We present four classes of results: (i) Cumulative time series of mean specific net balance, (ii) time series of mean specific winter, summer and net balance, (iii) the spatial distribution of mass balance and (iv) equilibrium line altitudes. By analyzing the model results, we identified four periods of decadal time scale with mass gain or exceptional rates of mass loss. The exact beginning and end of each period were set arbitrarily. Periods I (1912-1920) and III (1974-1981) are characterized by mass gains, Periods II (1942-1950) and IV (1998-2006) by extraordinarily high rates of mass loss (Fig. 2.7 and Table 2.4). The mean specific net balances of each period differ significantly from the values of the entire time series (Student's t test at a significance level of 99%).

The mass loss since 1865 is considerable for all glaciers analyzed. However, there are significant differences. The cumulative mass balance of Griesgletscher is three times greater compared to

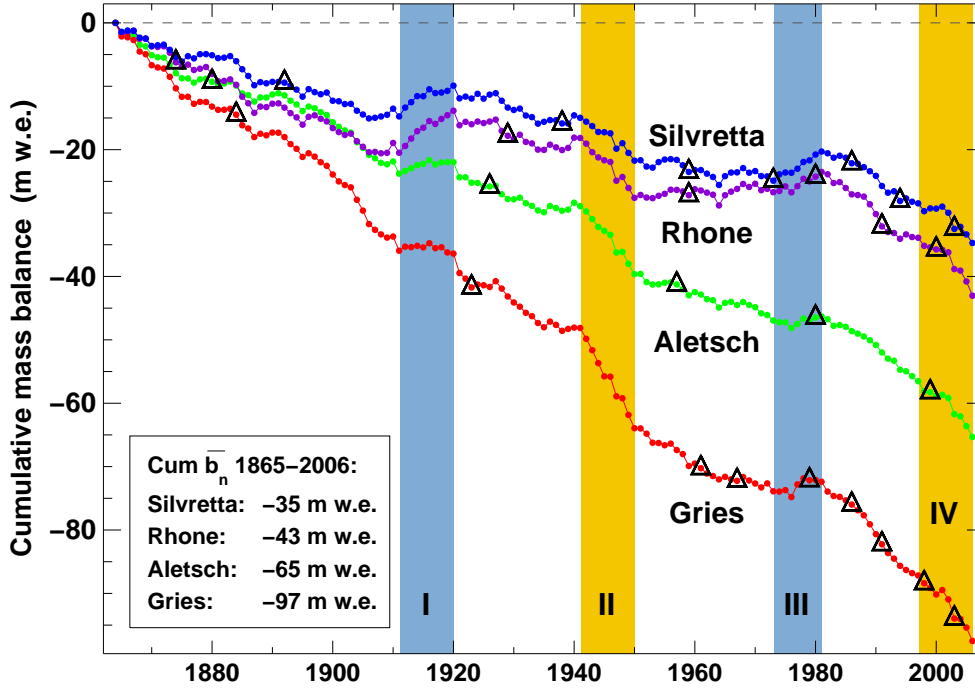


Figure 2.6: Time series of cumulative mean specific net balance ($\overline{\text{Cum } b_n}$) for Aletsch, Rhone, Gries and Silvretta in 1865-2006. Two decadal periods with positive (I, III) and strongly negative mass balances (II, IV) are highlighted. Triangles mark the years when DEMs are available. Note that the model was calibrated so that volume changes obtained from integrating annual mass balances over the periods between consecutive DEMs coincided with those obtained from DEM differencing.

Silvrettagletscher (Fig. 2.6 and Table 2.3). The cumulative mass balance curves show similar behavior during the entire study period. Aletschgletscher, Rhonegletscher and Griesgletscher are located within a distance of 30 km to each other, but their cumulative mass balances differ from each other by a factor of more than 2.

We averaged the mass balance series of the four investigated glaciers in order to investigate their year-to-year variability. Results are presented in Figure 2.7. Whereas winter balances display only minor changes during the last century, summer balances are subject to large fluctuations (Fig. 2.7a). Mean specific net balances in the Periods I and III were slightly positive and led to advances of numerous glacier tongues (Glaciological reports, 1881–2008). The Periods II and

Table 2.3: Calculated glacier mass balance quantities: $\overline{\text{Cum } b_n}$ is the cumulative net mass balance over the period 1865-2006. $\overline{b_n}$, $\overline{b_w}$, $\overline{b_s}$ are the mean specific net, winter and summer balances, db/dz the mass balance gradient in the ablation area and \overline{ELA} the equilibrium line altitude averaged over 1865-2006.

Glacier	$\overline{\text{Cum } b_n}$ (m w.e.)	$\overline{b_n}$	$\overline{b_w}$	$\overline{b_s}$	db/dz (-)	\overline{ELA} (m asl)
		(m w.e. a ⁻¹)				
Aletsch	-65.3	-0.46	1.14	-1.60	-0.0078	3003
Rhone	-43.0	-0.30	1.65	-1.95	-0.0080	2944
Gries	-97.5	-0.69	1.32	-2.01	-0.0088	2937
Silvretta	-34.7	-0.24	1.19	-1.43	-0.0069	2811

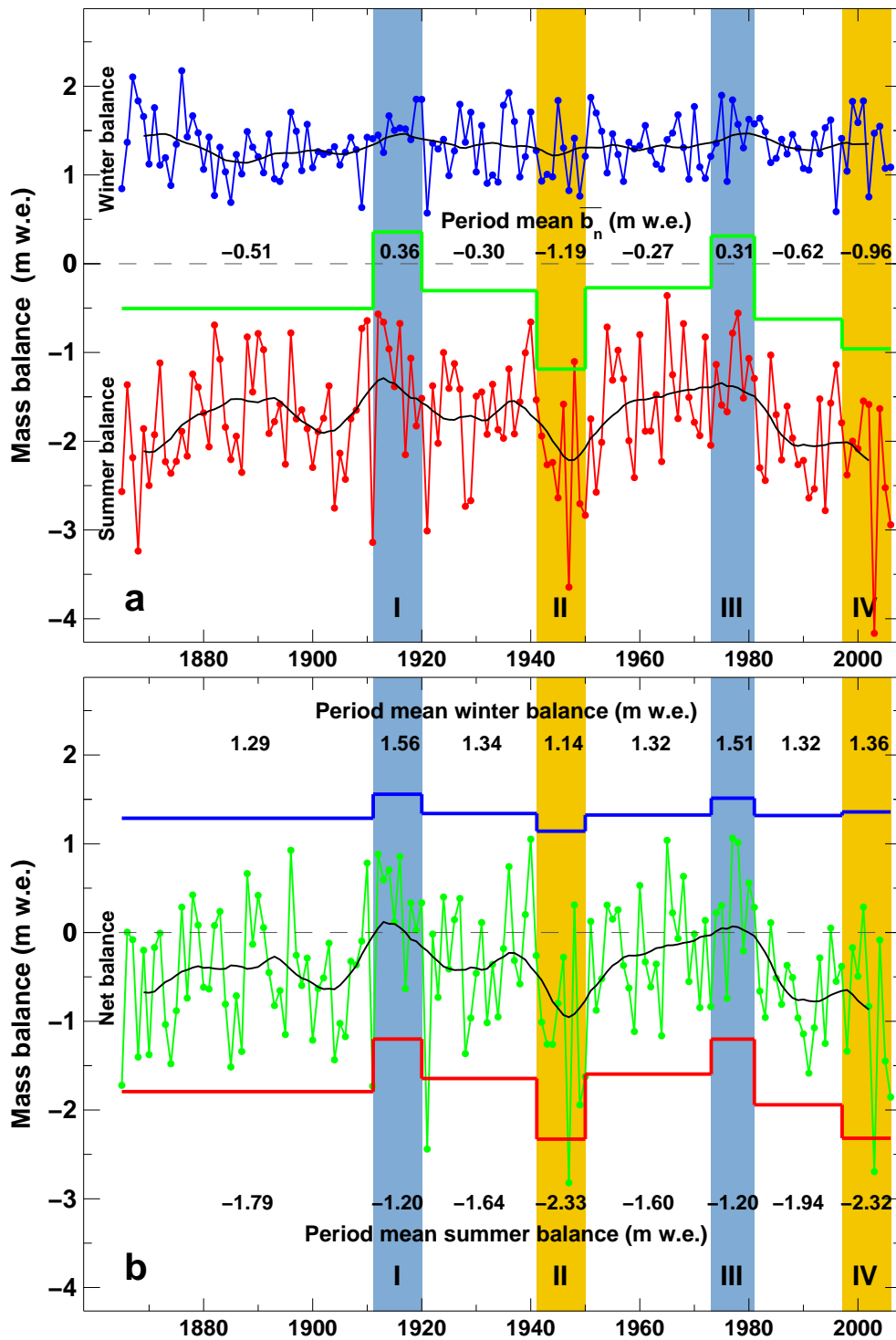


Figure 2.7: (a) Averaged seasonal mass balance series of Aletsch, Rhone, Gries and Silvretta, 1865-2006. Annual data points of winter balance \bar{b}_w (positive) and summer balance \bar{b}_s (negative) are smoothed using a 10-year running mean. The solid line shows the mean net balance in the four highlighted periods and in the interim. (b) Four-glacier average of surface net balances \bar{b}_n . The solid lines and the numbers correspond to the period means of winter and summer balance.

IV are characterized by strongly negative mass balances (Table 2.4). Period IV includes 1998, 2003 and 2006 – the years with the most negative net balances in the Swiss Alps determined within the conventional mass balance programs (Glaciological reports, 1881–2008). However,

Table 2.4: Calculated mean specific mass balances, ELA and AAR averaged over Periods I-IV and the four glaciers

Period	\bar{b}_n	\bar{b}_w	\bar{b}_s	ELA	AAR
	(m w.e. a ⁻¹)			(m a.s.l.)	(%)
I (1912-1920)	0.36	1.56	-1.20	2793	65
II (1942-1950)	-1.19	1.14	-2.33	3076	34
III (1974-1981)	0.31	1.51	-1.20	2857	65
IV (1998-2006)	-0.96	1.36	-2.32	3066	41
1865 - 2006	-0.42	1.33	-1.75	2923	48

the mass balances in the 1940s (Period II) were more negative than those of Period IV (1998-2006). The results indicate that this is due to low winter balances during Period II (Fig. 2.7b). Summer balances in Period IV are equally low as in the 1940s, but are partially compensated by relatively high amounts of winter precipitation. The two periods of mass gain are characterized by only slightly more winter accumulation, but significantly reduced melt in the summer months (Student's t test at a significance level of 99%). Summer balances are only half as negative as in the Periods II and IV (Fig. 2.7). The most negative mass balance year since the end of the Little Ice Age was not the year 2003 with its exceptional European summer heat wave (Schär and others, 2004), but 1947.

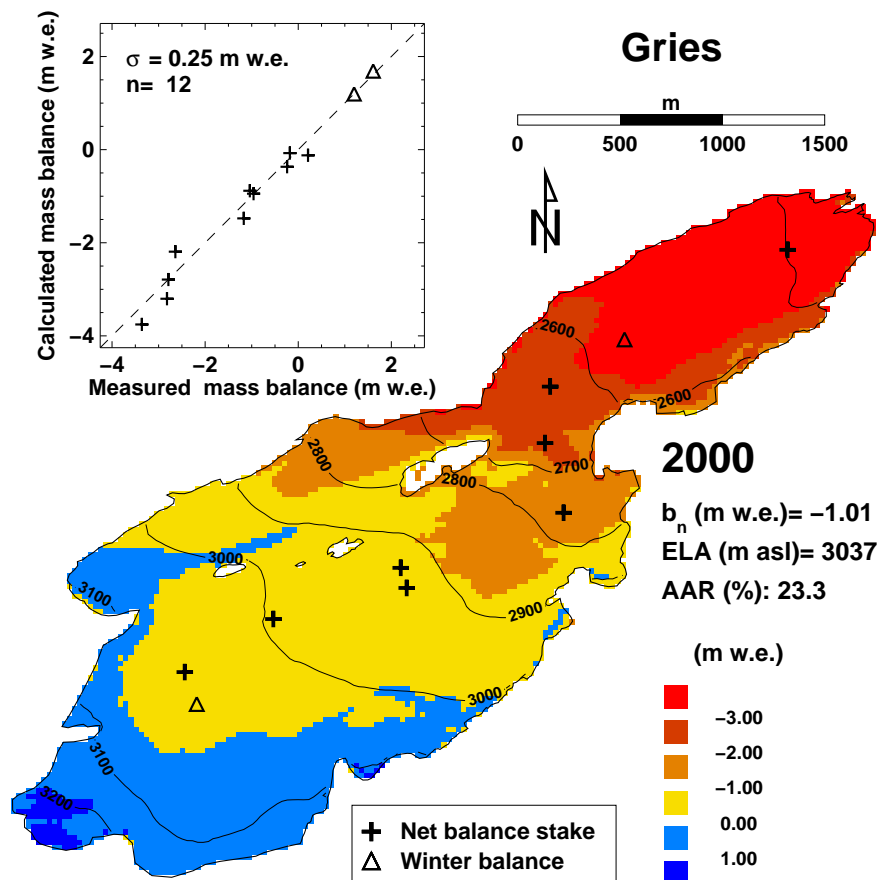


Figure 2.8: Spatial distribution of net balance as calculated for Griesgletscher in 2000. The dashed line follows the equilibrium line which is variable in altitude due to effects of aspect and snowdrift. Comparison of measured and calculated mass balance is shown in the inset.

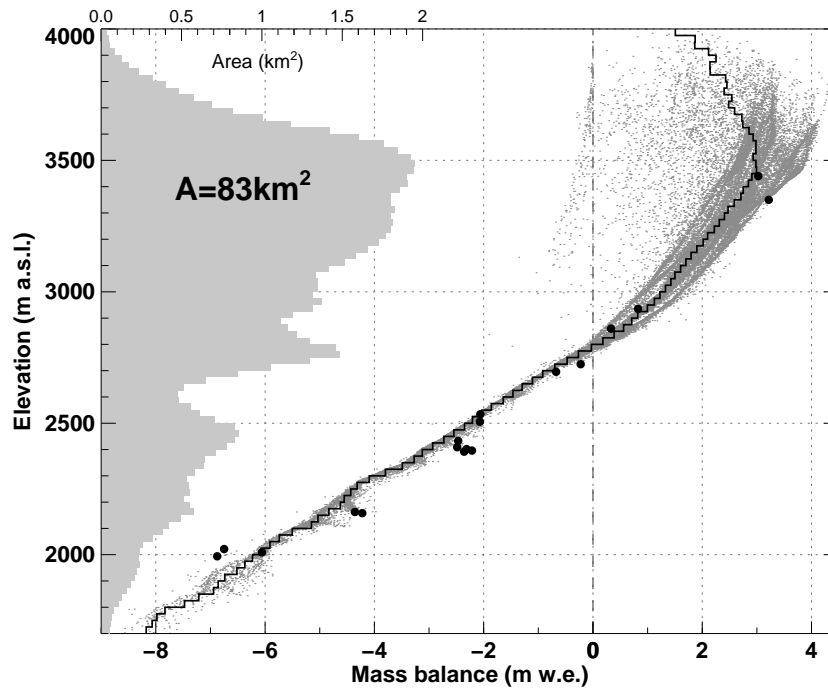


Figure 2.9: Altitudinal distribution of surface net balance as calculated for Grosser Aletschgletscher in 1977. Each small dot corresponds to one grid cell. The step function shows to the mean net balance in elevation bands. Differences in the balance gradient and in the variability of mass balance between the ablation and the accumulation area are evident. Decreasing values of mass balance above 3500 m a.s.l. are due to effects of snowdrift and avalanches. Solid dots show in-situ measurements of net balance. The area-elevation relation of the glacier surface is evaluated in 25 m elevation bands and is plotted in grey.

An important output of the model is the mass balance distribution. While comparison of two successive DEMs indicates only the elevation change at a given point which is determined by both mass balance and ice dynamics, we calculate effective rates of seasonal balance at every grid cell of 25 m (Fig. 2.8). This makes it possible to determine the equilibrium line altitude (ELA), the accumulation area ratio (AAR) and the mass balance gradients directly from the gridded data sets. The model is able to reproduce the higher mass balance gradients in the ablation area. In the accumulation area a larger spread of mass balance is modeled which is due to the effects of snowdrift and avalanches (Fig. 2.9).

The mean specific net balance \bar{b}_n is integrated over the annually updated glacier surface area, although the area cannot adapt immediately after a stepwise climate change. Therefore, the dynamic response time of the glacier influences the values of mean specific mass balance (Jóhannesson and others, 1989). \bar{b}_n is an indicator of the actual mass change and thus useful for hydrological and sea-level change applications (Harrison and others, 2005). It also allows the intercomparison of different glaciers and represents the mass balance quantity usually determined within the framework of mass balance monitoring programs worldwide. The ELA, by contrast, is a quantity that is determined by climate and the aspect of the glacier. It is not influenced by glacier dynamics, extent and hypsometry, and thus reveals a largely unfiltered climatic signal.

The annual variability of ELA is considerable (Fig. 2.10). The lowest and the highest ELA values differ by 600 m. Even decadal mean ELAs show variations of up to 300 m between periods

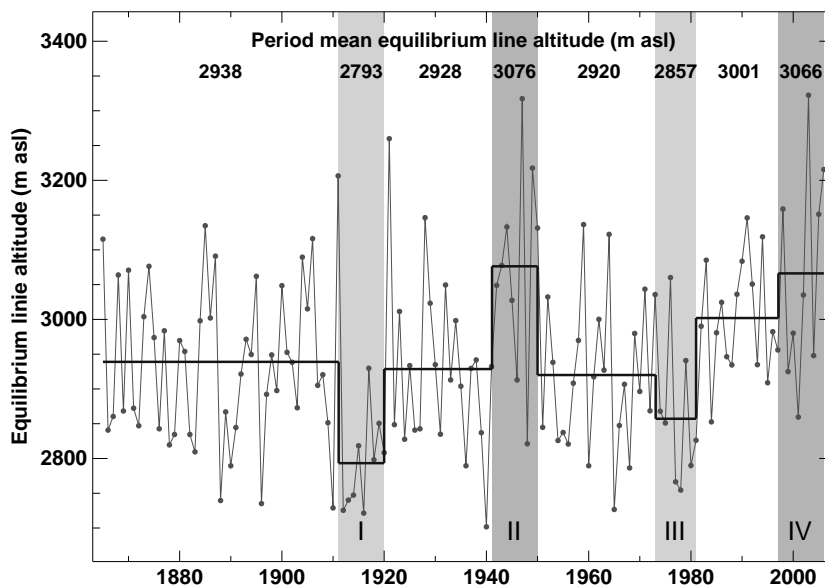


Figure 2.10: Annual ELAs averaged over Aletsch, Rhone, Gries and Silvretta. The solid line corresponds to the mean of ELAs in the Periods I to IV and in the interim.

of positive and negative mass balances. The mean ELA was slightly higher in Period II than in Period IV. This implies that the greater mass losses in the 1940s are a climatic signal. The 1940s were warm and dry, whereas the most recent period is even warmer but wetter (Fig. 2.3). The greater mass losses in Period II seem also to be favored by the larger glacier extents, i.e., lower-reaching glacier tongues. Some adaptation of the glaciers to the changed climatic conditions has taken place in the last century enabling the ice mass to be closer to equilibrium with higher ELAs (Fig. 2.10).

2.5 Discussion

The model approach used in this study is simple and well suited for long time periods. Glacier surface mass balance is determined using temperature and precipitation as input variables, but requires in-situ measurements for calibration. The good agreement of measured and calculated quantities indicate that the method presented has a potential in unifying all available data with modeling. Nevertheless, the applied model has some limitations: All variables of the energy balance other than air temperature are neglected.

For example, albedo variations of the glacier surface as a result of snow metamorphism and dust deposition are insufficiently parameterized. Also variations in cloudiness may influence the melt rates substantially (Pellicciotti and others, 2005) but are neglected in our approach. The relevance of these limitations, however, is larger for short time scales than for decadal periods. In the Swiss Alps, cloudiness was monitored at three high elevation sites for several decades (Auer and 31 others, 2007). The data show no consistent trend or change during the two periods of accelerated glacier recession (Period II and IV) but a general trend towards more cloudiness. We refrain from including more meteorological input variables into the calculations since they are not available for the glacier sites and extrapolation procedures are doubtful. By calibrating a parameter set for each subperiod, constrained by a known ice volume change, the limitations discussed above are minimized. The values of the model parameters show a decreasing trend in

the last decades which could be associated with the observed increase in global radiation after the 1980s (Ohmura and others, 2007).

The uncertainty of the calculated mass balance series depends critically on the quality of the DEM derived ice volume changes. However, since the individual DEMs are independent of each other, the imprecision of the ice volume change estimated as $\pm 5\%$ (Bauder and others, 2007) does not propagate throughout the calculation period. In addition, the entire set of point-based mass balance and runoff measurements is used in the calibration procedure. Random errors in individual point measurements most likely cancel out within a large number of data points.

Our method for determining mass balance time series of high temporal and spatial resolution is based on the meteorological input data. The knowledge about air temperatures in high alpine environments is relatively good, whereas little is known about the precipitation sum and its spatio-temporal distribution. Gridded data sets such as PRISM are known to have significant biases above 2500 m a.s.l. (Schwarb, 2000; Machguth and others, 2006). This is due to the lack of reliable measurements of precipitation in high mountain terrain.

Glaciers serve as precipitation gauges and could help to reduce this bias. The quality of the precipitation time series is assessed by comparison of the winter balance time series of individual stakes and the meteorological input of the model. Data of totalisators, precipitation gauges in high mountain areas, sampling annual to semi-annual precipitation sums, are available for some sites. However, they were rejected due to an inability to monitor data quality and measurement errors. The data set of point-based measurements of winter balance provides a possibility to enhance the knowledge about precipitation in areas relevant for glacier existence. In our model approach this is done in an iterative way by varying the precipitation correction factor c_{prec} until the model results are able to explain the measured winter balances. The precipitation of PRISM needs to be corrected by a factor of 1.3 for Rhonegletscher and by as much as 2.1 for Silvrettagletscher. Hence, the in-situ measurements contribute to reducing the uncertainty in the precipitation data. PRISM yields good estimates of the precipitation sum for Griesgletscher and for Grosser Aletschgletscher, however, it has to be corrected in the uppermost parts of the catchment for the latter.

In order to evaluate the transferability of our approach to glaciers where only some of the independent field data types are available, we consider three cases of field data availability and their effect on the quality of the mass balance determination: (1) no field data, (2) only volume changes ΔV , (3) ΔV and net balance b_n , but no b_w data.

1. No field data: The method is doomed to fail in this case. The melt parameters of temperature-index models are site-specific and must be calibrated. They are not transferable within a sufficient range of confidence between individual glaciers. If it is possible, however, to calibrate the parameters during a number of years for an individual glacier, we may expect them to be valid for an extended period without data. This is what we assume for the years before the first DEM.
2. ΔV : If only field data of ΔV are available the model may be tuned to reproduce the observed decadal scale volume changes but for the wrong physical reasons. For example, overestimation of precipitation might be compensated for by overestimation of melt. There is no possibility to validate the distribution of the balance terms and their seasonal values because both accumulation and melt parameters can not be constrained unambiguously.

3. ΔV , b_n : The spatial distribution of net balance can be validated and fitted to the measurements (Fig. 2.4). However, as for case 2 there is the risk of errors in winter and summer balances canceling out each other. We compared the mass balance series calibrated using only field data of ΔV and b_n to the reference time series obtained by considering all available measurements. The residuals of the mean specific net balance series show a standard deviation of $\sigma_d=0.06$ m w.e. and the winter balances display a mean absolute deviation of $\Delta \overline{b_w}=0.12$ m w.e. from the reference.

We conducted a sensitivity test concerning the number of available in-situ measurements. The data sets of b_n , b_w and Q_a were divided randomly into two groups of identical size. We obtained the almost identical results from the model calibration when applying either the first or the second of the reduced data sets.

The field data series may be of irregular temporal and spatial coverage to be valuable to the calibration procedure. The quality of the seasonal mass balance series and their spatial distribution increases with the available types of field data. A large number of measurements within one class of calibration data and in particular its extensive temporal coverage leads to a high statistical weight of the data set.

The differences in cumulative net mass balances over a period of one and a half century can be considerable for neighboring glaciers (Fig. 2.6 and Table 2.3). This was already observed for other Alpine glaciers (Kuhn and others, 1985). The spatial representativity of single glacier mass balance records must be assessed carefully as they may be biased by, for example, ice dynamics and glacier surface geometry. A mean specific mass balance value determined for one glacier might not be representative for a whole mountain range. Cumulative mass balance series may diverge of various reasons: e.g. uneven changes in the local climate since 1865, different glacier hypsometries and topographic effects, different mass balance gradients, or the dynamic reaction of the ice mass. The relative contributions of these effects are not easy to determine and beyond the scope of this paper.

Positive albedo feedback mechanisms may be another cause for the differential behavior of the investigated glaciers. Due to persistently negative mass balances, the firn line retreats, exposing ice surfaces with lower albedo. The albedo of the bare ice surface may change over time leading to further melt enhancement and increasing mass balance gradients. Our simple model approach is capable only of describing some of the albedo feedback mechanisms. More complex processes cannot be analyzed. The albedo feedback may be better able to explain the considerable mass losses in the 1940s that occurred in spite of lower summer temperatures than those experienced during the last two decades (Fig. 2.3). Low winter accumulation and the succession of several extremely negative mass balance years caused the firn line to rise considerably, which reduced the albedo of the glacier surface and led to high melt rates.

2.6 Conclusion

We present a method to resolve decadal to semicentennial ice volume changes obtained from repeated DEMs of the glacier surface to seasonal mass balance time series and to provide the spatial distribution of balance terms. The mass balance model requires only temperature and precipitation data which are widely available in the Alpine region as input. Our method incorporates all types of available in-situ measurements in order to determine and analyze homogenized

mass balance time series in seasonal resolution over centennial time scales tied directly to measured quantities. We are able to merge inhomogeneous or incomplete sets of field data covering different periods in varying density into time series of mean specific mass balances. Our approach allows direct comparison of the results from different glaciers, since the periods of mass balance determination are exactly the same for all glaciers.

We demonstrate that the mass balance evolution of four glaciers in the Swiss Alps has undergone significant fluctuations. Two decadal periods of mass gains are found, which are due to less negative summer balances. The general trend since 1865 is strongly negative, however, displaying large differences between neighboring glaciers. The most negative mass balances occurred in the 1940s. This is due to extraordinarily low winter accumulation and high summer temperatures. In future, we plan to extend the spatial coverage of the seasonal mass balance series to more than 20 glaciers in Switzerland in order to shed light on regional differences in high Alpine mass balance evolution. Our results emphasize the need to continue in-situ mass balance measurements in seasonal resolution over long periods. We provide a promising method for combining these point measurements with geodetic observations and mass balance modeling to obtain mass balance quantities with high spatial and temporal resolution and extend measured mass balance series back in time.

Acknowledgments

This work is supported by ETH Research Grant TH-17 06-1. Our results contribute to efforts in glacier monitoring. The weather data were recorded by MeteoSchweiz. The Federal Office for the Environment (BAFU) provided the runoff data. We thank Kraftwerke Aegina und Maggia AG for their support of the measurements on Griesgletscher. The immense contribution to mass balance measuring of previous researchers at the VAW is gratefully acknowledged. Swisstopo was responsible for the aerial photograph surveys. B. Nedela digitized old topographic maps and H. Bösch established DEMs from aerial photographs. We thank C. Frei for providing the PRISM data set and for helpful discussions. L.A. Rasmussen made valuable remarks on an earlier version of the manuscript. S. Braun-Clarke edited the English. The constructive comments of the scientific editor M. Church, the associate editor G. Hamilton, reviews by B. Brock and an anonymous reviewer substantially improved the clarity of the manuscript.

Chapter 3

Twentieth century climate change inferred from four long-term point observations of seasonal mass balance

MATTHIAS HUSS AND ANDREAS BAUDER

Versuchsanstalt für Wasserbau, Hydrologie und Glaziologie (VAW), ETH Zürich, 8092 Zürich, Switzerland

In press, *Annals of Glaciology*

Citation: Huss, M. and A. Bauder (in press). Twentieth century climate change inferred from four long-term point observations of seasonal mass balance. *Annals of Glaciology*, 50.

ABSTRACT: Four long-term time series of seasonal mass balance observations, all starting in 1914, have been compiled for two stakes on Claridenfirn and one stake on Grosser Aletschgletscher and Silvrettagletscher, Switzerland. These data represent the longest records of mass balance worldwide. A mass balance model based on the temperature index approach is used to correct field data for varying observation dates and data gaps and to separate accumulation and ablation. The homogenized continuous 93-year time series cover most of the 20th century and enable to investigate temporal, regional and altitudinal variability in mass balance and changes in the climatic forcing on glaciers. A high altitude site shows summer balance trends opposite to those at three stakes located near the equilibrium line. Since 1975 melt rates have increased by 10% per decade. Two periods of enhanced climatic forcing are detected, 1943-1953 and 1987-2007. The energy consumed for melt was higher in the 1940s in spite of lower air temperatures than during the last two decades. We find evidence for a change in the glacier surface heat budget having important implications for the long-term stability of degree-day factors in empirical temperature index modelling.

3.1 Introduction

Changes in glacier surface mass balance are considered to be a sensitive indicator for climatic variations (e.g. Vincent and others, 2004; Kaser and others, 2006). Point observations at fixed locations directly reflect climatic conditions and are not biased by uncertain spatial interpolation of mass balance or the change in glacier surface area (Ohmura and others, 2007). Glacier surface mass balance in mid latitudes is mainly determined by two processes: solid precipitation (accumulation) dominating the winter balance and snow- or icemelt (ablation) dominating the summer balance. Thus, seasonal mass balance components most clearly reveal the effect of the climatic forcing on glaciers (Vincent and others, 2004). Accumulation on glaciers is generally regarded as the best measure for precipitation in high mountain regions.

The direct observation of seasonal mass balance is laborious and requires two field surveys: one in spring when the maximum of snowcover is reached and one in late summer at the end of the melting season. In Switzerland, mass balance measurements were started in the 1910s on Claridenfirn, Grosser Aletschgletscher and Silvrettagletscher (Aellen, 1996). Seasonal observations at these locations were continued until today with almost no disruptions and represent the longest direct measurements of mass balance worldwide.

Müller and Kappenberger (1991) compiled a complete documentation of the measurements at the two stakes on Claridenfirn and reconstructed missing data using regression methods. The Claridenfirn data have been repeatedly analyzed (Müller-Lemans and others, 1995; Vincent and others, 2004; Ohmura and others, 2007) and turned out to be of great value for inferring climatic fluctuations at high altitudes in the Alps in the 20th century. The two comparable time series of Silvrettagletscher and Aletschgletscher, however, have not thus far been

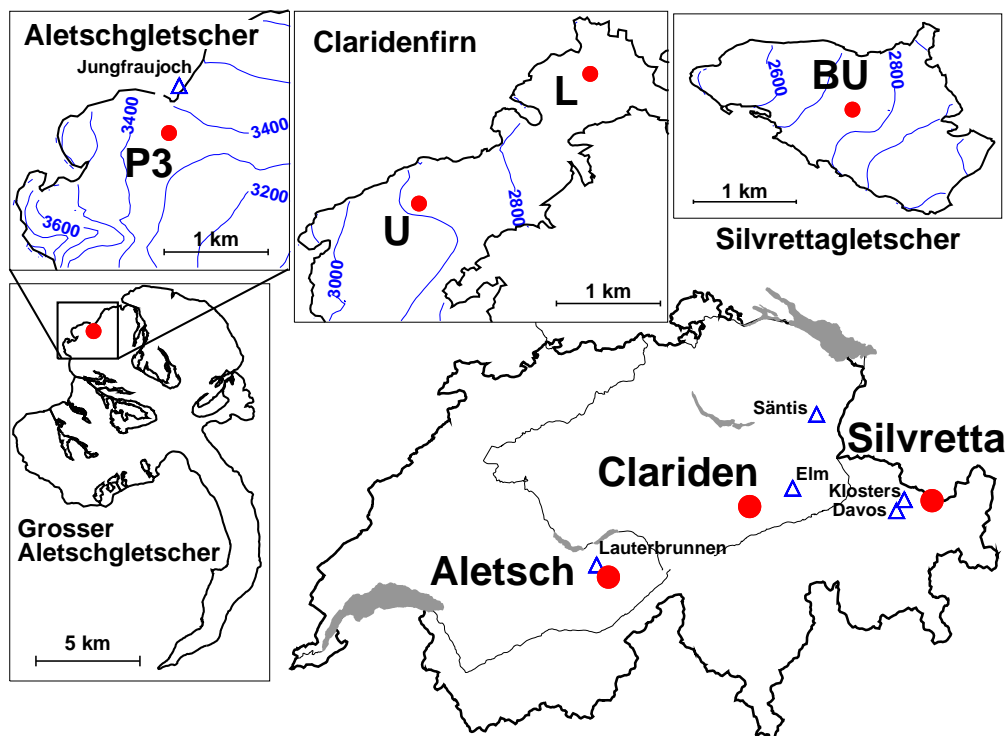


Figure 3.1: Location of the study sites in Switzerland. Weather stations of MeteoSchweiz used in this study are indicated with triangles (Table 3.1). The local topographic setting of each stake is shown in insets (a)-(d). The contour interval is 100 m.

considered in scientific discussions.

In this study we present four 93-year time series of seasonal point-based mass balance. The series are homogenized using a mass balance model based on the temperature index approach and now cover annual time periods of equal length. Accumulation and ablation components are separated enabling the calculation of the total energy consumed for melt. We aim at analyzing trends and regional differences in the context of 20th century climatic forcing on Alpine glaciers. Changes in the heat budget at four high alpine sites are investigated and the long-term stability of degree-day factors in empirical temperature-index modelling is assessed.

3.2 Study sites and field data

With the aim of better understanding the precipitation conditions in high mountains, snow accumulation and mass balance observations have been started at two sites on Claridenfirn in 1914 and 1915, at one site on Silvrettagletscher in 1915, and on Aletschgletscher in 1918 (Fig. 3.1). All series were continued until today (Table 3.1). The measurement sites are located at or above the long-term equilibrium line in locally flat terrain. Grosser Aletschgletscher is the largest ice mass in the Alps and borders to the main northern Alpine crest. Claridenfirn and Silvrettagletscher are smaller mountain glaciers situated at the northern flank of the Swiss Alps.

The monitoring program is consistent at all sites (Firnberichte, 1914–1978; Glaciological reports, 1881–2008). The winter field survey is mostly performed between April and June and the sites are visited again in September. Readings of the snow depth are complemented by density information, which is, however, not systematically reported before 1960. Snow depth is evaluated using three independent methods: (i) differences in snow depth from readings at the stake, (ii) snow probings and (iii) observations in snow pits or by drillings to a marked horizon including snow density measurements. Often results from more than one of these procedures are documented. The stake marks the measurement site and is annually moved back to the initial position. In some years the data sets are incomplete (Fig. 3.2): stakes were lost due to high accumulation, and in a few cases a whole campaign did not take place. The location of stake Silvretta BU was moved about 200 m to the north in 1987 with

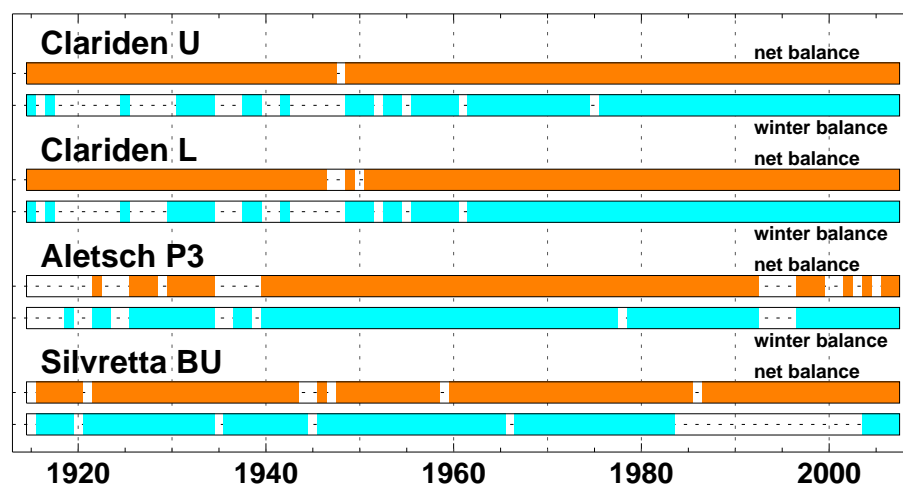


Figure 3.2: Seasonal observations of point-based net and winter balance since 1914. The bars are not shaded in years with missing data.

Table 3.1: *Measurement sites and data characteristics. The elevation of the stakes corresponds to the year 2003. The number of missing winter and net balance observations refers to the entire study period (1914-2007).*

Stake	Glacier	Elevation (m a.s.l.)	Period	Missing balance values	
				net	winter
U	Claridenfirn	2894	1915-2007	1	28
L	Claridenfirn	2679	1914-2007	3	27
P3	Gr. Aletschgletscher	3338	1918-2007	24	16
BU	Silvrettagletscher	2732	1915-2007	7	25

	Weather stations		Data source
	Temperature	Precipitation	
U	Säntis	Elm	[1], [2], [3]
L	Säntis	Elm	[1], [2], [3]
P3	Jungfrauoch	Lauterbrunnen	[1], [2]
BU	Davos	Davos, Klosters	[1], [2]

[1]: Firnberichte (1914–1978); [2]: Glaciological reports (1881–2008);

[3]: Müller and Kappenberger (1991)

no significant change in elevation. Until 1984 the data for the stakes Clariden U and L are taken from Müller and Kappenberger (1991). For our analysis we discarded reconstructed data points. The mass balance data of Aletsch P3 and Silvretta BU are digitized from annual reports (Firnberichte, 1914–1978; Glaciological reports, 1881–2008).

We also make use of topographical information and weather data (Table 3.1). For each of the three investigated glaciers 4 to 8 digital elevation models (DEMs) exist covering the last century (Bauder and others, 2007). This allows the surface elevation change at the stake sites to be inferred. From the network of the official Swiss weather service (MeteoSchweiz) we use time series of daily air temperature recorded at Säntis (2490 m a.s.l., 54 km from Clariden), Jungfrauoch (3580 m a.s.l., 500 m from stake site), and at Davos (1590 m a.s.l., 18 km from Silvretta). The temperature records of Säntis and Davos have been corrected for biases due changing measurement techniques or station relocation (Begert and others, 2005). Time series of daily precipitation are taken from Elm (965 m a.s.l., 21 km from Clariden), Lauterbrunnen (820 m a.s.l., 8 km from Aletsch), Davos and since 1961 Klosters (1200 m a.s.l., 13 km from Silvretta) (Fig. 3.1).

3.3 Methods

Time series homogenization

In order to compare the time series, homogenization of the measurements is required in order to account for inconsistency, systematic errors and gaps in the reported observations (Fig. 3.2). The measurements were taken at arbitrary dates. Year-to-year differences of several months in the date of the field surveys have a considerable impact on the representativeness of the seasonal mass balance results (Huss and others, in press). By applying a mass balance model at a daily

time scale the observations are projected to common periods with fixed dates. Net balance b_n given in m water equivalent (w.e.) is determined in the hydrological year (Oct. 1 - Sept. 30). We subdivided the year into a winter period (Oct. 1 - April 30) for determination of winter balance b_w and summer period (May 1 - Sept. 30) for summer balance b_s . According to Meier (1962) we term mass balance quantities at a single point 'specific' mass balance. The model further allows us to handle incomplete years, to close gaps in a consistent way and to separate the total annual accumulation c_a from the total annual ablation a_a . In the homogenization procedure, measured weather data are used to resolve the seasonal mass balance measurements at a daily scale.

Mass balance model

We calculate daily specific mass balance using a temperature index melt and accumulation model (Hock, 1999). Temperature index models are based on a linear relation between melt rate and positive air temperature (Ohmura, 2001). In our approach the degree-day factors are varied as a function of potential direct solar radiation in order to account for the effects of slope, aspect and shading (Hock, 1999). Daily temperature and precipitation are required as input data. Surface melt rates M (m d^{-1}) at the stake site are calculated by:

$$M = \begin{cases} (f_M + r_{\text{snow/firn}} I) T & : T > 0 \\ 0 & : T \leq 0 \end{cases} \quad (3.1)$$

where f_M ($\text{m d}^{-1} \text{ } ^\circ\text{C}^{-1}$) denotes a melt factor, $r_{\text{snow/firn}}$ ($\text{m}^3 \text{ W}^{-1} \text{ d}^{-1} \text{ } ^\circ\text{C}^{-1}$) are radiation factors for snow and firn surfaces and I (W m^{-2}) is the potential direct radiation. Air temperature T ($^\circ\text{C}$) at the stake is calculated using constant monthly temperature lapse rates determined by comparing several nearby weather stations. Annually updated surface elevation of the sites is obtained by linearly interpolating between two successive DEMs. The lapse rates vary between -4°C km^{-1} (Jan.) and $-6.5^\circ\text{C km}^{-1}$ (June). Accumulation is computed using the daily precipitation sums at the weather station multiplied with a correction factor c_{prec} . A threshold temperature of 1.5°C distinguishes snow from rainfall. Using calculated melt and accumulation the snow water equivalent S (m w.e.) at the stake site is updated daily. Ablation due to sublimation can occur on Alpine glaciers (Lang and others, 1977), but is of minor importance compared to melt. Sublimation is not included explicitly in the model. However, it is captured by the in situ mass balance measurements.

Model calibration

The model calibration is an automated iterative procedure that is repeated for every year of the study period. The calculated mass balance is matched with the two annual direct observations (b_w , b_n) aiming at an exact fit. In order to avoid an under-determined system the free parameters of the mass balance model are reduced to two: (i) The correction factor for precipitation c_{prec} and (ii) one melt parameter. f_M , $r_{\text{snow/firn}}$ (Eq. 3.1) are assumed to be directly proportional to each other. With $r_{\text{snow}} = c_s f_M$ and $r_{\text{firn}} = c_f f_M$ we reformulate the degree-day factor $DDF(I, c_{s/f}) = f_M(1 + c_{s/f} I)$ using Equation 3.1. $DDF(I, c_{s/f})$ is a function of the potential radiation I and the condition of the glacier surface. f_M is constant in the course of the year and is used for tuning. The simulated snow water equivalent S indicates whether the proportionality factor for snow ($S > 0$) or for firn c_f ($S = 0$) is used. c_s and c_f are taken from studies using the

Table 3.2: Mean degree-day factor for snow $\overline{DDF_{\text{snow}}(\bar{T})}$ ($\text{mm d}^{-1} \text{C}^{-1}$) and mean precipitation correction factor $\overline{c_{\text{prec}}}$ (-) in 1914-2007 and standard deviations σ of annual parameter values.

Stake	$\overline{DDF_{\text{snow}}(\bar{T})}$	σ_{DDF}	$\overline{c_{\text{prec}}}$	$\sigma_{c_{\text{prec}}}$
U	3.73	0.84	2.67	0.37
L	3.93	0.83	2.68	0.39
P3	3.97	0.99	3.10	0.64
BU	2.96	0.62	2.80	0.44

same temperature index model (e.g. Huss and others, 2007a) and have values of $c_s=0.035$ and $c_f=0.050$ (both in $\text{W}^{-1} \text{m}^2$). They represent albedo variations due to different surface types.

Basically, measured winter balance is used to obtain a first approximation of c_{prec} and summer balance allows us to estimate f_M . The mass balance model is calibrated in three separate steps for each year individually: (1) c_{prec} is tuned so that the observed snow water equivalent at the date of the winter survey is matched by the model. (2) The model is run between the exact dates of the two successive late summer surveys using c_{prec} calibrated in (1). The melt factor f_M is varied so that calculated specific mass balance matches the net balance measurement.

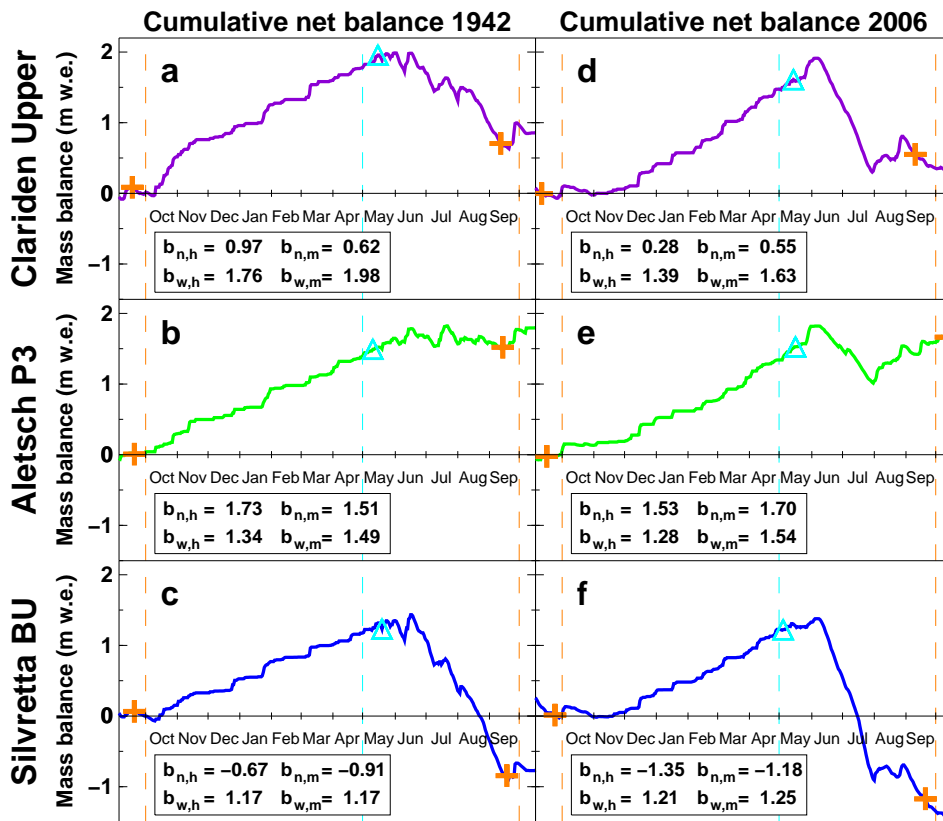


Figure 3.3: Cumulative daily mass balance in two arbitrarily selected years: (a-c) 1942, (d-f) 2006. Results of the stakes Clariden U, Aletsch P3 and Silvretta BU are shown. The winter balance measurement is indicated by a triangle, net balance measurements by crosses. Dashed vertical lines refer to fixed date time periods of homogenized mass balance. Comparison of homogenized ($b_{n,h}$, $b_{w,h}$) and measured mass balance quantities ($b_{n,m}$, $b_{w,m}$) in m w.e. is shown in the boxes.

(3) As the accumulation period is rarely free of melt and the ablation period rarely free of solid precipitation, respectively, the previously determined parameters c_{prec} and f_{M} represent an initial guess and need to be recalibrated in a final step iteratively in order to reproduce both the winter and net balance measurements within <0.05 m w.e. Thus, an individual parameter set for each year with a complete field data (b_{w} , b_{n}) is obtained. During years with incomplete data sets (Fig. 3.2) mean values of c_{prec} and f_{M} calibrated for all complete years are used (Table 3.2).

Examples for the calculated daily mass balance time series during an annual cycle are presented in Figure 3.3. The calculated mass balance curve matches the direct observations of winter and net balance and allows mass balance for arbitrary periods to be evaluated. Measured ($b_{\text{n,m}}$, $b_{\text{w,m}}$) and homogenized ($b_{\text{n,h}}$, $b_{\text{w,h}}$) mass balance quantities may vary considerably as a result of the differences between the effective observation dates and fixed evaluation periods (see boxes in Fig. 3.3).

Trend analysis

In order to analyze trends in the mass balance time series we apply the non-parametric Mann-Kendall (MK) test, which is widely used in hydrological applications for trend detection (e.g. Helsel and Hirsch, 1992). This rank-based procedure is especially suitable for non-normally distributed data and is robust against outliers and data gaps. The MK-test yields a trend test statistic that allows to reject the null hypothesis at a certain significance level (see Birsan and others, 2005, for details). The slope of trends significant at the 99% level of the MK-test is estimated using the Theil-Sen method, which is suitable for nearly linear trends and is little affected by non-normal data and outliers (Helsel and Hirsch, 1992).

3.4 Results

The mass balance regime at the four investigated sites shows significant differences (Fig. 3.3). Whereas high winter accumulation is observed at Clariden U and L, Silvretta BU exhibits a drier climate (Table 3.3). Aletsch P3 is characterized by a regime with positive summer balances, whereas the stakes U, L and BU suffer net ablation in the summer season. Clariden L and Silvretta BU are located near the long-term equilibrium line, Clariden U and Aletsch P3 are in the accumulation area in all years (Table 3.3).

Direct comparison of point balances is complicated by the different mass balance regimes. We subtract the 1914-2007 average of each time series from annual values (Table 3.3). Thus, time

Table 3.3: *Measurement site characteristics. Net balance $\overline{b_{\text{n}}}$, winter $\overline{b_{\text{w}}}$ and summer balance $\overline{b_{\text{s}}}$, total annual accumulation $\overline{c_{\text{a}}}$ and ablation $\overline{a_{\text{a}}}$ represent 1914-2007 averages in m w.e. a^{-1} .*

Stake	$\overline{b_{\text{n}}}$	$\overline{b_{\text{w}}}$	$\overline{b_{\text{s}}}$	$\overline{c_{\text{a}}}$	$\overline{a_{\text{a}}}$
U	1.31	2.00	-0.69	3.39	-2.08
L	0.32	1.93	-1.61	3.19	-2.87
P3	2.18	1.73	0.45	3.13	-0.95
BU	-0.10	1.37	-1.47	2.32	-2.42

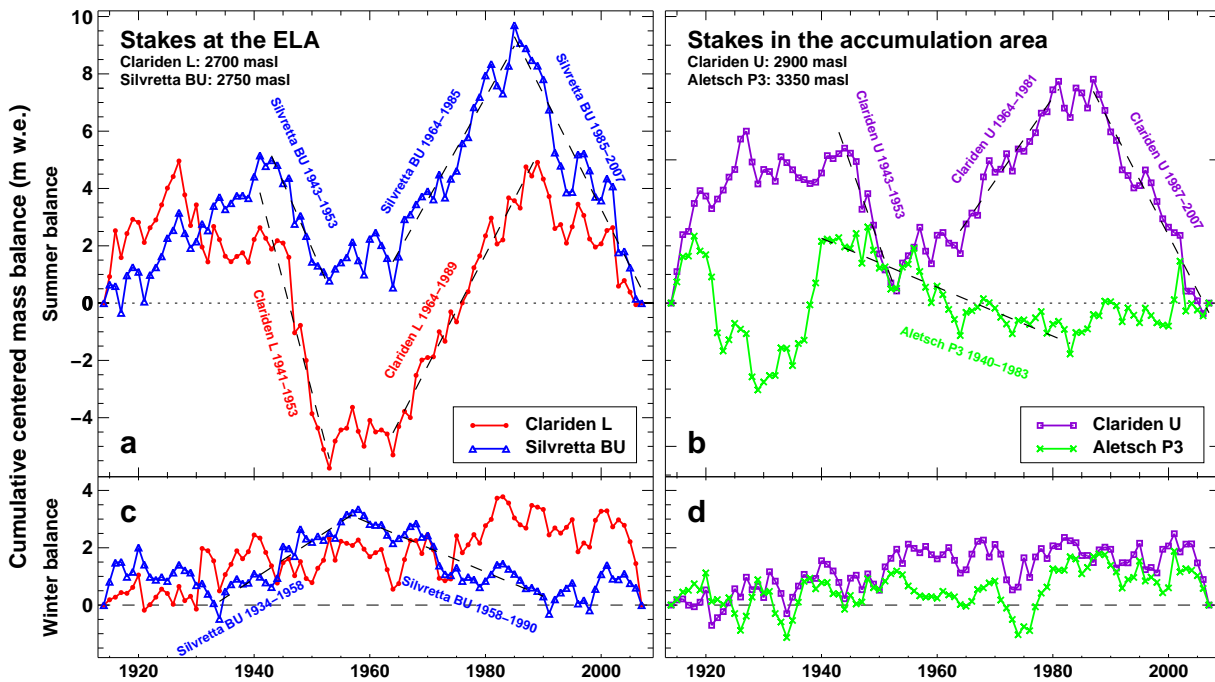


Figure 3.4: Cumulative centered time series of summer and winter balance for (a,c) Clariden L and Silvretta BU and (b,d) Clariden U and Aletsch P3. The scales for summer and winter balance are the same. Dominant trends are indicated by dashed lines and corresponding text lines. For a complete trend analysis see Figure 3.5.

series of the deviation from the long-term average are obtained. This quantity is referred to as 'centered' mass balance. Positive (negative) centered mass balances have to be interpreted as above (below) the stake-average of the considered quantity in the period 1914 to 2007. Centered mass balances allow the analysis of mass balance fluctuations, which are separated from the mass balance regime at the study site.

Significant regional and altitudinal differences between the individual sites are evident in the cumulative centered balance curves (Fig. 3.4). At all stakes the temporal variation in winter balance is much smaller than in summer balance. This is consistent with previous studies (Vincent and others, 2004; Huss and others, 2008a) and underlines that glacier recession in the 20th century is mainly driven by increased melt in the summer months. Clariden L exhibits notably low centered summer balances in the 1940s, whereas the most important decrease at Silvretta BU has taken place since the mid 1980s (Fig. 3.4a). The stakes located below 3000 m a.s.l. (U, L, BU) show positive trends in the cumulative centered summer balances between the mid 1960s and the mid 1980s. For the Aletsch P3, however, there is an opposite trend at the same time. This is not due to anomalously high winter balances at Aletsch P3, but reveals altitudinal differences in the reaction of summer balances to 20th century climate warming on summer balances (Fig. 3.4). A similar observation in the western Alps is reported by Vincent and others (2007).

The cumulative centered time series of summer and winter balance (Fig. 3.4) were systematically analyzed in terms of prevailing trends. Trends over periods with a length of more than 10 years were detected visually between break points in the time series. Between two and four long-term trends in both summer and winter balance significant at the 99% level according to the MK-test could be identified for each site (Fig. 3.5). Negative trends in the cumulative centered summer balance occurred between 1943 and 1953 and between 1987 and 2007, positive

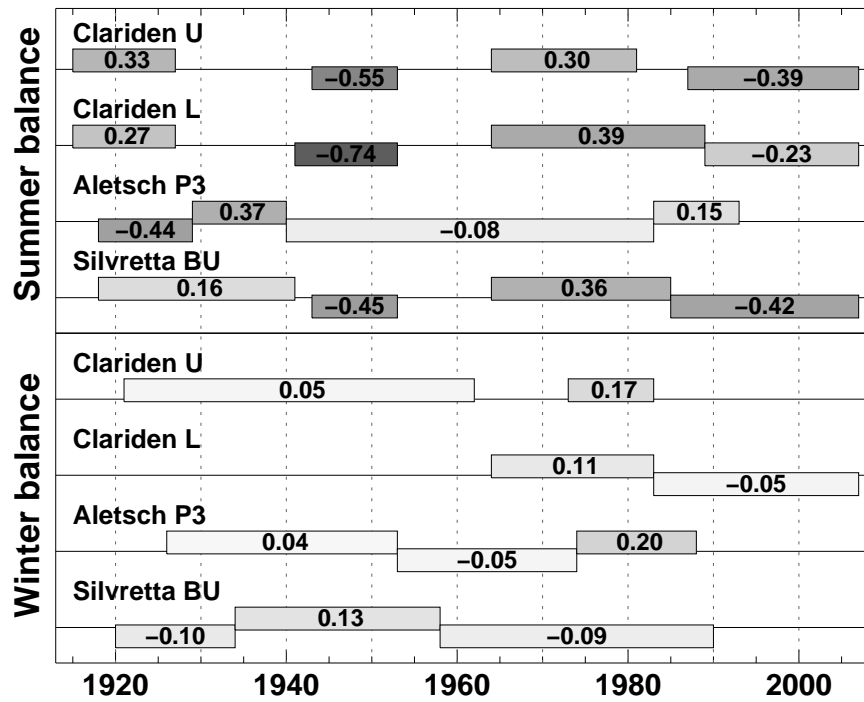


Figure 3.5: Dominant trends in cumulative centered summer and winter balance for the four stakes. The bars indicate the period and the sign of individual trends, the numbers give the slope of the trend (in m w.e. a⁻¹). 'Strong' trends (steep slope) have a darker shading.

trends are found between 1964 and 1985. However, Aletsch P3 exhibits completely different periods of dominant trends in summer and in winter (Fig. 3.4). The lengths of the trends are similar for Silvretta BU, Clariden U and L, but are rarely the same. The trends in the cumulative centered winter balance generally have smaller slopes and are even less consistent than the summer balance trends (Fig. 3.5).

We divided the study period into seven sub-periods (I-VII) of 13 years (Fig. 3.6). This arbitrary subdivision of the data set corresponds best to the periods of dominating trends (Fig. 3.5). Three sub-periods (II, IV, V) are controlled by positive centered summer balances and three periods (III, VI, VII) with predominantly negative values are found. The sign of the centered summer balance at Aletsch P3, however, is opposite in sub-periods IV-VII (Fig. 3.6). The summer balance at high altitudes is significantly different from that at the long-term equilibrium line. The anomalously low summer balances of Clariden L in Period III may be related to a complete wastage of the firn coverage in the succession of warm years in the 1940s, which caused a positive feedback of surface albedo on the summer ablation rates and is responsible for the large difference compared to Clariden U (Fig. 3.6). Above-average winter accumulation probably reduced the impact of the same process at Silvretta BU. Winter balances are below the long-term average in Periods VI and VII (Fig. 3.6b). This is partly due to a prolongation of the melting season that successively extends into the period used for the determination of winter balance. Our model results indicate significant trends of about two days per decade towards a longer melting season for all stakes except Aletsch P3. The trends are even steeper for the last two decades. The increase in days with melt occurring at the equilibrium line is attributed to higher air temperatures in early summer and late fall and leads to a longer exposure time of low albedo surfaces with enhanced melt rates.

We evaluated the annual fraction of solid precipitation compared to total precipitation

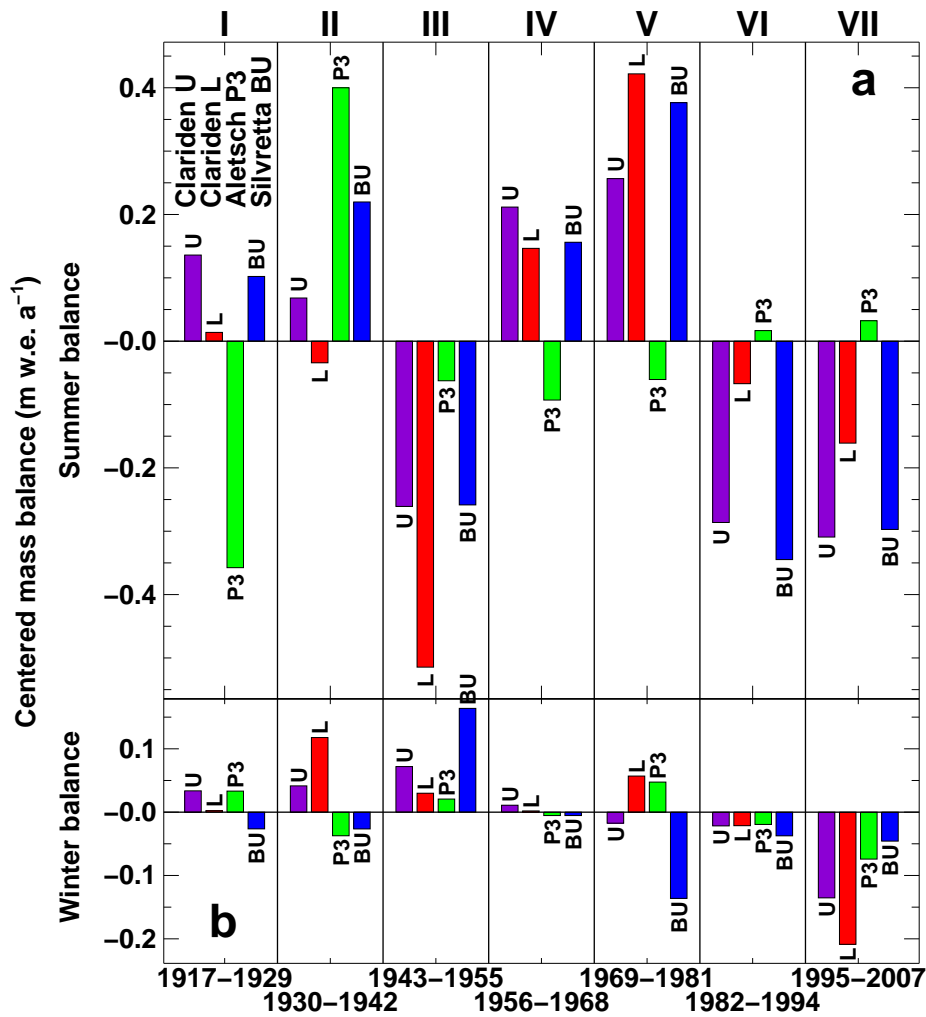


Figure 3.6: Mean centered summer and winter balances of the four stakes in seven 13-year periods.

(Fig. 3.7a). This variable was chosen to further highlight the potential impact of temperature change on accumulation. On average 79% of the annual precipitation occurs as snow at the stake sites. After a culmination around 1970, a significant decrease of the solid precipitation fraction is found. This implies that a considerable amount of potential accumulation is lost at elevations at or above the equilibrium line due to positive air temperatures during snow fall events (assuming no refreezing in the snow pack). This positive feedback effect (increasing temperature, decreasing solid precipitation fraction) has the potential to considerably accelerate glacier wastage.

The total annual ablation a_a at the site calculated based on field data and model is used to determine the corresponding energy consumed for melt E_m . We consider this quantity to be an excellent indicator for the climatic forcing on glaciers. a_a is converted into E_m (W m^{-2}) using the latent heat of fusion of 334000 J kg^{-1} . On average between 10 W m^{-2} (P3) and 30 W m^{-2} (L) were consumed for snow- and icemelt at the stake sites during the study period. There is an altitudinal gradient in climatic forcing of about -3 W m^{-2} per 100 m (Table 3.4). Our values of melt energy consumed are lower than those published by Vincent and others (2004) for the melting season on Glacier de Sarennes in the Western Alps. This is due to the fact that our study considers the total melt integrated over one year (Oct. 1 - Sept. 30). This allows the evaluation

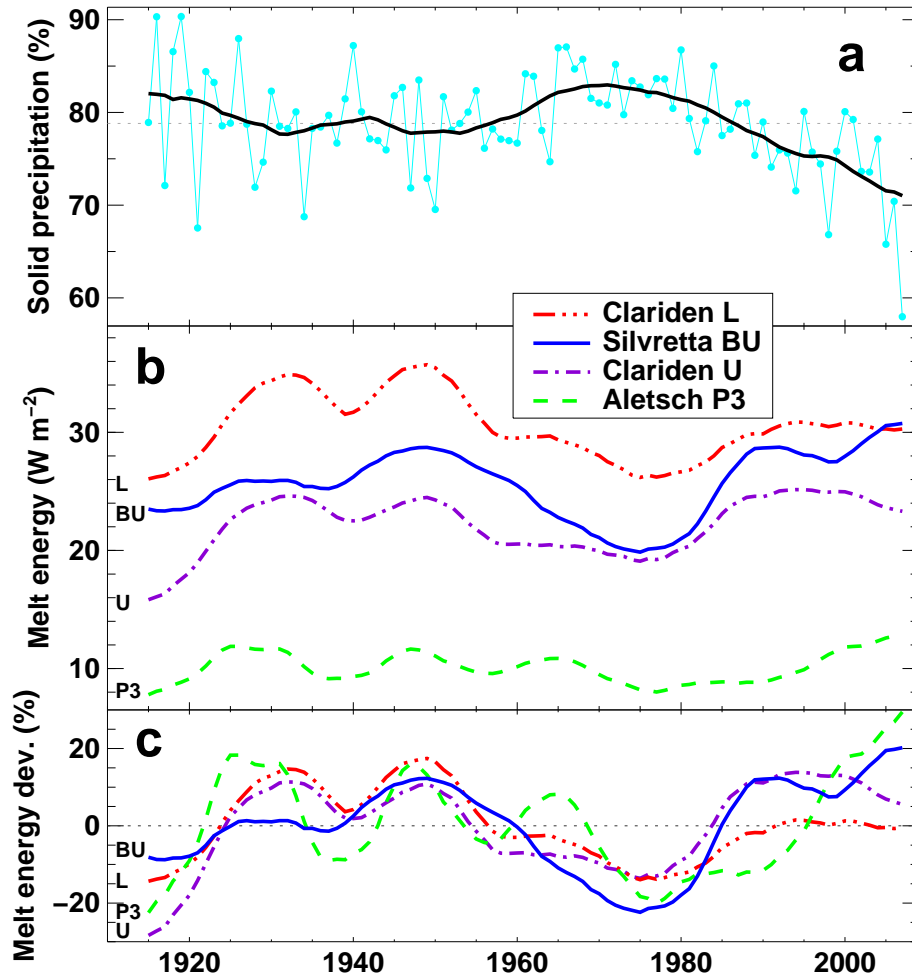


Figure 3.7: (a) Four-stake average of the fraction of solid precipitation relative to total precipitation smoothed with a 10-year running mean (bold). The dotted line is the 1914-2007 mean. 10-year running means of (b) the energy consumed for melt at the four stakes and (c) the relative deviations from the 1914-2007 mean. Annual values are not shown for clarity.

of E_m time series, which are not biased by the varying length of the melting season.

The climatic forcing at Clariden U and L is very similar except for a shift due to different elevation (Fig. 3.7b). Throughout most of the 20th century significantly less energy is consumed for melt at Silvretta BU than at Clariden L although the stake elevations only differ by 50 m. The mean degree-day factor is lower by 24% for Silvretta BU than for the other sites (Table 3.2). This can not be explained by an effect of aspect only. The lower climatic forcing at Silvretta BU inferred from the long-term point mass balance measurements is consistent with the observation of reduced rates of glacier wide mass loss of Silvrettagletscher compared to other Alpine glaciers (Bauder and others, 2007). The amount of energy consumed for melt significantly decreased during the 1960s to 1980s causing the specific summer balance at three stakes to be above average (Fig. 3.4 and Fig. 3.6). Strong regional differences in climatic forcing between Silvretta and Clariden are evident from Figure 3.7b. Whereas E_m at Silvretta BU was almost as low as at Clariden U, it meets the level of Clariden L at present. This shift in climatic forcing is interpreted as a result of regionally differing climate change conditions and has a magnitude of 6 W m^{-2} , corresponding to a shift in elevation of about 200 m.

We analyzed three periods with dominant trends in the cumulative centered summer balance

Table 3.4: Energy consumed for melt E_m at the four stakes. Mean E_m in 1914-2007 and relative mean deviations from the 1914-2007 average for three periods.

Stake	E_m (W m^{-2})	Deviation from 1914-2007 mean (%)		
		1943-1953	1964-1985	1987-2007
U	22.1	+14.0%	-9.7%	+12.2%
L	30.4	+20.3%	-10.3%	+1.0%
P3	10.0	+18.0%	-10.9%	+6.5%
BU	25.1	+13.1%	-21.0%	+13.9%

(Fig. 3.5) and calculated the relative deviation of the period mean E_m from the 1914-2007 stake-average (Table 3.4). The climatic forcing was significantly higher in the 1940s than in the last two decades except for Silvretta BU. During the period of positive centered mass balances (1964-1985) E_m was up to 20% below average. The time series analysis at the four locations reveals similar fluctuations and relative offsets of E_m from the mean values (Table 3.4 and Fig. 3.7c). This indicates that the trends in 20th century climate forcing have extended to all four stake sites located at different elevations. However, there are substantial regional differences: The increase in climate forcing observed in the 1980s at three sites starts one decade later at Aletsch P3 and is much stronger at Silvretta BU compared to those on Claridenfirn (Fig. 3.7c).

3.5 Discussion

Uncertainties in the homogenized seasonal time series of specific mass balance are due to several factors, which are either directly related to the measurements or to the homogenization procedure. Müller and Kappenberger (1991) identified the following biases in direct mass balance measurements (numbers in brackets give the estimated error in m w.e.): (a) accumulation before and ablation after field visits in late summer ($\sigma_a = \pm 0.2$), (b) melt in of stake ($\sigma_b = +0.1$), (c) compaction of firn layer ($\sigma_c = -0.1$), (d) determination of snow or firn density ($\sigma_d = \pm 0.05$), and (e) percolation with refreezing mainly at the onset of the melting season ($\sigma_e = +0.05$). Most importantly, ablation after the field visits in late summer can be responsible for considerable differences in snow depth resulting from stake reading and snow probings. We address this bias using the daily mass balance model. The other biases are difficult to detect and to correct and are assumed to be significant only in a few cases. The total uncertainty in the direct determination of mass balance is estimated to be ± 0.25 m w.e. a^{-1} .

Years with no measurements available (Fig. 3.2) are completed using average model parameters calibrated for all years covered with data. Considering the significant year-to-year variability of $DDF(I, c_{s/f})$ ($\pm 22\%$) and c_{prec} ($\pm 16\%$, Table 3.2), the uncertainty in the reconstructed values may be substantial. However, our statistical model is considered to be the best way to address data gaps in order to obtain continuous time series. In years with a complete set of field data (b_w, b_n) the potential for errors due to the mass balance model is low, as it is well constrained by the seasonal data points. We suspect a tendency of the model to overestimate melt after the late summer field survey. The radiation conditions often observed in autumn with high longwave outgoing radiation are not properly accounted for in our model and may substantially reduce the melt rates (Ohmura, 2001). The potential for erroneous results, however, is low as moderate air temperatures and reduced incoming radiation generally lead to relatively small

amounts of melt in this season of the year. Summer accumulation is insufficiently resolved by the seasonal mass balance data because it is continuously melted away. The mass balance model calculates summer accumulation, however, could overestimate this term by compensating for it with increased melt rates. This would have an impact on the calculated total ablation and consequently on E_m .

With glacier retreat a reduction in surface elevation at the stake location is inevitable. In order to shed light on the impact of this bias on specific mass balance we analyzed the elevation changes using repeated DEMs. Glacier surface subsided by between 10 m (P3) and 21 m (L) since 1914. We calculated the change in E_m between the maximum and the minimum stake elevation. Surface lowering causes an additional forcing of in the order of $+0.5 \text{ W m}^{-2}$, corresponding to 0.05 m w.e., or 2 % of the mean annual melt.

The mass balance observations used in this study are performed at fixed locations. The stakes are annually moved back to the original location. This implies that (i) the exposure to solar radiation is constant, (ii) the deposition or erosion of snow can be assumed to be similar in all years, and (iii) the observed mass balance quantities directly reflect the climatic forcing and are not biased by changing glacier surface area or uncertain spatial extrapolation of mass balance. This manifests an important advantage compared to glacier wide average mass balance quantities.

The evaluation of mass balance quantities between fixed dates allows the comparison of different mass balance time series on the basis of equal time periods. The choice of the fixed dates is debatable and has an impact on the evaluated values of winter and summer balance. The absolute maximum of snow cover often occurs in late May or June at the study sites (Fig. 3.3). We chose April 30 for the termination of the winter period because melt starts to be important around this date. When shifting the evaluation date to May 31 our conclusions remain valid.

The two parameters of the mass balance model are allowed to vary freely in order to obtain an exact match of the measurements. The year-to-year fluctuations in c_{prec} and $DDF(I, c_{\text{s/f}})$ do, however, not hamper the applicability of the mass balance model because it is not regarded as a strictly physical model but as a statistical tool for scaling measured weather data to direct mass balance observations. Moreover, the variation in c_{prec} and $DDF(I, c_{\text{s/f}})$ can be interpreted in terms of local climate at the glacier site. Fluctuations in c_{prec} correspond to varying differences in precipitation between the valley weather station and the stake site; c_{prec} is a measure for the altitudinal precipitation gradient and also captures anomalous snow drift in individual years. $DDF(I, c_{\text{s/f}})$ is the proportionality factor between positive air temperatures and snow- or icemelt. Year-to-year variations in $DDF(I, c_{\text{s/f}})$ can be due to the uncertain extrapolation of temperature from the valley station to the stake site. In addition, varying heat budget components, for example in terms of different air moisture or cloudiness (Pellicciotti and others, 2005), may influence the statistical relation between air temperature and melt rate.

We analyzed the calibrated annual values of $DDF_{\text{snow}}(\bar{I})$ with \bar{I} being the annual average of the potential direct radiation I . There is a constant level in $DDF_{\text{snow}}(\bar{I})$ until 1960 when a decreasing trend starts (Fig. 3.8a). Compared to the beginning of the 20th century more positive degree-days are required nowadays to melt the same quantity of snow. This is intriguing, as decreasing surface albedo, reported for alpine glaciers Paul and others (2007a), would have the opposite effect. A decrease in the temperature gradient between the weather station and the glacier site could explain the negative trend in the degree-day factors. This effect, however, is assumed not to be very important as temperatures used for the modelling were recorded at high-altitude stations with limited elevation differences to the glacier sites. We attribute the

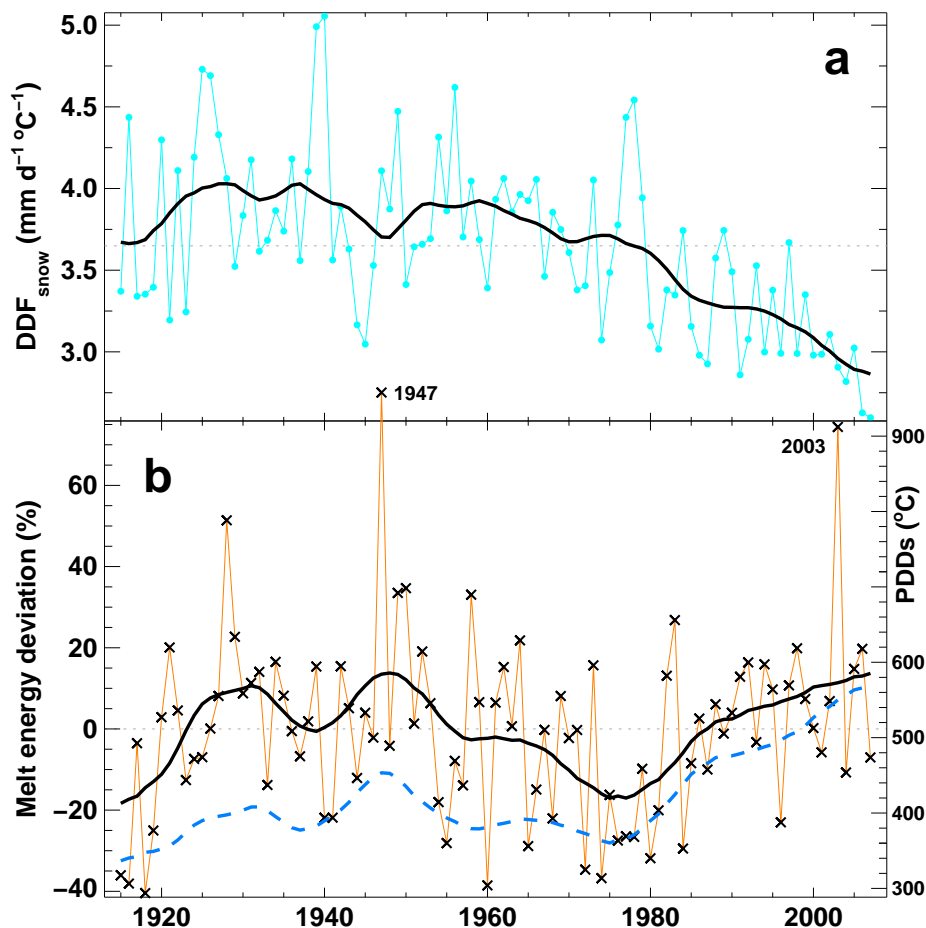


Figure 3.8: Annual four-stake average of (a) the calibrated degree-day factor for snow $DDF_{\text{snow}}(\bar{T})$ and (b) the four-stake average of the relative melt energy deviations from the mean and (dashed) the sum positive degree-days (PDDs). Bold lines indicate 10-year running means.

decreasing proportionality between positive air temperatures and the melt rate to a change in the relative importance of radiative fluxes at the study sites. Our present data basis does not allow to shed light on the drivers of these changes in the heat budget and further investigation is required.

The decadal fluctuations in melt energy consumed are consistent at all sites (Fig. 3.7c and Table 3.4) and were averaged over the four stakes (Fig. 3.8b). E_m culminates in the extreme year of 1947 that exhibits a higher climatic forcing than 2003 with its famous European heat waves. We observe an increase in climatic forcing of 30% between 1975 and 2005. Ohmura and others (2007) attributed the higher melt rates during the last decades to a global brightening of solar radiation and the enhanced greenhouse effect of terrestrial radiation.

The change in proportionality between the positive degree-days (PDDs) and the melt is evident from the comparison of these variables. At present, the annual sum of PDDs has increased to values unprecedented in the last century, however, the melt energy consumed shows no significant long-term trend (Fig. 3.8b). This discrepancy leads to a decrease in the calibrated degree-day factors. There is some anticorrelation of E_m and $DDF_{\text{snow}}(\bar{T})$; the degree-day factor is low in periods of intensive climatic forcing and higher during years with less melt (Fig. 3.8b). The observation of decreasing degree-day factors with increasing climatic forcing could sub-

stantially hamper the applicability of temperature index models for projections of future glacier melt. It is important to understand the drivers of this changing proportionality between PDDs and melt in order to develop methods to tackle this problem.

3.6 Conclusions

Four long-term time series of seasonal mass balance observations at fixed locations have been compiled. Each data set was homogenized using a mass balance model to account for the varying date of observations, correct for measuring bias, to fill gaps and to separate accumulation and ablation. A unique data basis has been assembled covering most of the 20th century. We find evidence for significantly different regional changes in the precipitation and melting conditions. A high altitude site exhibits opposite trends in summer balance compared to the other series. Since 1975 the melt rates have increased by 10% per decade. The analysis of the energy consumed for melt shows that the climatic forcing on Alpine glaciers was higher in the period from 1943 to 1953 than during the last two decades. We find differing trends in climatic forcing and positive air temperatures since 1960; an observation which is probably related to a change in the surface heat budget at the equilibrium line of glaciers and has important implications for the long-term stability of empirical degree-day factors in temperature index modelling over time.

The main goal of point mass balance observations is to study variability and changes in climate at high altitude sites. Our analysis shows the potential of long-term time series for inferring regional and altitudinal differences in climatic forcing. The four homogenized 93-year time series of point-based seasonal mass balance at different locations throughout the Alps are a unique data set for investigating high Alpine climatic changes throughout the 20th century. Thus, the continuation of long-term point mass balance time series is highly recommended in future mass balance monitoring strategies.

Acknowledgments

This study would not have been possible without the continuous and immense effort of a large number of field workers. We are particularly grateful to H. Müller and G. Kappenberger for their efforts to collect and homogenize the Claridenfirn data. Salome Duelli helped with digitizing old mass balance reports. This work is supported by ETH Research Grant TH-17 06-1. The meteorological data used were recorded by MeteoSchweiz. M. Funk is acknowledged for stimulating discussions and his interest in this study. We thank the scientific editor P. Jansson, an anonymous reviewer and K. A. Brugger for helpful comments that improved the clarity of the paper.

Chapter 4

Homogenization of long term mass balance time series

MATTHIAS HUSS, ANDREAS BAUDER, MARTIN FUNK

Versuchsanstalt für Wasserbau, Hydrologie und Glaziologie (VAW), ETH Zürich, 8092 Zürich, Switzerland

In press, *Annals of Glaciology*

Citation: Huss, M., A. Bauder and M. Funk (in press). Homogenization of long term mass balance time series. *Annals of Glaciology*, **50**.

ABSTRACT: The re-analysis of long term mass balance time series is important to provide bias-corrected mass balance data for climate change impact studies. A method to homogenize time series of comprehensive mass balance monitoring programs is presented and applied to the nearly 50-year mass balance records of Griesgletscher and Silvrettagletscher, Switzerland. Using a distributed mass balance model in daily resolution we correct the mass balance data for varying observation dates and direct point measurements are combined with independent geodetic mass changes, a prerequisite for a thorough homogenization of mass balance records. Differences between mass balance evaluated in the hydrological year or according to the measurement period and the stratigraphic system are analyzed and may be up to ± 0.5 m w.e. a⁻¹. Cumulative mass balance of both glaciers based on the glaciological method generally agrees well with geodetic mass change on the investigated glaciers. However, for Silvrettagletscher a significant bias of +0.37 m w.e. a⁻¹ was detected and corrected since 1994.

4.1 Introduction

Glacier surface mass balance clearly reflects climatic fluctuations and is important for the assessment of water resources and sea level rise (Kaser and others, 2006; Ohmura and others, 2007). Mass balance has been determined within numerous glacier monitoring programs for several decades (WGMS, 2000). Comparison of mass balance time series originating from the direct glaciological method and the indirect geodetic method often reveals inhomogeneities (e.g. Cox and March, 2004). Different dates of field surveys hamper the comparability of annual mass balance quantities (Anonymous, 1969) and changing methods for data evaluation affect the consistency of the results (Holmlund and others, 2005). Long term mass balance time series, thus, need homogenization in order to be a valuable contribution to the understanding of ongoing climate change.

The determination of glacier surface mass balance is often performed using the direct glaciological method. A network of measurement sites is used to evaluate point balances and to extrapolate them on the entire glacier area enabling to calculate glacier wide average mass balance (Dyrgerov and Meier, 2002). Only a small number of glaciers exist, for which seasonal mass balances are reported, aiming at a separation of accumulation and ablation (Ohmura and others, 2007). Comprehensive monitoring programs additionally include periodical geodetic surveys of the change in glacier surface elevation based on topographic maps, photogrammetrical analysis or laser scanning providing ice volume changes.

The time periods used for the evaluation of annual and seasonal mass balance quantities have a significant impact on the results – an issue rarely addressed in recent literature. Mass balance can be determined within a fixed date system or a stratigraphic system (Anonymous, 1969; Mayo and others, 1972). Often a correction of inhomogeneous results caused by varying evaluation periods is difficult as e.g. the amount of melt after the late summer field survey is not documented with measurements. A projection of annual and seasonal mass balance quantities to the same periods is required to ensure comparability of both individual years and different glaciers.

Several studies have previously approached the re-analysis of long term mass balance time series. Systematic errors in point mass balance data were detected and corrected by Müller and Kappenberger (1991). Funk and others (1997) used different methods to calculate glacier wide mass balance from stake data. Holmlund and others (2005) performed a re-analysis of the seasonal time series of Storglaciären, Sweden, highlighting the importance of homogenizing mass balance records.

In this study, we present a method for homogenizing long term time series of comprehensive mass balance monitoring programs and apply it to two glaciers in Switzerland. While point mass balance data provide a high temporal resolution and the distribution pattern of mass balance, geodetic surveys yield a wide spatial coverage of elevation change. A combination of both data sources is, thus, of benefit. A daily mass balance model calibrated annually using all available field data is applied to correct the time series for varying observation dates and to calculate the spatial mass balance distribution. The time series are corrected for deviations from independent geodetic mass changes derived from high-accuracy digital elevation models. The geodetic mass change provides a more accurate baseline for the homogenization process on decadal time scales. This central assumption is discussed in detail within the section 'Error analysis'.

4.2 Study sites and field data

This study focuses on two glaciers in the Swiss Alps (Griesgletscher and Silvrettagletscher, Fig. 4.1), for which mass balance has been determined for nearly 50 years using the glaciological method. For both glaciers exceptional data sets of point based seasonal mass balance measurements and geodetic ice volume changes are available (Table 4.1).

Table 4.1: *Glacier characteristics and field data basis. Area and elevation range are based on the DEM of 2007. n_{b_n} and n_{b_w} are the total number of point net and winter balance measurements.*

Glacier	Area (km ²)	Elevation (m a.s.l.)	Measurements		DEMs
			n_{b_n}	n_{b_w}	
Gries	4.97	2415 - 3307	1486	62	8
Silvretta	2.79	2467 - 3073	1047	112	6

Griesgletscher is a small alpine valley glacier situated south of the main Alpine crest. The glacier has a north-eastern exposure and has experienced dramatic retreat during the past two decades (Glaciological reports, 1881–2008). Since 1961 Griesgletscher has lost almost 40% of its ice volume (Fig. 4.1d). Silvrettagletscher is a small glacier in the north-eastern Swiss Alps with exposure to the west. Silvrettagletscher exhibits lower rates of mass loss than other Alpine glaciers (Huss and others, 2008a). The mass balance distribution on the investigated glaciers is considerably influenced by local effects of exposure and snow drift (Fig. 4.1b and c). Mass balance monitoring programs were set up on Griesgletscher in 1961 and on Silvrettagletscher in 1959 and are still operating.

In the 1970s a network of up to 80 mass balance stakes was maintained on Griesgletscher. A

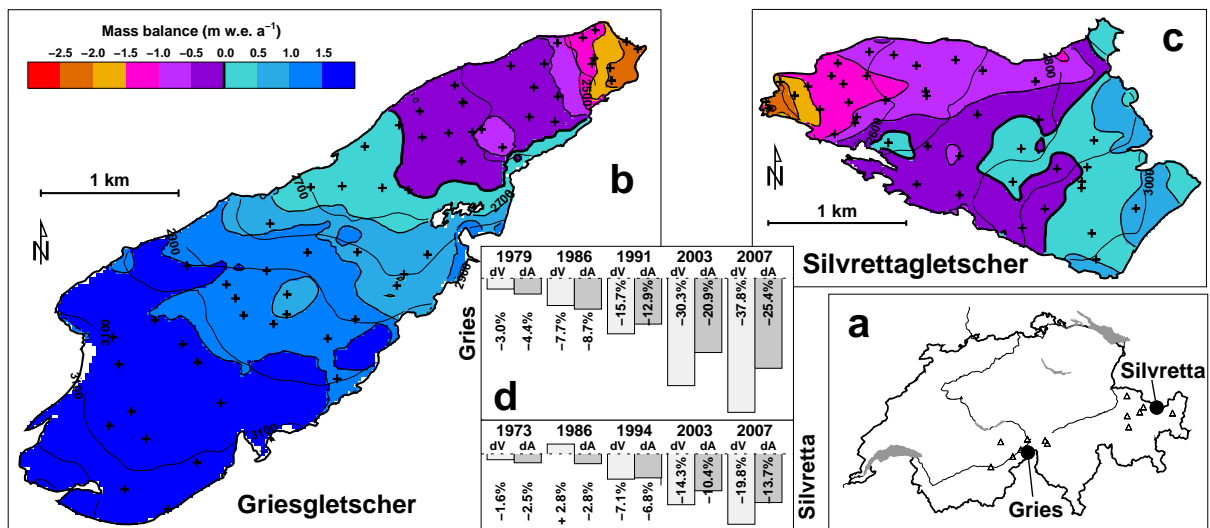


Figure 4.1: (a) Location of Griesgletscher and Silvrettagletscher in Switzerland. Triangles represent considered weather stations. (b) Mass balance distribution of Griesgletscher in 1978 and (c) Silvrettagletscher in 1972. Crosses indicate net balance stakes. (d) Percentage of ice volume (dV) and area change (dA) according to digital elevation models relative to 1961 (Gries) and 1959 (Silvretta). The total ice volume of the glaciers is known from radio-echo soundings (unpublished data, VAW-ETHZ).

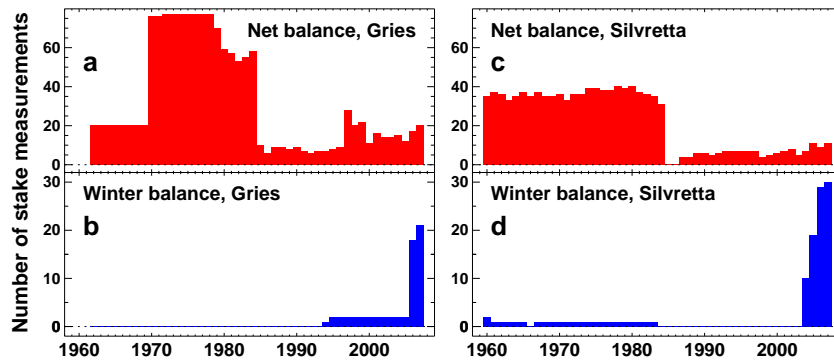


Figure 4.2: Number of point net and winter balance measurements per year.

network of almost 40 stakes on Silvrettagletscher was monitored during 25 years (Fig. 4.2). The maximum stake density was 12 km^{-2} on both glaciers. Additionally, measurements of winter accumulation exist, covering more than half of the study period in the case of Silvretta and the last 14 years for Gries (Fig. 4.2). Our study is based on a complete digital set of original data.

High-accuracy Digital Elevation Models (DEMs) are available for Gries (8 DEMs during the study period) and Silvretta (6 DEMs) in a spatial resolution of 25 m (Bauder and others, 2007). The DEMs are based on photogrammetrical evaluation of aerial photographs and provide ice volume changes in decadal to subdecadal periods. Volume changes are converted to mass changes assuming a density of $850 \pm 50 \text{ kg m}^{-3}$ (Sapiano and others, 1998).

We use time series of daily mean temperature recorded at Jungfraujoch (3580 m a.s.l., 30 km from Gries) and at Davos (1590 m a.s.l., 18 km from Silvretta). Lapse rates for monthly mean air temperature were determined by considering eleven nearby weather stations (Fig. 4.1a) and are used to shift the temperature time series of Jungfraujoch and Davos to the mean glacier elevation. Mean monthly precipitation sums for the period 1971-1990 are provided by a gridded data set (PRISM) with a spatial resolution of 2 km (Schwarb and others, 2001). The daily precipitation recorded at Airolo (1150 m a.s.l., 21 km from Gries) and Klosters (1200 m a.s.l., 13 km from Silvretta) are used for the downscaling of PRISM at the glacier site and thus provide the temporal variability in precipitation.

4.3 Methods

Determination of mass balance

For practical reasons glacier surface mass balance is often evaluated between the dates of two successive field surveys. This evaluation period is termed 'measurement period' throughout this paper. In order to directly compare mass balance quantities of individual years and different glaciers an evaluation between fixed dates, e.g. the hydrological year, is better suited and is termed here 'fixed date system'. The length of the 'natural' mass balance year is, however, best described by the 'stratigraphic system' (Anonymous, 1969; Mayo and others, 1972) based on annual minima and maxima of mass balance.

\bar{b}_n expressed in meter water equivalent (m w.e.) is the mean specific surface net balance. It corresponds to the annual sum of accumulation and ablation on the entire glacier divided by

that year's glacier surface area. $\overline{b_w}$ is the mean specific winter balance. For each year we evaluate net and winter balance according to the three mass balance systems with different evaluation periods. $\overline{b_n^{\text{meas}}}$ and $\overline{b_w^{\text{meas}}}$ refer to the exact dates of the field surveys, which vary between the years. $\overline{b_n^{\text{fix}}}$ is the net balance in the hydrological year (Oct. 1 - Sept. 30) and the fixed date winter balance $\overline{b_w^{\text{fix}}}$ is determined in the period October 1 - April 30. We define the mean specific stratigraphic net balance $\overline{b_n^{\text{strat}}}$ as the sum of accumulation and ablation between the minima of glacier mass in two successive years. $\overline{b_w^{\text{strat}}}$ is the absolute maximum of snow cover in the course of one year.

We calculate 'conventional' mass balances (Elsberg and others, 2001), i.e. glacier extent and elevation are updated annually. An annual time series of glacier area is obtained by linearly interpolating the glacier surface geometry between successive DEMs. Using this technique both the annual change in glacier surface elevation and the change in glacier extent are estimated and step changes in the glacier geometry are avoided (Huss and others, 2008a).

Mass balance model

The homogenization procedure is performed using a distributed accumulation and temperature index melt model (Hock, 1999; Huss and others, 2008a). This mass balance model is not regarded as a physical model, but as a tool to resolve annual and seasonal mass balance measurements on a daily time scale and to perform the spatial 'inter- and extrapolation' of sparse data points based on a consistent algorithm taking into account the principal factors of mass balance distribution.

Temperature index models are based on a linear relation between positive air temperature and melt rate (Ohmura, 2001). In the applied model, degree-day factors are varied as a function of potential direct radiation in order to account for the effects of slope, aspect and shading. Daily surface melt rates M are computed for each cell of the DEM by:

$$M = \begin{cases} (f_M + r_{\text{ice/snow}} I) T & : T > 0 \\ 0 & : T \leq 0 \end{cases} \quad (4.1)$$

where f_M denotes a melt factor, $r_{\text{ice/snow}}$ are radiation factors for ice and snow surfaces and I is the potential solar radiation. Air temperature T at every grid cell is determined by a constant lapse rate dT/dz . Parameter values and units are given in Table 4.2.

Precipitation is assumed to increase linearly with elevation (dP/dz). A correction factor c_{prec} allows the adjustment of precipitation sums and a threshold temperature $T_{\text{thr}}=1.5^\circ\text{C}$ distinguishes

Table 4.2: Mean values of model parameters and units.

Parameter	Units	Gries	Silvretta
f_M	$10^{-4} \text{ m h}^{-1} \text{ }^\circ\text{C}^{-1}$	1.689	0.832
r_{ice}	$10^{-6} \text{ m}^3 \text{ W}^{-1} \text{ h}^{-1} \text{ }^\circ\text{C}^{-1}$	0.720	0.635
r_{snow}	$10^{-6} \text{ m}^3 \text{ W}^{-1} \text{ h}^{-1} \text{ }^\circ\text{C}^{-1}$	0.525	0.466
dT/dz	$^\circ\text{C m}^{-1}$	-0.0054	-0.0048
dP/dz	$\% \text{ m}^{-1}$	0.008	0.033
c_{prec}	-	1.26	2.07

snow from rainfall (Hock, 1999). The spatial variation of accumulation on the glacier surface is substantially influenced by snowdrift. The measurements of net balance carried out in high spatial resolution until 1984 (Fig. 4.2) provide detailed information on distribution patterns (Fig. 4.1b and c). In order to parametrize snow redistribution by wind drift we determine a spatial accumulation anomaly A^{acc} , which is calculated for all years with a dense coverage of stakes ($>6 \text{ km}^{-2}$) as follows: (1) Point net balance is interpolated spatially using an inverse distance technique. (2) A linear mass balance gradient and an equilibrium line altitude are determined from the result – the most simple mass balance distribution. (3) By subtracting the mass balance given by this linear trend with elevation from the interpolated value of mass balance at every grid cell an offset is obtained. We consider these offsets to be measure for anomalous snow deposition and convert them into dimensionless quantities by normalizing the grid. This accumulation anomaly grid A^{acc} provides percental solid precipitation deviations from the expected value and is applied to all snow fall events. A factor f_{anom} is used to scale the amplitude of A^{acc} . In years with low spatial coverage of stakes ($<6 \text{ km}^{-2}$) we use the average anomaly pattern of all years for which mass balance distribution is well constrained with field data. The anomaly maps show significant year to year variability, but also reveal constant features, which can be explained by preferential wind erosion of snow in convex topography and redeposition in lee side depressions. The model precipitation P_{xy}^{mod} at the location (x, y) is calculated as

$$P_{xy}^{\text{mod}} = P_{xy} \cdot c_{\text{prec}} \cdot (1 + f_{\text{anom}} \cdot A_{xy}^{\text{acc}}), \quad (4.2)$$

where P_{xy} is the measured precipitation extrapolated to the grid cell using dP/dz , c_{prec} the precipitation correction factor, A^{acc} the accumulation anomaly and f_{anom} the scaling factor.

Ablation due to geothermal heat flux, internal deformation and basal friction are insignificant components of glacier mass balance and is accounted for in the model. Based on simple considerations we estimate the contribution of these processes to mass balance as $-0.01 \text{ m w.e. a}^{-1}$. Griesgletscher exhibited non-negligible mass loss due to calving into a proglacial lake until the mid-1980s. Annual calving rates are well documented (Glaciological reports, 1881–2008) and were subtracted from the calculated surface mass balance.

Time series homogenization

The homogenization procedure is subdivided into two steps (Fig. 4.3): (1) Tuning the model to the point mass balance data, and (2) correcting the results obtained in (1) using independent geodetic mass changes. Basically, (1) represents the direct glaciological method with a model used for temporal downscaling and for determining the spatial distribution of mass balance, and (2) fits the mean specific mass balance to the geodetic mass change, which is assumed to have a higher accuracy. The measurements of point mass balance are the best indicator of the local meteorological conditions on the glacier (Huss and Bauder, in press). Daily temperature and precipitation from a nearby weather station serve to resolve the seasonal data at a daily scale. As the model is tuned to the field data for every year individually, the fluctuations in seasonal mass balance are given by the in situ measurements and not by the meteorological conditions at weather stations.

First, the accumulation parameters of the mass balance model are calibrated using the measurements of winter balance. c_{prec} and dP/dz are tuned so that the calculated snow water equivalent at the winter survey date matches the measured value (Fig. 4.3). If no winter balance data are

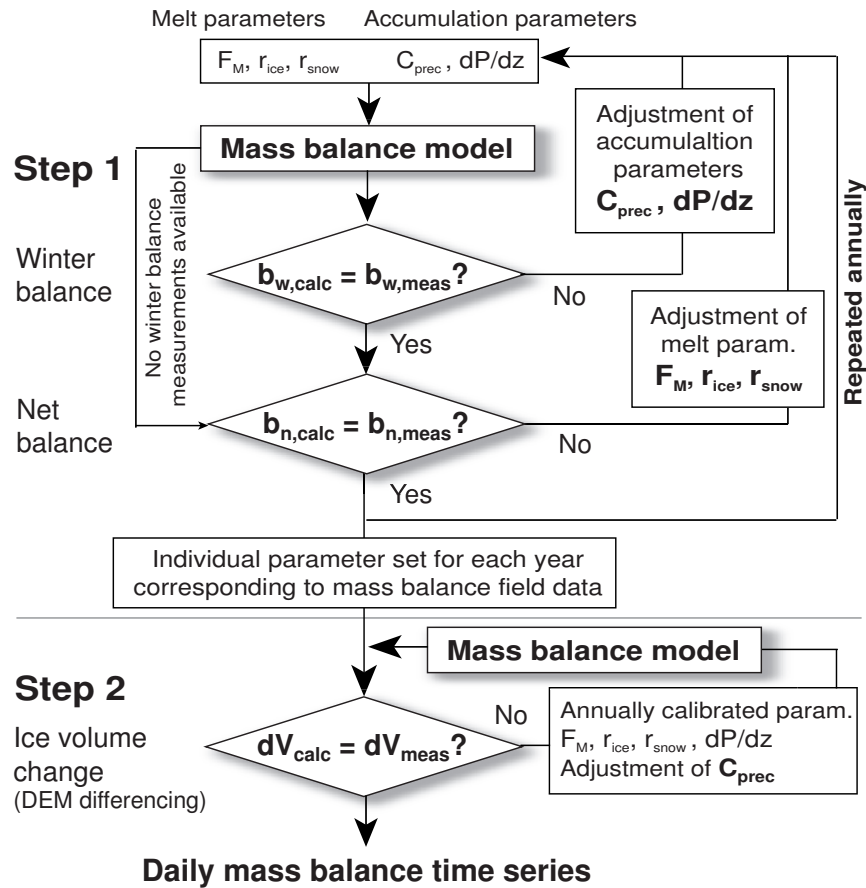


Figure 4.3: Homogenization procedure. The daily model is tuned annually to match the seasonal point mass balances optimally (step 1). If necessary, the misfit with geodetic volume changes is corrected by adjusting the parameter C_{prec} (step 2).

available C_{prec} has the average value of all years with winter measurements and dP/dz is set to values found for the investigated glaciers by Huss and others (2008a).

The calibration of the melt parameters f_M and $r_{ice,snow}$ (Eq. 4.1) is performed annually using the measurements of point net balance. Mass balance calculated between the exact dates of the late summer field surveys in two successive years is tuned to the field data. The parameters are varied systematically in order to obtain (i) an average difference of field data and calculation equal to zero and (ii) a minimization of the root-mean-square error ($rmse_d$) of measurement and model (Fig. 4.3). Using f_{anom} the accumulation anomaly is scaled such that $rmse_d$ is minimized. The use of the anomaly significantly increases the performance of the model to capture the spatial variation in net balance; $rmse_d$ is reduced by 20% compared to model runs excluding this component.

The aerial photographs used for DEM production were acquired between mid August and end of September; the exact dates are known. All geodetic mass changes were corrected for melt or accumulation occurring between the acquisition date and the end of the hydrological year using the mass balance model. The mean specific corrections applied are smaller than ± 0.5 m w.e. They are, thus, important in short time intervals between successive DEMs and almost negligible in longer subperiods.

In the second homogenization step, the resulting time series are compared to the density- and

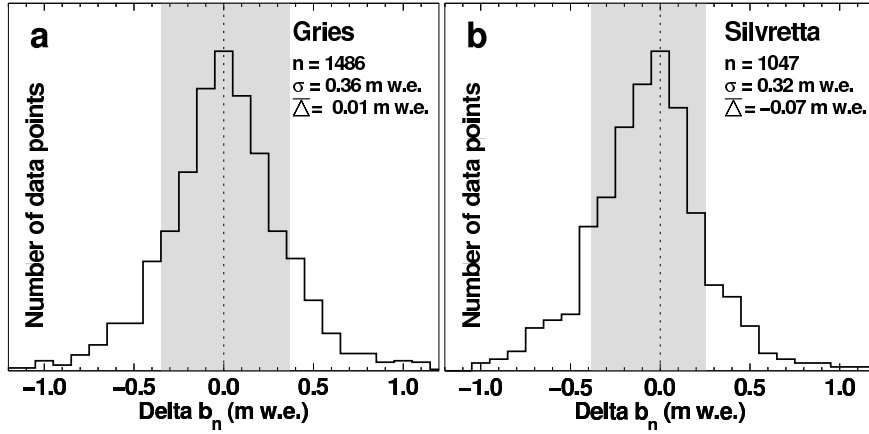


Figure 4.4: Distribution of differences Δb_n of measured and calculated point net balance for (a) Griesgletscher and (b) Silvrettagletscher. The shaded bar corresponds to ± 1 standard deviation (containing 70% of the data points).

date-corrected ice volume changes. In the ideal case, the cumulative direct mass balance coincides with the geodetic mass change. If not, the mass balances calculated in step 1 are corrected (Fig. 4.3). The difference between the cumulative mass balance and the geodetic mass change in a period given by two successive DEMs is distributed evenly over the years. When doing so, a misfit with the point mass balance data in each year of the period has to be accepted. The parameters obtained in step 1 are updated in order to yield the corrected cumulative mass balance matching the geodetic mass changes. This is achieved by adjusting the correction factor for precipitation c_{prec} and keeping all other parameters constant. c_{prec} was chosen for this purpose, because a relatively high uncertainty is attributed to the measurement and the modelling of high-mountain precipitation. A change in the total precipitation also affects the ablation area and distributes the increased misfit with the stakes across the glacier without significantly changing the previously determined mass balance distribution.

4.4 Results

The differences between measured and calculated point net balances cluster in a gaussian-shaped distribution (Fig. 4.4). In the case of Silvrettagletscher there is a systematic negative misfit of -0.07 m w.e., because in step 2 of the homogenization process a significant correction was required. 70% of the stake measurements can be reproduced within ± 0.37 m w.e. (Gries) and ± 0.32 m w.e. (Silvretta).

The homogenization procedure provides daily time series of mean specific mass balance (Fig. 4.5). These allow us to visualize the characteristics of the mass balance year, e.g. the occurrence of summer snow fall events (Fig. 4.5b) or melt after the late summer field survey (Fig. 4.5c). In individual years the mass balance quantities can differ considerably due to the choice of the evaluation period.

Since 1982 mean specific net balances have been predominantly negative, in particular in 2002/03 (Fig. 4.6a). Net balance values corresponding to different evaluation periods mostly have the same sign, but often differ significantly. The homogenized time series refer to the same periods and, thus, allow comparison of both individual years and different glaciers. When

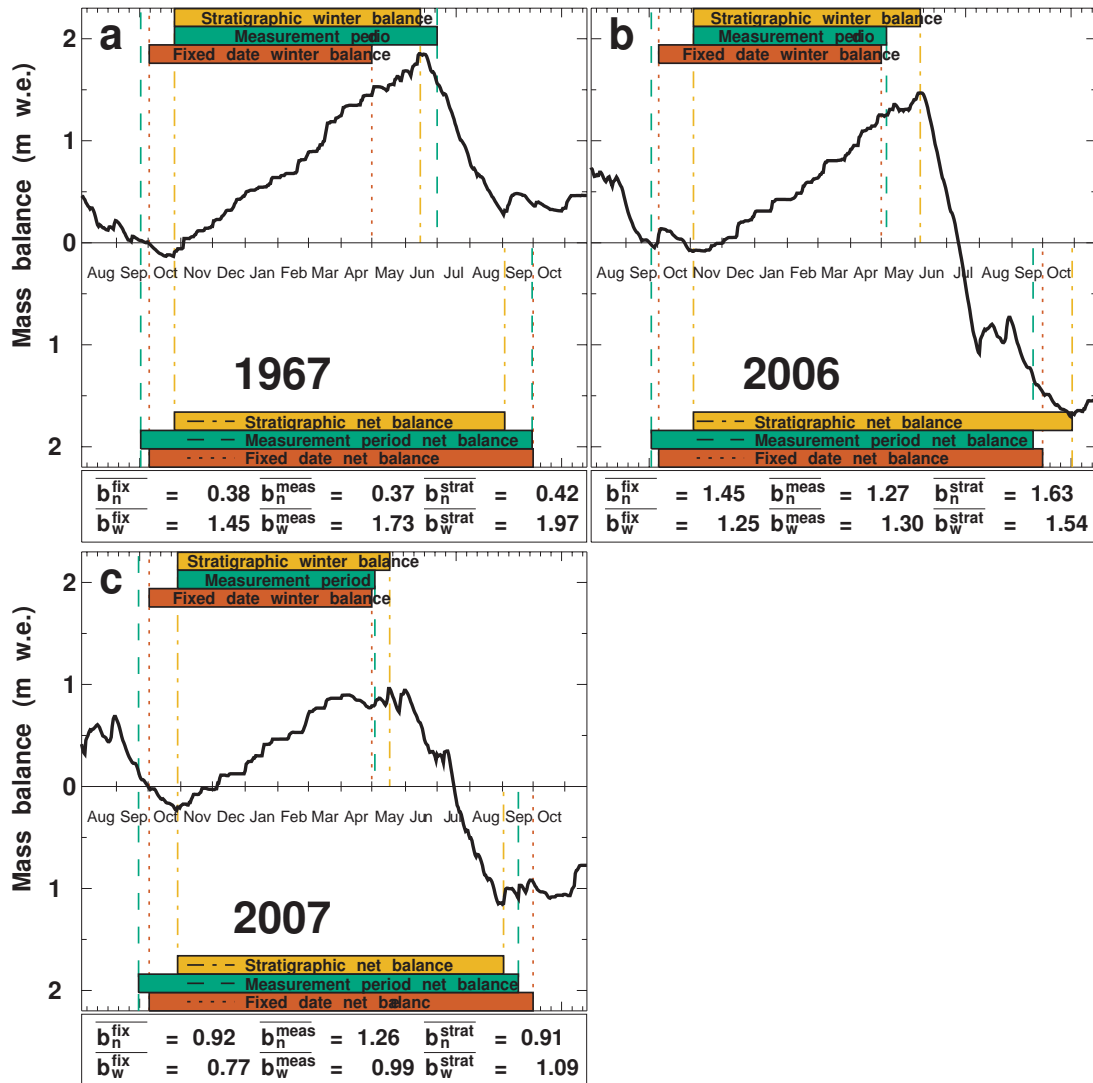


Figure 4.5: Cumulative daily area-averaged mass balances of Silvrettagletscher for selected years: (a) 1967, (b) 2006 and (c) 2007. Bars and vertical lines visualize the length of the different evaluation periods.

considering cumulative net balances the differences due to the choice of the evaluation period cancel out.

The homogenized mass balance time series are compared to the previously reported values (Glaciological reports, 1881–2008; WGMS, 2000), which have been determined based on the traditional glaciological method. In the case of Griesgletscher the homogenized mass balances agree well with the published data (Fig. 4.7b). The mass loss according to this study is slightly larger. However, a significant bias is found for Silvrettagletscher since 1994 (Fig. 4.7a). Whereas the cumulative mass loss was -3.1 m w.e. according to the previous evaluation, the homogenized time series yield -8.0 m w.e. in the same period, resulting in a net balance bias of $+0.37$ m w.e. a^{-1} .

In order to find additional evidence for the bias in the Silvretta time series we compared them to those of Jamtalferner (3.7 km²), Austria, located 7 km apart (WGMS, 2000). Since 1994 the non-homogenized net balance of Silvrettagletscher is on average $+0.54$ m w.e. a^{-1} more positive compared to Jamtalferner. This indicates that the correction towards higher mass losses

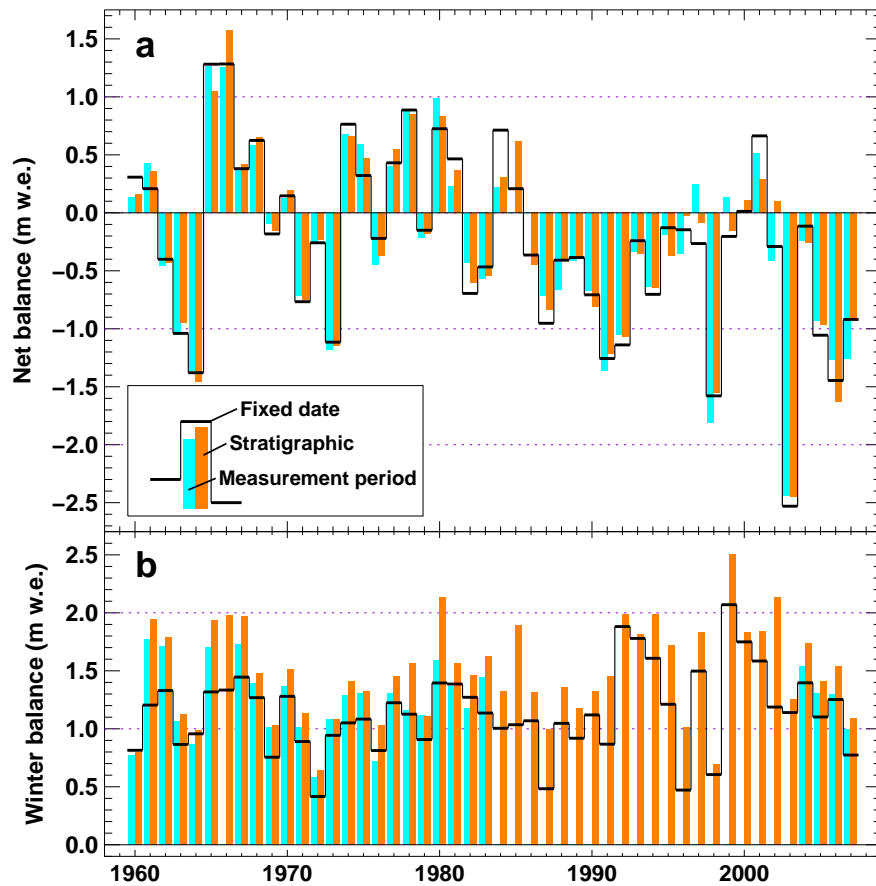


Figure 4.6: Homogenized mass balance time series of Silvrettagletscher 1959-2007. Mean specific (a) net balances and (b) winter balances in the fixed date system (solid line), the measurement period and the stratigraphic system (shaded bars).

performed within the homogenization is also supported by a nearby mass balance record.

The method presented allows us to separate accumulation and ablation (inset in Fig. 4.7b). It is often assumed that winter and summer balance are a good approximation of the total annual accumulation \bar{c}_a and the total annual ablation \bar{a}_a (Dyurgerov and Meier, 1999). The values contained in Table 4.3 show that this assumption is hampered by non-negligible amounts of accumulation during summer and ablation during winter, respectively. The evaluation of mass balance according to the stratigraphic system leads to closer agreement of \bar{c}_a and \bar{a}_a with winter and summer balance (Table 4.3). For Silvrettagletscher summer accumulation is a more important term than for Griesgletscher. On average 13 summer snow fall events per year (during June to Sept.) with >0.01 m w.e. accumulation occurred on Silvretta, compared to only 6 events per year on Gries. This may have contributed to the more moderate retreat of Silvrettagletscher during the study period (Fig. 4.7) due to an albedo feedback effect. The winter maximum of glacier mass is reached 10 days later on Silvretta than on Gries, indicating a shorter ablation period (Table 4.3).

We investigate the differences in net and winter balances evaluated according to the fixed date system, the measurement period and the stratigraphic system for all years analyzed of both glaciers. For 50% of the years the difference is within ± 0.1 m w.e. (Fig. 4.8a), and, thus, almost negligible. However, this range is exceeded in the other half of the years. Net balance determined in the measurement period may deviate by more than ± 0.5 m w.e. from that in the

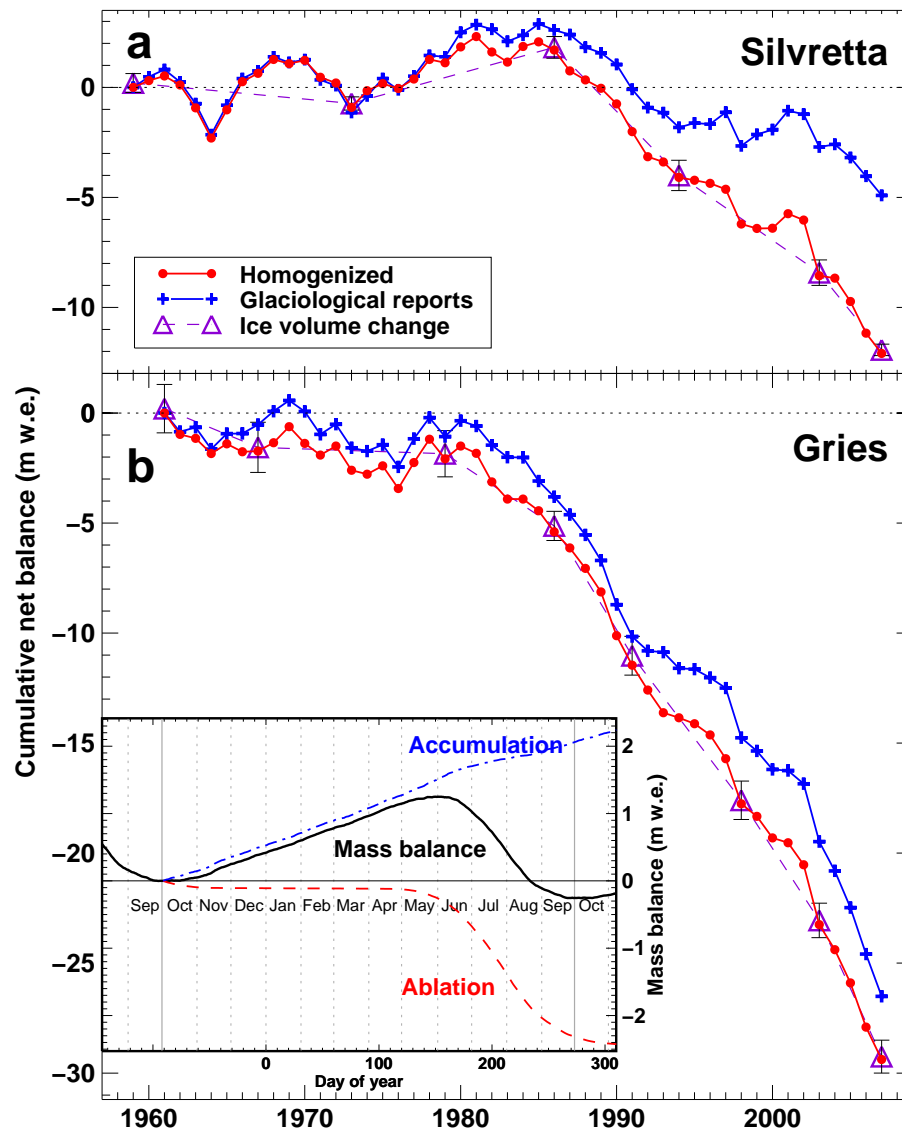


Figure 4.7: Cumulative mass balance time series of (a) Silvrettagletscher and (b) Griesgletscher. Note that the scales are the same. Error bars indicate the uncertainty of each DEM (triangles). The averaged annual course of mass balance quantities for Griesgletscher in 1961-2007 is displayed in the inset in (b).

hydrological year. Note that, over decadal periods the differences in net balance average out. Fixed date winter balance systematically underestimates the winter maximum of glacier mass (Fig. 4.8b); the stratigraphic winter balance is 0.26 m w.e. higher on average. Nevertheless, April 30 is proposed as termination of the fixed date winter balance, because melt starts to be important around this date (inset in Fig. 4.7b).

Table 4.3: Comparison of fixed date and stratigraphic winter and summer balances averaged over the entire study period to mean annual totals of accumulation (\bar{c}_a) and ablation (\bar{a}_a) in the hydrological year. Numbers in brackets give the percentage of the analyzed variable compared to \bar{c}_a and \bar{a}_a , respectively.

Glacier	\bar{c}_a	\bar{b}_w^{fix}	\bar{b}_w^{strat}	\bar{a}_a	\bar{b}_s^{fix}	\bar{b}_s^{strat}
Gries	1.80	1.23 (68%)	1.48 (82%)	-2.46	-1.88 (76%)	-2.13 (87%)
Silvretta	2.06	1.15 (56%)	1.48 (72%)	-2.32	-1.40 (60%)	-1.73 (75%)

Mean date of max. / min. glacier mass		
Gries	May 24	October 3
Silvretta	June 3	October 1

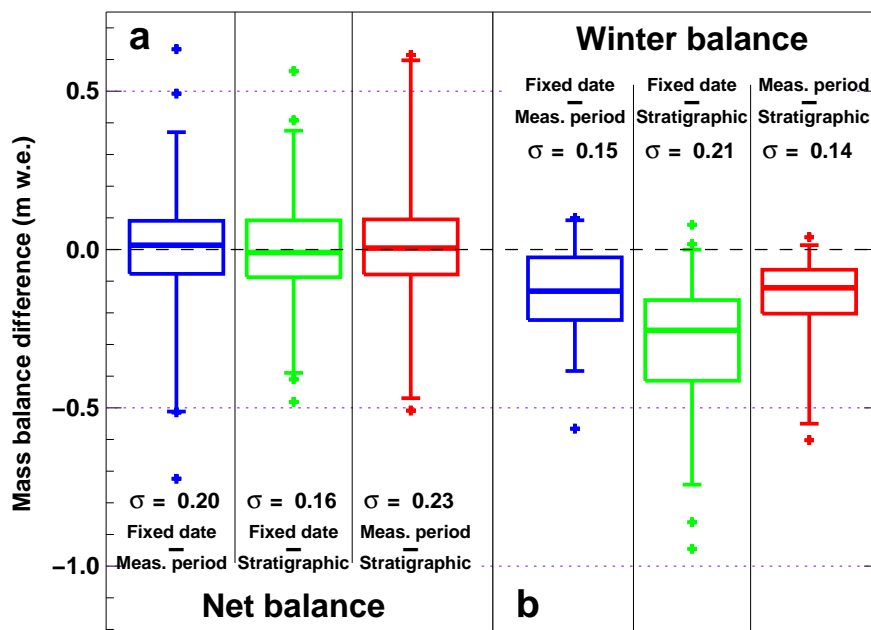


Figure 4.8: Comparison of mean specific (a) net balance and (b) winter balance according to different evaluation periods using boxplots. All years analyzed of both glaciers are included. The box ranges from the 25%-quantile to the 75%-quantile, the thick horizontal line represents the median. Vertical bars include 95% of the data points and outliers are marked with crosses. For each boxplot the standard deviation σ is given in m w.e.

4.5 Error analysis

Several studies have estimated the uncertainty in the determination of mass balance using the direct glaciological method as ± 0.2 m w.e. a^{-1} (Dyurgerov and Meier, 2002, and references therein). We separate five sources of errors contributing to the uncertainty in mean specific net balance:

1. Uncertainty in the net balance determination at individual stakes arises due to reading and reporting errors, uncertain snow or firn density, melt in of the stake, compaction of the firn layer, or refreezing of melt water (Müller and Kappenberger, 1991) and is estimated as $\sigma_{\text{stake}} = \pm 0.1$ m w.e. in the ablation area and ± 0.3 m w.e. in the accumulation area.
2. Mass balance often varies significantly on small spatial scales (some meters) due to ice surface roughness or differential accumulation due to snow drift. Thus, a point measurement may poorly represent its closest vicinity. In order to quantify this effect we scanned the data sets of both glaciers for measurements in the same year with distances of < 50 m from each other and elevation differences of < 5 m. We found standard deviations $\sigma_{\text{local}} = \pm 0.30$ m w.e. (Silvretta) and $\sigma_{\text{local}} = \pm 0.54$ m w.e. (Gries) of net balance at neighboring stakes.
3. Determining glacier wide mass balance from point data induces considerable uncertainty, which is difficult to estimate. Errors are due to (i) a non-representative distribution of stakes over the glacier surface, (ii) insufficient spatial density and (iii) inter- and extrapolation to unmeasured areas. We assessed the uncertainty due to these factors by computing and comparing mean specific net balance obtained with randomly reduced annual stake data sets and find $\sigma_{\text{int}} = \pm 0.12$ m w.e.
4. The effect of inaccurate glacier surface areas used for the mass balance calculation (Elsberg and others, 2001) was evaluated by comparing net balances referring to annually updated glacier areas or to the last DEM available. The uncertainty is small for both glaciers due to a high temporal coverage of the geodetic surveys ($\sigma_{\text{area}} = \pm 0.03$ m w.e.).
5. The evaluation of net balance in a measurement period system leads to variations of $\sigma_{\text{period}} = \pm 0.2$ m w.e. relative to a fixed date system (Fig. 4.8a).

Only some of these significant uncertainties in the determination of mass balance based on the direct glaciological method can be addressed in the homogenization process. Errors in individual stake measurements are difficult to detect and remain in the data set used for the re-analysis. Some obviously implausible data points were discarded (about 1%). Snow density is missing in some years and is assumed to correspond to the mean of all years with available data. The re-analysis cannot account for error source (2) as no information on the small scale variability in mass balance is available. We address (3) applying a mass balance model that accounts for the effects of aspect and wind drift and is assumed to reproduce the spatial pattern of mass balance more accurately than common interpolation algorithms. By annually updating the glacier surface area the errors due to (4) are corrected and the daily model accounts for varying evaluation periods (5).

We conservatively assume that σ_{local} includes the uncertainty in the stake measurements σ_{stake} and compute the annual uncertainty in the calculated mean specific net balance based on direct

observations as

$$\sigma_{\text{dir}} = \sqrt{\sigma_{\text{local}}^2 + \sigma_{\text{int}}^2} \quad (4.3)$$

As annual mass balance data are independent from each other (Cogley and Adams, 1998) the uncertainty in an n -year record is $\sigma_{\text{dir}}^{\text{sample}} = \sigma_{\text{dir}}/\sqrt{n}$ and ranges from 0.09-0.28 m w.e. a⁻¹ (Table 4.4).

The uncertainty in the geodetic method is given by four principal error sources:

1. The orientation and the geolocation of the individual aerial photographs is the most important. An error of ± 0.2 - 0.5 m is estimated by comparing photogrammetric measurements with 10 to 20 georeferenced ground control points.
2. The elevation information for single points can be retrieved with an accuracy of ± 0.1 m in the ablation zone and ± 0.3 m in the area of low contrast (McGlone and others, 2004). As this error is randomly distributed its contribution to the total uncertainty is reduced to ± 0.01 m (Thibert and others, in press).
3. The interpolation to unmeasured grid points induces an uncertainty of between ± 0.05 - 0.5 m depending on the spatial coverage of the photogrammetrical analysis (Bauder and others, 2007).
4. A considerable uncertainty of $\pm 6\%$ (Sapiano and others, 1998) arises due to the unknown density for the conversion of the change in ice or firn volume to a mass change (Krimmel, 1999). During periods of growing or decreasing firn thickness Sorge's law (Bader, 1954) assuming a constant density profile in the accumulation area may not be valid. Thus, the density used for the conversion would have to be adapted according to the changes in the depth-density profiles, which are unavailable during the study period.

Error sources (1)-(3) depend on the quality of the DEM production and (4) is proportional to the magnitude of the volume change. Our homogenization procedure distributes the misfit of glaciological cumulative mass balance and geodetic mass change in each subperiod evenly over the years in the time interval Δt between two successive DEMs. Thus, it is possible to calculate the uncertainty σ_{geod} in the homogenized annual mass balance results due to errors in the geodetic mass change with

$$\sigma_{\text{geod}} = \sqrt{\overline{\Delta z}^2 \cdot \sigma_{\rho}^2 + \rho^2 \cdot \sigma_z^2} \quad (4.4)$$

where $\rho=850 \text{ kg m}^{-3}$ is the density used to convert ice volume to mass change and $\sigma_{\rho}=50 \text{ kg m}^{-3}$ the related uncertainty. $\overline{\Delta z}$ is the mean geodetic elevation change and

$$\sigma_z = \frac{1}{\Delta t} \sqrt{\sigma_{\text{DEM}_1}^2 + \sigma_{\text{DEM}_2}^2} \quad (4.5)$$

the related uncertainty depending on the accuracy of both DEMs (Table 4.4).

The error analysis shows that the uncertainty σ_{geod} due to errors in the geodetic mass change is significantly lower in all subperiods than the uncertainty in the direct glaciological method $\sigma_{\text{dir}}^{\text{sample}}$ (Table 4.4). Furthermore, there is a potential for additional systematic errors in the direct glaciological method, which are difficult to detect, e.g. substantial melt in of stakes in the accumulation area (resulting in too positive mass balance) or locally high accumulation rates

Table 4.4: *Error analysis for direct and geodetic mass balances in all DEM subperiods of Griesgletscher (G) and Silvrettagletscher (S). $\overline{\Delta z}$ is the mean geodetic elevation change and σ_z the related uncertainty due to DEM evaluation. σ_{geod} is the total annual uncertainty due to errors in the geodetic mass change. $\sigma_{\text{dir}}^{\text{sample}}$ is the uncertainty in the direct glaciological method. $\overline{\Delta b_n^{\text{stake}}}$ is the mean annual misfit of measured point net balances required to match geodetic mass change.*

Period	$\overline{\Delta z}$ mm a ⁻¹	σ_z	σ_{geod}	$\sigma_{\text{dir}}^{\text{sample}}$	$\overline{\Delta b_n^{\text{stake}}}$ mm w.e. a ⁻¹
G 1961-1967	-345	±117	±101	±226	-48
G 1967-1979	-27	±58	±50	±160	+57
G 1979-1986	-550	±83	±75	±210	-44
G 1986-1991	-1388	±84	±100	±248	-6
G 1991-1998	-1020	±54	±68	±210	-64
G 1998-2003	-1238	±104	±108	±248	-66
G 2003-2007	-1790	±126	±140	±277	+46
S 1959-1973	-78	±50	±43	±87	-18
S 1973-1986	+230	±44	±39	±90	-68
S 1986-1994	-854	±53	±62	±115	-68
S 1994-2003	-577	±51	±52	±108	-313
S 2003-2007	-1032	±98	±98	±162	-313

due to avalanche deposits. The geodetic method, in contrast, allows a thorough analysis of all its uncertainties, which is a major advantage. For these reasons, the use of geodetic mass changes is considered to be the best data source for detecting biases and homogenizing long term mass balance time series.

In most DEM subperiods cumulative mass balances obtained using the direct glaciological method correspond reasonably well with the geodetic mass changes (Fig. 4.7).

$$\overline{\Delta b_n^{\text{stake}}} = \frac{1}{m} \sum (b_n^{\text{hom}} - b_n^{\text{stake}}) \quad (4.6)$$

is the mean annual misfit of net balances b_n^{stake} measured at m stakes required to match the homogenized point net balances b_n^{hom} that agree with the geodetic mass change. In general, $\overline{\Delta b_n^{\text{stake}}}$ is in the range of both $\sigma_{\text{dir}}^{\text{sample}}$ and σ_{geod} ; there is no bias and the methods agree well (Table 4.4). Since 1994, however, the mass balance of Silvrettagletscher determined based on the glaciological method is significantly too positive and needs to be corrected. We can only speculate about the reasons for this bias and attribute it to errors in accumulation measurements and a non-representative distribution of the stakes. The uncertainty in the final homogenized mean specific mass balance time series is equivalent to σ_{geod} (Table 4.4).

4.6 Conclusion

We presented a method for homogenizing time series of long term mass balance monitoring programs. A distributed mass balance model is used to resolve annual and seasonal mass balance measurements at a daily scale and to calculate spatial mass balance variations based on point measurements. The time series are corrected in order to match the independently determined density-corrected ice volume changes. Mass balance data with different characteristics

are combined; stake measurements provide high temporal resolution and altitudinal mass balance distribution, but have incomplete spatial coverage, whereas the geodetic data cover the entire glacier, but do not yield information on interannual variability. Our method further allows us to address the problem of varying evaluation periods, which have a significant impact on annual results and tend to blur the natural variability in mass balance. We derive homogenized and complete time series of seasonal mass balance of two alpine glaciers for fixed time periods and provide a comparable data basis for climate impact studies.

Geodetic mass changes are assumed to be most appropriate to detect biases in the direct glaciological method and are an indispensable prerequisite for a thorough homogenization of long term mass balance time series. Re-analysis requires a variety of meta-information (dates of the field surveys, location of the measured stakes etc.), which was often not systematically reported in the past. We strongly suggest gathering all information available and to document not only final mass balance results, but also raw data. The homogenization procedure presented is recommended in comprehensive mass balance monitoring programs of alpine glaciers for re-analysis of the previous data series and as a tool for current evaluation of the glacier wide mass balance.

Acknowledgments

This work is supported by ETH Research Grant TH-17 06-1. The weather data were recorded by MeteoSchweiz. The effort of previous researchers measuring mass balance is gratefully acknowledged. Swisstopo was responsible for the aerial photograph surveys. H. Bösch established DEMs from aerial photographs. R. Hock provided an important contribution to the development of the mass balance model. We thank the scientific editor A. G. Fountain, an anonymous reviewer and J. G. Cogley for helpful comments that improved the clarity of the paper.

Part II

Applications to glacier hydrology and Arctic regions

Chapter 5

Glacier-dammed lake outburst events of Gornersee, Switzerland

MATTHIAS HUSS,¹ ANDREAS BAUDER,¹ MAURO WERDER,¹
MARTIN FUNK,¹ REGINE HOCK^{2,3}

¹Versuchsanstalt für Wasserbau, Hydrologie und Glaziologie (VAW), ETH Zürich, 8092 Zürich, Switzerland

²Department of Earth Sciences, Uppsala University, 75236 Uppsala, Sweden

³Geophysical Institute, University of Alaska Fairbanks, Alaska 99775-7320

Published, Journal of Glaciology

Citation: Huss M., A. Bauder, M. Werder, M. Funk and R. Hock (2007). Glacier-dammed lake outburst events of Gornersee, Switzerland. *Journal of Glaciology*, **53**(181), 189–200.

ABSTRACT: Gornersee is an ice marginal lake, which drains almost every year sub-glacially within a few days. We present an analysis of the lake outburst events between 1950 and 2005, as well as results of detailed field investigations related to the lake drainage in 2004 and 2005. The latter included measurements of lake geometry, water pressure in nearby boreholes, and glacier surface motion. A distributed temperature-index melt model coupled to a linear-reservoir runoff model is used to calculate hourly discharge from the catchment of Gornergletscher in order to distinguish between the melt-precipitation component and the outburst component of the discharge hydrograph. In this way, drainage volume and timing are determined. There is a clear trend since 1950 for the outburst flood to occur earlier in the melt season, though lacking any relation to lake discharge volumes. Peak discharges from the lake lie significantly below the values obtained with the empirical relation proposed by Clague and Mathews (1973). The shapes of the 2004 and 2005 lake outflow hydrographs differ substantially, thereby suggesting different drainage mechanisms. From water balance considerations we infer a leakage of the glacier-dammed lake starting one week prior to the lake outburst in 2005. During the drainage events up to 50% of lake water is temporarily stored in the glacial system causing substantial uplifts of the glacier surface.

5.1 Introduction

Glacier-dammed lakes can release their water suddenly causing a so-called outburst flood or 'jökulhlaup' (e.g. Björnsson, 1998). They represent a severe threat in many mountain ranges and have caused major destruction in historical time (e.g. Haeberli, 1983; Richardson and Reynolds, 2000; Björnsson, 2002; Raymond and others, 2003). Discharge at the glacier tongue may increase by more than one order of magnitude (e.g. Björnsson, 1992). High water pressure gives rise to extensive perturbations of the glacial drainage system and of the dynamics of the ice mass (Röthlisberger and Lang, 1987).

Glacier outburst floods have been addressed empirically and theoretically. Clague and Mathews (1973) proposed a widely known empirical relation to predict peak discharge, indicative for the hazard potential, from lake volume. Further studies elaborated on this relation (Costa, 1988; Walder and Costa, 1996; Ng and Björnsson, 2003). Theory postulates that the drainage of glacier-dammed lakes can be controlled by two different processes: Firstly, the classical Röthlisberger-channel enlargement (Röthlisberger, 1972; Nye, 1976), inducing a gradually rising limb of the hydrograph; and, secondly, flotation of the ice dam, producing a sharp and sudden runoff peak (e.g. Flowers and others, 2004). Based on these theories many attempts have been made to simulate glacier-dammed lake outburst events numerically (e.g. Nye, 1976; Spring and Hutter, 1981; Clarke, 1982, 2003; Flowers and others, 2004). Only few theories exist focusing on the initiation of the drainage (e.g. Fowler, 1999).

Data about glacier-dammed lake outbursts are sparse and the understanding is still incomplete owing to the complex nature of these events. Many of the processes involved are only partially known. Exceptional data sets exist for Grímsvötn, Iceland (Björnsson, 1988, 1998, 2002) and Hidden Creek Lake, Kennicott Glacier, Alaska (Anderson and others, 2003, 2005; Walder and others, 2005, 2006). The project on Gornergletscher presented in this paper is the first integrated study of a lake outburst event in the Alps (Sugiyama and others, 2007b).

Our project investigates the outburst events of an ice-marginal lake, Gornersee, that forms annually in spring and drains in summer. The present study deals with the hydrological part of the outbursts. Various studies have been carried out on Gornergletscher focusing on glacial hydrology (Röthlisberger, 1972; Elliston, 1973; Collins, 1979; Aschwanden and Leibundgut, 1982; Collins, 1986; Iken and others, 1996). Gornergletscher is particularly suited for an hydrological study of glacier dammed-lake outburst events due to the long time-series of discharge measurements at the terminus of more than three decades and the long-term climate records available in the vicinity. Additionally, observations of lake drainage by Bezinge and others (1973) in the 1950s and 1960s provide the possibility of an assessment of glacier floods over more than half a century.

The paper consists of two parts: Firstly, an analysis of the 50-year time series of the annual lake outburst events including trends in flood timing and drainage volume, and, secondly, an analysis of detailed field investigations performed in 2004 and 2005.

In order to separate the outburst component of the discharge hydrograph from the melt-precipitation component we perform a hydrograph separation using a coupled melt-runoff model (Hock, 1999). This is necessary for Gornergletscher since background discharge is relatively large during the outbursts. By calculating hourly discharge in the period 1970-2005 we are able to derive timing and drainage volume of the annual outburst events. Data of the extensive field campaigns in 2004 and 2005 allow an integrated investigation of the processes

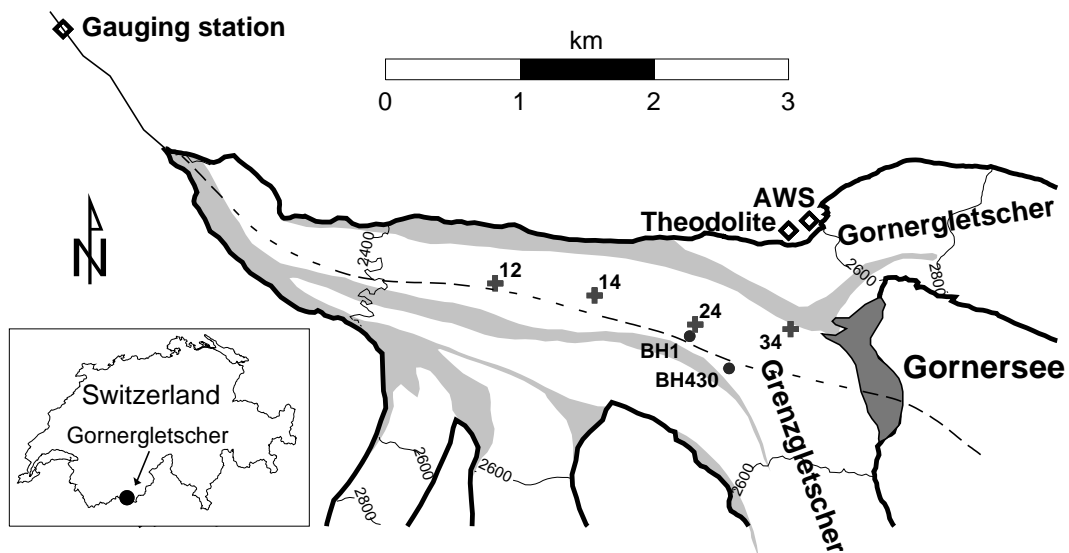


Figure 5.1: Map of the ablation area of Gornergletscher. Dots mark two boreholes and crosses indicate the position of four stakes for ice motion measurement. Debris-covered ice is grey-shaded. The central flowline used for the profiles in Figure 5.2 is dashed.

involved in the drainage event focusing on short time scales, thus providing a unique opportunity for a comprehensive study of glacier-dammed lake outbursts. For both years we compute the water volume impounded in the lake, the lake outflow and the drainage hydrograph at the glacier terminus. The hydrographs are interpreted with respect to water pressure records in boreholes and ice motion. We detect different initiation mechanisms of the glacier outburst flood and infer on water storage processes during the drainage event.

5.2 Field Site

Gornergletscher, Switzerland, is the second largest glacier in the Alps (Fig. 5.1). It consists of several tributaries and covers an area of nearly 60 km². The glacier spans an elevation range from 2200 to 4600 m a.s.l. Most parts of the glacial system are temperate. The main tributary, however, Grenzletscher, accumulates cold firn at altitudes higher than 4000 m a.s.l. (Suter, 2002). The cold ice reappears on the flat glacier tongue, which extends 5 km further downstream from the lake, causing a polythermal regime (Haeberli, 1976). Radio-echo soundings and borehole temperature measurements indicate that the base of the glacier is temperate, thus not inhibiting water flow (personal communication from O. Eisen, 2006). The maximum ice thickness is 450 m (Huss, 2005) and the main glacial valley is slightly overdeepened (Fig. 5.2b).

Gornersee is situated in a deep basin at the confluence of two tributaries (Figs. 5.1 and 5.2). Significant changes of glacier geometry during the last century caused shifts in lake location and volume (Fig. 5.2a). The lake usually starts to fill in May and drains annually between June and August (Bezinge and others, 1973). Each year $1\text{--}5 \times 10^6$ m³ of meltwater are impounded by the lake. Often, the lake is filled to the maximum level beyond which supraglacial outflow would occur at the start of the drainage. However, it has also been known to drain earlier (Bezinge and others, 1973; personal communication from H. Röthlisberger, 2005). In 2004 we observed a supraglacial outflow for a few days before water left the basin subglacially. The duration of the lake drainage varies between 2 and 7 days. The peak discharges during the

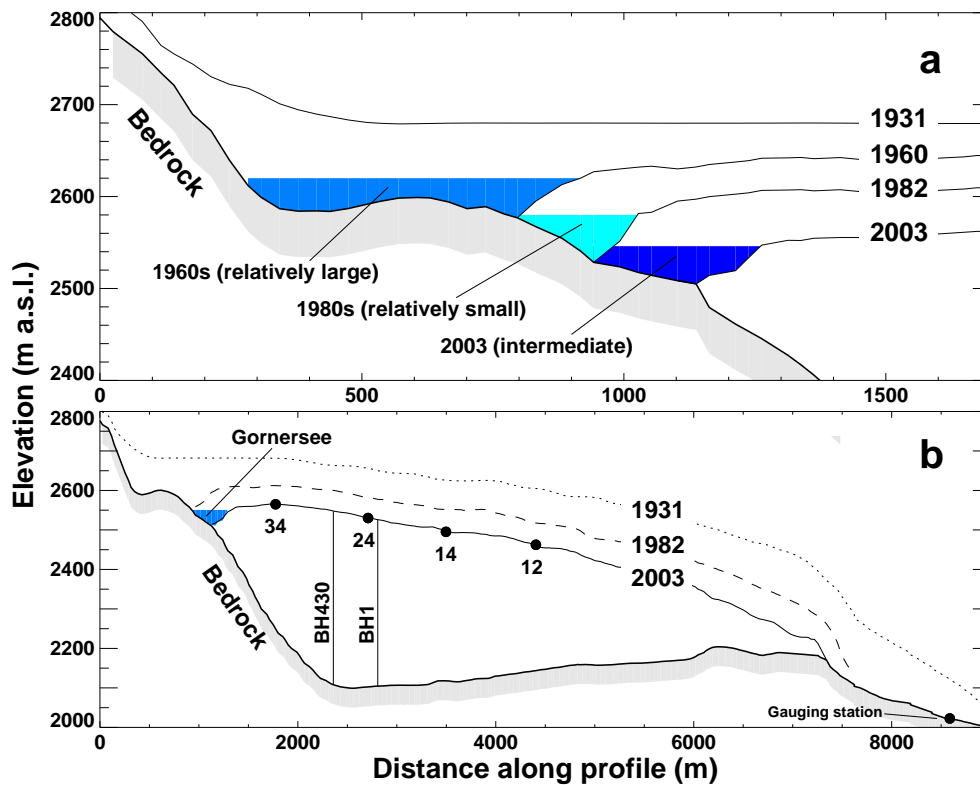


Figure 5.2: (a) Schematic profile of the evolution of Gornersee in the last decades. The glacier surface of 1931 is based on a digitized map of the official Swiss topographic survey, 1960 on an unpublished map by Wilhelm (1967), 1982 and 2003 on evaluated aerial photographs (Bauder and others, 2007). (b) Longitudinal profile of the tongue of Gornergletscher. Bed topography is obtained from radio-echo sounding. Two boreholes and four stake locations are indicated.

outburst events measured at the glacier terminus reach 20 to $50 \text{ m}^3 \text{ s}^{-1}$, of which (as calculated in this study) 40 - 75% is lake water. In the first half of the 20th century flood intensities of more than $100 \text{ m}^3 \text{ s}^{-1}$ were reported, regularly causing severe damage in the valley of Zermatt (Raymond and others, 2003).

5.3 Field Campaigns and Methods

Data collection and field methods

A gauging station operated by Grande Dixence hydropower company is situated 1 km from the glacier snout, recording hourly discharge since 1970 (Fig. 5.1). Long-term climate data since 1982 is provided at hourly resolution by the weather station of MeteoSchweiz, Zermatt, 1638 m a.s.l, 5 km from the glacier terminus. For the period 1970-1981 we used subdaily data from a weather station at Grächen, 1550 m a.s.l, 25 km downvalley from Gornergletscher. During the field studies in 2004 and 2005 we operated an automatic weather station (AWS), 2650 m a.s.l, that measured ventilated air temperature and precipitation at 30 min intervals at the northern margin of Gornergletscher (Fig. 5.1). A network of up to 30 stakes was maintained and ablation readings were taken at intervals of one to three weeks. In April 2004, the

water equivalent of the snow cover was determined at several positions. An automatic camera on Gornergrat provides daily photographs to map the extent of snow cover and monitor the lake evolution. Digital elevation models (DEMs) of the glacier surface topography were derived from aerial photographs for 1982, 2003, 2004 and 2005 (Bauder and others, 2007). We installed pressure transducers in the lake in 2004 and 2005, recording the water depth every 10 minutes. Surface ice motion was continuously monitored both by differential GPS at 3 h-intervals, and a theodolite surveying 30 stakes hourly providing a distributed picture of ice motion. In both years we drilled several boreholes to the glacier bed using a hot water drilling system. In the boreholes, we recorded water pressure, englacial temperature, and conducted measurements of vertical strain with magnetic rings. Tracer injections were carried out and seismic activity was monitored.

Hydrograph separation

The discharge of lake outburst events is superimposed on melt-precipitation induced runoff variations. Since the latter, in contrast to other previous studies (e.g. Björnsson, 1998; Anderson and others, 2003) is not negligible in case of the Gornersee outburst floods it is indispensable to conduct a hydrograph separation. We apply a distributed temperature-index melt model coupled to a linear-reservoir runoff model (Hock, 1999) to compute hourly discharge from the catchment of Gornergletscher. The model and its calibration are described in the Appendix. By subtracting simulated melt-precipitation induced discharge from discharge measured at the gauging station we extract the outburst component of the hydrograph (Fig. 5.3).

The analysis of the drainage events of Gornersee includes two stages: Firstly, discharge in all years with available runoff data (1970-2005) was simulated using the calibrated melt-runoff model. Thus, based on the difference between measured and modeled discharge, the timing of the drainage event could be identified for every year of the 35-year period considered. Secondly, the model was re-calibrated for every year over a period of 25 days around the drainage event. An initial snow cover for this reduced period was generated with a model run starting in October of the previous year providing information about hibernal snow accumulation. By re-calibrating the model, an individual parameter combination was found for each year that maximized agreement between modeled and measured discharge before, after and, thus, presumably during the outburst. This enables the determination of outburst volume, peak lake discharge, timing and flood duration with optimal accuracy. Estimates of drainage volume and timing between 1950 and 1970 by Bezingue and others (1973) were connected with our new 35-year data series.

The measured and simulated quantities have two sources of uncertainty: (1) errors in the runoff measurements (estimated as $\pm 5\%$) and (2) modeling uncertainties. The accuracy of the model is difficult to judge during the outburst floods as no experimental validation is possible in this period. Therefore, the potential errors were estimated arbitrarily for every year mainly based on model performance before and after the outburst event. The occurrence of heavy rainfall events during the flood influences the quality of the model results in a negative way and were also considered. We come up with an error of between $\pm 5\text{-}30\%$ of both drainage volume and peak lake discharge for individual years.

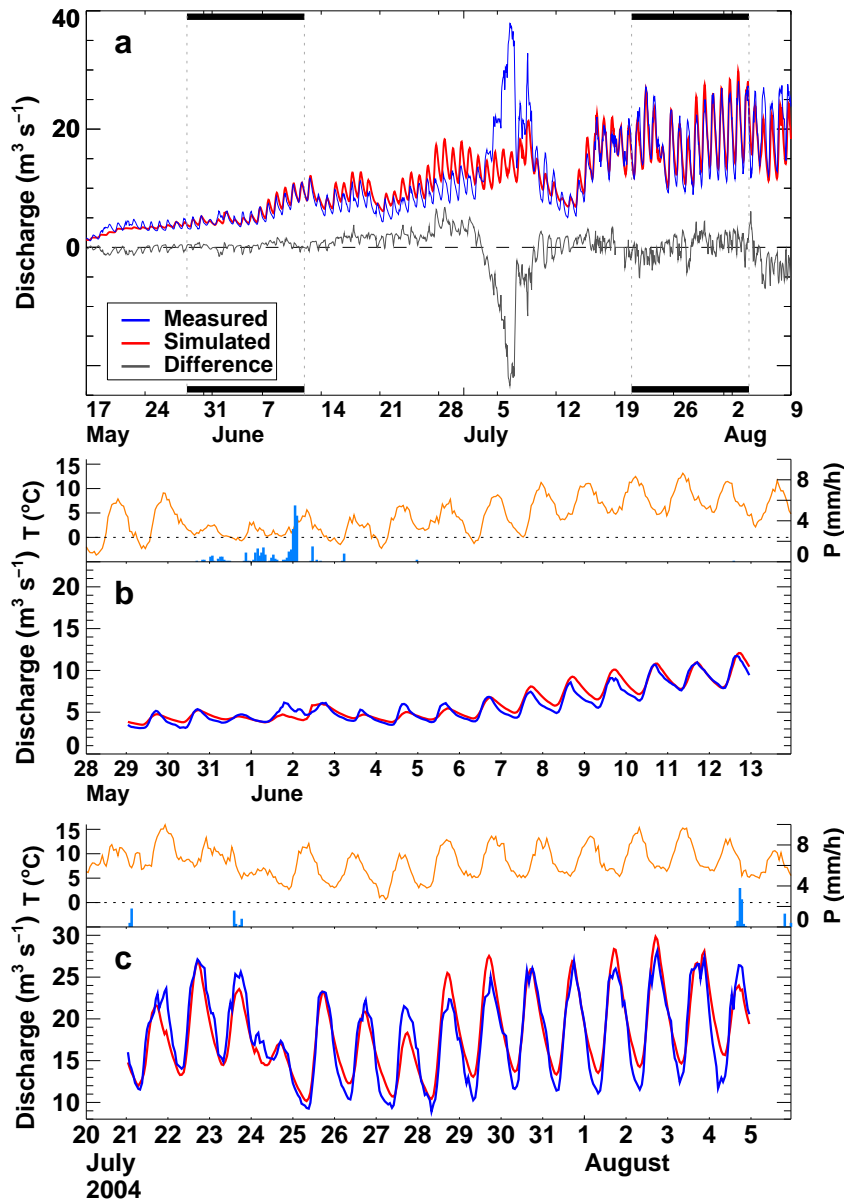


Figure 5.3: (a) Measured and simulated hourly discharge of Gornergletscher during summer 2004. The lake drainage event is eye-catching. Periods marked with bars are shown in detail in sub-figures (b) and (c). Temperature (T) and precipitation (P) are shown for comparison.

Lake bathymetry and meltwater input

As a more extended data base exists for 2004 and 2005, we are able to determine the bathymetry of the lake basin from highly resolved digital elevation models derived from aerial photographs taken right after the drainage for both years. By combining lake level measurements and bathymetry we calculate lake volume. Errors may arise due to floating icebergs or partial flotation of the ice dam. These uncertainties are minor and are not incorporated in the computation. They contribute to an estimated uncertainty of lake volume of $\pm 5\%$.

For water balance considerations we simulate the meltwater input into the lake for the pre-drainage periods of 2004 and 2005 with the melt-runoff model (see Appendix). The catchment basin of the glacier-dammed lake has an extent of 8.6 km^2 . We define it as the surface watershed. To model runoff from the lake catchment basin we use the parameters calibrated for the entire

glacial system.

5.4 Results

Lake outburst events 1950-2005

Since 1970 we identified significant drainage events in every year except for 1984, 1991 and 1995. Figure 5.4a presents the evolution of the lake outburst timing showing an obvious trend. Between 1950 and 2005 a shift of about two months has been observed, moving the expected date of the event from late August to late June. In contrast, the temporal evolution of drainage volume does not show a uniform trend. In addition to the year-to-year variability, long-term fluctuations of drainage volumes also occurred (Fig. 5.4b). Since only very limited direct observations exist in the past, we do not know to what extent the volume fluctuations are caused by changing lake basin geometry or different filling levels of the lake.

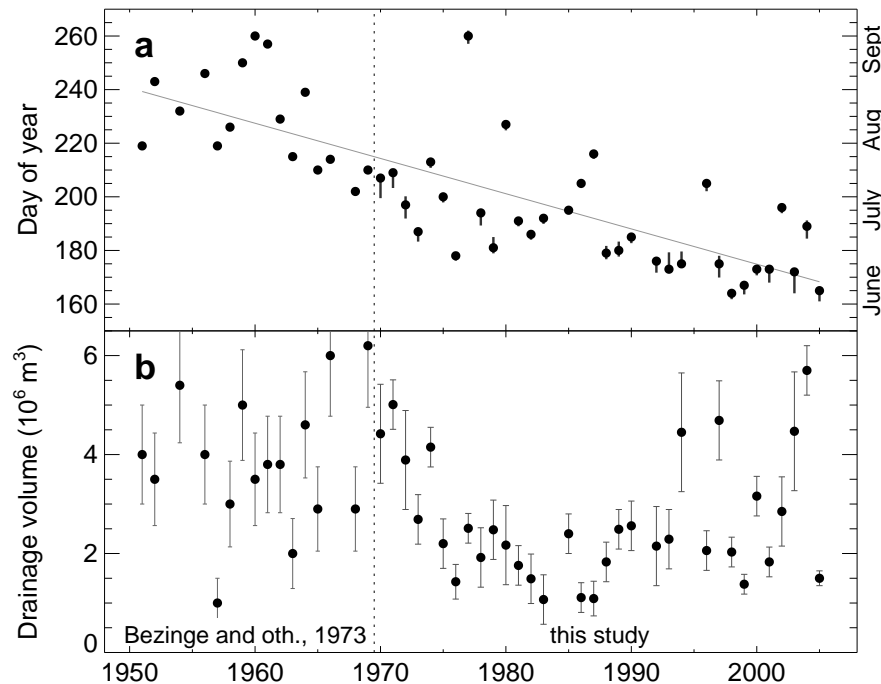


Figure 5.4: (a) Evolution of lake outburst timing. The dots correspond to the date of the peak discharge. In 1984, 1991 and 1995 no drainage events could be found. Vertical bars (after 1970) show the duration of the drainage event. (b) Evolution of drainage volume. Error bars indicate the uncertainty range of the calculated values.

We find a power-law relation between peak lake discharge Q_{\max} ($\text{m}^3 \text{s}^{-1}$) and drained volume V (10^6 m^3) as proposed by Clague and Mathews (1973) in the form of

$$Q_{\max} = k \cdot V^b \quad (r^2 = 0.61, n = 33) \quad (5.1)$$

with constant $k=10$ and exponent $b=2/3$ yielding the best fit for the drainage events of Gornerssee. Considering the range of drainage volumes involved, which is much lower than in previous studies (Clague and Mathews, 1973; Walder and Costa, 1996), the two variables show a strong

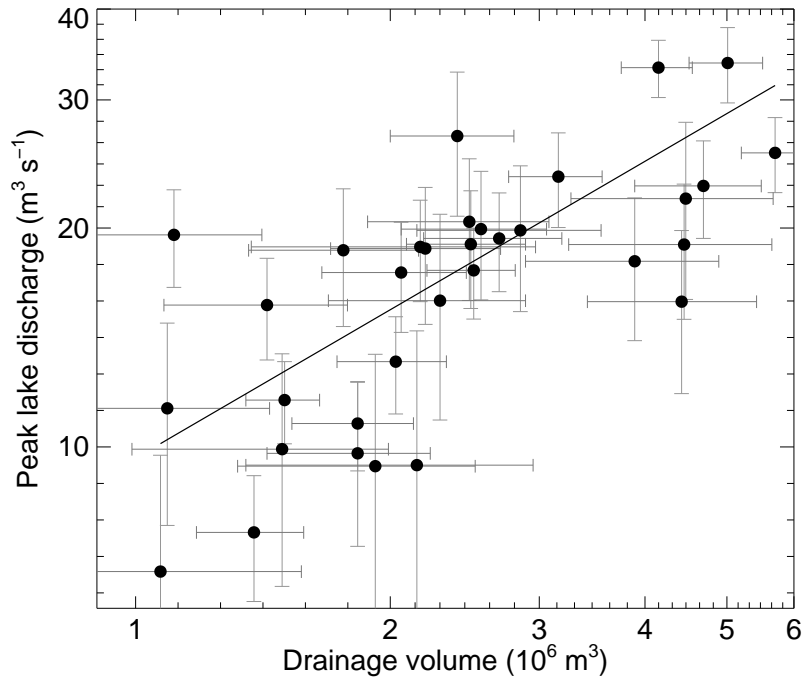


Figure 5.5: Log-log-plot of drainage volumes and peak lake discharges for the outburst events 1970-2005. The relation $Q_{\max} \sim V^{2/3}$ is given corresponding to the Clague-Mathews formula with a constant of $k=10$ ($r^2=0.61$, $n=33$).

correlation (Fig. 5.5). The peak lake discharges of the analyzed drainage events of Gornerssee are lower than those predicted by the Clague-Mathews relation. However, the proportionality $Q_{\max} \sim V^{2/3}$ seems applicable to Gornerssee.

Outburst events 2004 and 2005

Lake filling

The glacier-dammed lake reached a maximum volume of $4 \pm 0.2 \times 10^6 \text{ m}^3$ in 2004 and $1.3 \pm 0.1 \times 10^6 \text{ m}^3$ in 2005. The maximum water volume stored in the lake varies strongly between both years although the lake basin size was nearly the same. In 2004, the cumulative modeled lake input and the measurements of lake volume agree well (Fig. 5.6). In 2005 the simulated cumulative meltwater input matches the measured lake volume well until 2 June. Afterwards lake volume rises at a slower rate (Fig. 5.6). Based on these considerations we suggest that a leak be opened one week prior to the beginning of the lake outburst in 2005.

Lake outflow and river flood hydrographs

In this section we analyze two types of hydrographs. The *lake outflow hydrograph* describes the discharge from the lake and the *river flood hydrograph* refers to the discharge at the glacier terminus that solely results from the outburst. The hydrographs are defined as:

$$Q_{\text{lake outflow}} = Q_{\text{modeled lake inflow}} - \frac{dV_{\text{lake}}}{dt} \quad (5.2)$$

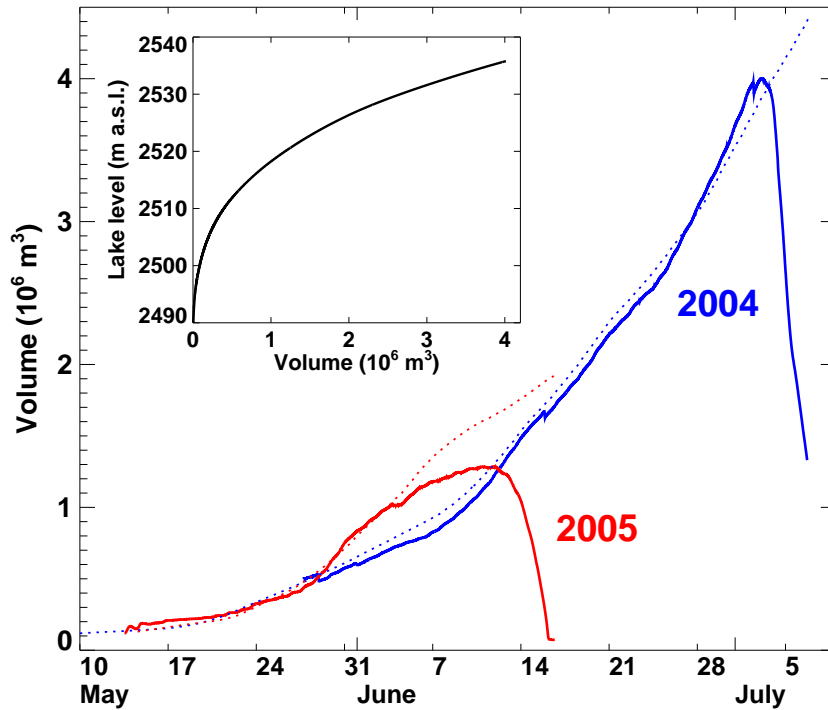


Figure 5.6: Temporal evolution of water volume stored in Gornersee in 2004 and 2005 (solid lines). Dotted lines correspond to the cumulative modeled input of meltwater into the lake basin. The hypsometric relation between lake level and water volume in 2004 is shown in the inset.

$$Q_{\text{river flood}} = Q_{\text{measured}} - Q_{\text{simulated}} \quad (5.3)$$

Comparison of the hydrographs provides information about the modification of the flood wave during its passage through the glacial system. Unfortunately, in 2004 an iceberg buried the pressure transducer in the lake four days after the initiation of the outburst and terminated the measurement.

As shown in Figure 5.7d, the lake outflow hydrographs for 2004 and 2005 display significantly differing shapes. In 2004 a rapid rise of lake outflow is observed, reaching its peak two days after the start. In contrast, the drainage event in 2005 is characterized by a progressive increase of lake outflow followed by an abrupt termination. Furthermore, the lake outflow hydrograph reveals fluctuations with amplitudes of $\approx 1 \text{ m}^3 \text{ s}^{-1}$ (Fig. 5.7d, right). They reach their maxima in morning and their minima in afternoon, behaving anticyclicly to water pressure in the glacial system. The lake outflow peaks at $17 \text{ m}^3 \text{ s}^{-1}$ in 2004 and at $10 \text{ m}^3 \text{ s}^{-1}$ in 2005.

In 2004 and 2005, runoff at the glacier terminus before and after the drainage event is modeled well (Fig. 5.7b). By integrating the river flood hydrograph a drainage volume of $5.7 \pm 0.5 \times 10^6 \text{ m}^3$ is determined for 2004, which differs by $1.7 \times 10^6 \text{ m}^3$ from the lake volume derived from bathymetry. The flood duration was 7 days. The peak discharge at the glacier terminus was $38 \text{ m}^3 \text{ s}^{-1}$, of which $25 \pm 3 \text{ m}^3 \text{ s}^{-1}$ did not originate from surface melt or precipitation (Fig. 5.7e, left). Unlike the lake outflow hydrograph, the river flood hydrograph increases over a time span of almost five days and culminates three days after the maximum of lake outflow. This indicates a significant internal storage of lake water in the glacier. The main part of the flood ends with a sudden drop in runoff. However, for two days after the apparent termination of the drainage event, discharge still remains significantly greater than explainable by melt and rainfall processes (Fig. 5.7b, left).

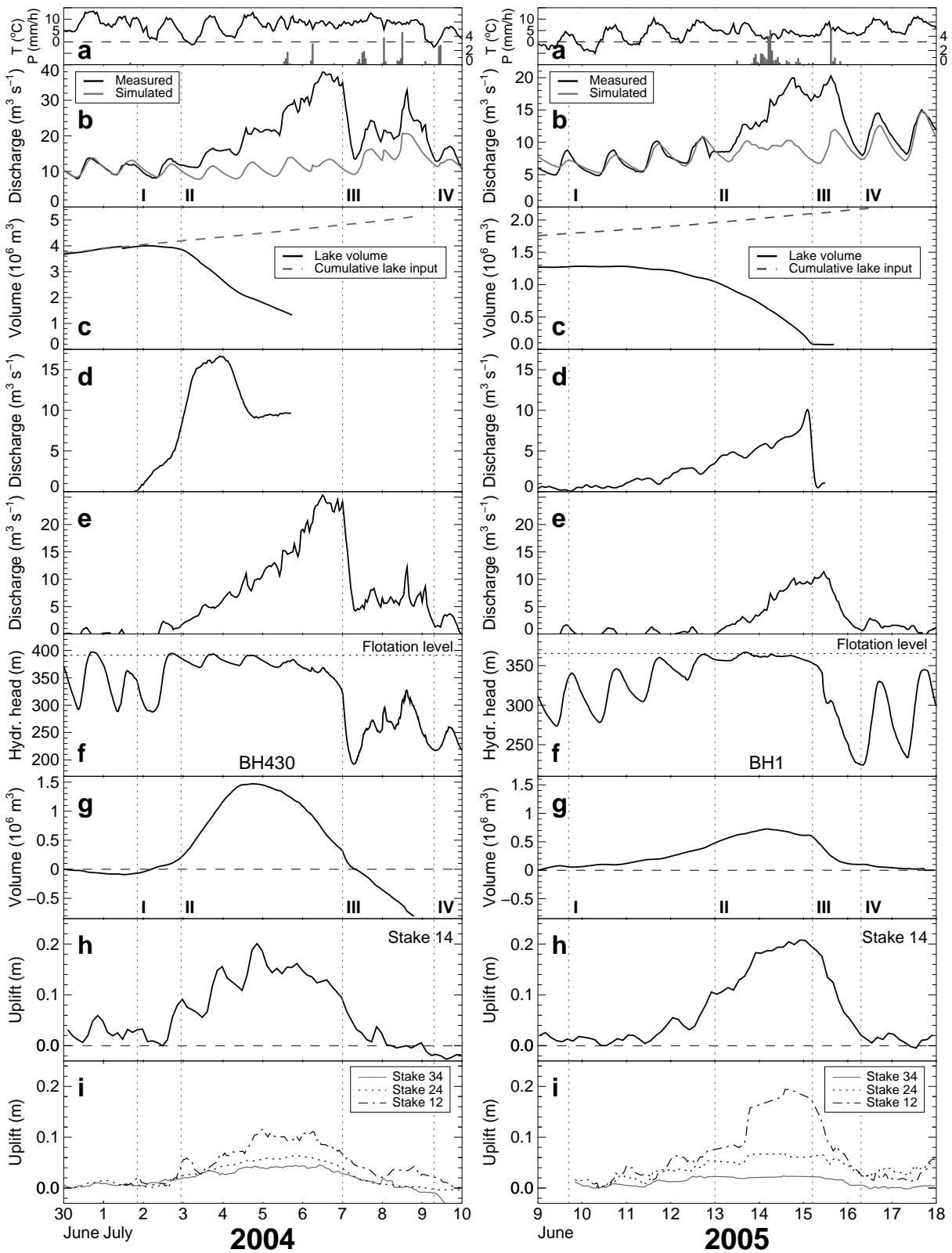


Figure 5.7: Compilation of measurements and simulations around the drainage events of 2004 (left) and 2005 (right). (a) Temperature (T) and precipitation (P), (b) measured and simulated discharge at the gauging station, (c) measured and simulated lake volume, (d) lake outflow hydrograph, (e) river flood hydrograph, (f) water pressure in a borehole (BH430, BH1) reaching the glacier bed, (g) sub- or englacially stored lake water, (h) uplift of glacier surface at stake 14 (GPS measurement), (i) uplift of glacier surface at stakes 34, 24 and 12 surveyed by theodolite. Note that for sub-figures b, c and f the scales differ between 2004 and 2005. All data except the GPS measurements (3-hourly) have hourly resolution. Thin vertical lines in all sub-figures correspond to the start of lake outflow (I), the arrival of lake water at the tongue (II), the culmination of the flood (III) and its termination (IV).

In 2005, we determined a drainage volume of $1.5 \pm 0.2 \times 10^6 \text{ m}^3$ over a period of 5 days. The peak discharge was $20 \text{ m}^3 \text{ s}^{-1}$ with a contribution of $12 \pm 1.5 \text{ m}^3 \text{ s}^{-1}$ from the lake. The flood at the glacier terminus starts more than three days after the onset of lake evacuation and culminates within 2.5 days (Fig. 5.7e, right).

The temporal evolution of lake water storage in the glacial system is determined from the cumulated difference between the lake outflow and the river flood hydrograph (Fig. 5.7g). In 2004 a fast accumulation of water in the glacial system is computed, reaching a maximum of $1.5 \times 10^6 \text{ m}^3$. The temporary storage of lake water amounts to $0.7 \times 10^6 \text{ m}^3$ in 2005. In 2004 a "negative storage" of $0.8 \times 10^6 \text{ m}^3$ results by the end of the glacier flood (Fig. 5.7d, e and g, left). This value lies beyond errors of the modeling procedure and the measurements and is due to the fact that the drainage volume is significantly larger than the lake volume. The negative storage implies that water stored previously to the drainage event in the glacial system is released. Such a process was not observed in 2005, when the temporary storage of lake water drops to zero by the end of the flood.

Water pressure and ice surface uplift

Water pressure is recorded in the boreholes BH430 and BH1 at distances of 1 km from the lake (Figs. 5.1 and 5.2). During the flood, water pressure remains close to flotation level in 2004 and 2005 with reduced diurnal amplitudes (Fig. 5.7f). The end of the lake drainage is marked in both years by a significant drop of 30-40% of the water column in the boreholes coinciding with a simultaneous decrease in discharge at the glacier terminus (Fig. 5.7e and f). After the flood, the diurnal minima of water pressure are significantly lower than before, indicating a more efficient drainage system.

Vertical uplift at stake 14 on the central flowline is measured by GPS and shows a clear signal during the flood event (Fig. 5.7h). The accuracy of the records is $\pm 0.3 \text{ cm}$ (Sugiyama and Gudmundsson, 2004). The glacier surface was lifted up by as much as 20 cm at this location compared to pre-drainage conditions. To show the spatial distribution of surface uplift we also present results of the theodolite survey at chosen stakes along the central flowline (Fig. 5.7i). Gudmundsson and others (2000) estimate an accuracy of $\pm 5 \text{ cm}$ for single data points in z-direction derived by theodolite. By filtering the error can be reduced to one third of this value. The ice motion data show that a glacier surface uplift of 2 to 20 cm occurred along the central flowline of Gornergletscher with a maximum at stake 14. An interesting aspect is the similar temporal evolution of the uplift curve (Fig. 5.7h and i) and the lake water storage in both 2004 and 2005 (Fig. 5.7g).

5.5 Discussion

Decadal trends

Analysis of the lake drainage events of Gornersee from 1950-2005 indicates trends in lake outburst timing and large variations in the drainage volume (Fig. 5.4). Several processes may be the cause for these findings. Rapid shrinkage of ice volume and glacier extent took place in recent decades due to climate change (Fig. 5.2b). An influence of these modifications of glacier

geometry on the lake drainage is likely. The position of Gornersee moved westwards out of a tributary valley accompanied by a decrease in ice thickness in the central parts of the glacier (Fig. 5.2a).

Timing of outburst

A shift in lake outburst timing of 70 days is observed since 1950 (Fig. 5.4a). We can only speculate about the driving factors of this significant trend. To investigate the possible influence of an earlier start of the melting season and thus earlier filling of the lake we conducted additional model simulations. They show a slight trend towards more melting in late spring and early summer. However, this change is only able to explain shifts in timing of some days.

For our calculations, the size of the lake catchment area was kept fixed for all years. It is probable that fluctuations in the extent of the catchment basin due to changes in glacier geometry occurred during the last decades. Assuming that the catchment basin remained at its current extent over the last 35 years, the results of the model simulations indicate that more meltwater was produced when the drainage event occurred than was in fact impounded in the lake at that time. Based on these findings we suggest that the catchment area of the lake has increased during the last three decades, causing an earlier filling of Gornersee. A contribution of this effect on the observed trend in the outburst timing is likely, but its relative importance is difficult to estimate.

The hydraulic gradient Δh is given by the elevation difference Δz (lake level - glacier terminus) divided by the length of the drainage path Δx . Δh dropped from 0.09 in 1950 to 0.07 in 2000. Clarke (2003) demonstrated a major influence of the location of the seal on timing as well as on magnitude of the flood. The changes in glacier geometry around the lake are considerable (Fig. 5.2a). Although we do not know the exact position of the seal for all past glacier geometries a shift may have occurred influencing the timing of the outburst event.

Drainage volume

A maximum of drainage volumes was observed in the early 1970s, whereas a significant minimum occurred in the 1980s (Fig. 5.4b). In the 1990s the data reveal a more variable pattern of flood magnitude than before with either quite large or small floods. There is no correlation between drainage volume and the timing of the lake outburst. The volume of the lake is subject to substantial long-term changes which are attributed to fluctuations in glacier geometry (Fig. 5.2a). For 1982 a potential lake basin size of about $2 \times 10^6 \text{ m}^3$ is determined from a digital elevation model. However, drainage volumes in the order of $6 \times 10^6 \text{ m}^3$ at the end of the 1960s suggest that a much greater amount could have been stored in the lake basin at that time, which is also supported by photographs and descriptions (Wilhelm, 1967; Bezingé and others, 1973). The glacier retreat in the last decade favored a rapid enlargement of the ice-marginal basin, mainly due to calving. We suspect that the geometry change in the lake basin cannot be the sole reason for the variations in drainage volume. In particular, the interannual fluctuations may be caused by different initiation mechanisms provoking the lake to drain subglacially, either partially filled (as observed in 2005) or after an antecedent supraglacial outflow (2004).

Volume – peak discharge relation

Several empirical studies confirmed the exponent $b=2/3$ for the power-law relation (Eq. 5.1) between Q_{\max} and V (Clague and Mathews, 1973; Costa, 1988; Desloges and others, 1989; Walder and Costa, 1996). The constant k varies between the studies from 46 to 113. These values originate from analysis of different lake systems and not multiple outbursts of one lake. Ng and Björnsson (2003) developed a theoretical approach to shed light on the background of the Clague-Mathews relation. For the incomplete drainage of Grímsvötn they predict an exponent b of 1-2, corresponding well with observations for the same lake (Björnsson, 1992). The exponent $b=2/3$ seems to be a combined result due to effects of different system size and geometry and the conditions at flood initiation (Ng and Björnsson, 2003).

Our relation between Q_{\max} and V satisfies the proportionality proposed by Clague and Mathews (1973) and is in line with the other empirical studies although we consider one single lake. However, bearing in mind the dramatic changes in both glacier and lake geometry in the last century, it is hardly possible to speak of the 'same' lake during the entire period (Fig. 5.2a). The peak discharges of Gornerssee are small compared to other lakes. k (Eq. 5.1) is nearly one order of magnitude lower than in the previous studies. This may be caused by the setting of Gornergletscher. The ice extending downstream of the lake has a thickness of more than 400 m and the bed is overdeepened. It is not known to what extent the polythermal character of the ice influences the lake outburst mechanism. Still, it remains puzzling that in the first half of the 19th century, much higher flood magnitudes – estimated indirectly from observations – were reported, although the lake basin was never significantly larger than it is at present (Wilhelm, 1967; Bezing and others, 1973).

By analyzing a 50-year time series of annual lake outburst events, the complexity and diversity of the jökulhlaup-system becomes evident. The data from 2004 and 2005 illustrate that the triggering mechanisms of an outburst event can be various for the same lake. The year-to-year variability in drainage volume in the last decades is remarkable.

Drainage events of 2004 and 2005

Initiation mechanisms

The data sets of 2004 and 2005 show some similarities as well as significant differences. The outburst events differ greatly in terms of lake volume, drainage volume, peak lake discharge (by a factor of 2 to 4) and timing. However, the patterns of water pressure fluctuations and ice motion on the central flowline of the glacier downstream of the lake are similar in both years (Fig. 5.7f, h and i). Also the river flood hydrographs at the glacier terminus exhibit a gradually rising limb and a sharp termination (Fig. 5.7e). In contrast, the lake outflow hydrographs differ remarkably, hinting at different initiation mechanisms of the floods. In 2005, a progressive increase in lake outflow (Fig. 5.7d, right) suggests a classical enlargement of R-channels as proposed by Nye (1976). On the other hand, the abrupt flood initiation in 2004 could indicate a temporary flotation of the ice dam near the lake. This claim is supported by the observation of short-term uplifts of the ice dam of up to three meters during the main drainage phase (Weiss, 2005).

Flowers and others (2004) present a model that simulates a drainage system in a subglacial water sheet feeding a nascent system in discrete channels. The lake outflow hydrograph of 2004

suggests similar processes (Fig. 5.7d, left). In a first stage of the drainage event, the ice dam was lifted, causing lake outflow to increase rapidly. The slight increase in lake outflow measured after the first culmination suggests a channel enlargement as a second phase of the lake drainage. Due to the breakdown of the pressure transducer in 2004, the further course of the lake outflow hydrograph is unknown. From the bathymetry, however, we know the water volume left in the lake basin at that time. The termination of lake water input into the glacial system coincides most probably with the rapid loss of hydraulic head at borehole BH430 (Fig. 5.7f, left). To evacuate the remaining lake water after the termination of the measurement a constant lake outflow would have to be $13 \pm 3 \text{ m}^3 \text{ s}^{-1}$ for the period without data. Thus, a second culmination of the lake outflow hydrograph (Fig. 5.7d, left) does not seem implausible.

Leakage of the lake

The start of the 2005 outburst event merits further comment. It was one of the earliest since 1950, starting when the lake was only filled to less than one third of its potential volume. After 2 June 2005, the time series for the measured lake volume and the cumulative simulated lake input diverge (Fig. 5.8b). In 2005 the discharge modeling was performed with the same parameters and boundary conditions as in 2004, when good agreement between model and field data was achieved. The simulated lake input from 2 June 2005 until the start of the lake drainage on 10 June is more than twice as great as the measured one. Inaccuracies in the runoff-modeling procedure are not able to explain this discrepancy. Two reasons could account for the divergence: Firstly, there is a slowly expanding leak in the dam of Gornersee; secondly, the subglacial drainage system has changed in such a way that the water no longer enters the lake, but benefits from new subglacial pathways directing the meltwater directly downglacier. Stagnations or drops in the lake level would support the hypothesis of a leak. In fact, the measured lake volume slightly decreases during nighttime in the days preceding the flood (inset in Fig. 5.8b). The leakage is very limited. It ceases almost completely during daytime and attains about $0.7 \text{ m}^3 \text{ s}^{-1}$ in periods of low water pressures in the glacial drainage system (inset in Fig. 5.8c). Model sensitivity tests showed that this observation is not an artefact of the melt-runoff model. For more than one week the leak does not grow substantially. On 10 June, lake outflow starts to increase over-night, provoking a progressive rise in the minimal water pressure at borehole BH430 (Fig. 5.8b and c).

In Figure 5.8b the water pressure recorded in borehole BH430 shows the transition of a 'winter drainage system' to a well developed 'summer drainage system' with pronounced diurnal amplitudes (Schuler and others, 2002). The position of the transition from an inefficient to an efficient drainage system slowly moves upglacier as is observed by dye tracing experiments (unpublished data, VAW/ETHZ). The transition at BH430 takes place two days before the melt-runoff model fails to explain the volume stored in the lake (Fig. 5.8b). It seems plausible that leakage starts once an efficient drainage system has developed close to the lake.

Internal water storage

Water storage plays an important role in glacial hydrology and is manifested in various processes (Schuler and others, 2002; Jansson and others, 2003). Storage of water in the glacial system can occur in subglacial cavities (e.g. Iken and others, 1996) or englacially in channels

or voids (e.g. Fountain and Walder, 1998). Drainage events of glacier-dammed lakes are excellent subjects to study water storage processes in glaciers as large perturbations of the drainage system occur.

Associated with the strong drainage event of 2004, we observe a period of enhanced runoff for two days after the abrupt drop in discharge forming a hydrograph "tail" (Fig. 5.7e, left). In this period a volume of approximately $1 \times 10^6 \text{ m}^3$ water is released that cannot be due to melt or rainfall. This value lies above the uncertainties of model and measurement. This feature may yield an explanation for the considerable difference between lake volume (determined by bathymetry of the lake basin) and drainage volume (integration of river flood hydrograph). We suggest that the additional water recorded at the glacier terminus during the flood results from water storage in the glacial system prior to the lake drainage event. Presumably, this water is released during the two days after the main phase of the outburst event, benefiting from the

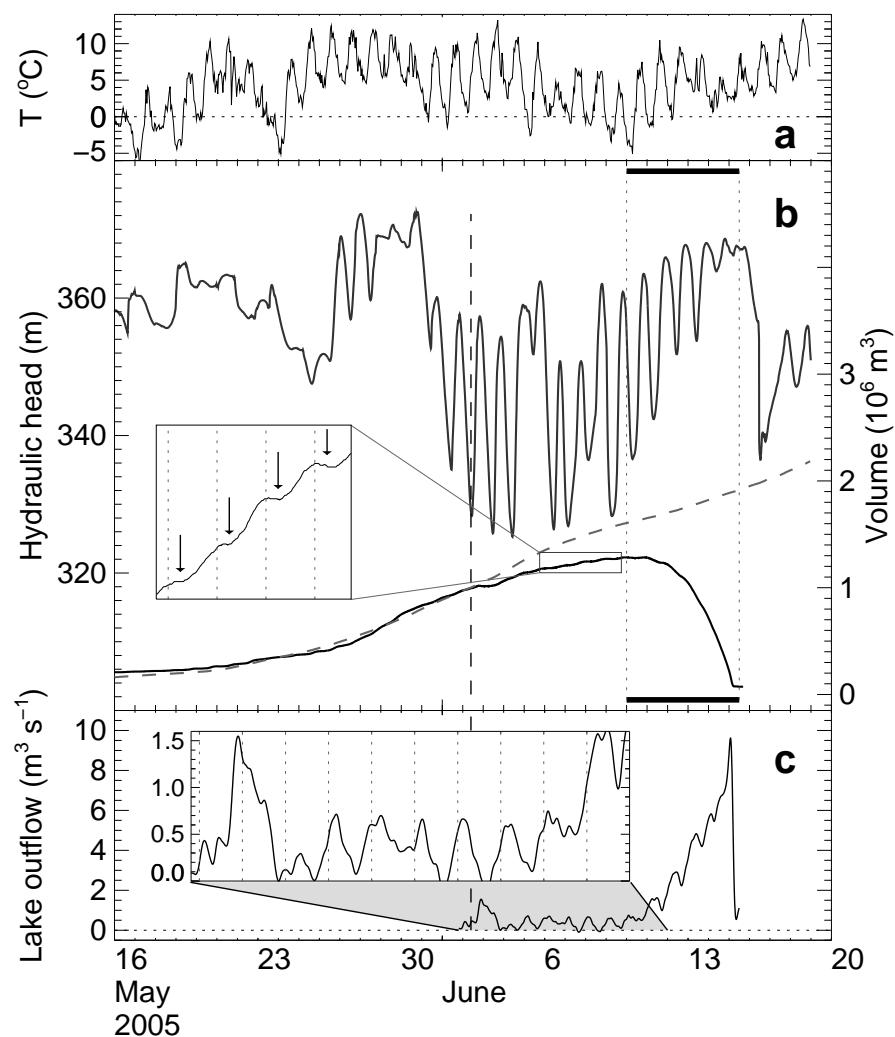


Figure 5.8: (a) Hourly air temperature at AWS. (b) Filling of the lake in 2005 in comparison with water pressure fluctuations in borehole BH430. The solid line indicates the measured evolution of lake volume and the dashed line the cumulative simulated melt in the lake catchment basin. Bars mark the timing of lake outflow. The inset shows the lake volume enlarged during the period of leakage. Thin vertical lines correspond to midnight. (c) Lake outflow hydrograph with the period of the leakage enlarged in the inset. Local outflow maxima occur between 3 and 6 a.m local standard time.

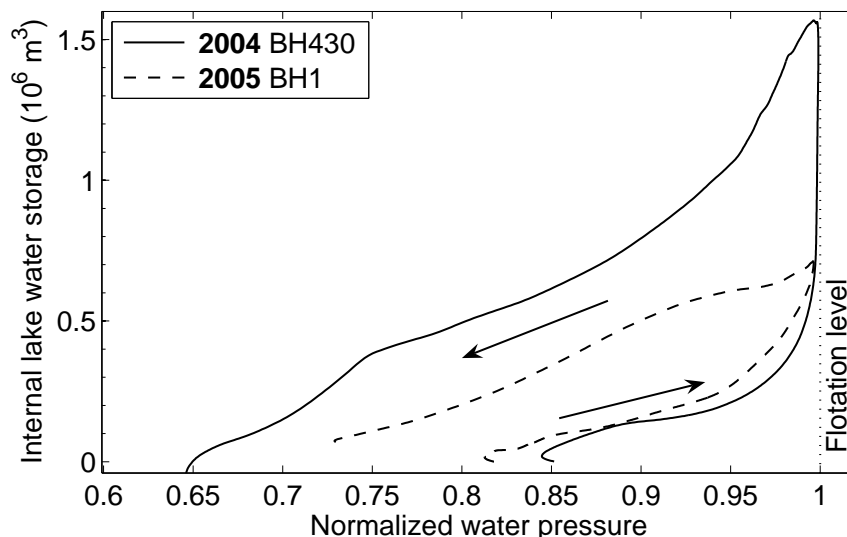


Figure 5.9: *Hysteresis of relationship between water pressure, normalized to flotation level, and en- and subglacial lake water storage for 2004 (solid) and 2005 (dashed line). Arrows indicate the direction of time.*

well-developed drainage pathways. Anderson and others (2003) report a similar hydrograph tail for Kennicott glacier, Alaska, and explained it with the presence of a floated part of the ice dam and its dampening effect with lower water pressures.

Compared to the total lake volume, temporary storage of lake water in the glacial system during the drainage event reaches fractions of 38% (2004) and 54% (2005), emphasizing the importance of this storage term. The uplifts of the glacier surface of up to 20 cm follow the evolution of the storage curve (Fig. 5.7g, h and i). Obviously, glacier surface uplift and lake water storage are closely related. When distributing the temporarily stored flood water uniformly over the total area downstream of the lake the storage water column corresponds to 35 cm in 2004 and to 17 cm in 2005.

Uplift of the glacier surface can be due to (i) vertical straining, (ii) sliding over an inclined bed or (iii) cavity formation at the bed (Sugiyama and Gudmundsson, 2004). The measurements of vertical strain show no stretching signal during the outburst events (unpublished data, VAW/ETHZ). The inclination of the bedrock underneath the tongue of Gornergletscher is small, thus (ii) is excluded. This leaves the cavity formation as responsible for the observed surface uplifts. The glacier surface elevation returns to its starting point after the termination of the flood, which supports our assumption.

In Figure 5.9 water pressures in BH430 (2004) and in BH1 (2005) are plotted normalized to flotation level pressure, versus en- and subglacial lake water storage. The pressure data is smoothed using a 24h -running mean. We obtain a hysteresis of storage that reveals some interesting aspects. The findings by Hubbard and others (1995) on Haut Glacier d’Arolla, Switzerland, help to interpret our observations. With a dense network of boreholes, they succeeded in showing two different pressure regimes at the glacier bed. Water pressure around an efficient drainage channel reacts immediately to external meltwater input, whereas the variations in hydraulic head decrease sideways. The hydraulic gradient between hydraulically well connected and unconnected parts of the glacier bed changes direction in the course of a day (Hubbard and others, 1995).

At the beginning of the drainage events in both 2004 and 2005, water level in a borehole, well connected to the main drainage system, increases abruptly as shown in Figure 5.9. Due to the limited amount of englacial voids in the zone of high water pressure, the potential to store water is minimal. However, the storage increases abruptly near overburden pressure. We attribute this to a partial detachment of the glacier from its bed, allowing the water to penetrate into subglacial cavities sideways from the main drainage channels. Thus, the pressure perturbations spread out into regions hydraulically unconnected with the efficient drainage system under normal conditions. Storage at the bed and in englacial voids in these parts of the glacier increases. The internal lake water storage increases by roughly $1 \times 10^6 \text{ m}^3$ in 2004, when the water column is at flotation level. In 2005 by contrast, the hydraulic head soon starts to decrease after reaching flotation level due to the smaller lake volume. The hysteresis curves have comparable slopes in 2004 and 2005. This indicates that similar processes contribute to internal storage in both years. However, the pressure perturbation seems to spread out over a wider range of the glacier in 2004.

More water is stored in the glacial system with decreasing than with increasing water pressures. After the end of lake water input, stored water slowly flows back from englacial voids and subglacial cavities into the main drainage system. Then, the pressure is lower than before the outburst event owing to the channel enlargement during flood conditions.

As discussed above, surface uplift is mainly due to cavity formation at the bed. The measured surface elevation changes during the outburst events are not sufficient to accommodate the sub- or englacially stored lake water, also given the unlikely assumption of a uniform distribution of lake water. We conclude that only parts of the stored water penetrated into subglacial cavities and that the rest is stored in englacial voids or in water pockets that are not detectable by measurements of ice motion.

The importance of englacial voids

Based on our data of glacier surface uplift subglacial storage alone cannot account for the additional water volume in the glacial system. Therefore, we attribute a particular importance to englacial voids. The volumetric content of englacial voids was quantified as 0.5% by Copland and others (1997) using borehole video methods in a temperate alpine glacier. Also on Gornergletscher we observed englacial voids and crevasses with a borehole video camera.

In this section we combine our data of water input into the glacial system (lake outflow hydrograph), water output (river flood hydrograph), glacier surface uplift, and water pressure records and attempt to estimate an integrated void ratio r_v for the ice downstream of the lake. r_v is

Table 5.1: *Estimated ranges of input data for the calculation of the void ratio r_v .*

Symbol	Range of values	Unit	Source
V_s	$0.7 \times 10^6 - 1.5 \times 10^6$	m^3	Hydrographs
Δz_s	0.05 – 0.2	m	GPS, Theodolite
Δh_b	20 – 100	m	Boreholes
A_a	$0.5 \times 10^6 - 5 \times 10^6$	m^2	DEM, Theodolite
r_v	$10^{-3} - 10^{-1}$	–	

defined as the ratio between the volume of englacial voids and the total ice volume, and is calculated as follows:

$$r_v = \frac{V_s}{\Delta h_b A_a} - \frac{\Delta z_s}{\Delta h_b}, \quad (5.4)$$

where V_s is the stored lake water volume, Δh_b the change of water column height, A_a the area of the glacier bed accessible to water storage, and Δz_s the glacier surface uplift. We estimated possible ranges for the values of all quantities. Whereas V_s is well known from the data, we cannot be sure about the representativity of the point based measurements for Δh_b and Δz_s . Δh_b is recorded in boreholes connected to the main drainage system. However, an important part of the storage seems to take place in hydraulically unconnected parts of the ice mass, as could be inferred from the hysteresis of storage (Fig. 5.9). There, smaller pressure variations Δh_b are expected (Hubbard and others, 1995). Δz_s is measured by GPS and theodolite in 2004 and 2005 (Fig. 5.7h and i). The amounts of uplift are not uniformly distributed and lie between 2 and 20 cm (Weiss, 2005). This demonstrates the inhomogeneity of surface elevation change in reaction to the flood. A quantity difficult to estimate is A_a . If we presume the drainage to take place in one or a few discrete drainage channels and the pressure perturbations spreading out from these, the accessible area A_a for water storage should be less than the total subglacial area downstream of the lake. We calculate the void ratio r_v for a reasonable range of input data (Tab. 5.1) and obtain a value of $r_v=0.1\% - 10\%$. Our estimates imply that the amount of englacial voids is not negligible.

5.6 Conclusions

This study investigates the annual drainage events of an ice-marginal lake, Gornersee, in detail. Using a distributed temperature-index model coupled to a linear-reservoir runoff model, we simulate glacial discharge due to melt and precipitation in hourly resolution. We can extract lake drainage hydrographs from measured runoff at the glacier terminus and determine outburst timing, lake volume and peak lake discharge.

Since 1950 the lake has been draining progressively earlier in the course of the year. The drainage volumes show remarkable long-term and interannual fluctuations. The relation between peak lake discharge and drainage volume follows the proportionality $Q_{\max} \sim V^{2/3}$ proposed by Clague and Mathews (1973), but exhibits a lower constant k leading to reduced runoff peaks during the flood events.

Extensive field measurements around the drainage events of 2004 and 2005 provide the data basis for an integrative assessment of the outburst of Gornersee. We detected two different drainage mechanisms, a temporary flotation of the ice dam in 2004 and the classical channel enlargement in 2005 after a leakage during eight days. Lake outflow hydrographs differ greatly between 2004 and 2005. During the passage of the flood wave through the glacier, however, these differences are blurred and a canonical drainage hydrograph is recorded at the tongue in both years. Water pressure and glacier surface motion show a close interrelation to the lake drainage characteristics. Temporary storage of lake water in the glacial system causes uplifts of up to 20 cm at the glacier surface with a similar temporal evolution. In 2004 a large amount of water stored sub- or englacially prior to the drainage event is released during the two days after the outburst.

The detailed data sets of two years, and the analysis of the annual outbursts of the last decades proves that even for an individual system, a variety of different processes are involved which

alter the character of the drainage to varying degrees of importance. This study shows the need for an integrative assessment of glacier-dammed lake floods to better understand the nature of these events.

Acknowledgments

The project was funded by the Swiss National Science Foundation, Grant-No. 200021-103882/1. Regine Hock is Royal Swedish Academy of Science Research Fellow supported by a grant from the Knut Wallenberg Foundation. We are grateful to many members of VAW/ETHZ who helped with data acquisition and field work. Grande Dixence SA provided the discharge data and MeteoSchweiz made climate data available for Zermatt and Grächen. Hermann Bösch processed aerial photographs for 1982, 2003, 2004 and 2005. Shin Sugiyama provided the GPS data. Thomas Schuler and Olaf Eisen made valuable remarks on an earlier version of the manuscript. Susan Braun-Clarke edited the English. Together with constructive comments of the scientific editor J. Walder, reviews of R. Bingham, P. Jansson and an anonymous reviewer improved the manuscript.

Appendix: Melt and discharge modelling

A distributed temperature-index melt-accumulation model coupled to a linear-reservoir discharge model (Hock, 1999) is used to compute hourly meltwater production and runoff from the catchment of Gornergletscher. It elaborates on classical models using degree-day factors by varying these as a function of potential clear-sky radiation in order to account for the effects of slope, aspect and shading. The model has been shown (Hock, 1999) to be capable of reproducing the large diurnal runoff amplitudes typical of glacier discharge regimes, although driven only by air temperature and precipitation data. Surface melt rates M are computed by:

$$M = \begin{cases} (f_M + r_{\text{snow/ice}} I) T & : T > 0 \\ 0 & : T \leq 0 \end{cases} \quad (5.5)$$

where f_M denotes a melt factor, $r_{\text{snow/ice}}$ are radiation factors for snow and ice and I is the potential direct solar radiation (Tab. 5.2). Reduced melt rates over debris-covered surfaces are accounted for.

The surface characteristics (snow/ice) were either modeled using an initial distribution of winter snow cover (1970-2003), or prescribed by weekly evaluation of photographs of the automatic camera (2004 and 2005).

The air temperature and precipitation at every grid cell is calculated using constant gradients with altitude. In this model approach, correction factors account for rain gauge under-catch errors and increased losses in the case of solid precipitation. A threshold temperature distinguishes snow from rainfall (Hock, 1999).

To derive hydrographs of glacial discharge, the melt model is coupled to a simple runoff model which routes meltwater through the glacier using a linear-reservoir approach (Baker and others,

Table 5.2: Optimized parameters of the distributed temperature-index model on Gornergletscher obtained from the calibration period (April-September 2004).

Parameter	Sym.	Value	Unit
Melt factor	f_M	0.31×10^{-4}	$\text{m h}^{-1} \text{ } ^\circ\text{C}^{-1}$
Radiation factor ice	r_{ice}	0.61×10^{-6}	$\text{m}^3 \text{ W}^{-1} \text{ h}^{-1} \text{ } ^\circ\text{C}^{-1}$
Radiation factor snow	r_{snow}	0.35×10^{-6}	$\text{m}^3 \text{ W}^{-1} \text{ h}^{-1} \text{ } ^\circ\text{C}^{-1}$
Temperature gradient	dT/dz	-6×10^{-3}	$^\circ\text{C m}^{-1}$
Precipitation gradient	dP/dz	2.5×10^{-4}	m^{-1}
Retention const. ice	c_{ice}	14	h
Retention const. firn	c_{firn}	600	h
Retention const. snow	c_{snow}	500	h

1982; Hock and Noetzli, 1997). Melt- and rainwater is distributed to three water reservoirs – ice, firn and snow – according to the surface characteristics of the grid cell where the water originates. The firn reservoir is defined as the area above 3500 m a.s.l. The reservoirs are characterized by different retention constants c_i which need to be calibrated. The model is based on the assumption that discharge $Q_i(t)$ from reservoir i is proportional to the stored water volume $V_i(t)$:

$$V_i(t) = c_i \cdot Q_i(t). \quad (5.6)$$

The constants c_i correspond to the mean residence time of water in the reservoir i and have values of hours to days (Tab. 5.2).

The climatic constraints are obtained from comparison of overlapping periods of the weather data (dT/dz , dP/dz) or from literature (precipitation corrections, threshold liquid-solid precipitation; Hock, 1999; Schwarb, 2000; see Tab. 5.2). Melt parameters (f_M , r_{ice} , r_{snow}) and runoff parameters (c_{ice} , c_{firn} , c_{snow}) are obtained from calibration. The parameters are chosen to achieve maximum agreement between three types of data providing optimal constraint of the model: (i) simulated and measured melt at ablation stakes, (ii) simulated and measured hourly discharge and (iii) simulated and observed snowline retreat. We choose the ablation season 2004 as calibration period because of the existing extensive data basis and 2005 as validation period. Two different parameter sets were calibrated based on the meteorological input data (temperature and precipitation) of the AWS (2004, 2005) and the weather stations at Zermatt and Grächen (1970-2003).

At all ablation stake locations good agreement between field data and model results is achieved for the calibration period. Measured and simulated runoff during the melt season 2004 (April to September) agree well (Fig. 5.3). To judge the model performance we use the R^2 -efficiency criterion (Nash and Sutcliffe, 1970) defined as

$$R^2 = 1 - \frac{\sum (Q_{\text{meas}} - Q_{\text{sim}})^2}{\sum (\overline{Q_{\text{meas}}} - Q_{\text{meas}})^2} \quad (-\infty < R^2 < 1) \quad (5.7)$$

with Q_{meas} the measured and Q_{sim} the simulated discharge. For 2004 (2005) R^2 is 0.91 (0.73) with weather input data from the AWS and 0.88 (0.79) with data from Zermatt / Grächen, respectively. Simulated snowlines were compared with the photographs of the automatic camera and good agreement was obtained (Huss, 2005).

Chapter 6

Temporal and spatial changes of Laika Glacier inferred from satellite remote sensing and mass balance modelling

MATTHIAS HUSS¹, RETO STÖCKLI^{2,3}, GIOVANNI KAPPENBERGER⁴ AND HEINZ BLATTER⁵

¹ Versuchsanstalt für Wasserbau, Hydrologie und Glaziologie (VAW), ETH Zürich, Switzerland

² NASA Earth Observatory, Goddard Space Flight Center, Greenbelt, USA

³ MeteoSchweiz, Zürich, Switzerland

⁴ MeteoSvizzera, Locarno Monti, Switzerland

⁵ Institut für Atmosphäre und Klima, ETH Zürich, Switzerland

Published, Journal of Glaciology

Citation: Huss, M., R. Stöckli, G. Kappenberger and H. Blatter (2008). Temporal and spatial changes of Laika Glacier, Canadian Arctic, since 1959 inferred from satellite remote sensing and mass balance modelling. *Journal of Glaciology*, **54(188)**, 857–866.

ABSTRACT: The retreat of Laika Glacier (4.4 km²), part of a small ice cap situated on Coburg Island, Canadian Arctic Archipelago, is analyzed using field data, satellite remote sensing and mass balance modelling. We present a methodology for merging various data types and numerical models and investigate the temporal and spatial changes of a remote glacier during the last five decades. A glacier mass balance and surface evolution model is run for the period 1959-2006 forced with in situ weather observations and climate re-analysis data (ERA-40, NARR). The model is calibrated using the ice volume change observed between 1959 and 1971, and measured seasonal mass balances. Calculated glacier surface elevation is validated against ICESat GLAS altimeter data and ASTER-derived elevation. Landsat-derived glacier outlines are used to validate calculated ice extent. The piedmont tongue of Laika Glacier has retreated considerably and is in a state of disintegration. The modelled glacier mass balance between 1959 and 2006 was -0.41 m w.e. a⁻¹ on average. Model results indicate a significant trend towards higher mass balance gradients. A complete wastage of Laika Glacier by 2100 is predicted by model runs based on climate scenarios.

6.1 Introduction

Mountain glaciers and ice caps are sensitive indicators of climate change (IPCC, 2007). They contribute significantly to sea level rise and will continue to do so during the decades to come (Kaser and others, 2006; Meier and others, 2007). Thus, it is vitally important to understand their reaction to climate warming, which is particularly pronounced at high latitudes of the Arctic (Moritz and others, 2002). However, field monitoring of remote ice masses is resource-consuming and data are available only for a limited number of glaciers in Arctic environments (e.g. Dowdeswell and others, 1997; Hagen and others, 2003; Oerlemans and others, 2005). Satellite remote sensing allows temporal and spatial changes of inaccessible glaciers and ice caps to be assessed and is frequently used in climate change impact studies (e.g. Rignot and Thomas, 2002; Abdalati and others, 2005; Paul and Kääb, 2005). However, satellite remote sensing data need to be compared to ground-truth measurements, and require a careful assessment of their limitations in order to characterize their accuracy and suitability to such applications.

Since 1959 glacier surface mass balance has been determined on several glaciers in the Canadian Arctic (Koerner, 1970; Adams and others, 1998; Koerner, 2005). Burgess and Sharp (2004) and Mair and others (2005) assessed the mass balance and the geometrical changes of Devon Ice Cap in recent decades. Blatter and Kappenberger (1988) determined the seasonal mass balance of Laika Ice Cap, Coburg Island, and measured englacial temperatures and surface ice velocities. Greuell and Oerlemans (1989) computed the temperature distribution in the superimposed ice zone of Laika Ice Cap.

In this study we assess the temporal and spatial changes of Laika Glacier, the largest outflow glacier of the small Laika Ice Cap, over the period 1959 to 2006, and make projections of future glacier extent based on climate scenarios. A methodology that combines previous field measurements, current satellite remote sensing data and numerical modelling is presented, since none of these sources alone is complete in terms of temporal and spatial coverage. A temperature index mass balance model (Hock, 1999) coupled with a simple glacier surface evolution model is used to calculate the change in glacier extent and surface mass balance based on meteorological variables. The model is calibrated using in situ measurements and is validated using satellite remote sensing data. The present study puts forth a methodology to assess the impacts of climate change on glaciers in areas where field measurements are scarce.

6.2 Study site

Laika Ice Cap (unofficial name) is a small icefield with a surface area of about 10 km² on Nirjutiqavvik (Coburg Island), Canadian Arctic Archipelago (Fig. 6.1). It is situated at the western edge of the North Water Polynya, a region with no sea ice during large parts of the year (Barber and others, 2001). Laika Ice Cap extends from close to sea level to an elevation of 530 m a.s.l. and has three outlet glaciers (Fig. 6.1c). Our study focuses on the main outlet glacier of the ice cap that forms a piedmont tongue on the coastal plain. In the paper the piedmont tongue and its catchment (4.4 km²) on the ice cap are referred to as Laika Glacier (Fig. 6.1c).

Superimposed ice formation and internal accumulation are significant components of the mass balance of Arctic glaciers (Woodward and others, 1997; Schneider and Jansson, 2004). On

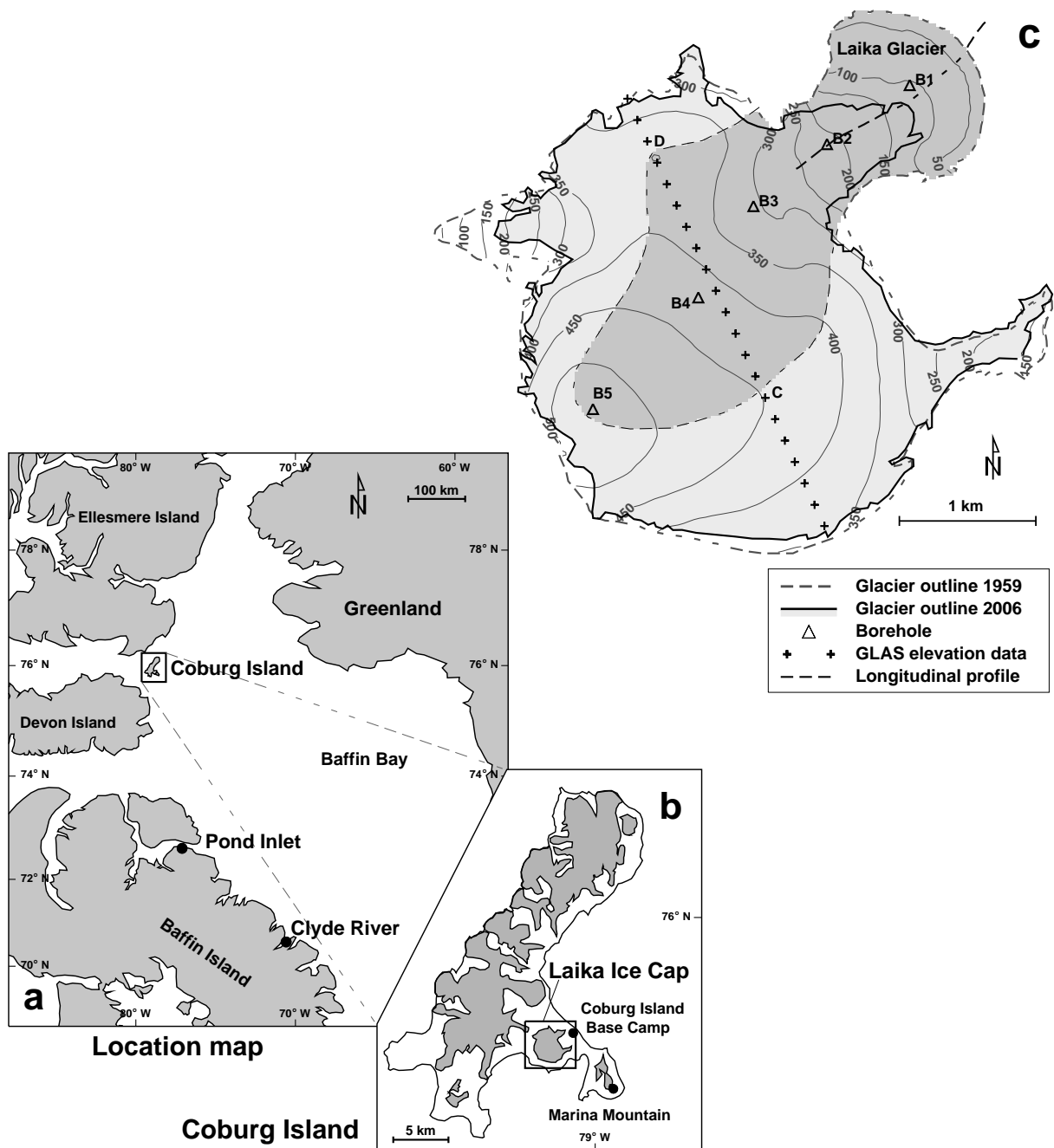


Figure 6.1: (a) Location map. Coburg Island with Laika Ice Cap is enlarged in (b). The location of relevant weather stations is indicated by dots. (c) Map of Laika Ice Cap. Glacier outlines for 1959 and 2006 are obtained from aerial photographs and satellite remote sensing data. The catchment of Laika Glacier has darker shading. Triangles indicate boreholes drilled to the bedrock in 1975 and crosses show a trace with ICESat GLAS elevation data acquired in 2006.

Laika Ice Cap almost the entire net accumulation is due to superimposed ice formation as was shown by analysis of a 20 m firn core from the top of Laika Ice Cap (Kappenberger, 1976). Melt water over the cold and impermeable bare ice surface contributes to runoff. The importance of internal accumulation by refreezing of melt water below the last summer surface is, thus, assumed to be minor on Laika Ice Cap.

Coburg Island exhibits an Arctic maritime climate as it is influenced by the North Water

Polynya. It experiences stronger winds and higher precipitation than is usual in that latitude of the Canadian Arctic. Despite the low altitude of the mountaintops (lower than 900 m a.s.l.) more than half of Coburg Island is glacierized (Fig. 6.1b). Important factors for the mass balance of Laika Ice Cap are the precipitation and the wind pattern. Precipitation increases with elevation due to orographic uplift of air masses (Blatter and Kappenberger, 1988). The strongest winds blow from the west and redistribute considerable amounts of snow from the windward slopes and the top of Laika Ice Cap to leeward slopes (Blatter and Kappenberger, 1988). This process causes an accumulation pattern which is not well correlated with elevation (Fig. 6.2).

6.3 Data sources and methods

A wide range of different data types is used in this study: (i) mass balance measurements on Laika Ice Cap, (ii) local weather observations on Coburg Island, (iii) long-term meteorological time series measured at Pond Inlet and Clyde River, (iv) climate re-analysis data (ERA-40, NARR), and (v) satellite observations (Landsat, ICESat, ASTER).

Field data

During the 1970s a field study was performed on Laika Glacier (Blatter and Kappenberger, 1988). Seasonal mass balance of the glacier surface was determined at up to forty stakes. The surveys were complemented with snow probings and density measurements in snow pits in May or June. The mass balance data include accumulation due to superimposed ice formation. Seasonal mass balance data are available in the form of manually interpolated contour maps. We digitized maps of the net balance distribution for 1973/74-1978/79 and winter balance maps for 1973/74-1977/78.

Aerial photographs of Laika Ice Cap were taken in 1959 and 1971 providing accurate glacier outlines (Blatter and Kappenberger, 1988). The photographs were co-registered using seven ground control points, which were geolocated in a local coordinate system by triangulation. The photogrammetrical evaluation was performed using a Kern P62 analogue stereo-plotting instrument. The elevation accuracy is estimated as ± 2 m (Kappenberger, 1976). For 1959 a map of the entire Laika Ice Cap was drawn, for 1971 only the piedmont tongue of Laika Glacier, delimited by the glacierized region below 250 m a.s.l. (Fig. 6.1c), was mapped due reduced contrast in the accumulation area. The scale of the maps is 1:20'000 and the contour line-spacing is 25 m. The maps were digitized and interpolated on a regular 25 m grid providing a digital elevation model (DEM) of the glacier surface. The change in ice volume of the Laika Glacier tongue was determined by differencing the DEMs of 1971 and 1959 and converted to a mass change assuming an ice density of 900 kg m^{-3} . We estimate the uncertainty in the ice volume change as $\pm 12\%$. The estimate is based on the uncertainty in the elevation information and the observed mean 12-year thinning of the glacier tongue of -16.9 m. The topographical data refer to a local coordinate system for Coburg Island. The coordinates of georeferenced satellite images were shifted into this local system using a coordinate transformation established based on eight common points (landmarks). We estimate a spatial error of the geolocation of ± 10 m arising from the coordinate transformation.

The ice thickness is known at five boreholes (Fig. 6.1c) drilled in 1975 to measure englacial temperatures (Blatter and Kappenberger, 1988). Ice thickness data were spatially interpolated

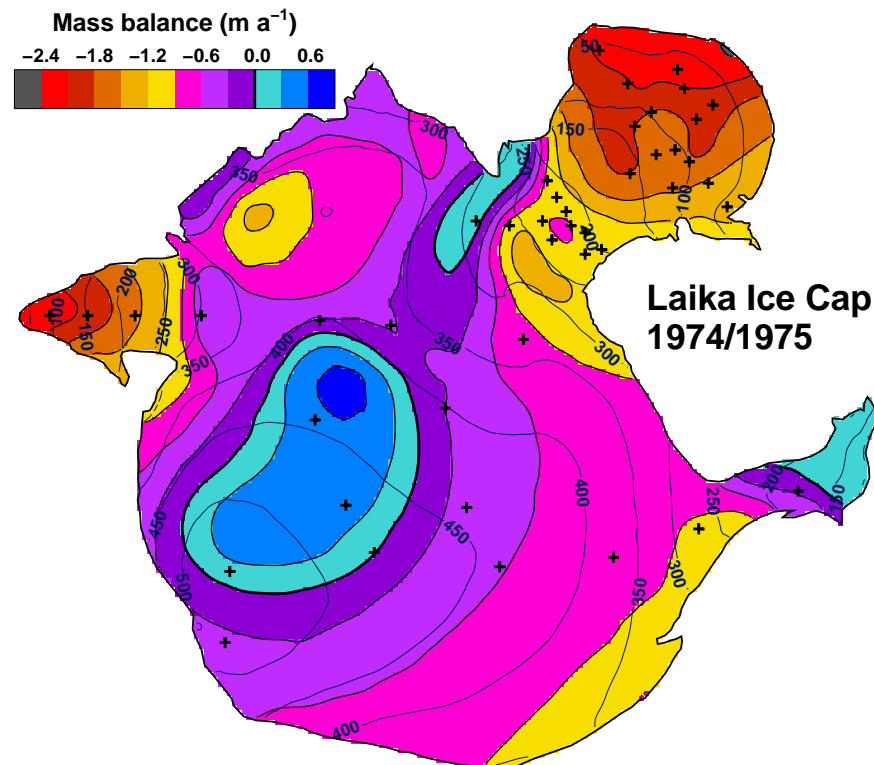


Figure 6.2: *Distribution of net balance as measured between September 24, 1974 and August 23, 1975. Mass balance stakes are indicated by crosses.*

to provide a map of approximate bedrock elevation of Laika Glacier. The maximum ice thickness is slightly above 100 m.

Meteorological time series

Homogeneous and continuous time series of daily air temperature and precipitation are required to drive the mass balance model. However, continuous meteorological data for the Canadian Arctic are sparse and climatic variability is high. Therefore, we combine various observational series in the vicinity of the glacier and re-analysis data spanning over different time periods to obtain a composite daily temperature and precipitation series (1959 - 2006) for Coburg Island.

Data sets

Measurements of air temperature and precipitation on Coburg Island are available for the period 1973-1978. An automatic weather station was located 1 km from the terminus of Laika Glacier at "Coburg Island Base Camp". The air temperatures were recorded every 3 hours using a System Lambrecht 809 Pt100 temperature sensor mounted in a Stevenson screen. The nominal accuracy of the temperature sensor is $\pm 0.3^{\circ}\text{C}$ at 0°C . The measurements during winter are not used because of lower data quality due to rime formation. The data of the automatic weather station were complemented with routine manual observations (Blatter and Kappenberger, 1988). A Canadian standard snow and rain gauge with Nipher inverted bell wind shield was manually read every 6 hours. A significant underestimation of precipitation is likely in the case of strong

Table 6.1: Meteorological time series and re-analysis data (T: air temperature, P: precipitation). The elevation of the weather station and the re-analysis grid cell, respectively, is given in m a.s.l.

Station	Time period	Variable	Elevation
Coburg Isl. Base Camp	1973 - 1978	T	4
Coburg Isl. Base Camp	1973 - 1976*	P	4
Marina Mountain	1973 - 1978	T	730
Pond Inlet	1975 - 2006	T, P	55
Clyde River	1946 - 1996	T, P	26
ERA-40	1959 - 2001	T, P	192
NARR	1979 - 2006	T, P	115

* only during March to September in 1975 and 1976.

winds during snow fall events. Additional measurements of daily air temperature during the summer months are available from an automatic weather station on the top of Marina Mountain at a distance of 7 km from Coburg Island Base Camp (Fig. 6.1b and Table 6.1).

Daily data of mean air temperature and total precipitation at Pond Inlet and Clyde River (Fig. 6.1a and Table 6.1) were downloaded from the climate archive of Environment Canada. These stations are at distances of 194 km and 373 km, respectively, from Laika Ice Cap and were chosen because their topographic setting is similar to Coburg Island and their data is almost void of data gaps.

Additional information about the meteorological conditions is provided by climate re-analysis data sets. We used the European Centre for Medium-Range Weather Forecasts (ECMWF) 40-yr Re-Analysis (ERA-40) air temperature and precipitation time series 1959-2001 (Uppala and 46 others, 2005). The ERA-40 re-analysis data set provides continuous and consistent time series of 6-hourly air temperature and precipitation on the N80 reduced gaussian grid, which was resampled to a cylindrical $1^\circ \times 1^\circ$ grid for this study. Daily mean values of 2 m air temperature and total precipitation (liquid and solid) of the grid point nearest to Laika Ice Cap were downloaded. ERA-40 precipitation is based on a daily forecast model and is not assimilated from measured station data. Daily precipitation forecasts were assembled as in Schmidli and others (2006).

Data from the NCEP North American Regional Re-Analysis (NARR) is available for the period 1979-2006 (Mesinger and 18 others, 2006). The NARR data set has a higher spatial resolution than ERA-40. Three-hourly temperature and precipitation data are available on a grid of approximately 32 km, however, with no overlapping period with in situ weather observations at Coburg Island Base Camp. Thus, no direct comparison of measurements and re-analysis is possible.

Composite temperature and precipitation series

We now describe how meteorological information originating from different sources was combined to obtain a 50-year time series of daily temperature and precipitation for Coburg Island. The weather data of Coburg Island Base Camp are assumed to be the best representation of the local climate conditions. Daily air temperatures are highly correlated with those at Marina Mountain during June to September ($r^2=0.80$), indicating that the weather conditions at the

coastal station are not heavily affected by stable inversions and can be extrapolated over the entire elevation range of Laika Ice Cap.

The ERA-40 air temperature data could not be used to extend the Coburg Island time series since correlation between ERA-40 and Coburg Island Base Camp monthly summer temperatures was absent or weak. The interannual variations are insufficiently represented.

We compared measured weather station data from Pond Inlet and Clyde River to the records of Coburg Island Base Camp. Daily air temperatures showed unsatisfactory correlations between the three sites. We resampled the time series to monthly resolution and found good correlation between both Pond Inlet and Coburg Island Base Camp, as well as Clyde River and Pond Inlet with linear correlation coefficients of $r^2=0.85$ and $r^2=0.82$, respectively. This allows transfer functions for monthly mean air temperatures between these weather stations to be established. Using these linear regression relationships, the temperatures recorded at Clyde River (1959-1974) and at Pond Inlet (1975-2006) were scaled to Coburg Island. In order to obtain a daily series we downscaled the 1959-2006 monthly air temperature time series by applying the daily temperature deviations from the monthly mean values of the year 1977 of Coburg Island Base Camp.

We used daily average values of 2 m air temperature of the NARR grid point nearest to Laika Ice Cap to check the plausibility of the temperature series obtained using the regression method. Due to its higher spatial resolution the NARR data set performs slightly better than ERA-40 in capturing the year-to-year fluctuations of temperature on Coburg Island and provides some validation of the composite temperature series.

The precipitation sums measured at Pond Inlet and Clyde River do not correlate with the time series of Coburg Island and are significantly lower. The precipitation time series of ERA-40 and NARR extracted for the grid points closest to Laika Glacier (about 10 km apart) were compared. In the overlapping period the annual precipitation sums of ERA-40 and NARR are well correlated ($r^2=0.64$) and only differ by 1% on average. ERA-40 annual precipitation (liquid and solid) matches the data for Coburg Island Base Camp in 1973-1976 within 10%. We use daily precipitation provided by the ERA-40 data set for the period 1959-1979 and NARR daily precipitation for 1980-2006. Summer temperature and annual precipitation according to the composite time series are shown in Figure 6.3.

Satellite remote sensing data

Satellite data from various sensors are used to assess the current state of Laika Glacier (Table 6.2). Glacier outlines were digitized from the panchromatic channel of the Landsat ETM sensor for the years 2000, 2002 and 2006 at a spatial resolution of 15 m. The spatial uncertainty in the delineation of the ice margin due to shadows, limited contrast in the image and perennial snow patches is estimated as ± 100 m.

One track of the Laser Altimeter system GLAS on board of NASA's ICESat (Ice, Cloud and land Elevation Satellite) is available for 2006 across Laika Glacier (Fig. 6.1c). GLAS provides surface elevation data with a spatial footprint of 60 m and an along-track resolution of 170 m. The accuracy of the elevation information is estimated as ± 0.2 m for smooth terrain (Shuman and others, 2006). In rough terrain the accuracy is lower due to the size of the laser footprint.

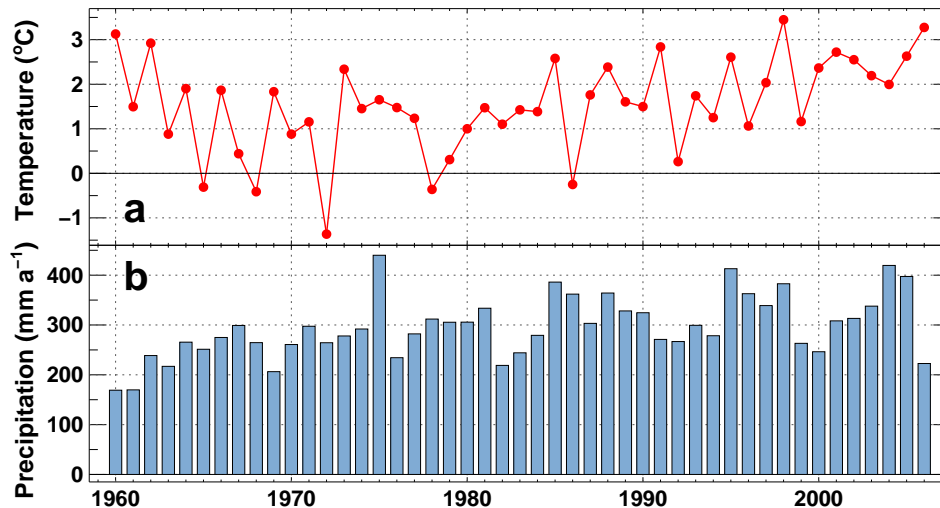


Figure 6.3: (a) Mean June-September air temperature and (b) annual precipitation according to the composite data set for Coburg Island.

ASTER (Advanced Spaceborne Thermal Emission and Reflection Radiometer) is a joint effort between NASA and Japan's Ministry of Economy Trade and Industry (METI) and includes stereo viewing capability for digital elevation model creation at 30 m spatial resolution. The accuracy of the altitudinal information of the DEMs is estimated as ± 10 m by Stearns and Hamilton (2007). However, also larger errors of ± 60 m in complex high-mountain topography are reported (Kääb and others, 2003). Retrieval of the ASTER DEM seems to be particularly unreliable over fresh snow due to limited contrast variability and generally high reflectance values.

One good quality ASTER scene covering Coburg Island is available for June 2004 and was used to generate a DEM. We assessed the accuracy of the ASTER DEM by comparing it to GLAS ICESat elevation data in the vicinity of the ice cap over non-glacierized regions. We find a root-mean-square error $RMSE=14.5$ m ($n=185$). Above 200 m a.s.l. the ASTER DEM underestimates surface elevation given by GLAS systematically by 9 m; at lower altitudes the elevation of the GLAS tracks is reproduced well on average. Over open sea the $RMSE$ of the ASTER DEM is 13 m. We assign an uncertainty of ± 15 m to elevation information provided by ASTER. In general, the ASTER DEMs are capable of yielding information on significant spatial changes in glacier geometry. However, they are not accurate enough to allow the calculation of ice volume changes for a small glacier. In this study, we use the ASTER DEM of 2004 as an independent spatially distributed data set for validation of the model results.

Mass balance and surface evolution model

The temporal and spatial changes of Laika Glacier since 1959 are assessed using a grid-based numerical model consisting of a mass balance model and a simple surface evolution model.

Surface mass balance

Glacier surface mass balance is calculated using an accumulation model coupled to a distributed temperature index melt model (Hock, 1999; Huss and others, 2008a). In this model the degree-

day factors are varied as a function of potential direct solar radiation to account for the effects of slope, aspect and shading. Temperature index models are based on a linear relation between positive air temperature and melt rate (Hock, 2003). Several studies have shown that off-ice temperature is well suited to simulate melt using temperature index models (e.g. Lang and Braun, 1990).

Daily surface melt rates M are computed by

$$M = \begin{cases} (f_M + r_{\text{ice/snow}} I) \cdot T & : T > 0 \\ 0 & : T \leq 0 \end{cases} \quad (6.1)$$

where f_M denotes a melt factor, $r_{\text{ice/snow}}$ are radiation factors for ice and snow and I is the potential clear-sky direct radiation. Due to the empirical character of the temperature index model the site-specific parameters f_M and $r_{\text{ice/snow}}$ must be calibrated using field data. Air temperature T at every grid cell is derived using a constant lapse rate dT/dz . Precipitation is assumed to increase linearly with elevation (dP/dz). A correction factor allows the adjustment of precipitation sums (c_{prec}), and a threshold temperature $T_{\text{thr}}=1^\circ\text{C}$ distinguishes snow from rainfall. Liquid precipitation does not contribute to mass balance. Parameter values and units are shown in Table 6.3.

Regions with positive net balance at the end of the previous year define the firn area. Firn is treated as snow in Equation 6.1. The distribution of snow on Laika Ice Cap is highly influenced by wind (Fig. 6.2) and is relatively constant during the years with observations. In order to account for the substantial effect of snow drift we derived a mean distribution pattern of snow from the in situ measurements of winter mass balance. The winter balance maps between 1974 and 1978 were normalized and averaged. This measured accumulation pattern is used to redistribute solid precipitation during each precipitation event.

Table 6.2: *Satellite remote sensing data used in this study. The estimated accuracy refers to the digitized glacier outlines (xy) and to the elevation information (z).*

Satellite	Sensor	Date	Source	Spatial resol.	Used for	Accuracy (xy)	Accuracy (z)
Landsat	ETM	Jul 24, 2000	USGS/NASA	15 m	gl. outline	± 100 m	-
Landsat	ETM	Sept 14, 2002	USGS/NASA	15 m	gl. outline	± 100 m	-
Landsat	ETM	Aug 26, 2006	USGS/NASA	15 m	gl. outline	± 100 m	-
TERRA	ASTER	June 12, 2004	NASA/METI	30 m	DEM	-	± 15 m
ICESat	GLAS	Feb 3, 2006	NASA	170 m	elev. track	-	± 0.2 m

Table 6.3: *Mass balance model parameters, values and units.*

Parameter	Value	Units
f_M	0.5×10^{-3}	$\text{m d}^{-1} \text{ }^\circ\text{C}^{-1}$
r_{ice}	4.32×10^{-5}	$\text{m}^3 \text{ W}^{-1} \text{ d}^{-1} \text{ }^\circ\text{C}^{-1}$
r_{snow}	1.32×10^{-5}	$\text{m}^3 \text{ W}^{-1} \text{ d}^{-1} \text{ }^\circ\text{C}^{-1}$
dT/dz	-5×10^{-3}	$^\circ\text{C m}^{-1}$
dP/dz	0.03	$\% \text{ m}^{-1}$
c_{prec}	75	$\%$

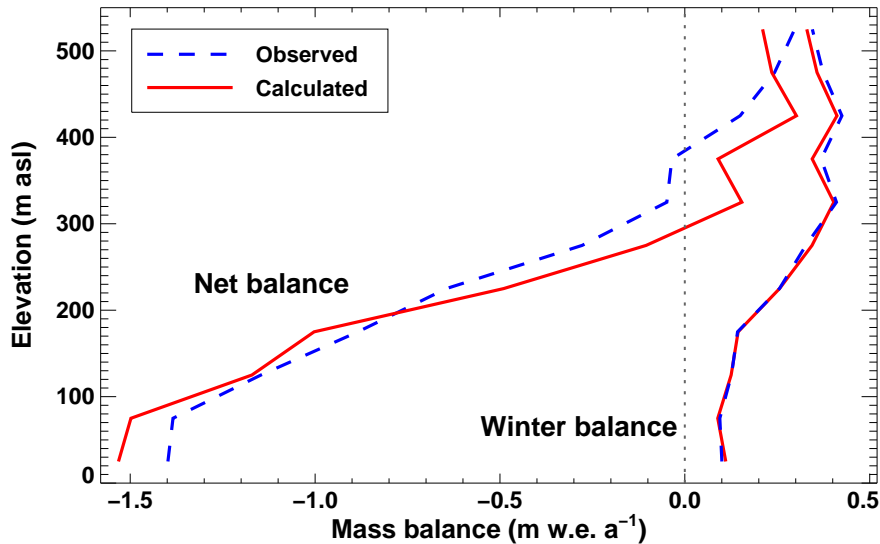


Figure 6.4: Comparison of observed and calculated net balance and winter balance in 50 m elevation bands as a mean of the years 1973/74-1978/79.

The comparison of daily air temperatures measured at Coburg Island Base Camp and Marina Mountain (Fig. 6.1b) reveals a lapse rate of $dT/dz = -5^{\circ}\text{C km}^{-1}$ during July and August. As these months are the most important for melt we used this lapse rate for the modelling. The effect of refreezing melt water in the winter snow cover is indirectly considered by tuning the parameters of the temperature index model such that the direct seasonal mass balance data are matched and the observed mass balance gradients are reproduced (Fig. 6.4). Given the paucity of field data additional parameters that explicitly take into account refreezing (as e.g. in Reeh, 1991) could not be constrained.

We define the mean specific net balance \bar{b}_n (in m water equivalent) as the sum of accumulation (solid precipitation) and ablation (snow- or icemelt) over the entire glacier during the hydrological year (Oct. 1 - Sept. 30) divided by that year's glacier surface area. We calculate 'conventional' mass balance (Elsberg and others, 2001), i.e. the glacier area is updated annually. The mean specific winter balance \bar{b}_w is determined during the period October 1 to May 30 and summer balance \bar{b}_s over June 1 to September 30.

Glacier surface elevation change

In order to account for the change in glacier surface elevation and ice extent over time we use a simple model based on mass conservation. Glacier surface geometry and extent are updated annually in response to the calculated mass balance distribution. We refrain from applying a more sophisticated ice flow model because of the uncertain bedrock elevation (in particular in the accumulation area) and the missing in situ data for validation. Several rigorous assumptions have been made in order to simplify the ice flow dynamics in our grid-based approach. We assume the glacier to adjust its geometry immediately to a change in surface mass balance. Considering the size and the relatively high mass balance gradients of Laika Glacier this approximation is reasonable. The importance of ice flux replacing mass lost by ablation in the tongue is small in periods of glacier retreat, allowing elevation change rates in the ablation area of Laika Glacier to approach surface melt rates (Blatter and Kappenberger, 1988).

Our method to update glacier surface considers two cases of mass change: (1) $\overline{b_n} < 0$ (mass loss of the glacier): Regions where positive mass balances occur in the individual year are assumed to remain constant in surface elevation. The accumulated ice volume B_{acc} is equally distributed over the ablation area. For each grid cell in the ablation area the surface elevation change is given by the sum of the net balance b_n and the compensating effect of ice flow b_{comp} in ice equivalent. b_{comp} is obtained with B_{acc}/A_{abl} , where A_{abl} is the area with net ablation. Consequently, near the equilibrium line $b_n + b_{comp}$ may be positive. We condition the surface elevation not to increase and distribute positive residuals of $b_n + b_{comp}$ further downglacier. For almost 90% of the study period case (1) occurs. The assumptions are supported by the observation of small elevation changes in the accumulation area and rapid thinning in the ablation area during a period of glacier retreat on several Arctic ice caps (e.g. Abdalati and others, 2005). (2) $\overline{b_n} > 0$ (mass gain): Elevation on the entire glacier surface increases with the calculated rate of the mean specific net balance $\overline{b_n}$ in ice equivalent. This uniform thickening is assumed to occur immediately in our model, whereas in nature the spatial elevation change patterns are more complex and are delayed by several years. However, we consider this simple parameterization to be a first order approximation of glacier geometry change in the case of a mass gain (calculated for only 6 years of the study period). The glacier extent at the end of each year is inferred by comparing the updated glacier surface elevation with the bedrock elevation at all grid cells. The glacierized area shrinks where the ice thickness drops below zero.

The applied procedure is simple and does not require input data other than the mass balance distribution, as well as being insensitive to uncertainties in the bedrock elevation except for regions near the glacier terminus. In comparison to physical ice flow modelling, our method is an alternative well suited to glaciers for which neither long-term measurements of flow speeds nor exact knowledge of the entire bedrock geometry exist.

Table 6.4: Measured and calculated net balance $\overline{b_n}$ and winter balance $\overline{b_w}$, and observed equilibrium line altitude (ELA) for Laika Glacier in all years with field data.

Year	Area (km ²)	$\overline{b_n}^{meas}$ (m w.e. a ⁻¹)	$\overline{b_n}^{calc}$ (m w.e. a ⁻¹)	$\overline{b_w}^{meas}$ (m w.e. a ⁻¹)	$\overline{b_w}^{calc}$ (m w.e. a ⁻¹)	ELA ^{obs} (m a.s.l.)
1973/1974	4.17	-0.41	-0.32	0.39	0.29	410
1974/1975	4.17	-0.55	-0.46	0.46	0.19	420
1975/1976	4.15	-0.19	-0.33	0.18	0.21	300
1976/1977	4.14	-0.40	-0.24	0.29	0.33	400
1977/1978	4.13	-0.15	0.23	0.27	0.28	300
1978/1979	4.13	0.02	-0.16	-	0.20	260

Model calibration and validation

The glacier mass balance and surface evolution model is calibrated and validated in a multilayer procedure including all available data: (i) ice volume change of the Laika Glacier tongue for 1959-1971, (ii) measured distribution of glacier surface net and winter mass balances for 1974-1979, (iii) extent of Laika Glacier known from aerial photographs in 1971 and the Landsat scenes for 2000-2006, (iv) GLAS ICESat elevation data for 2006, and (v) the ASTER DEM of 2004. Data types (i) and (ii) are used for calibration of the mass balance model, (iii)-(v) are used for validation of the combined glacier mass balance and surface evolution model.

The parameters of the mass balance model are tuned to match the measured ice volume change 1959-1971. This is achieved by varying the melt parameters f_M and $r_{ice/snow}$. The accumulation parameters c_{prec} and dP/dz are calibrated simultaneously to optimize agreement between the calculated and the observed seasonal mass balance gradient (Fig. 6.4). Comparison of observed point mass balances interpolated on a regular 25 m grid with model results showed a RMSE of 0.32 m w.e. for net balance and of 0.08 m w.e. for winter balance. Measured and calculated mean specific mass balance quantities are shown in Table 6.4. Some of the differences are due to varying evaluation periods; calculated mass balance is given in a fixed-date system, whereas field mass balance refers to a measurement period. This bias could only be accounted for in some years as the dates of the field surveys were not documented systematically.

The model is run for the period 1959-2006 and achieves good agreement with the GLAS elevation data (Fig. 6.5). The RMSE of model and measurements is 1.7 m. Measured glacier outlines in 1971 (aerial photographs) and 2006 (Landsat) are compared to the model results and the observed glacier extent is reproduced well (Fig. 6.6). The distribution of surface elevation change of the tongue of Laika Glacier is captured by the model in 1971 (Fig. 6.7). The ASTER scene of 2004 provides an independent validation of the model results in the spatial domain. The differences are within the range of uncertainty (± 15 m) of the satellite DEM (Fig. 6.7).

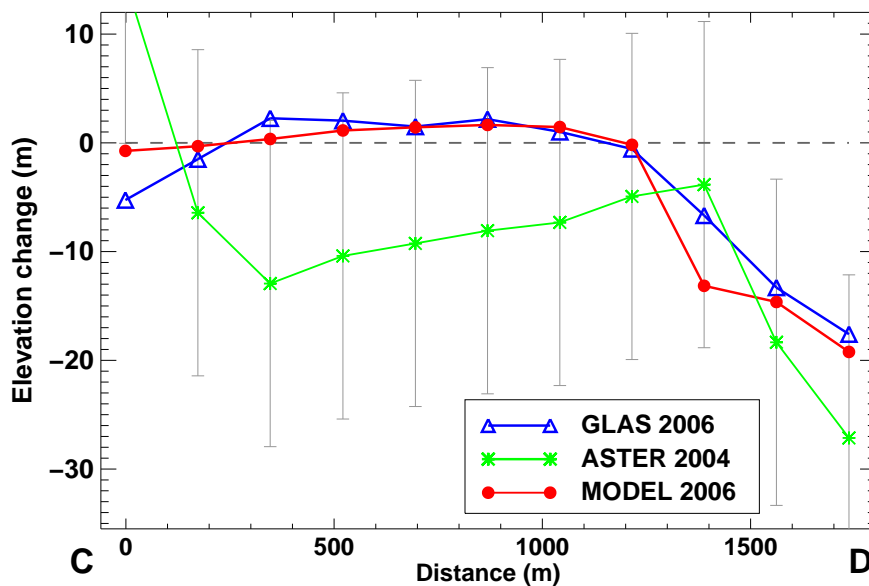


Figure 6.5: Comparison of the ICESat GLAS and ASTER elevation data with model results on the glacier cross-profile C-D displayed in Figure 6.1c. Elevation changes are relative to the glacier surface in 1959. Error bars show the uncertainty in the ASTER DEM.

6.4 Results and discussion

An increase in surface elevation of about two meters is found in the upper reaches of the glacier by comparing the 1959 DEM and the ICESat GLAS elevation data of 2006 (Fig. 6.5) in spite of a substantial overall mass loss of the glacier. A similar observation was previously made in different regions of the Arctic during subdecadal time periods (Krabill and others, 2000; Bamber and others, 2004; Abdalati and others, 2005). Interior thickening was attributed to an increase in precipitation by Abdalati and others (2005). Shallow ice-coring on Devon Ice Cap,

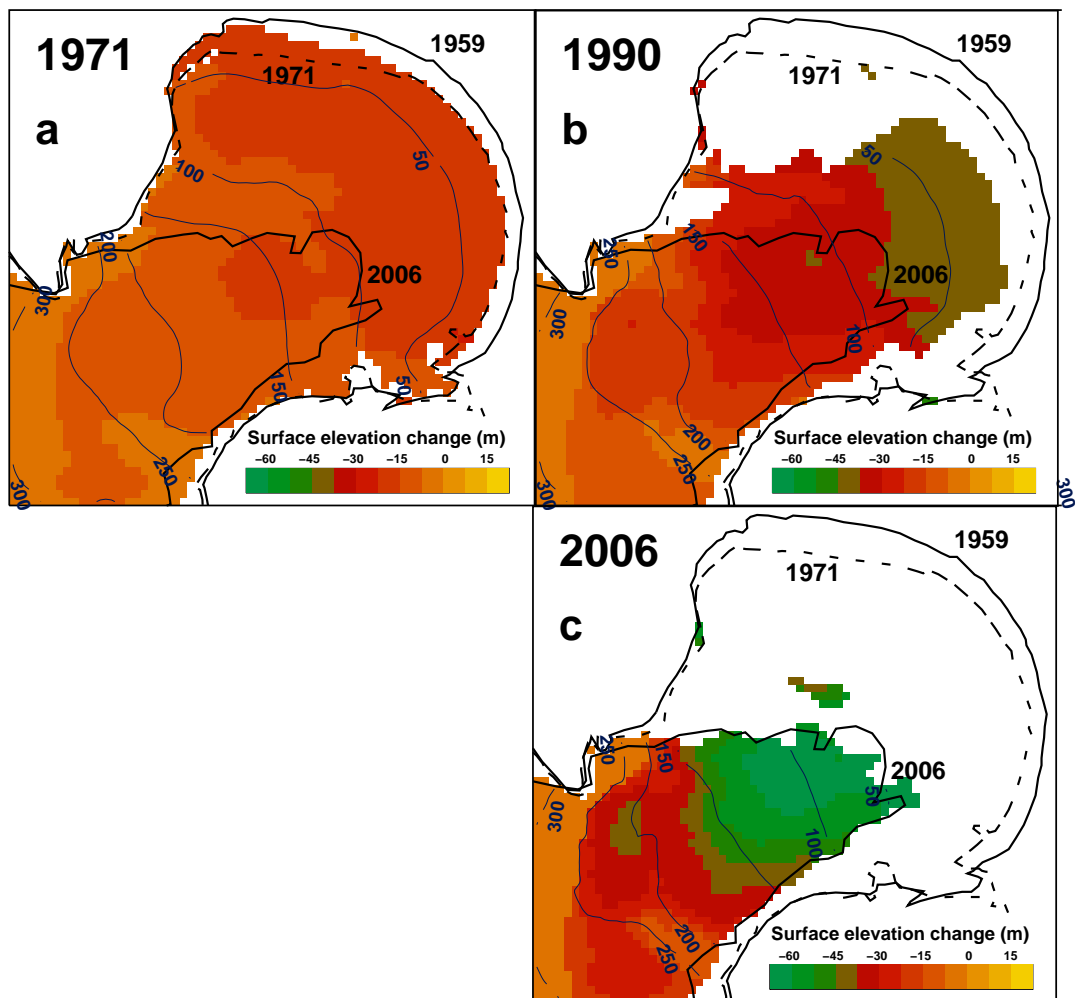


Figure 6.6: Calculated extent of the piedmont tongue of Laika Glacier for snapshots in (a) 1971, (b) 1990 and (c) 2006. Observed glacier outlines in 1959, 1971 and 2006 are shown. Grey scales indicate the calculated surface elevation change since 1959.

however, does not support this interpretation (Colgan and Sharp, 2008). Koerner (2005) explains the observed thickening with a change in ice dynamics. Ice flow from the accumulation to the ablation area has decreased leading to a rapid thinning at the glacier margin and an increase in surface elevation in the interior. Our study cannot provide a final solution to this question, but shows that a small Arctic glacier exhibits a behavior similar to that reported for larger ice caps. Furthermore, our results indicate that the trend of peripheral thinning and interior thickening is even revealed when considering a period of five decades.

Significant lowering of the surface occurs in the lower reaches of the glacier (Fig. 6.6 and 6.7). Glacier surface elevation decreased by up to 50 m near the current glacier tongue, which corresponds to mean thinning rates of more than 1 m a^{-1} . This has led to a substantial retreat of Laika Glacier over the past five decades. A disintegration of its piedmont tongue was initiated two decades ago. Interestingly, about one third of the elevation changes on the piedmont tongue of Laika Glacier occurred in the period 1959-1971, the first decade of the study period. Glacier retreat slowed down in the 1970s and displayed increasing rates again in the 1980s and 1990s (Fig. 6.8). Laika Glacier has decreased in area by 23% and has lost 24% of its volume between 1959 and 2006.

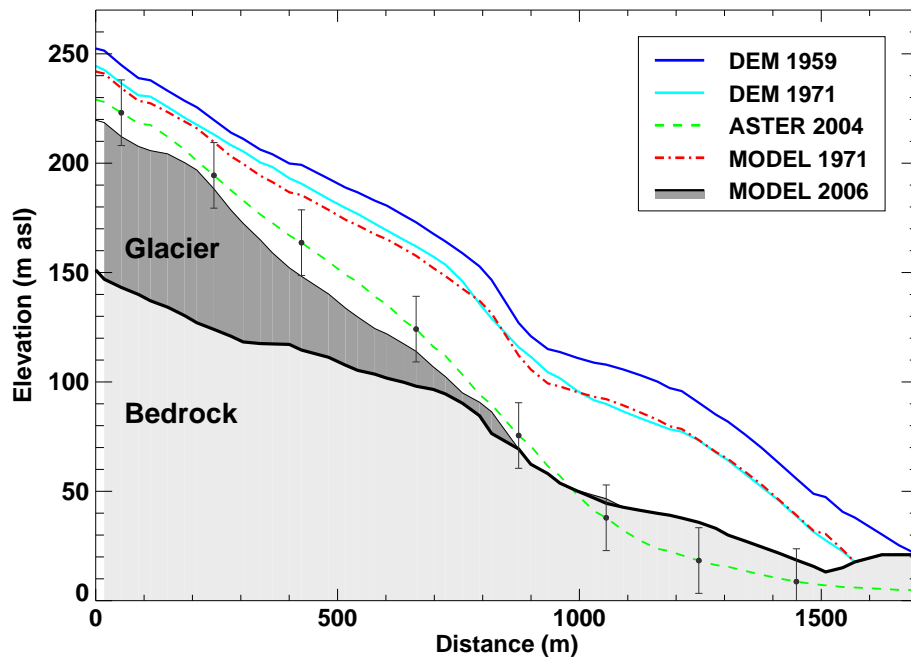


Figure 6.7: Longitudinal profile of the piedmont tongue of Laika Glacier (dash-dotted line in Fig. 6.1c). The model is capable of reproducing the surface elevation change of the glacier tongue between 1959 and 1971 and is consistent with the ASTER DEM within its uncertainty (± 15 m). Dark shading represents the glacier in 2006, light shading the bedrock.

The cumulative modelled mass balance is -19.6 m w.e. (Fig. 6.9). The first three years of the study period are characterized by highly negative summer balances. The rate of mass loss shows no accelerating trend (Fig. 6.9). Mass loss by increased melt due to rapidly rising air temperatures (Fig. 6.3) is partly compensated by higher precipitation sums and the substantial decline in glacier area at low elevations (Fig. 6.6).

We compare the mass balance time series derived in this study to the data of Devon Ice Cap NW (WGMS, 2000; Koerner, 2005) situated at a distance of about 80 km from Coburg Island. Laika Glacier exhibits much higher cumulative mass losses and larger annual fluctuations of the mass balance (Fig. 6.9). The average mean specific net balance of the entire Devon Ice Cap is

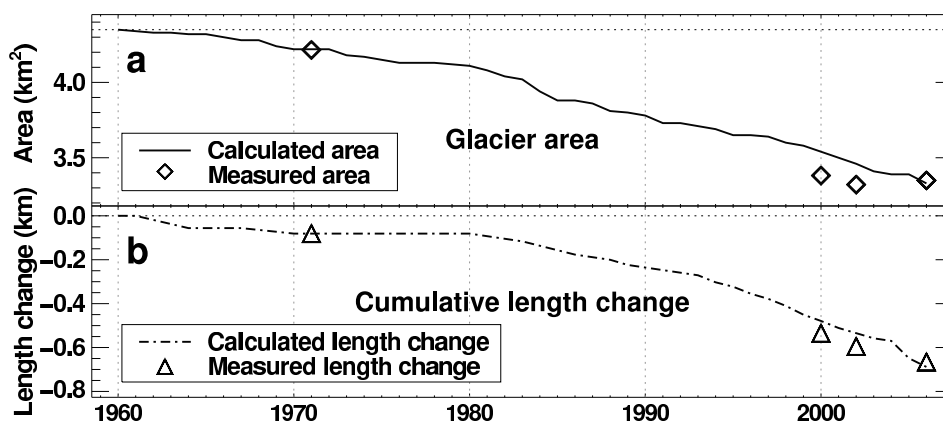


Figure 6.8: Calculated time series of (a) glacier area and (b) length change of Laika Glacier in 1959-2006. Measured data points (area and length) based on photogrammetry and Landsat images are shown.

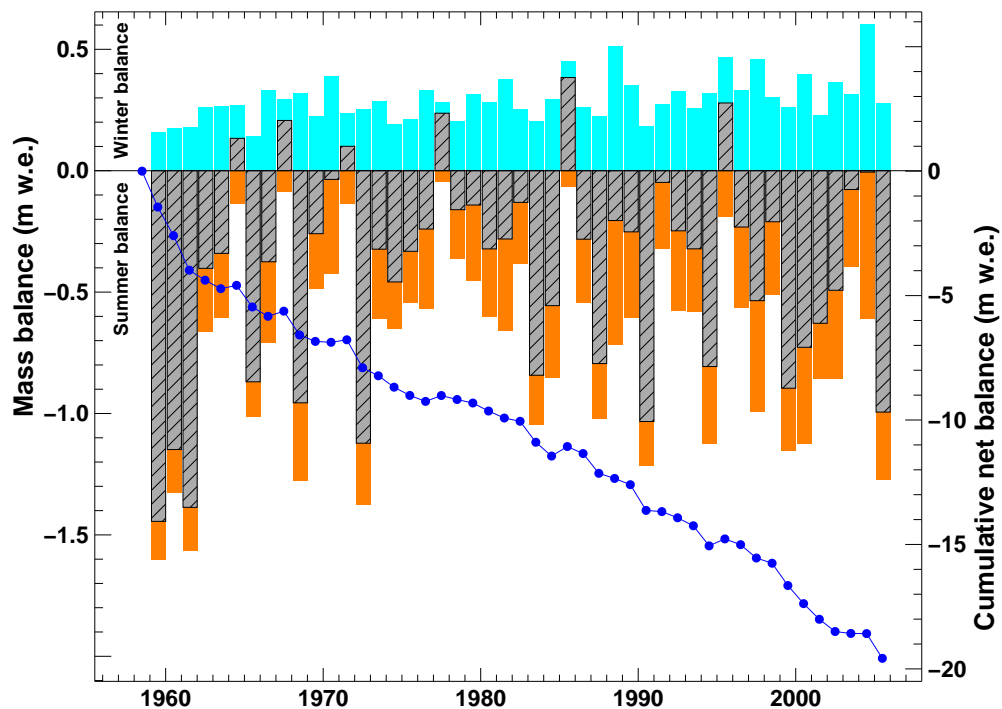


Figure 6.9: Calculated mean specific mass balance quantities shown in bars: winter balance $\overline{b_w}$ (positive), summer balance $\overline{b_s}$ (negative), net balance $\overline{b_n}$ (hatched), and cumulative net balance of Laika Glacier in 1959-2006.

estimated as $-0.13 \text{ m w.e. a}^{-1}$ for the period 1963-2000 (Mair and others, 2005), whereas it is $-0.33 \text{ m w.e. a}^{-1}$ for Laika Glacier during the same period.

The mean equilibrium line altitude is at about 350 m a.s.l. on Laika Glacier (Table 6.4). This is much lower than on Devon Ice Cap or on White Glacier, where the multi-decadal ELA is situated at about 1000 m a.s.l. (WGMS, 2000). We attribute this difference to higher precipitation sums on Coburg Island due to the vicinity to the North Water Polynya. The low elevation of Laika Ice Cap makes it highly sensitive to changes in air temperature.

The model results enable us to calculate altitudinal mass balance gradients directly derived from the gridded data sets of mass balance distribution. The mean mass balance of Laika Glacier was evaluated in 5-year intervals in five elevation bands (Fig. 6.10). In the lower reaches of Laika Glacier the mass balance becomes increasingly negative, whereas there is only a minor decrease in net accumulation in the highest regions of the glacier. We find a mass balance gradient of -0.005 a^{-1} during the first two decades of the study period and -0.007 a^{-1} at the beginning of the 21st century (Fig. 6.10). Increasing mass balance gradients have been observed on various glaciers and indicate higher mass turn-over and, thus, increased sensitivity to climate change (Dyurgerov, 2003).

The calibrated glacier mass balance and surface evolution model is run for the 21st century in order to estimate the stability of Laika Glacier during the next decades. We assume linear trends of air temperature and precipitation based on the SRES A1B scenario (IPCC, 2007). In order to force the glacier model we construct a future daily meteorological time series. We randomly select years of the composite 1959-2006 series, shift their annual means to the anticipated mean values of temperature and precipitation and perform 10 model runs in order to eliminate effects of intra-annual meteorological variability on the results. The means of these multiple model

runs are presented. The parameters calibrated in the past are assumed to be constant in the future.

A rate of air temperature rise of $+0.05^{\circ}\text{C a}^{-1}$ and a change in annual precipitation of $+0.2\% \text{ a}^{-1}$ are assumed (Fig. 6.11 a and b). The model results indicate a decrease in glacier area of 48% by

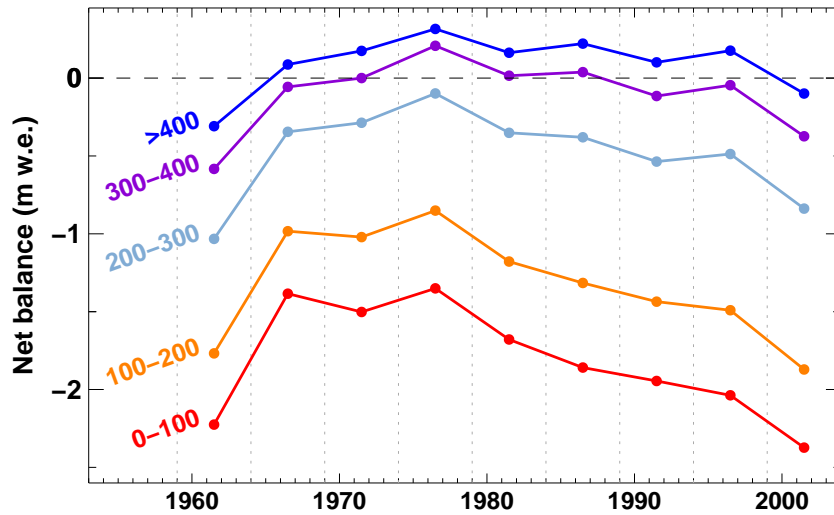


Figure 6.10: Calculated mean net balances evaluated in 5-year intervals for five elevation ranges of Laika Glacier. Numbers on the left give the altitudinal extent in m a.s.l. of the elevation band considered.

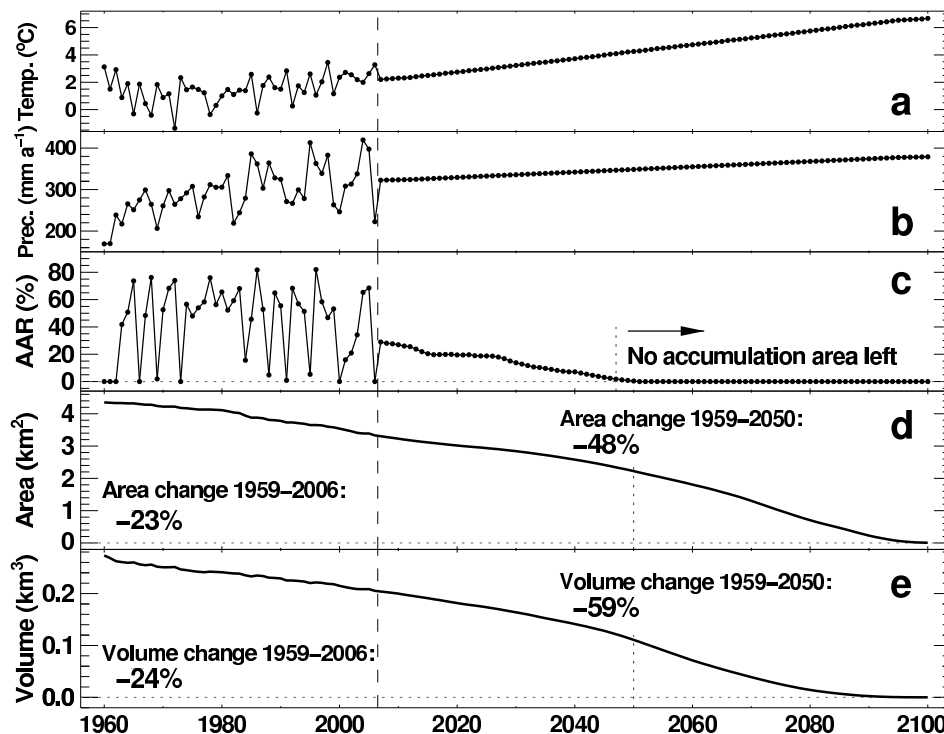


Figure 6.11: Projections of future changes in Laika Glacier based on the SRES A1B scenario (IPCC, 2007). Time series of (a) June-September air temperatures and (b) annual precipitation, (c) calculated Accumulation Area Ratio (AAR) of Laika Glacier and (d) changes in glacier area and (e) ice volume. Data points before 2006 are modelled using the composite meteorological series (Fig. 6.3).

2050 compared to 1959. Laika Glacier is expected to have lost 59% of the 1959 ice volume by 2050 (Fig. 6.11d and e). After about 2045 the equilibrium line lies above the summit of Laika Glacier in all years, impeding net accumulation (Fig. 6.11c). This leads to accelerated glacier wastage and a complete disappearance of Laika Glacier before the end of the 21st century.

The glacier model has several limitations. (i) By calibrating the melt parameters using the direct mass balance measurements performed in the 1970s the percentage of melt water refreezing in the snow cover is implicitly assumed to remain constant over time. This may not be the case in a dynamically changing climate system and could lead to errors in the projections of future ice extent. (ii) The representation of the change in firn cover and the parameterization of the melt rates over firn are not well backed up with in situ measurements. (iii) Altitudinal temperature gradients over glacierized surfaces display significant variations (e.g. Marshall and others, 2007). We assume a constant lapse rate found by comparing two weather stations on Coburg Island. Nevertheless, the glacier mass balance and surface evolution model is able to match various field data types covering different time periods within their range of uncertainty. Our model approach seems to be a reasonable description of the most important processes governing the retreat of Laika Glacier.

6.5 Conclusions

The temporal and spatial changes of Laika Glacier during the past five decades were assessed using in situ measurements, observations from space, and modelling. We provide homogenized long-term mass balance time series for a small glacier in the Canadian Arctic. A substantial mass loss of Laika Glacier during the last five decades is inferred; the calculated cumulative mass balance is -19.6 m w.e., corresponding to -0.41 m w.e. a^{-1} . Laika Glacier has decreased in area and ice volume by more than 20% between 1959 and 2006, and its piedmont tongue is in a state of disintegration. Our results indicate a significant trend towards higher mass balance gradients. Model runs driven by climate scenarios predict an acceleration of glacier retreat and the disappearance of Laika Glacier before the end of the 21st century. This study provides evidence for the rapid wastage of small arctic glaciers in response to recent climatic warming.

Our methodology merges large-scale climate re-analysis data sets (ERA-40, NARR), satellite remote sensing data from various sensors (Landsat, ICESat, ASTER) with direct field measurements. None of these data sets is complete in terms of spatial coverage and temporal resolution. A distributed glacier mass balance and surface evolution model allows gaps to be closed and glacier mass changes in high temporal and spatial resolution to be derived. The combination of data sets complementing each other and modelling is of benefit and may provide comprehensive and accurate information on long-term glacier change. We emphasize that such research needs to be concurrently executed with field measurements, not only to provide a "reality check", but also to maintain and further develop glacier models and satellite remote sensing algorithms.

Acknowledgments

This study was funded by ETH Research Grant TH-17 06-1 and by Science Systems and Applications, Inc. through NASA contract NAS5-02041, subcontract 2207-06-016. Weather data for Pond Inlet and Clyde River were provided by Environment Canada. We are indebted to R. Hock who contributed to the development of the mass balance model. The U.S. Geological Survey (USGS) Earth Resources Observation System (EROS) Data Center,

the Land Processes Data Center (LPDAAC) and the National Snow and Ice Data Center (NSIDC) at the Cooperative Institute for Research in Environmental Sciences (CIRES), University of Colorado, provided Landsat 7 ETM data, TERRA ASTER data and ICESat GLAS data. We acknowledge the respective space agencies for delivering high quality data as part of their earth observation systems. Helpful comments of A. Arendt, an anonymous reviewer and the scientific editor R. Hock contributed to improve the clarity of the manuscript.

Part III

Projections of future glacier extent and runoff

Chapter 7

Modelling the future retreat of Unteraargletscher

MATTHIAS HUSS¹, SHIN SUGIYAMA^{1,2}, ANDREAS BAUDER¹, MARTIN FUNK¹

¹Versuchsanstalt für Wasserbau, Hydrologie und Glaziologie (VAW), ETH Zürich, 8092 Zürich, Switzerland

²Institute of Low Temperature Science, Hokaido University, 060-0819 Sapporo, Japan

Published, Arctic, Antarctic and Alpine Research

Citation: Huss M., S. Sugiyama, A. Bauder, M. Funk (2007). Retreat scenarios of Unteraargletscher, Switzerland, using a combined ice-flow mass-balance model. *Arctic, Antarctic and Alpine Research*, **39**(3), 422–431.

ABSTRACT: The future evolution of Unteraargletscher, a large valley glacier in the Swiss Alps, is assessed for the period 2005 to 2050 using a flowline model. Detailed measurements of surface velocity from the last decade allow us to relate ice flux to glacier thickness and width. Mass balance is calculated using a distributed temperature-index model calibrated with ice volume changes derived independently from comparison of repeated digital elevation models. The model was validated for the period 1961 to 2005 and showed good agreement between the simulated and observed evolution of surface geometry. Regional climate scenarios with seasonal resolution were used to investigate the anticipated response of Unteraargletscher to future climate changes. Three mass balance scenarios were defined, corresponding to 2.5 %, 50 % and 97.5 % quantiles of a statistical analysis of 16 different climate model results. We present a forecast of the future extent of Unteraargletscher in the next five decades and analyze relevant parameters with respect to the past. The model predicts a retreat of the glacier terminus of 800-1025 m by 2035, and of 1250-2300 m by 2050. The debris coverage of the glacier tongue reduces the retreat rate by a factor of three. The thinning rate increased by 50-183% by 2050 depending on the scenario applied, compared to the period 1997 to 2005.

7.1 Introduction

Glaciers are considered to be sensitive indicators of climate change (e.g. IPCC, 2001; Oerlemans and Fortuin, 1992; Haeberli, 1995). During the last century, Alpine glaciers suffered major mass losses (e.g. Vincent and others, 2004). Large rearrangements in alpine systems due to glacier retreat or complete disappearance will result from the likely acceleration of climatic warming during the next decades. These changes affect the environment on local and on global scales. Water resources are expected to diminish and significant societal impacts in peripheral regions are anticipated. Therefore, the investigation of glacier retreat and the development of methods for its prediction are important in order to be prepared for the new environmental situation.

The parameterization of glacier mass balance is of crucial importance to the investigation of glacier reaction to a warming climate. In recent years a wide range of models has been developed to calculate mass balance using climatological observations (e.g. Braithwaite, 1995; Hock, 1999; Hock and Holmgren, 2005; Schaeffli and others, 2005; Pellicciotti and others, 2005; Gerbaux and others, 2005). Energy balance models directly address the physical processes at the glacier surface. Temperature-index models are based on a linear relation between positive air temperature and melt rate. Ohmura (2001) demonstrated that the physical base of temperature-index modeling is stronger than previously assumed. Melt is highly correlated with longwave heat flux, for which air temperature is a good indicator.

Several studies investigated the consequences of changing temperature and precipitation on alpine glaciers. Some works are focused on sea level change (e.g. Zuo and Oerlemans, 1997; Braithwaite and Zhang, 1999; Van de Wal and Wild, 2001). Schaeffli (2005) conducted a study on the change in hydrological variables in several highly glacierized alpine catchment basins with a statistical distribution of regional climate models, but without taking the ice motion into account. The reaction of the glacier front to a shift in climate variables is related to the ice flow (Jóhannesson and others, 1989). Therefore, reasonable predictions of the response of an individual glacier with sufficient spatial and temporal accuracy are only possible using a combined ice-flow mass-balance model approach. Wallinga and van de Wal (1998) and Oerlemans and others (1998) applied flowline models with simple parameterizations of climate change to a number of alpine glaciers. Schneeberger and others (2001) used a 3-dimensional flow model and a glacier melt model forced by downscaled GCM outputs to calculate the response of Storgläciären, Sweden.

The assessment of ice volume and glacier extent in the next decades requires the incorporation of climate change scenarios. There are several factors of uncertainty in climate projections. First of all, the socio-economic and technological development of our civilization, which will determine the future emission of greenhouse gases, is not known. Our knowledge of the climate system and its processes and feedback mechanisms is still limited and there are various ways to describe the system by using quantitative models. In recent years, a large number of climate change models has been developed (IPCC, 2001). A probability-distribution function (PDF) can be derived by evaluating a whole set of model results with different, but realistic, boundary conditions. This has been done on global (Wigley and Raper, 2001) and on regional scales (e.g. Frei and others, 2006). A PDF provides a better quantitative estimation of the modeling uncertainties, and allows the future range of climate change to be inferred.

In this study we present a combined ice-flow mass-balance model, which is driven by regional climate scenarios for temperature and precipitation changes with seasonal resolution. The high

temporal and spatial resolution used for this work allows us to perform detailed predictions of future glacier evolution based on field measurements and robust modeling approaches.

The presented study was initiated as part of an extension project of the hydro-electric power company Kraftwerke Oberhasli AG (KWO). The company manages a system of several dammed lakes in the catchment basin of the Aare river. To increase the system performance, the possibility is considered of raising the maximum lake level of Grimsensee (lake), its largest reservoir, by 23 m. This lake is situated in the valley of Unteraargletscher, 1 km downstream from the current glacier terminus. The planned raising of the lake level would flood the glacier forefield up to the current glacier snout. In order to assess whether the lake water would come into contact with the glacier after the completion of the project (in 2012), we performed numerical simulations of the future glacier evolution until 2050. To achieve this goal, we developed a flowline model applying novel approaches to ice-flow and mass-balance computation by carrying out the following steps:

- the setup of an empirical ice-flow model based on flow-speed measurements,
- distributed modeling of mass-balance using temperature and precipitation data,
- verification of the flowline model in the past by comparing the results with measured glacier surface geometries, and
- incorporation of state-of-the-art climate scenarios into the mass-balance model to simulate future conditions.

7.2 Study area and relevant data

With a length of approximately 13 km, Unteraargletscher is the fourth largest glacier in the Swiss Alps. The temperate valley glacier covers an elevation range from 1900 to 4000 m a.s.l. Two main tributaries, Lauteraargletscher and Finsteraargletscher, merge to form the Unteraargletscher extending about 5 km eastward of the confluence area with a mean slope of 4° (Fig. 7.1). Unteraargletscher is largely debris-covered and characterized by the dominant feature of an ice-cored medial moraine. The thickness of the debris cover is generally 0.1-0.2 m, but increases progressively toward the glacier terminus (Sugiyama, 2003).

In the last two decades Unteraargletscher was the object of extensive field studies focusing on the geometry of the glacier and its bed (Funk and others, 1994; Bauder and others, 2003), mass balance (Bauder, 2001), basal processes (Fischer and others, 2001; Rousselot, 2006), hydrology (Schuler, 2002; Fischer and others, 2005) and dynamics (Gudmundsson, 1999; Sugiyama and Gudmundsson, 2004; Helbing, 2005).

The relevant data sets for the setup of the flowline model can be divided into five categories: (i) surface and bed topography, (ii) thickness changes, (iii) surface velocity measurements, (iv) ablation measurements and (v) climate data. Since 1924 annual measurements of thickness changes and surface velocities at 13 profiles have been conducted. After 1990, photogrammetric analysis of aerial photographs replaced previous field surveys and the measurements on profiles were expanded by applying digital elevation models (DEM) to the whole ablation area (Flotron, 1924-1998). We used the velocity measurements on Unteraargletscher at profiles 1 to 6

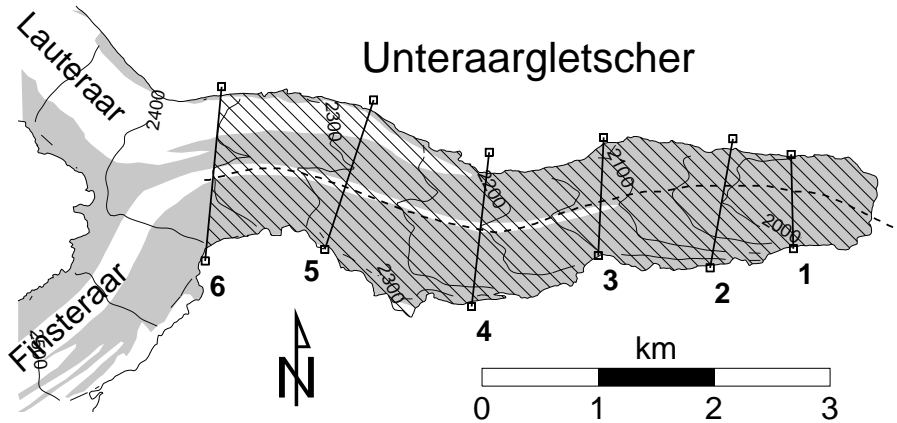


Figure 7.1: Map of the ablation zone of Unteraargletscher. The extent of debris-covered ice is grey-shaded. The hatched area confines the part of the glacier on which the modeling was performed and the dashed line marks the central flowline. Annual measurements of surface velocity are available for the cross-section profiles 1 to 6.

(Fig. 7.1) in the period 1989-2001 for the development of the ice-flow model. DEMs of the ablation area are available for 1990-1992, 1995-1999, 2003 and 2005 (Flotron, 1924-1998; Bauder, 2001; unpublished data VAW/ETHZ). By comparing the elevation changes of the DEMs volume balances were derived (Bauder, 2001). A dense network of radio-echo sounding profiles covers the ablation area of the glacier (Bauder and others, 2003). The accuracy of the bed topography is in the range of 5% of the ice thickness (Bauder, 2001). Direct ablation measurements on Unteraargletscher are available at up to 40 stakes for the period 1996 to 2001 (Bauder, 2001). Temperature and precipitation have been measured since 1959 at subdaily resolution and since 1989 at hourly resolution at the MeteoSchweiz weather station at Grimsel Hospiz, 1980 m a.s.l, located within 7 km from the glacier terminus.

Additional data cover the entire last century and provide possibilities for comparing the predictions of the flowline model with long data series of the past. Annual records of length change of Unteraargletscher extend back to 1871. Six DEMs of the whole glacial system were derived by evaluating old maps and aerial photographs (Bauder and others, 2007). Volume changes and rates of glacier thinning can be established for more than 125 years. A nearly constant glacier retreat has been observed since the records began. Short periods of positive mass balance (for example in the 1980s) are not revealed in the length change record. This is because Unteraargletscher has a response time of 70 to 100 years according to the volume-time scale of Jóhannesson and others (1989) and does not reflect short-term climate variations.

7.3 Flowline model

A site-specific one-dimensional flowline model was developed for Unteraargletscher below profile 6 (Fig. 7.1). The temporal evolution of the glacier surface is given by the continuity equation

$$\frac{\partial h(x, t)}{\partial t} = \dot{b}(x, t) - \frac{\partial Q(x, t)}{\partial x W(x, t)}, \quad (7.1)$$

where Q denotes the ice flux through a cross section, W the glacier width, \dot{b} the mass-balance rate and h the ice thickness. The x -axis follows the flowline. Equation 7.1 is solved explicitly with a grid spacing of $\Delta x = 25$ m along the flowline and a time step of $\Delta t = 1$ d. At each grid point and time step, Q , W and \dot{b} are calculated as described in the following subsections.

Ice-flow model

Ice velocity u observed on a glacier surface is composed of a component u_d due to deformation of the ice mass and a component u_b due to sliding over the bed (Paterson, 1994). The deformation of ice can be described by the conservation equations of mass and momentum together with a constitutive relationship accounting for ice rheology (e.g. Glen, 1955). The motion at the base including a variety of relevant processes for sliding and deformation of the bed itself is an important, but poorly understood, element of ice-flow dynamics. Under real conditions the stress field in glacier ice is very complex and can only be solved numerically (e.g. Gudmundsson, 1999). The detailed measurements of surface geometry and velocity made over a period of more than one decade in recent years offer an alternative way to calculate the ice flux along the flowline.

To incorporate two-dimensional effects into the ice-flow model, we define an empirical relationship between the ice flux through a glacier cross section and the central ice thickness by using measured data. The ice flux Q through the profiles 1-6 is calculated by integrating flow speed in cross sections.

$$Q = \int_0^W \int_0^{h(y)} u(y, z) dz dy, \quad (7.2)$$

taking y across the glacier and z perpendicular to the bed. W is given in Flotron (1924-1998) and the thickness h is obtained from radio-echo sounding and DEM. The vertical distribution of the horizontal flow speed u is calculated from measured surface velocity with an assumption of simple shearing (Paterson, 1994),

$$u(z) = u_b + u_s \left\{ 1 - \left(\frac{h - z}{h} \right)^{n+1} \right\}. \quad (7.3)$$

The surface speed u_s across the profiles was measured annually from 1989 to 2001 and $n = 3$ is used as the exponent in Glen's flow law. We assume, that the basal sliding speed u_b accounts for 50% of the surface speed based on bore-hole inclinometry on Unteraargletscher (Gudmundsson and others, 1999; Helbing, 2005). Variations in the fraction of u_b would lead to a maximum sensitivity in the calculated flux of 10%, which lies in the range of uncertainty of the other variables.

The calculated fluxes through the six cross profiles for the years 1989 to 2001 enable us to parameterize ice flux with ice thickness at the center line of the glacier (Fig. 7.2a). For this

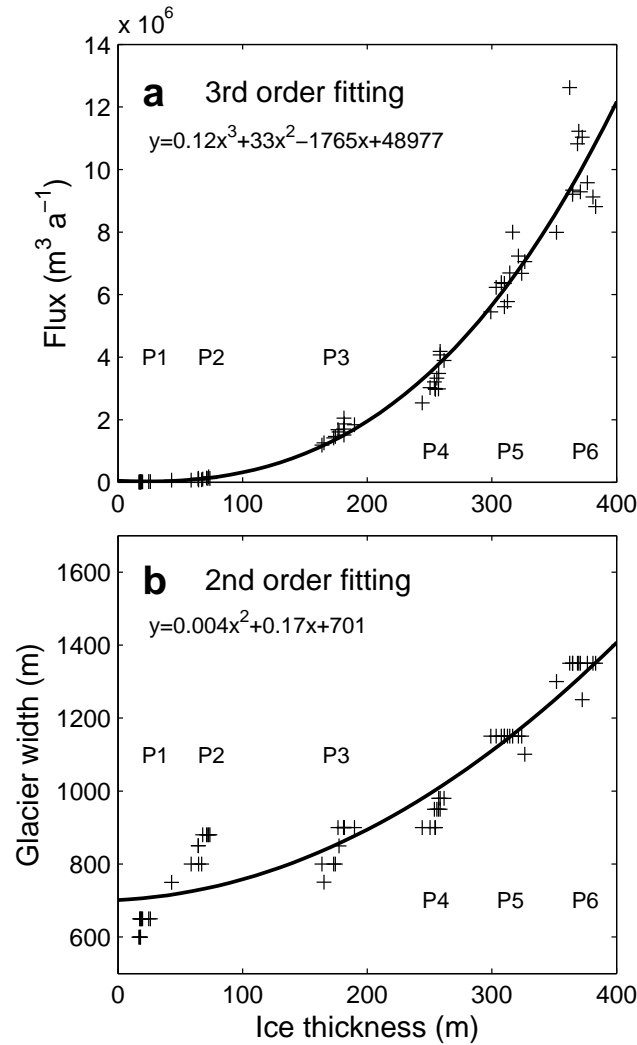


Figure 7.2: Empirical site-specific relations between central ice thickness and ice flux (a), and ice thickness and glacier width (b) for Unteraargletscher. Crosses correspond to data of individual years. Data clusters relate to the position of the profiles indicated by P1-P6 (Fig. 7.1). Equations of the polynomial fits are given.

empirical relation a third order fit yields good agreement for all profiles. Another empirical relation (Fig. 7.2b) between ice thickness and glacier width is used to obtain W in Equation 7.2. The values for the lowest two profiles do not match well with the fitted curve. Their influence on the computation, however, is not substantial as ice thickness and flow speed are minimal.

Using this approach we can calculate the two-dimensional ice flux through cross sections directly from the central ice thickness (Fig. 7.2a) and obtain the one-dimensional flux based on the glacier width (Fig. 7.2b) at every point along the flowline. The ice flux needs to be prescribed as the boundary condition at the upper end of the model domain. This quantity is obtained from the empirical relationship shown in Fig. 7.2a. Thus the upstream evolution of the glacier is taken into account in an indirect manner only. This parameterization is justified if we assume a constant mass-balance gradient over time.

Mass-balance model

We use a distributed temperature-index model (Hock, 1999) coupled with an accumulation model for the calculation of the spatial distribution of mass balance. It elaborates on classical models using degree-day factors by varying these as a function of potential clear-sky radiation in order to account for the effects of slope, aspect and shading. Temperature and precipitation at a nearby weather station are required field data. Surface melt rates M are computed by:

$$M = \begin{cases} (f_M + r_{\text{snow/ice}}I)T & : T > 0 \\ 0 & : T \leq 0 \end{cases} \quad (7.4)$$

where f_M denotes a melt factor, $r_{\text{snow/ice}}$ are radiation factors for snow and ice and I is the potential clear-sky radiation. I is calculated with a DEM on a 25 m grid at hourly resolution.

Large parts of Unteraargletscher are debris-covered. If the coverage is continuously thicker than several centimeters, this causes a significant reduction of ablation (Kayastha and others, 2000). Stake measurements on Unteraargletscher show strong spatial variability of icemelt. To account for the effect of debris-covered ice, ablation was corrected using a constant reduction factor f_{debris} (Schuler and others, 2002). The melt rate M over debris-covered surfaces is calculated as

$$M = (f_M + r_{\text{ice}}I)T \times f_{\text{debris}} \quad : T > 0 \quad (7.5)$$

The factor f_{debris} is determined as the mean reduction of measured ablation at stakes on debris-covered ice in comparison to stakes on bare ice surfaces in the same elevation range. f_{debris} is 0.5 and is supposed to remain unchanged over time. This assumption will be discussed later on.

Air temperature at every grid cell is calculated with a constant lapse rate of $-6 \times 10^{-3} \text{ }^\circ\text{C m}^{-1}$. The hourly measurements of temperature and precipitation at Grimsel Hospiz are taken to be representative of the modeling area. In this model approach, correction factors account for gauge under-catch errors and increased losses in the case of solid precipitation. Precipitation is assumed to increase linearly by 1.5% /100 m. A threshold temperature distinguishes snow from rainfall with a linear transition range (0.5°C to 2.5°C) of the fraction of the solid and the liquid phase (Hock, 1999). The spatial distribution of solid precipitation is corrected by taking into account the effects of snowdrift and avalanches. This is achieved by evaluating curvature and slope based on a DEM, similar to a procedure discussed in Blöschl and others (1991).

The applicability of temperature-index models depends on the calibration of the key parameters with field data. A site-specific relationship is established between melt rate M and positive air temperature (Hock, 2005). For the presented model there are three melt parameters to calibrate: f_M , r_{ice} and r_{snow} . The precipitation parameters mainly affect accumulation. The modeled area lies in the ablation zone in all years considered. Therefore, the results in this region are less sensitive to the precipitation parameters and they are set to standard values.

For the determination of an optimal set of the melt parameters we use ice volume changes derived from DEMs. 10 DEMs for the calibration period 1990-2005 are obtained from grid-based high resolution evaluation of aerial photographs. Uncertainty is estimated as ± 0.3 m (Bauder, 2001). Border lines of the glacier are digitized from the aerial photograph. This step can pose some problems as the limit of the glaciated area is not always visible because of debris coverage. By comparing elevation changes between the DEMs within the glacierized area of the modeled region we calculate mean thickness changes. By assuming an ice density of 900 kg m^{-3} we obtain the change in water equivalent between two DEMs. The overall accuracy

of the volume change evaluation is estimated as $\pm 10\%$ for annual time steps and $\pm 5\%$ for longer periods. Bauder and others (2007) give a detailed overview about the calculation of volume changes based on DEMs and their uncertainties.

As the DEMs do not cover the entire glacierized area, the derived volume changes cannot be compared directly to the simulated mass balances. The volume change ΔV_{mr} of the modeled region has to be corrected with the ice flux from the accumulation area counteracting the thinning of the glacier tongue due to ablation. The mean specific mass balance of the modeled region \overline{b}_{mr} is therefore

$$\overline{b}_{\text{mr}} = \frac{\Delta V_{\text{mr}} - Q_{\text{P6}}}{A_{\text{mr}}}, \quad (7.6)$$

where Q_{P6} is the ice flux through cross profile 6 and A_{mr} the area of the modeled region.

The applied calibration procedure proved to be well suited for the purpose of this study, because all quantities in Equation 7.6 are not point based, rather they integrate overall spatial changes of the entire glacier. Our focus when calibrating was on cumulative results of simulated mass balance and corrected volume change. Thus deviations in individual years due to inaccurate determination of mass balance, ice flux or volume change are averaged out. Good agreement was achieved between calculated mass balance and corrected volume change in the modeled region (Fig. 7.3). Subsequently, the results are compared to the measured melt at ablation stakes (Bauder, 2001), which serve as independent verifiers of the calibration procedure. The field data correspond well to the simulations. Mass balance is not modeled accurately at all stake locations, which can be explained by the considerable inhomogeneity of the debris coverage. However, the variability of ablation is averaged out spatially. The simulations of the mass-balance model calibrated with corrected volume changes are thus consistent with the direct ablation measurements.

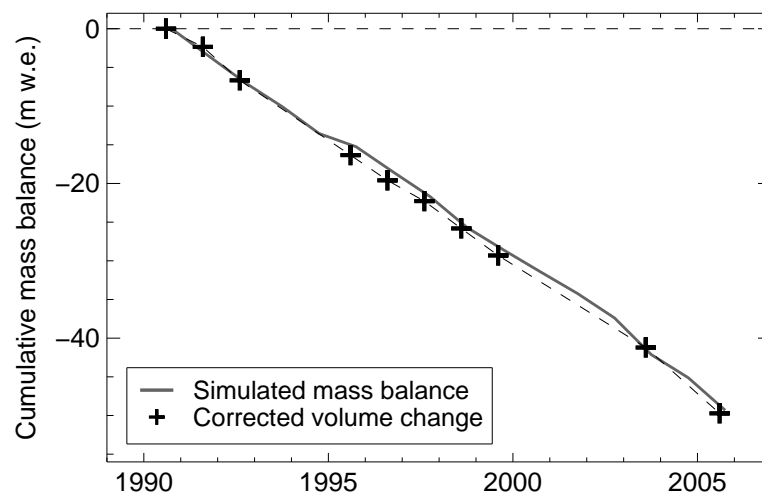


Figure 7.3: Calibration of the model parameters with simulated mass balance (solid line) and corrected volume change (crosses) in the modeled region.

Melting in the ablation area is characterized by two different mass-balance gradients (below 2500 m a.s.l.) due to the two different ice surfaces: debris-covered, and bare (Fig. 7.4). The measurements at ablation stakes support this finding (Bauder, 2001). The larger scatter in the accumulation area (above ≈ 2900 m a.s.l.) is due to snowdrift and slope effects.

In order to relate mass balance to the flowline with a variable geometry, we parameterize mass balance dependent on elevation. Accumulation and ablation at a given altitude is a function of

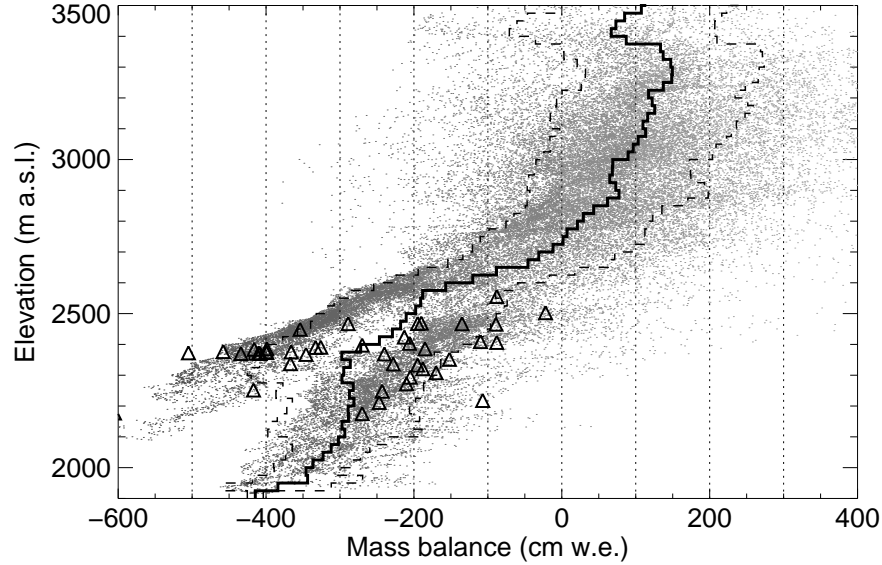


Figure 7.4: *Distribution of mass balance with elevation: October 1998 - October 1999. The solid line represents the mean mass balance in elevation classes of 25 m and the dashed lines the rms-deviations of mass balance from the mean value at grid cells (dots). Below 2500 m a.s.l. there are two clearly distinguishable gradients for bare and debris-covered ice. Triangles show the measured ablation in 1998/1999.*

climate variables and is calculated by the model described above. We assume slope and aspect at a fixed elevation to remain unchanged. Thus, the mass-balance gradient does not change, which corresponds to observations on alpine glaciers (Hoinkes, 1970). It is shifted according to the perturbations of the climate variables.

Table 7.1: *Model parameters, values and units*

Parameter	Symbol	Value/Range	Units
Ice flux in cross section	Q	$0 - 12 \times 10^6$	$\text{m}^3 \text{a}^{-1}$
Glacier width	W	$0 - 1200$	m
Ice thickness	h	$0 - 330$	m
Mass-balance rate	\dot{b}	$-7 - 4$	m a^{-1}
Melt rate	M	$0 - 0.018$	m h^{-1}
Potential clear-sky radiation	I	$0 - 1368$	W m^{-2}
Melt factor	f_M	0.63×10^{-6}	$\text{m h}^{-1} \text{ } ^\circ\text{C}^{-1}$
Radiation factor ice	r_{ice}	0.82×10^{-6}	$\text{m}^3 \text{W}^{-1} \text{h}^{-1} \text{ } ^\circ\text{C}^{-1}$
Radiation factor snow	r_{snow}	0.60×10^{-6}	$\text{m}^3 \text{W}^{-1} \text{h}^{-1} \text{ } ^\circ\text{C}^{-1}$
Reduction factor debris-covered ice	f_{debris}	0.5	—

7.4 Future climate

Climate scenarios for the Alpine region

The climate projections are based on simulations of the PRUDENCE project (Christensen and others, 2002). A statistical analysis from results of 16 regional climate models for Switzerland was performed by Frei (2007). These results are derived from model chains of different emission-scenarios and downscaled GCM outputs. Frei (2007) computed a 95% confidence interval for the evolution of temperature and precipitation in a seasonal resolution for 2030, 2050 and 2070. Figure 7.5 shows the results of this study. The given values are changes relative to 1990. The temperature rise is most pronounced in the summer season and is $+1.4^{\circ}\text{C}$ until 2030 and $+2.7^{\circ}\text{C}$ until 2050, respectively. In winter, a slight increase of precipitation $+8\%$ until 2050 is expected, whereas a decrease of -17% until 2050 in summer is predicted (Frei, 2007).

Mass-balance scenarios

We define three climate change scenarios: two extreme evolutions and a median scenario, expected to be the most probable evolution. Scenario 1 is most favorable to glacier existence, Scenario 2 adopts the median of the statistical analysis (Frei, 2007) and Scenario 3 is based on the most dramatic climate change assumptions (Fig. 7.5 and Tab. 7.2).

We use the model presented in Section 7.3 to calculate future mass balances. By applying this method we do not have to rely on statistical relations between climate variables and mass balance as proposed by previous studies, but calculate accumulation and melt directly in high

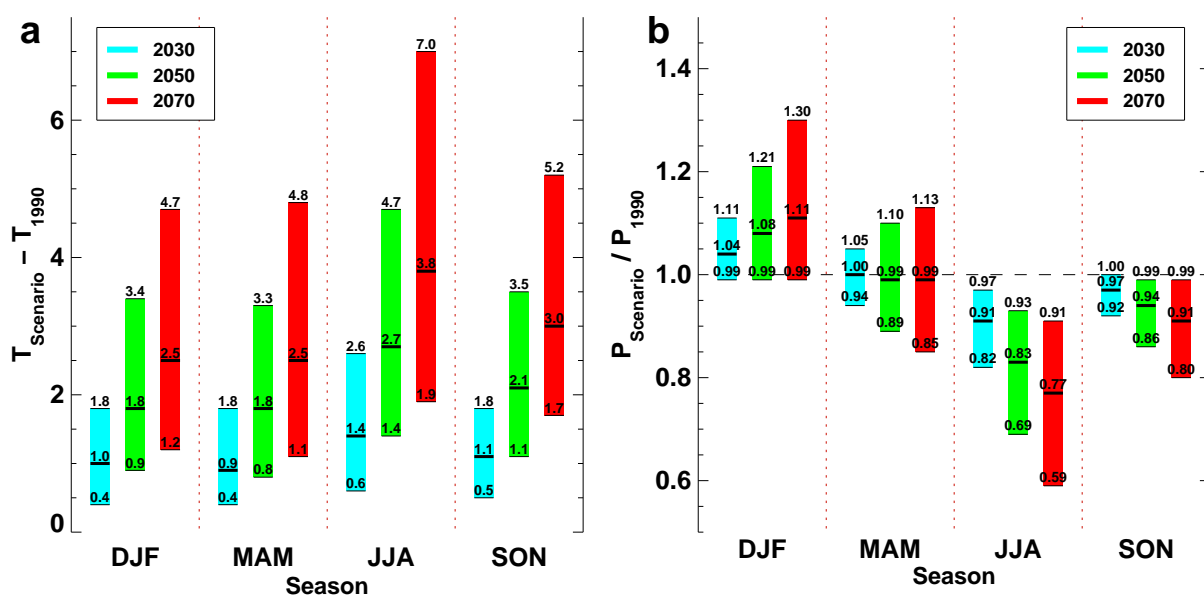


Figure 7.5: Expected climate change for the northern flank of the Alps in seasonal resolution for 2030, 2050 and 2070. The bars show the 95% confidence interval, the horizontal lines the median value. Temperature (a) and precipitation (b) scenarios are relative to 1990. Figure by Frei (2007).

Table 7.2: Definition of the climate scenarios according to Frei (2007) and Figure 7.5.

Scenario	Temperature change quantile	Precipitation change quantile
Scenario 1	2.5%	97.5%
Scenario 2	50%	50%
Scenario 3	97.5%	2.5%

temporal resolution. Thus, feedback mechanisms, such as longer ablation seasons, larger portions of liquid precipitation etc., are implicitly included. The parameters of the mass-balance model were calibrated for the period 1990 to 2005. To simulate mass balances in the next 50 years using the same parameter set, time-series of temperature and precipitation with identical temporal resolution are required. In the future, the mean of climate variables is supposed to change, whereas we assume their characteristics (e.g. diurnal amplitudes) to remain the same, thus justifying the applicability of the model parameters for the next decades.

Based on each year of a 1990 to 1999 reference period, a temperature time-series of hourly resolution was generated as follows: each hour value i of year j ($j=1990,\dots,1999$) is corrected with a normalization offset OT computed with the mean seasonal temperature of the individual year $\overline{T_{s,j}}$ and the mean seasonal temperature of the reference period $\overline{T_{s,rp}}$ with the relation

$$OT_{s,j} = \overline{T_{s,j}} - \overline{T_{s,rp}}, \quad (7.7)$$

where the subscript s denotes the season, rp the reference period. The normalization offset OT is a matrix with a value for each season and each year of the reference period (4×10). Subsequently, all data are normalized with OT :

$$T_{i,j}^{\text{norm}} = T_{i,j} - OT_{s,j}. \quad (7.8)$$

The temperature time-series $T_{i,j}^{\text{norm}}$ of all years of the reference period has identical seasonal means and are, thus, comparable. Their interannual variability is removed. The annual temperature changes ΔT_k ($k=2005,\dots,2050$) for the future are calculated with a linear interpolation between the measured reference values and the expected changes for 2030, 2050 and 2070 (Frei, 2005 and Fig. 7.5). A hourly time-series for each year k of the modeling period is obtained by the relation

$$T_{i,j,k} = T_{i,j}^{\text{norm}} + \Delta T_{s,k}. \quad (7.9)$$

The precipitation time-series is generated by the same method. The normalization offset OP for precipitation is computed as a ratio

$$OP_{s,j} = \frac{P_{s,j}}{P_{s,rp}}, \quad (7.10)$$

where P denotes the seasonal precipitation sum. OP as well as $\Delta P_{s,k}$ are therefore applied to the precipitation values as a factor. By applying these time-series of temperature and precipitation as input for each year between 2005 and 2050 the mass balance was calculated using the temperature-index model.

7.5 Results

Model validation

The model was applied to two periods in the past, for which the model output can be compared with corresponding measured glacier surface geometry. For the short period of 1990 to 2005, good agreement was found. Even for the longer period of 1961 to 2005, the simulated glacier surface matches the observed one (Fig. 7.6). We conclude that the combined ice-flow mass-balance model is capable of simulating glacier evolution caused by a modification of present climate input parameters over a period of a few decades. The good performance of the model between 1961 and 2005 without tuning of the parameters of both the ice-flow and the mass-balance model strongly supports the application of the flowline model for a period of comparable length in the future.

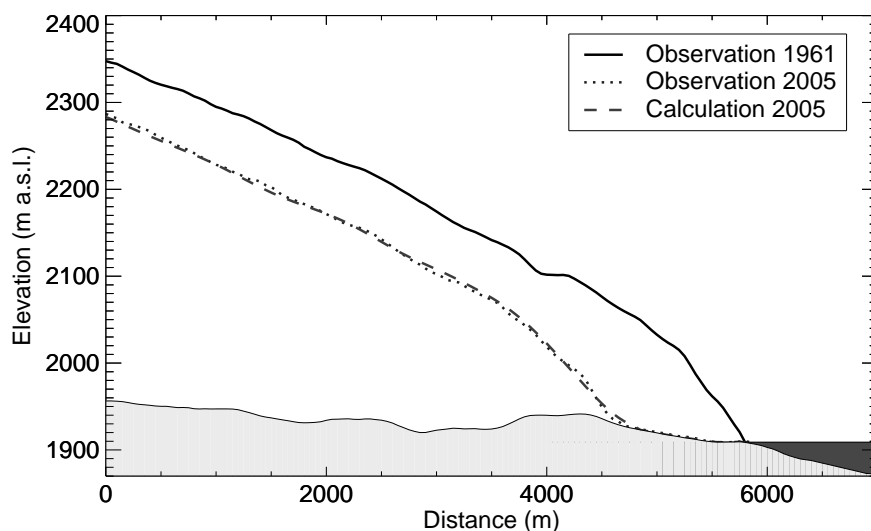


Figure 7.6: Test run of the coupled ice-flow mass-balance model in the past (1961-2005). Good agreement between calculated (dashed) and observed (dotted) surface geometry is obtained.

Retreat of Unteraargletscher

By forcing the model with the climate scenarios described in Section 7.4 we calculate the future evolution of Unteraargletscher until 2050. We present the results focused on 2035 and 2050. The model runs until 2035 show a retreat of the snout of Unteraargletscher between 800 m and 1025 m, depending on the scenario applied. A retreat of between 1250 m and 2300 m is predicted by 2050. Between 2035 and 2050 the rate of retreat increases substantially. Figure 7.7 demonstrates the glacier evolution along the central flowline. The simulated ice surfaces for the three climate scenarios corresponding to the 95% confidence interval of expected climate change all show a major retreat (Fig. 7.7a).

As the climate scenarios given by Frei (2007) provide information until 2070, we conducted model runs with less reliable mass-balance assumptions due to an extremely accelerated climate change until 2070. For Scenario 1, only a slight acceleration of the retreat rate can be observed, whereas for Scenario 3 a complete disintegration of the glacier in the model domain is predicted (Fig. 7.8a).

Table 7.3: Compilation of model results for Scenarios 1 to 3 for two periods (2005 to 2035, 2035 to 2050).

Scen	Length change		Thickness change		Volume change		Area loss	
	total (m)	annual (m a ⁻¹)	total (m)	annual (m a ⁻¹)	total (10 ⁶ m ³)	annual (10 ⁶ m ³ a ⁻¹)	total (km ²)	relative (% of 2005)
between 2005 and 2035								
1	-800	-26.7	-81	-2.7	-317	-10.6	-1.19	-26.7
2	-875	-29.2	-97	-3.2	-368	-12.3	-1.43	-32.0
3	-1025	-34.2	-120	-4.0	-436	-14.6	-1.69	-37.9
between 2035 and 2050								
1	-450	-30.0	-50	-3.3	-143	-9.6	-0.61	-40.3
2	-725	-48.3	-67	-4.5	-175	-11.6	-0.74	-48.6
3	-1275	-85.0	-90	-6.0	-202	-13.5	-1.04	-61.0

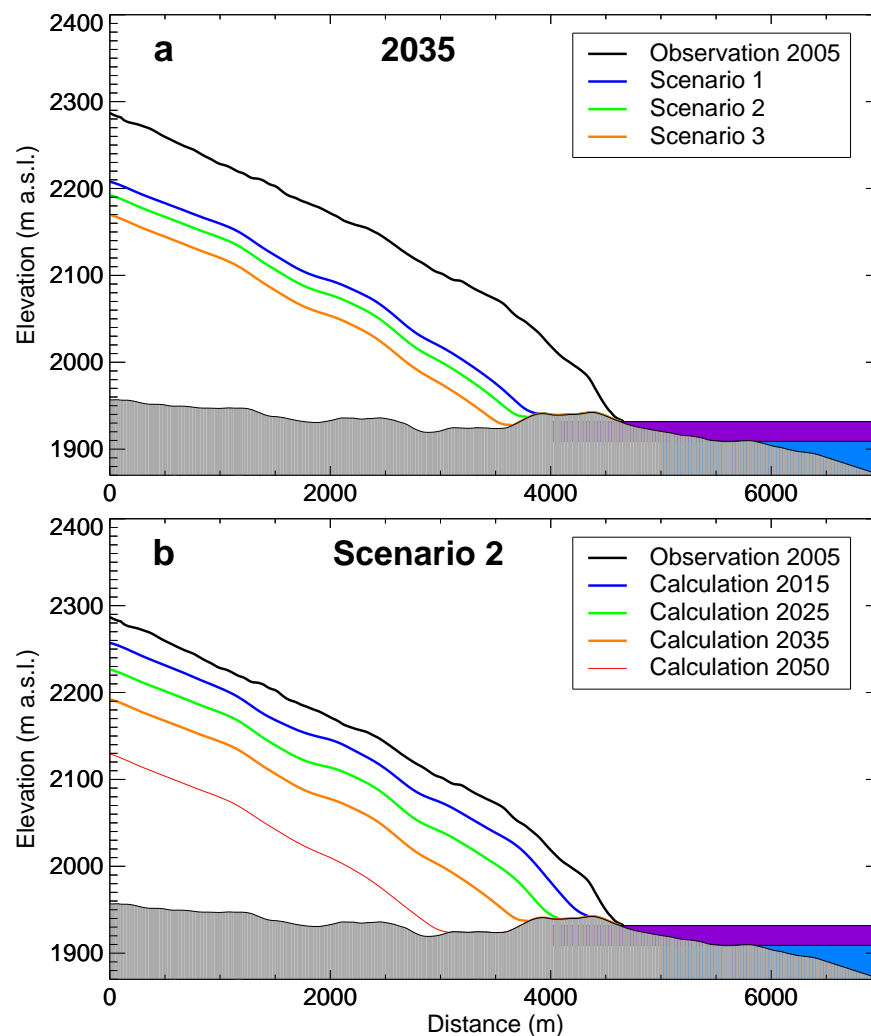


Figure 7.7: (a) Comparison of the model results for Scenarios 1 to 3 (2035) along the central flowline; (b) Simulated glacier surface elevation for 2015, 2025, 2035 and 2050 according to Scenario 2. Shaded areas in front of the glacier snout mark the extension of the current lake (dark grey) and the projected lake (light grey).

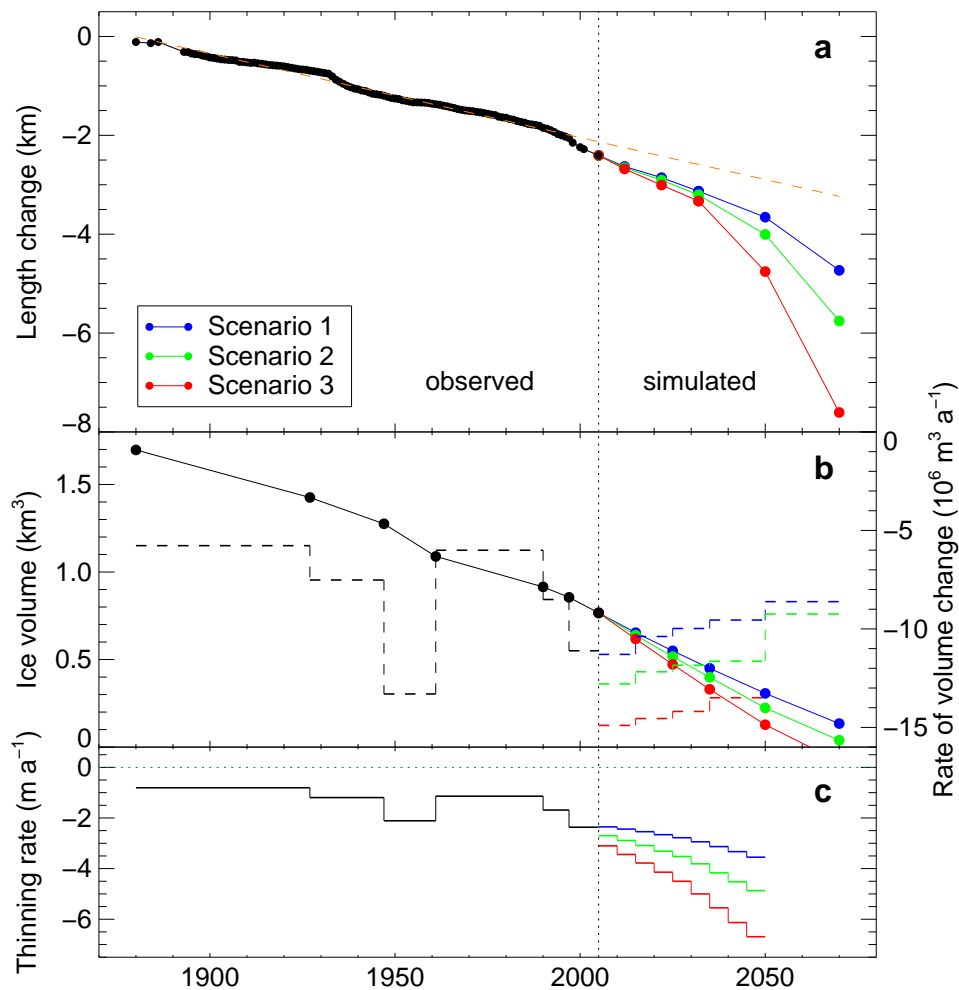


Figure 7.8: (a) Observed and simulated length change of Unteraargletscher. The dashed line shows the trend of the measured length change extrapolated into the future. (b) Ice volumes in the modeled region and corresponding volume change rates derived from DEMs since 1880 until present and from simulation results until 2070. (c) Thinning rates derived from DEMs and simulations.

Simulated length, volume changes and thinning rates are presented in Figure 7.8 with respect to observations in the past century. Ice volume in the modeled region will decrease by 41-57% by 2035 and by 60-83% by 2050 relative to 2005. However, the rate of volume change remains nearly constant (Fig. 7.8b). The thickness changes of Unteraargletscher were computed for six periods in the last century. Annual thinning rates in the modeled region lie in the range of -0.8 to -2.3 m a^{-1} with a weighted mean of -1.24 m a^{-1} between 1880 and 2005 (Fig. 7.8c). In the period 2005 to 2035 the ice thickness in the modeled region changes at an average rate of -2.7 m a^{-1} for Scenario 1, -3.2 m a^{-1} for Scenario 2 and -4 m a^{-1} for Scenario 3 (Table 7.3). The simulated thinning rates were evaluated in 5-year periods until 2050. An acceleration of thinning is predicted. Compared to the latest evaluated period, 1997 to 2005, an increase in the thinning rate of 50% by 2050 for Scenario 1, of 106% for Scenario 2 and of 183% for Scenario 3 is calculated.

We assess the mass budget of the modeled region by comparing mass gain due to ice flux through profile 6 with mass loss due to ablation. According to the applied climate scenario, the ratio of the importance of ice flux to mass balance falls from between 30 and 45% in 2005

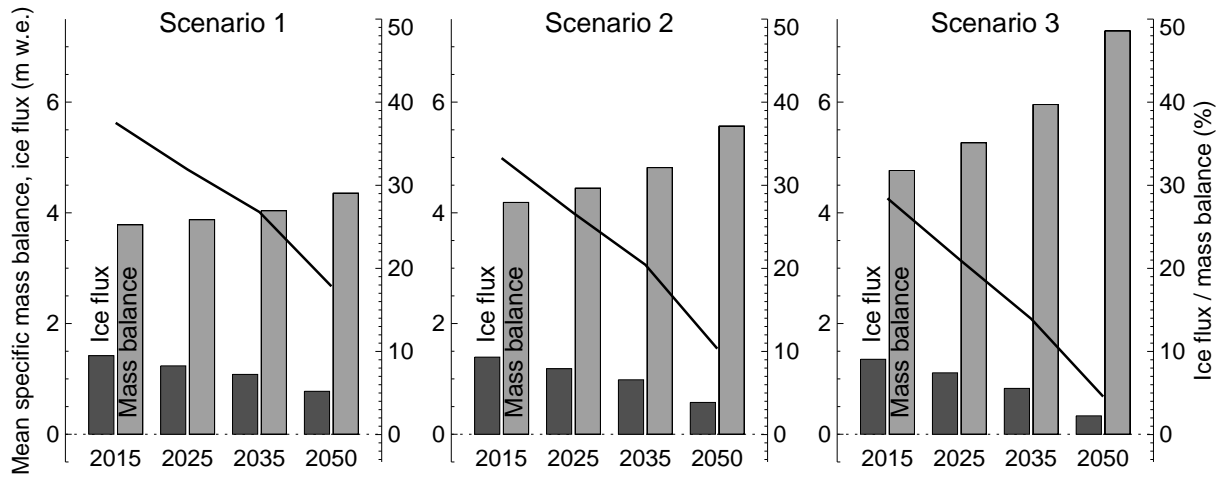


Figure 7.9: Comparison of absolute specific values (m WE) of mass fluxes in the modeled region. Ice flux through profile 6, positive, is plotted in dark grey; mean specific mass balance in the modeled region, negative, in light grey. The solid line is the ice-flux mass-balance ratio.

to between 13 and 2% in 2035 and between 5 and 18% in 2050 depending on which scenario is adopted (Fig 7.9). The computed mean specific mass balance $\overline{b_{mr}}$ of the modeled region of Unteraargletscher shows a progressive decrease. Because of the accelerated retreat due to climatic forcing, the importance of ice flow becomes increasingly marginal but not negligible compared to mass balance.

The computed glacier margins in the future are projected on a map assuming the thickness change on the flowline to be identical at the same elevation on the whole glacier. In Figure 7.10 the spatial extent of retreat is depicted. Close to the snout the glacier shrinks considerably. The model results predict that Unteraargletscher will lose 27-38% of its area downstream of profile 6 by 2035 and 40-61% by 2050 (Fig. 7.10 and Table 7.3).

The debris coverage of Unteraargletscher delays the retreat of the glacier tongue considerably. We performed two sensitivity tests, in which we either removed the debris cover completely (1) or decreased f_{debris} (Eq. 7.5) at constant rates corresponding to a gradual 50%-thickening of the debris cover by 2050 (2). The results of experiment 1 show that the retreat of the glacier tongue would be about three times faster without any debris coverage compared to the reference runs. For experiment 2 we observe a deceleration of glacier retreat rate by 20%. In both experiments the perturbations of mass balances caused by different debris coverages are amplified by a positive feed-back due to ice flow.

7.6 Discussion and Conclusion

Studies forecasting the future have to cope with problems of extrapolation. While our model was successfully tested for five decades in the past (Fig. 7.6) its performance in the future cannot be proved. This poses limitations on the time period of extrapolation into the future. The parameters of the temperature-index model were calibrated over the past 15 years by integrating the prevailing climate characteristics through this period. With major changes in the climate variables the tuned melt parameters may be influenced over the following decades by altered circulation patterns and the redistribution of heat fluxes, which are difficult to predict (Hock,

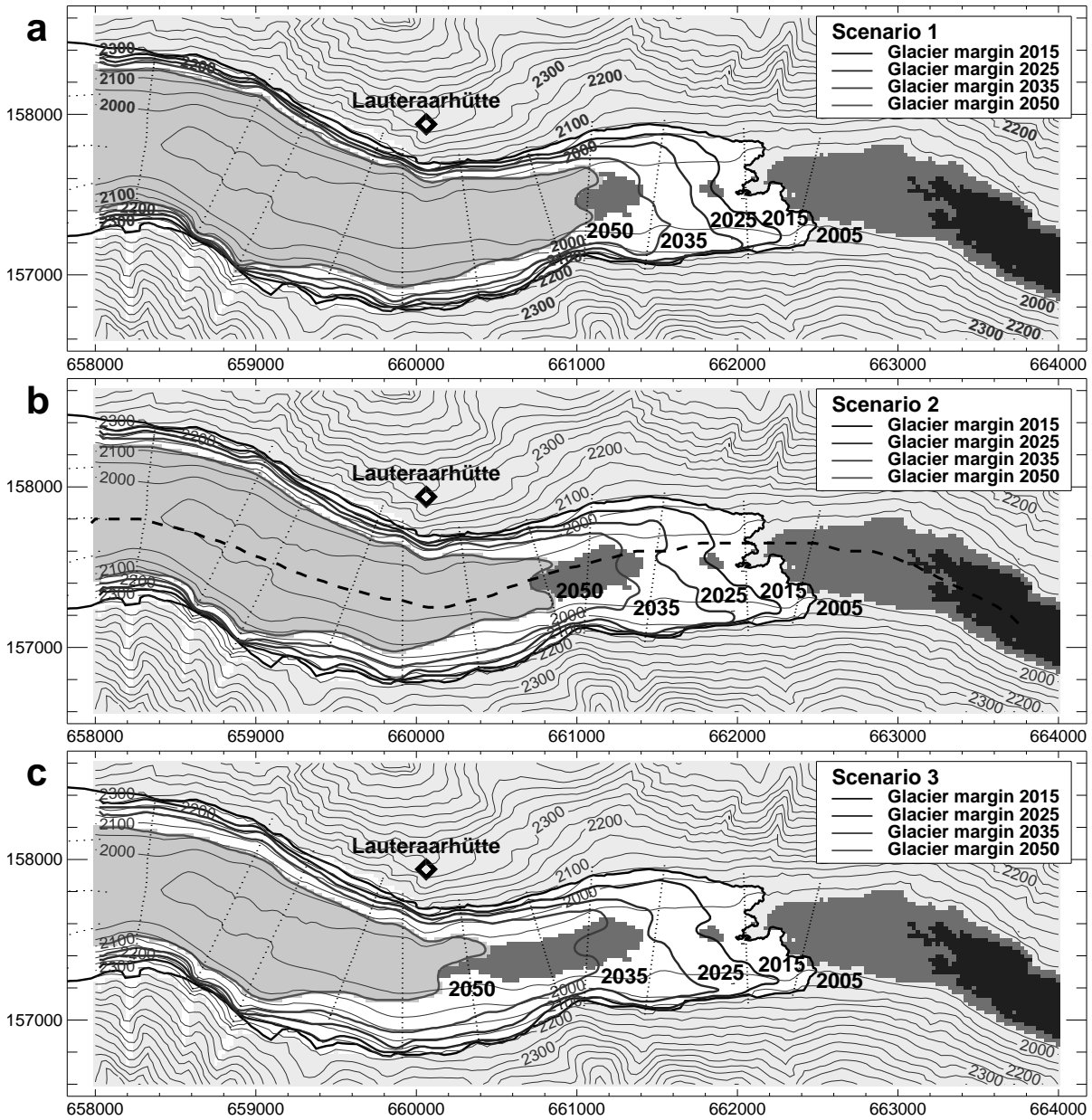


Figure 7.10: Simulated retreat of Unteraargletscher in 2015, 2025, 2035 and 2050 for the three different climate change scenarios. Dotted transverse lines indicate the location of radio-echo sounding profiles. The dashed line in (b) follows the central flowline used for the calculations. After 2035 a proglacial lake starts to form, shown by grey patches. Shaded areas in front of the glacier snout mark the extension of the current lake (dark grey) and the projected lake (light grey). Axes are labeled in km of the Swiss national coordinate system, with North at the top.

2005). Thus, the reliability of the mass-balance predictions decrease with extreme climate change and could be subject to question by the end of the 21st century. Therefore, we confine our main conclusions to 2050.

Debris coverage is an important factor when modeling the retreat of Unteraargletscher. It is a difficult task to predict the evolution of the debris cover and its insulating effect over time spans of several decades. Long-term observations of debris thickness evolution have not yet been conducted. For Unteraargletscher we evaluated the extent of debris-covered glacier surface from topographical maps of 1880 and 1927 and from aerial photographs of the last four decades. We find that the boundaries of debris-covered ice change very slowly over time. The debris-covered surfaces shifted to higher elevations with glacier retreat, but their total area remained constant during the last century. This implies that there is some long-term balance of debris coverage although no information about debris thickness is given.

Many studies have addressed ablation on debris-covered glaciers either theoretically (e.g. Anderson, 2000) or empirically (e.g. Lundstrom and others, 1993; Kayastha and others, 2000; Sugiyama, 2003). Generally, a thickening of the debris coverage must be expected with glacier retreat. This leads to a reduction of icemelt (Lundstrom and others, 1993). However, on down-wasting debris-covered glacier tongues some processes exist that contribute to an evacuation of debris into the forefield. Lukas and others (2005) report supraglacial debris flows exposing steep ice cliffs which melt back at an enhanced rate. Supraglacial streams also contribute to debris transport (Anderson, 2000; Lukas and others, 2005). Such melt-water channels as well as ice cliffs are presently observed on Unteraargletscher. The cliffs concentrate at the glacier terminus and along the medial moraine. The combination of all processes mentioned above inhibit well-founded forecasts of the evolution of f_{debris} (Eq. 7.5) in the next 50 years. We believe that debris thickening and thinning will balance itself out with ongoing glacier retreat. Therefore, we decided to fix the reduction factor for debris on a constant value.

The model results show retreat rates until 2035 in the range of 30 m a^{-1} . The mean retreat rate between 1871 and the present amounts to 17.5 m a^{-1} (Fig. 7.8a). We therefore predict an increase of glacier retreat rate of approximately 70% in the next three decades compared to the past century. At first, the reaction of the glacier is rather moderate compared to anticipated increase of summer temperature given by the climate models. Homogenized data sets show a trend of $\approx 0.009^\circ\text{C a}^{-1}$ between 1864 and 2004 (Begert and others, 2005). Summer temperature is expected to rise by between $0.023^\circ\text{C a}^{-1}$ and $0.078^\circ\text{C a}^{-1}$ according to Frei (2007) by 2050. However, length variations of a glacier are largely affected by the geometry of the ice mass and its underlying bedrock topography. The rapid retreat of the glacier snout takes place with a delay of several decades after the climate change (Fig. 7.8a). This lag is due to a substantial thinning of the flat glacier tongue of Unteraargletscher, which precedes a major length change.

If ice flux through profile 6 equals mass loss due to negative mass balance over the modeled region, the glacier surface remains unchanged and the position of the snout is stationary, as long as no modifications of material and basal properties occur. At present, the ratio ice-flux to mass-balance in the modeled region lies in the range of 40%, indicating a pronounced imbalance of the mass budget. Under the influence of climate variations this ratio can change rapidly, as it is directly influenced by the glacier mass balance (Fig. 7.9). The boundary condition at the upper end of the model, i.e., the starting point of the flowline, is the ice flux. Assuming a changing mass-balance gradient, this may pose some problems. With large changes in climate variables the mass-balance gradient is likely to be altered and, hence, some of our assumptions may no longer be justified. However, the importance of ice flux compared to mass balance

decreases with time and approaches 10% by 2050 (Fig. 7.9). Thus, the flux at the upper model boundary loses its influence on the final results in a gradual way. Additionally, the test runs (Fig. 7.6) indicate that the parameterization of the boundary condition at the upper end of the model domain reproduces reasonable results, also for conditions that are not steady state.

Ice flux should not be neglected in glacier retreat studies. Although the influence of icemelt exceeds the compensating effect of ice flow by far in the case of Unteraargletscher in the 21st century, significant underestimation of glacier extent occurs when assuming solely non-dynamic down-wasting of the ice. Test runs excluding ice flow show that the mean thinning rate is overestimated by 10% to 25% by 2050 with larger errors for Scenario 1 than for Scenario 3.

Ice volume is an important parameter for the assessment of water resources. The total ice volume in the modeled region currently amounts to 0.75 km^3 , corresponding to a decrease of 60% since 1880 (Fig. 7.8b). For all climate scenarios ice volume in the modeled region shrinks steadily, but not with an accelerated trend. The rate of volume change even shows an upward trend in future in spite of continuing climate warming. Due to the progressive decrease of glacier area the meltwater production will be reduced as well. This is a key observation for the management of water resources in catchment areas dominated by glaciers. The future meltwater discharge from highly glacierized drainage basins is expected to increase, favored by additional ablation in a first stage after the shift of climate variables. As ice volume and glacier area shrink, meltwater discharge drops below the preceding level. Thus, the short-term (daily to annual scales) and long-term (decadal scales) storage capacities of glaciers are lost. This will almost certainly lead to a reduction of water resources during dry and hot summers (Hock and others, 2005).

This work shows the impact of expected climate change on the evolution of a typical Alpine glacier. Detailed simulations of future glacier mass balance were performed using a probability-distribution function of different regional climate scenarios for temperature and precipitation change in seasonal resolution. By combining the calculations of ice flow and mass balance, predictions of the glacier extent in the next 50 years are possible.

The unique data base existing for Unteraargletscher allows an empirical ice-flow model to be set up based on velocity and ice thickness measurements and optimal calibration and verification facilities for the mass-balance model. According to the results of this study, the projected lake will never reach the glacier terminus. In the next decades, the glacier snout will retreat substantially and considerable growth of the proglacial area is expected. The retreat and thinning rates will double by the middle of the 21st century, leading to a dramatic decrease of ice volume.

Acknowledgments

The study was commissioned by Kraftwerke Oberhasli AG (KWO). Flotron AG made available surface velocities at different profiles and evaluated digital elevation models. We acknowledge C. Frei for the climate scenario data. R. Hock provided the code of her model used to calculate the mass balances. We thank H. Blatter for valuable comments on an earlier version of the manuscript. Suggestions of the scientific editor S. Anderson and reviews of B. Hubbard and an anonymous reviewer helped to improve the paper.

Chapter 8

Modelling runoff from highly glacierized drainage basins in a changing climate

MATTHIAS HUSS, DANIEL FARINOTTI, ANDREAS BAUDER
AND MARTIN FUNK

Versuchsanstalt für Wasserbau, Hydrologie und Glaziologie (VAW), ETH Zürich, 8092 Zürich, Switzerland

Published, Hydrological Processes

Citation: Huss M., D. Farinotti, A. Bauder and M. Funk (2008). Modelling runoff from highly glacierized alpine drainage basins in a changing climate. *Hydrological Processes*, 22(19), 3888–3992, doi:10.1002/hyp.7055.

ABSTRACT: The future runoff from three highly glacierized alpine catchments is assessed for the period 2007-2100 using a glacio-hydrological model including the change in glacier coverage. We apply scenarios for the seasonal change in temperature and precipitation derived from regional climate models. Glacier surface mass balance and runoff are calculated in daily time steps using a distributed temperature-index melt and accumulation model. Model components account for changes in glacier extent and surface elevation, evaporation and runoff routing. The model is calibrated and validated using decadal ice volume changes derived from four digital elevation models between 1962 and 2006, and measured monthly runoff at a gauging station (1979-2006). Annual runoff from the drainage basins shows an initial increase which is due to the release of water from glacial storage. After some decades, depending on catchment characteristics and the applied climate change scenario, runoff stabilizes and then drops below the current level. In all climate projections the glacier area shrinks dramatically. There is an increase in runoff during spring and early summer, whereas the runoff in July and August decreases significantly. This study highlights the impact of glaciers and their future changes on runoff from high alpine drainage basins.

8.1 Introduction

Climate change will alter the runoff characteristics of high alpine drainage basins substantially (IPCC, 2007; Braun and others, 2000; Bradley, 2006) and lead to drastic glacier retreat or complete wastage during the next decades. These changes affect the environment on global and on local scales (Oerlemans and Fortuin, 1992; Huss and others, 2007b). Water resources are expected to diminish in glacier-fed watersheds, and significant societal impacts in peripheral regions are anticipated (Burlando and others, 2002; Barnett and others, 2005; Hagg and others, 2006). For this reason it is important to assess the impact of climate change and glacier retreat on high alpine runoff and to develop methods for its prediction in order to be prepared for the new environmental situation.

Glaciers are known to have a significant impact on stream-flow runoff (e.g. Hock and others, 2005). During the summer months glacial meltwater may provide the only source of water for alpine valleys and dry lowlands (Singh and Kumar, 1997; Bradley, 2006). With decreasing glacierization, the annual cycle of runoff is transformed from an icemelt to a snowmelt dominated regime (Horton and others, 2006). At decadal time scales, glaciers store water as snow and ice in cold and wet years, and provide additional runoff in warm and dry years. The reduction in ice volume will yield a significant increase in annual runoff for several decades, followed by a shift in the peak discharge towards early summer and spring, combined with a decrease in runoff (Braun and others, 2000). The changed runoff characteristics of high mountain catchments will pose new challenges to water resources management in many mountain ranges of the Earth.

Changes in stream-flow runoff related to climate change were studied e.g. in the European Alps (Collins, 2006), in Iceland (Adalgeirsdóttir and others, 2006), the Himalayas (Singh and Kumar, 1997; Hagg and others, 2007) and in the tropical Andes (Bradley, 2006; Juen and others, 2007). Numerous models exist for calculating runoff from drainage basins of various sizes (e.g. Bergström, 1995; Braun and others, 1995; Gurtz and others, 1999; Schulla and Jasper, 2000; Schaeffli and others, 2005). In highly glacierized catchments these models may yield good agreement of calculated and observed runoff (Klok and others, 2001; Verbunt and others, 2003; Huss and others, 2007a). However, glaciers are often represented crudely in hydrological models and are mostly assumed to remain constant in surface geometry and extent over time (e.g. Bergström, 1995). Schaeffli and others (2007) considered a step-wise adaptation of glacial area when modelling runoff using different Regional Climate Models (RCMs) for the period 2070-2099.

Future changes in ice volume have been assessed using combined models of glacier mass balance and ice dynamics for individual glaciers (Oerlemans and others, 1998; Schneeberger and others, 2003). Coupled mass balance and ice flow models are able to supply information on long-term geometrical changes in ice sheets and alpine glaciers (Flowers and others, 2005; Huss and others, 2007b). However, they require substantial field data input and computational time, which make them difficult to apply to complex drainage basins.

This study presents a glacio-hydrological model which includes the annual adaptation of the 3D glacier surface topography and determines all components of the water balance in alpine terrain at high spatial and temporal resolution. The model requires a minimum of data input and is well suited to make predictions of the transient evolution of future ice volume, runoff and the discharge regime.

The present study focuses on the transition of discharge from glacierized catchments to ice-free conditions. The impact of glacier wastage on runoff from high alpine drainage basins is discussed. The model approach is based on a distributed temperature-index melt model including accumulation (Hock, 1999). Evaporation, runoff routing and glacier surface evolution are described in subroutines. In this paper we call the combined glacio-hydrological model **Glacier Evolution Runoff Model (GERM)**. GERM is forced using different regional climate scenarios in seasonal resolution (Frei, 2007). A random variability is superimposed on the mean expected changes in temperature and precipitation in order to account for the year-to-year fluctuations in climate and to draw inferences on the impact of extreme years. We present time series of glacier area, surface mass balance and runoff for the period 2007–2100 and investigate the distribution of runoff in the course of the year.

8.2 Study site and field data

The study site is the uppermost valley of Zinal, Valais, Switzerland. The area of interest is surrounded by several peaks reaching nearly 4500 m a.s.l. and is occupied by one large valley

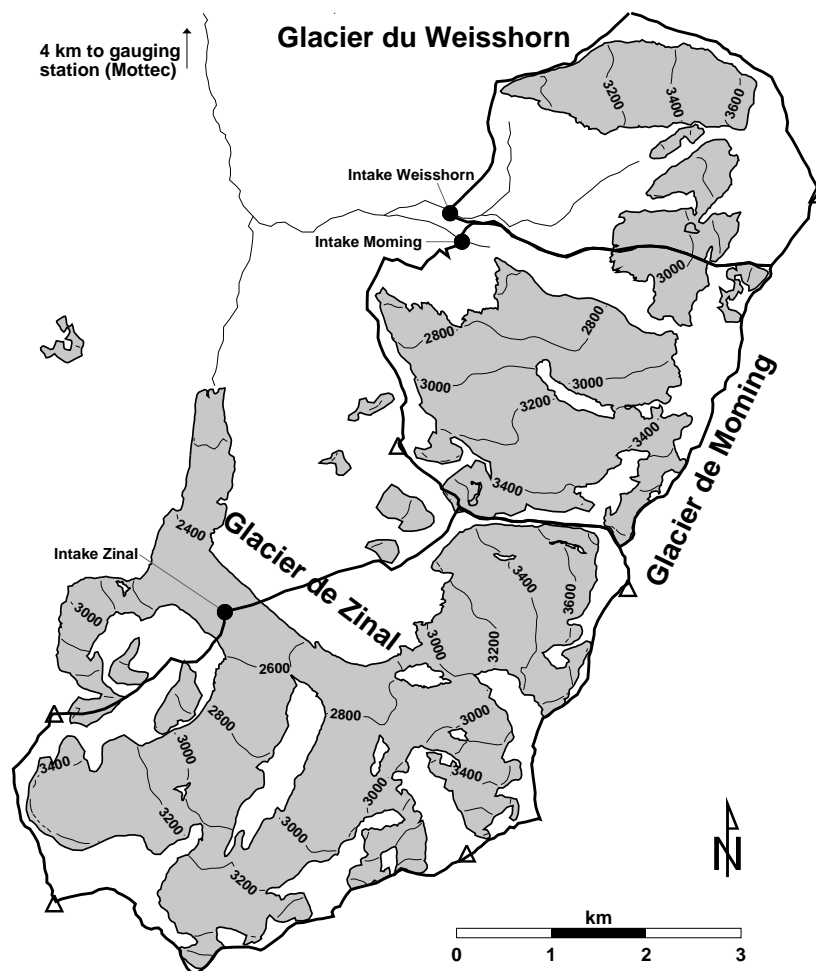


Figure 8.1: Overview map of the study site. Planned water intakes are indicated by solid dots. Ice covered regions are shaded and the three investigated drainage basins are bordered using thick lines. The presented results refer to these catchments.

Table 8.1: *Characteristics of the three investigated drainage basins based on the DEM from 2006. The elevation range and the area refer to the ice-covered regions within the catchment.*

Catchment	Gl. elevation (m a.s.l.)	Gl. area (km ²)	Ice vol. (km ³)	Glacierization (%)
Zinal	2483 - 3857	11.4	0.93	65
Moming	2525 - 4070	6.0	0.35	63
Weisshorn	2847 - 3714	2.7	0.17	39

glacier – Glacier de Zinal – and two medium-sized glaciers – Glacier de Moming and Glacier du Weisshorn (Fig. 8.1 and Table 8.1). Glacier de Zinal is a complex glacier system with five main tributaries and a debris-covered glacier tongue. Glacier de Moming is a steep, north-exposed mountain glacier, which reaches 4000 m a.s.l. Glacier du Weisshorn has a south-western aspect. Several small glaciers and ice patches lie within the study area. The local climate is relatively dry and determined by the meteorological conditions at the southern flank of the Alps.

The Forces Motrices de la Gougra SA hydropower company plans to set up one subglacial and two proglacial water intakes to capture the meltwater at an elevation of 2330 m a.s.l. The location of the water intakes defines the three catchments which are analyzed in the scope of this study (Fig. 8.1).

A wide range of field data is available for the study site: (i) meteorological data, (ii) radio-echo soundings of the ice thickness, (iii) discharge measurements, (iv) observations of the glacier equilibrium line altitude (ELA), and (v) digital elevation models (DEMs) and ice volume changes.

We use homogenized time series of temperature recorded at Sion (542 m a.s.l., 29 km from Glacier de Zinal), available continuously since 1864 (Begert and others, 2005). Lapse rates for monthly mean air temperature were determined by considering seven weather stations with shorter time series recording daily temperature and precipitation located closer than 20 km to the study site. Using these lapse rates the temperature time series of Sion were shifted to the mean elevation of the study site. The distribution of precipitation in high alpine regions is complex and cannot be extrapolated with confidence (Huss and others, 2008a). We take the spatial distribution of precipitation sums from a gridded data set (PRISM) with a spatial resolution of about 2 km (Schwarb and others, 2001). The temporal fluctuations of precipitation are scaled to those measured at local weather stations. Thus, we obtain time series of temperature and precipitation in daily resolution scaled to the study site.

During the winters 2006 and 2007 we conducted field campaigns on Glacier de Zinal to determine the elevation of the glacier bed using radio-echo sounding techniques. Twelve glacier cross-profiles on the main valley glacier are available (Fig. 8.2). Runoff measurements are provided by a gauging station at Mottec 7 km downvalley from the glaciers. The data are in monthly resolution and cover the period 1979-2006. The gauged drainage basin comprises the three analyzed catchments and is 25% glacierized. Besides the investigated ice masses, only some small perennial snow fields are within the catchment of Mottec. Between 1969 and 1986 the Grande Dixence SA hydropower company derived the ELA every year, based on aerial photographs. The data are available for about 30 glaciers close to the study site, however, not for the investigated glaciers.

Four high-accuracy DEMs were evaluated at 25 m spatial resolution. The first DEM (1962) is based on a digitized topographic map. The DEMs of 1988, 1995 and 2006 were produced

by photogrammetric analysis of aerial photographs. By comparing two successive DEMs, a decadal ice volume change was calculated. The accuracy of the volume change determination is within 5% (Bauder and others, 2007). The glaciers in the study area achieved slight mass gains between 1962 and 1988 and have lost between 10% and 20% of their ice volume during the last two decades (insets in Fig. 8.2).

8.3 Methods

Ice thickness distribution

Long-term runoff forecasts for glacierized drainage basins must account for the change in ice volume. In order to compute glacier retreat in response to annual mass balance fluctuations the initial ice thickness distribution has to be known. The ice thickness of every glacier within the study site was determined using two different methods. The measurements of radio-echo sounding performed in the ablation area of Glacier de Zinal (Fig. 8.2) allow an evaluation of the glacier bed according to standard procedures (Funk and others, 1994; Bauder and others, 2003). However, large parts of the glacierized area are not accessible for ground based radio-echo sounding as they are steep and crevassed. No measurements are available for those ice masses. In order to obtain estimates of the glacier bed topography in these regions we developed a method to determine the ice thickness distribution based on considerations of mass turnover and glacier surface characteristics.

The input for the method to estimate the ice thickness is limited to a DEM, two mass balance gradients, a central flowline (several for glacier systems with individual branches) and a catchment of ice flux contributing to each flowline. The calculated ice thickness is a function of the steady-state ice flux, glacier width and surface slope. The procedure is defined as follows:

1. Assuming typical mass balance gradients for Alpine glaciers of -0.009 a^{-1} for the ablation and of -0.005 a^{-1} for the accumulation area (Huss and others, 2008a) we derive the mass balance distribution using a DEM. The area-averaged mass balance of the glacier surface is assumed to be equal to zero.
2. A balance ice flux is calculated by summing up the gained or lost ice volume during one year in each elevation band of 10 m starting from the uppermost point of the glacier.
3. An integrated form of the ice flow law (Glen, 1955; Paterson, 1994) is solved for the ice thickness h on the central flowline.

$$h = \sqrt[5]{\frac{q}{\frac{2}{5} \cdot A \cdot (S_f \rho g \sin \alpha)^3}}, \quad (8.1)$$

where q ($\text{m}^2 \text{ s}^{-1}$) is the ice flux normalized with the glacier width, g the acceleration of gravity, A is the rate factor of the ice flow law (Glen, 1955), S_f is a factor accounting for the valley shape (Nye, 1965), ρ is the ice density and α is the slope of the glacier surface. A is calibrated to optimize agreement with the radio-echo sounding profiles. We find a value of $A=6.0 \times 10^{-15} \text{ s}^{-1} \text{ kPa}^{-3}$ which is consistent with previous studies (e.g. Paterson, 1994). $S_f=0.6$ is taken from the literature and α is equal to the mean slope along the flowline.

4. Using a boundary condition of $h=0$ at the entire glacier margin the ice thickness is interpolated spatially by assuming a parabolic valley shape.
5. We apply corrections to the spatially distributed values of h by accounting for the local surface slope α at every grid cell and assuming $h \sim (\sin \alpha)^{3/5}$. This proportionality is used to redistribute ice along the crossflow section. The proportionality factor is chosen such that the previously determined total ice volume is not changed.

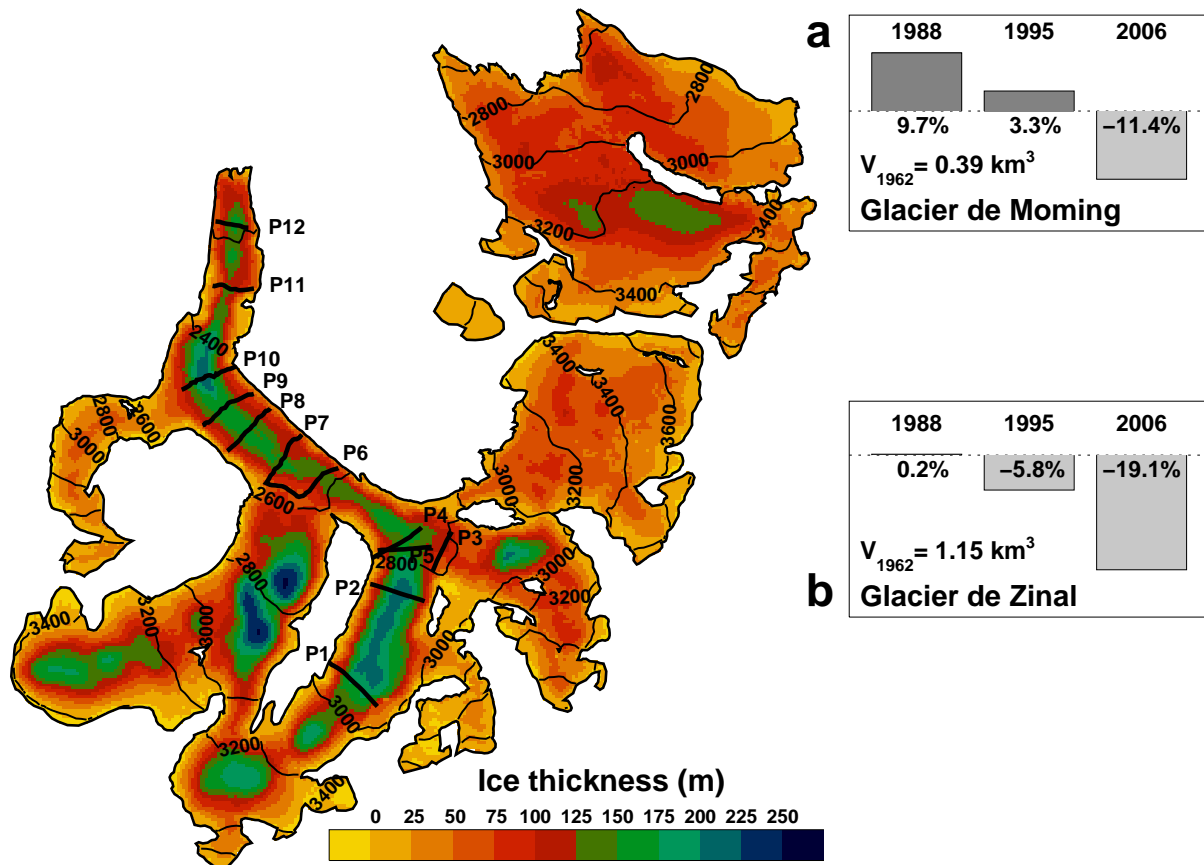


Figure 8.2: Ice thickness distribution of Glacier de Zinal and Glacier de Moming obtained by measurements and calculation. Radio-echo sounding profiles are indicated by bold lines and coded with P1-P12. Contours show surface elevation. The insets show the changes in ice volume in percent relative to 1962 for (a) Glacier de Moming and (b) Glacier de Zinal.

The ice thickness distribution of Glacier de Zinal (Fig. 8.2) is obtained in two steps: (i) ice thickness in regions covered with radio-echo soundings is interpolated spatially based on the measurements, and (ii) the ice thickness of ice masses with no field data is determined using the method described above. These data complement the ice thickness map where no information from step (i) is available. Ice thickness in the ablation area of glacier de Zinal reaches 220 m and is lower in the relatively steep accumulation area. A maximum ice thickness of 150 m in a trough at 3200 m a.s.l. is determined for Glacier de Moming (Fig. 8.2). By subtracting the calculated ice thickness from the smoothed glacier surface topography a bedrock DEM is obtained.

A validation of the distributed ice thickness estimation was conducted by comparing the results of our method to the radio-echo sounding measurements on Glacier de Zinal (Fig. 8.3). We also

tested our method on Grosser Aletschgletscher and Rhonegletscher, two large Alpine valley glaciers. For those ice masses some radio-echo soundings are available (unpublished data, VAW-ETHZ; Zahno, 2004). We found a correlation of measured and calculated ice thickness of $r^2=0.72$ for Glacier de Zinal, Aletschgletscher and Rhonegletscher. The mean relative error of the ice thickness is 26%. The cross sectional area of the radio-echo sounding profiles is reproduced within a range of $\pm 22\%$ by our method (21 profiles). The validation shows that the proposed method yields reasonable estimates of the ice thickness and is, thus, applicable on glaciers without field measurements.

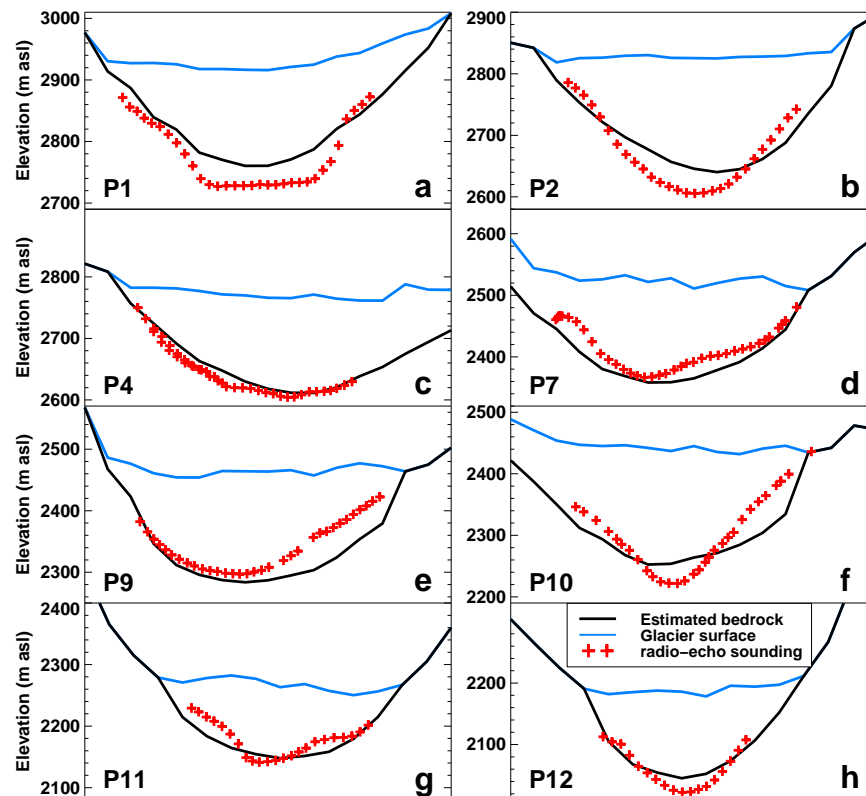


Figure 8.3: (a)-(h) Validation of the method to estimate ice thicknesses using radio-echo soundings along cross-section profiles on Glacier de Zinal (Fig. 8.2).

Glacier change and runoff modelling

A glacio-hydrological model (GERM) was developed in order to calculate runoff from highly glacierized catchments using daily temperature and precipitation as climatic input. The system model comprises components for (i) glacier surface mass balance (accumulation and ablation), (ii) evaporation, (iii) runoff routing and (iv) the change in glacier surface topography and glacier retreat. A schematic overview of GERM is shown in Figure 8.4. In this study we run GERM on a 25 m grid in daily time steps.

Glacier surface mass balance

Glacier surface mass balance is calculated using an accumulation model coupled to a distributed temperature-index melt model (Hock, 1999). The degree-day factors are varied as a function

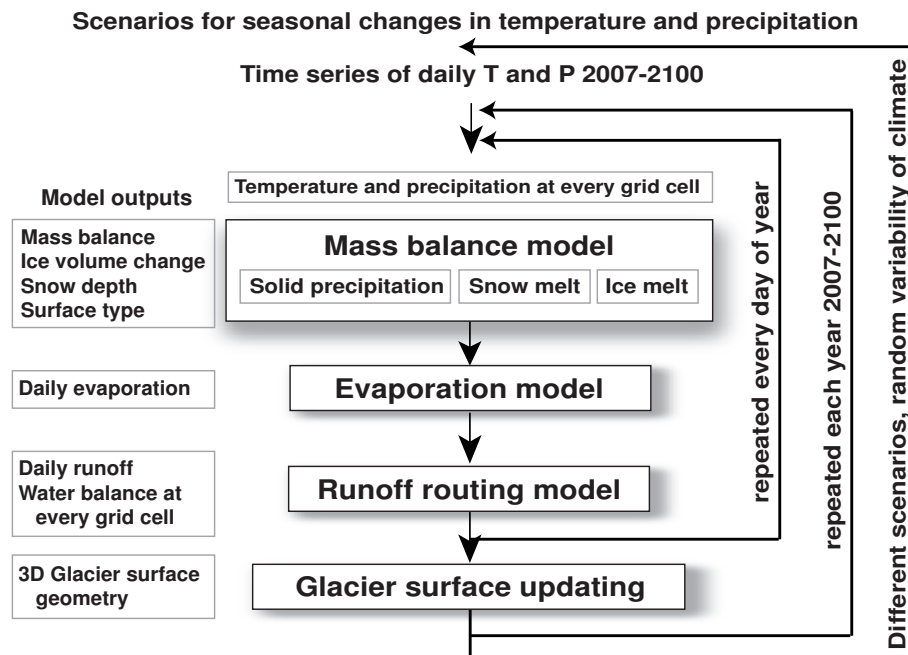


Figure 8.4: Schematic overview of GERM.

of potential direct solar radiation in order to account for the effects of slope, aspect and topographic shading. Temperature-index models are based on a linear relation between positive air temperature and melt rate (Hock, 2003). Melt is highly correlated with long-wave heat flux, for which air temperature is a good indicator (Ohmura, 2001).

Surface melt rates M are computed by

$$M = \begin{cases} (f_M + r_{\text{ice/snow}} I) \cdot T & : T > 0^\circ\text{C} \\ 0 & : T \leq 0^\circ\text{C} \end{cases} \quad (8.2)$$

where f_M denotes a melt factor, $r_{\text{ice/snow}}$ are radiation factors for ice and snow. I is the clear-sky direct radiation (Hock, 1999). Due to the empirical character of the temperature-index model the site-specific parameters f_M and $r_{\text{ice/snow}}$ must be calibrated using direct observations.

Daily air temperature at every grid cell is determined using a constant lapse rate (dT/dz). Precipitation is assumed to increase linearly with elevation (dP/dz). A correction factor accounts for gauge under-catch errors (c_{prec}) and a threshold temperature T_{thr} distinguishes snow from rainfall (Hock, 1999). Melt over debris-covered surfaces is multiplied by a constant reduction factor $f_{\text{debris}} < 1$. Regions with positive net balance at the end of the previous hydrological year (Oct 1 – Sept 30) define the firn area. Firn is treated as snow in Equation 8.2. The spatial variation of accumulation on the glacier surface is modelled by taking into account effects of snow redistribution due to drift and avalanches. This is achieved using curvature and slope evaluated based on a DEM (Huss and others, 2008a). The large-scale precipitation field is derived from the PRISM data set (Schwarb and others, 2001). Glacier surface mass balance is determined as the sum of solid precipitation and snow or icemelt at the end of the hydrological year. The integration of mass balance at every grid cell of the glacier yields an annual ice volume change which is used to determine the updated glacier surface geometry (see "Glacier surface updating").

Evaporation model

Evaporation has a limited importance in the water balance of high mountain catchments (Braun and others, 1995). In summer even net condensation can occur over bare ice surfaces (Lang and others, 1977; Bernath, 1991). However, a warmer climate induces a deglaciation and a corresponding rise of the vegetation zones and, thus, evaporation is likely to increase and to affect high alpine runoff more strongly than at present. Because the available data are limited, an empirical evaporation model is implemented in GERM. This model component is based on an approach for calculating potential evaporation by Hamon (1961). It was improved and made applicable to high mountain catchments by accounting for the effect of different surface types on evaporation, interception and actual evaporation.

Based on the air temperature T ($^{\circ}\text{C}$) and the saturation vapor pressure e_s the potential evaporation E_{pot} (mm d^{-1}) is calculated daily at every grid cell using:

$$E_{\text{pot}} = \frac{35.77 \cdot DL \cdot e_s}{T + 273.3} \cdot S_{\text{type}}, \quad (8.3)$$

where DL is the fraction of daylight per day and S_{type} is a factor to distinguish the properties of different surfaces. The model considers five surface types – snow, ice, rock, low vegetation and forest. Parameters describe their properties in terms of evaporation. The evaporation over snow-covered surfaces varies in the course of the year and is higher during winter. This is supported by energy balance measurements in the Arctic (Semadeni and others, 2004; personal communication A. Ohmura, 2007). The extent of ice surfaces is updated annually, the snow coverage is calculated each day using the mass balance model, and the outlines of the surface types rock, low vegetation and forest were taken from a map. Their extent is estimated in bidecadal time steps in the future by inferring a slow rise of the vegetated zones from the expected increase in air temperature. Potential evaporation is provided from an interception reservoir filled by rainfall. The values of E_{pot} (Eq. 8.3) are reduced to actual evaporation using a constant reduction factor depending on the surface type when the interception reservoir is empty. On snow-covered surfaces the evaporational water loss is subtracted daily from the snow water equivalent. On snow-free grid cells evaporation is subtracted from the interception reservoir (if not empty), or from the actual storage in the slow reservoir (see "Runoff routing").

Runoff routing

High alpine glacial systems yield relatively quick reaction in runoff due to the low retention capacity of ice and rock, the limited extent of vegetated surfaces and the generally shallow soils. The water volume available for runoff is determined daily at every grid cell by solving the water balance using the calculated quantities for liquid precipitation, melt and evaporation. By using a runoff routing model, a discharge hydrograph is obtained. The runoff routing model is based on the concept of linear storage (e.g. Jansson and others, 2003). The discharge Q is proportional to the actual storage S in the reservoir:

$$S = k \cdot Q. \quad (8.4)$$

The water is routed through two parallel linear reservoirs – a fast and a slow one, characterized by the different retention constants k_{fast} and k_{slow} , respectively. Melt and rain in glacierized grid cells is added to the fast reservoir, while for non-glacierized grid cells melt and rain is

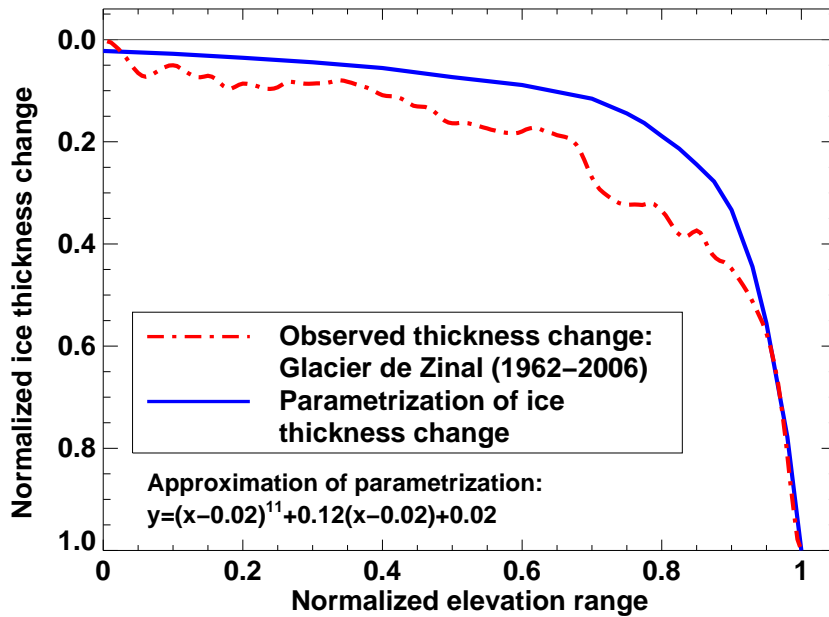


Figure 8.5: Observation (Glacier de Zinal, 1962-2006) and parameterization of ice thickness change as a function of the normalized elevation range based on Jóhannesson and others (1989). The origin of the x-axis corresponds to the maximum glacier elevation and the elevation range for the observation refers to 2006. An approximation function of the normalized Δh -parameterization is given.

divided into a portion I_{slow} infiltrating the slow reservoir and a portion I_{fast} contributing to the fast reservoir (both in mm d^{-1}) according to a relation described in Schaeffli and others (2005):

$$I_{\text{fast}} = (M + P_{\text{liq}}) \cdot (S_{\text{slow}}/S_{\text{max}})^c \quad \text{and} \quad (8.5)$$

$$I_{\text{slow}} = (M + P_{\text{liq}}) - I_{\text{fast}}, \quad (8.6)$$

where M is the melt, P_{liq} the liquid precipitation (both in mm d^{-1}), S_{slow} is the actual storage in the slow reservoir, S_{max} the maximum storage capacity (both in mm) and c a constant set to $c=2$ (Schaeffli and others, 2005). k_{fast} is varied as a function of the surface type of the grid cell (snow, ice, rock, vegetation) which is considered to be an indicator of its hydrological properties.

Glacier surface updating

When modelling the future runoff from highly glacierized drainage basins, the reduction in ice volume and glacial area due to glacier retreat should not be neglected. The ice thickness change between two steady-states is not uniformly distributed over the glacier area but is most pronounced at the glacier terminus (Jóhannesson et al., 1989; Fig. 8.5). We parametrize the annual glacier surface evolution using an ice thickness change pattern based on theoretical considerations of ice dynamics (Jóhannesson and others, 1989) displayed in Figure 8.5. A similar pattern is observed on Glacier de Zinal (Fig. 8.5) and on other retreating alpine glaciers. Comparable patterns of surface elevation change along a central flowline were found by applying a flowline model to an alpine glacier (Huss and others, 2007b). Jóhannesson and others (1989) analyzed the evolution of glacier geometry between two steady-states after a mass balance perturbation. According to these results the shape of the glacier surface becomes rapidly similar to the final steady-state geometry.

The 3D glacier geometry is updated in annual time steps. At the end of the hydrological year the lost or gained ice volume determined using the mass balance model is converted into a distributed ice thickness change (Δh). For practical reasons the Δh -parameterization (Fig. 8.5) is normalized with the altitudinal extension of the glacier and not with glacier length as presented by Jóhannesson and others (1989). Integration of the Δh -parameterization over the glacier surface and weighted with the relative area of elevation bands must be equal to the total annual change in glacier mass given by the mass balance computation. In order to satisfy this criterion, the magnitude of the Δh -function is adapted in an iterative procedure so that its curvature remains constant. Thus, for each elevation band of 10 m an annual surface elevation change is determined. Our approach is based on mass conservation. However, it accounts for ice dynamics only in an empirical way. We assume that the annual surface mass balance is immediately converted into a spatially distributed ice thickness change according to the pattern corresponding to Figure 8.5b and that the curvature of the Δh -parameterization is constant. If the glacier is in a state of non-dynamic downwasting, the surface elevation change is assumed to equal the calculated mass balance rate in ice equivalent. The ice extent is determined by comparing the updated glacier surface elevation and the DEM of the glacier bedrock topography.

Model calibration and validation

The calibration of GERM is performed in a stepwise procedure that focuses on individual parameter groups. The glacier mass balance model is the central element of GERM (Fig. 8.4). It is calibrated using (i) the ice volume changes derived from DEMs during the last four decades, (ii) observations of the equilibrium line altitude (ELA) and (iii) measurements of monthly runoff volumes recorded at the gauging station at Mottec for 27 years. The calibration procedure is similar to a method described in Huss and others (2008a). In each period given by two successive DEMs the melt model parameters f_M and $r_{\text{ice/snow}}$ are optimized so that modelled cumulated annual ice volume change matches the geodetically determined ice volume change. The accumulation parameters c_{prec} and dP/dz are calibrated simultaneously aiming at maximum agreement between modelled and observed ELAs. The ELA observations available for 30 neighboring glaciers were averaged in exposition classes to make them comparable to the investigated glaciers. Calculated and observed ELAs correlate; however, there is a slight underestimation of the ELA by the model (Fig. 8.6b). Furthermore, the accumulation parameters are constrained by the comparison of calculated and measured discharge (Fig. 8.6a). To judge the model performance in terms of runoff we use the Nash and Sutcliffe (1970) efficiency criterion defined as

$$R^2 = 1 - \frac{\sum (Q_{\text{meas}} - Q_{\text{sim}})^2}{\sum (Q_{\text{meas}} - \overline{Q_{\text{meas}}})^2} \quad (-\infty < R^2 < 1) \quad (8.7)$$

with Q_{meas} the measured and Q_{sim} the simulated monthly discharge. We found a value of $R^2=0.90$ during the period 1979-2006. Optimized parameter values are given in Table 8.2.

The calibration of the evaporation model is difficult due to lack of observational data. We optimized the calculated values of evaporation to estimates of evaporational water loss for different surface types in the course of the year at a high elevation site close to Rhonegletscher (Bernath, 1991). The parameters of the runoff routing model are chosen to optimize agreement between calculated and measured runoff (Table 8.2).

The parameterization of glacier retreat is validated by comparing modelled glacier extent to the observed glacier outlines in 1988, 1995 and 2006. The Δh -parameterization gives good results

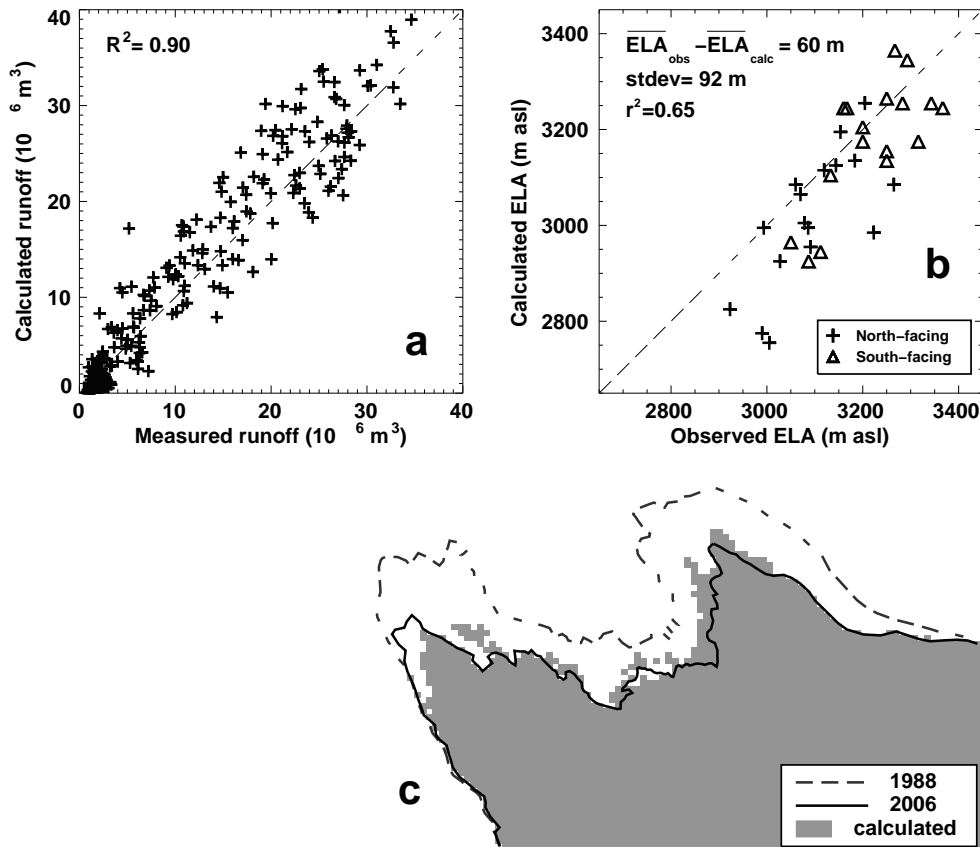


Figure 8.6: Validation of GERM in the past. Comparison of measured and calculated (a) monthly runoff at Mottec, (b) equilibrium line altitude, (c) terminus of Glacier de Moming. Lines correspond to observed glacier margins in 1988 and in 2006. The shaded area is the calculated glacier extent in 2006 when the model was initialised in 1988.

for periods of glacier retreat (Fig. 8.6c). This could also be confirmed by testing the approach on other alpine glaciers (Grosser Aletschgletscher, Rhonegletscher, unpublished data). However, our parameterization fails to yield correct glacier outlines in periods of glacier advance even though it reproduces ice volume changes correctly.

Table 8.2: Parameters of GERM, values and units

Parameter	Symbol	Value	Units
Melt factor	f_M	0.622×10^{-3}	$\text{m d}^{-1} \text{ } ^\circ\text{C}^{-1}$
Radiation factor	r_{ice}	1.493×10^{-5}	$\text{m}^3 \text{ W}^{-1} \text{ d}^{-1} \text{ } ^\circ\text{C}^{-1}$
	r_{snow}	1.267×10^{-5}	$\text{m}^3 \text{ W}^{-1} \text{ d}^{-1} \text{ } ^\circ\text{C}^{-1}$
Reduction debris	f_{debris}	0.6	–
Temp. gradient	dT/dz	-5.67×10^{-3}	$^\circ\text{C m}^{-1}$
Temp. threshold	T_{thr}	1.5	$^\circ\text{C}$
Prec. gradient	dP/dz	3.0×10^{-4}	m^{-1}
Prec. correction	c_{prec}	45	%
Retention constant	k_{fast}	1.0-3.0	days
	k_{slow}	30.0	days

Future climate

We use results of a climate change study for Switzerland by Frei (2007) based on simulations of the PRUDENCE project (Christensen and others, 2002; Christensen and Christensen, 2007). A statistical analysis from results of 16 Regional Climate Models for Switzerland was performed (Frei, 2007). These results are derived from model chains of the emission scenarios SRES A2 and B2 and downscaled Global Circulation Model outputs. Frei (2007) computed a 95% confidence interval for the evolution of temperature and precipitation in a seasonal resolution for time snapshots in 2030, 2050 and 2070 (Fig. 8.7). The given values are changes relative to the climate in 1990. The temperature increase is most pronounced in the summer season ($+5\pm 3.1^\circ\text{C}$ per century). An increase in winter precipitation ($+20\pm 25\%$ per century) and a decrease in summer precipitation ($-32\pm 25\%$ per century) is expected (Frei, 2007). These changes are consistent with a climate impact study in Switzerland by Hingray and others (2007).

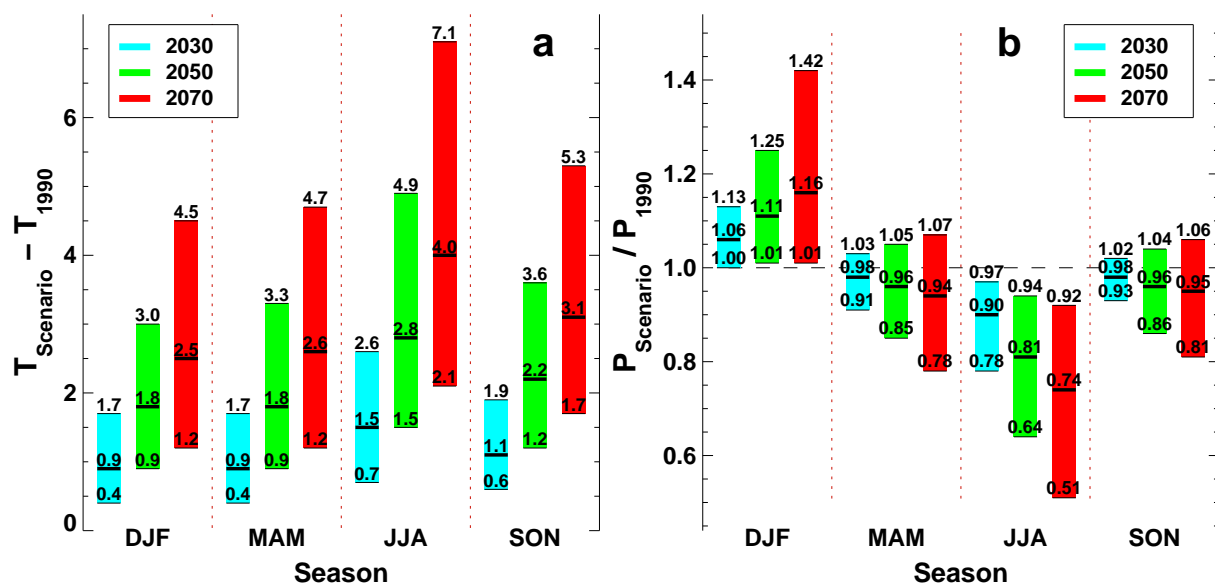


Figure 8.7: Expected climate change for the southern flank of the Alps in seasonal resolution for 2030, 2050 and 2070 (Frei, 2007). The bars show the 95% confidence interval evaluated from 16 regional climate models. The horizontal lines indicate the median value. (a) Temperature and (b) precipitation scenarios are relative to the climate in 1990. Figure adapted from Frei (2007).

We define three climate change scenarios: two extreme and a median scenario. Scenario 1 (cold-wet) is most favorable to glacier existence. It adopts the lowest expectable increase in temperature within the 95% confidence interval of climatic change (2.5% quantile) and the 97.5% quantile for precipitation change (upper limit of the bars in Figure 8.7). Scenario 2 refers to the median of the statistical analysis by Frei (2007). Scenario 3 (warm-dry) is based on the 97.5% quantile for temperature change and the 2.5% quantile for precipitation change (Fig. 8.7). Values in between the given time slices are obtained by linear interpolation and by extrapolation after 2070.

Frei (2007) provides mean changes of temperature and precipitation in the future. However, climate has an internal variability, which substantially influences stream-flow runoff and the management of the water resources. Especially extreme years may have considerable impact on the environment. In order to simulate a range of possible year-to-year fluctuations based on

given mean changes of the meteorological variables, random deviations are superimposed on these (Fig. 8.8). We assume the past and future climate variability to be equal.

The parameters of temperature-index models are sensitive to the characteristics (e.g. daily temperature range) of the meteorological time series used to calibrate them (Hock, 2003). This implies that we should use meteorological time series with the same characteristics in the future so that the calibrated parameter set is valid. Therefore, we use the time series measured in the past, but we adapt their seasonal means to the anticipated future seasonal mean values when running the temperature-index model during the 21st century. (1) We randomly select one year from the period 1900-1990. (2) We determine the deviation of that year's mean seasonal temperature and precipitation from the 30-year running mean of these variables. (3) This deviation is added to the expected seasonal mean in the future obtained from the climate scenarios given by Frei (2007). (4) The measured daily time series of the randomly selected year are shifted to the generated future seasonal mean value obtained in (3). Using this technique we obtain meteorological time series with the same resolution, characteristics and variance as in the past. In order to determine a range of the uncertainty in the calculated variables due to the internal variability of climate, we perform 20 model runs for each scenario using different randomly generated time series for temperature and precipitation for the period 2007 to 2100.

Our approach downscales the anticipated climate changes in three steps: (i) We define three scenarios for mean changes in temperature and precipitation in seasonal resolution, (ii) ran-

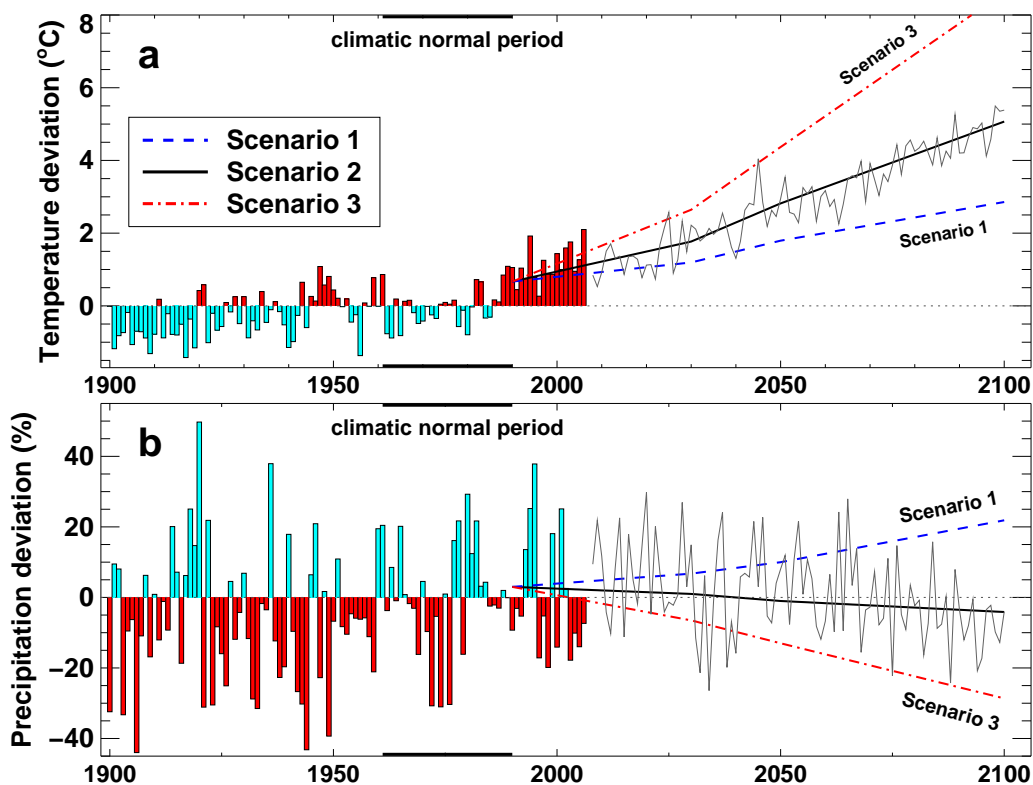


Figure 8.8: Deviations of annual (a) mean temperature and (b) precipitation from the 1961-1990 climatic normal period. Measured data of the weather station at Sion for the 20th century are displayed by bars, annual changes as assumed by the three climate scenarios are shown until 2100. Superimposed on the mean changes in the future are randomly generated deviations that correspond to the year-to-year fluctuations in climate. One random time series is shown referenced to the baseline changes of Scenario 2.

dom offsets corresponding to the year-to-year fluctuations in climate are superimposed on the seasonal changes of temperature and precipitation obtained from the climate scenarios (Frei, 2007), and (iii) the model is run in daily resolution using measured meteorological data scaled to future climate.

8.4 Results

We present results for three drainage basins for the period 2007–2100 (Fig. 8.1). Time series of glaciological and hydrological parameters are shown and discussed for Scenario 2 (median), Scenario 1 (cold-wet) and Scenario 3 (warm-dry). The results are determined as the mean of 20 multiple model runs using different year-to-year fluctuations in climate. A 95% confidence interval based on the multiple model runs is evaluated and provides a range of the expected variability in the calculated variables. Model results in the future are compared to the climatic normal period 1961-1990. For this period GERM is forced using measured meteorological variables. Some of the time series are only presented for the medium-sized Glacier de Moming.

Figure 8.9 shows the evolution of the glacier extent for three snapshots in the future based on Scenario 2. Small glaciers have disappeared by 2050 and dead ice patches are isolated on the debris-covered tongue of Glacier de Zinal. By 2075 the large glaciers are in a state of disintegration and have retreated above 3000 m a.s.l. Glacier de Zinal shows a more dramatic retreat than the medium-sized ice masses of Glacier de Moming and Glacier du Weisshorn (Fig. 8.9). This is due to the distribution of its former accumulation area. A large portion of Glacier de Zinal is situated at elevations between 2800 and 3300 m a.s.l., a region where net balances are expected to be negative already in the near future (Table 8.4). Furthermore, the current glacier extent is too large for the present climate. Only a small glacier at a steep north-exposed slope above 3600 m a.s.l. is left in the study area by 2100.

Glacial area and ice volume decrease significantly in all three climate change scenarios. The uncertainty in the climate projections, however, leads to large differences in estimates of glacier extent (Fig. 8.10a, Table 8.3). Glacier surface mass balances are expected to be negative in the

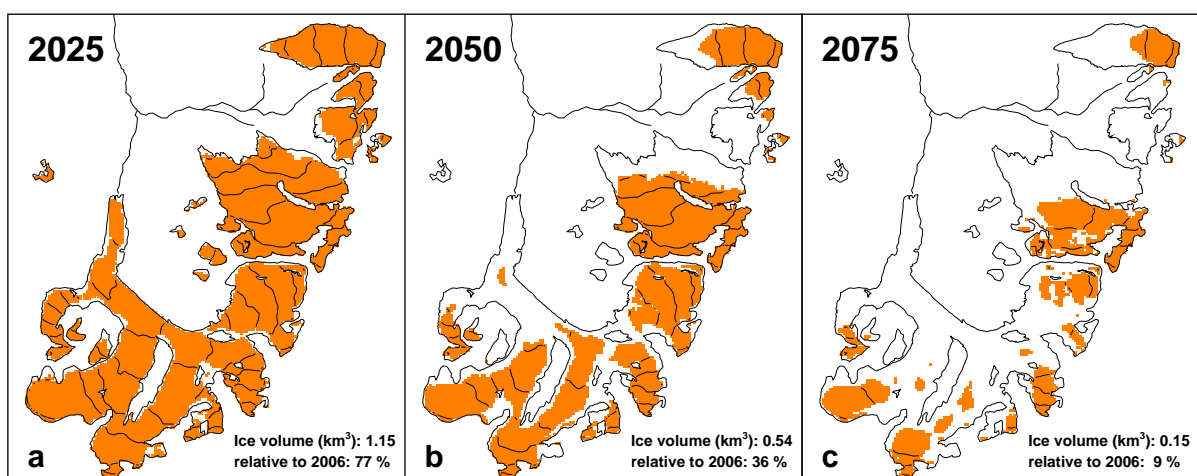


Figure 8.9: Calculated extent of Glacier de Zinal, Glacier de Moming and Glacier du Weisshorn in (a) 2025, (b) 2050 and (c) 2075 according to Scenario 2 (median).

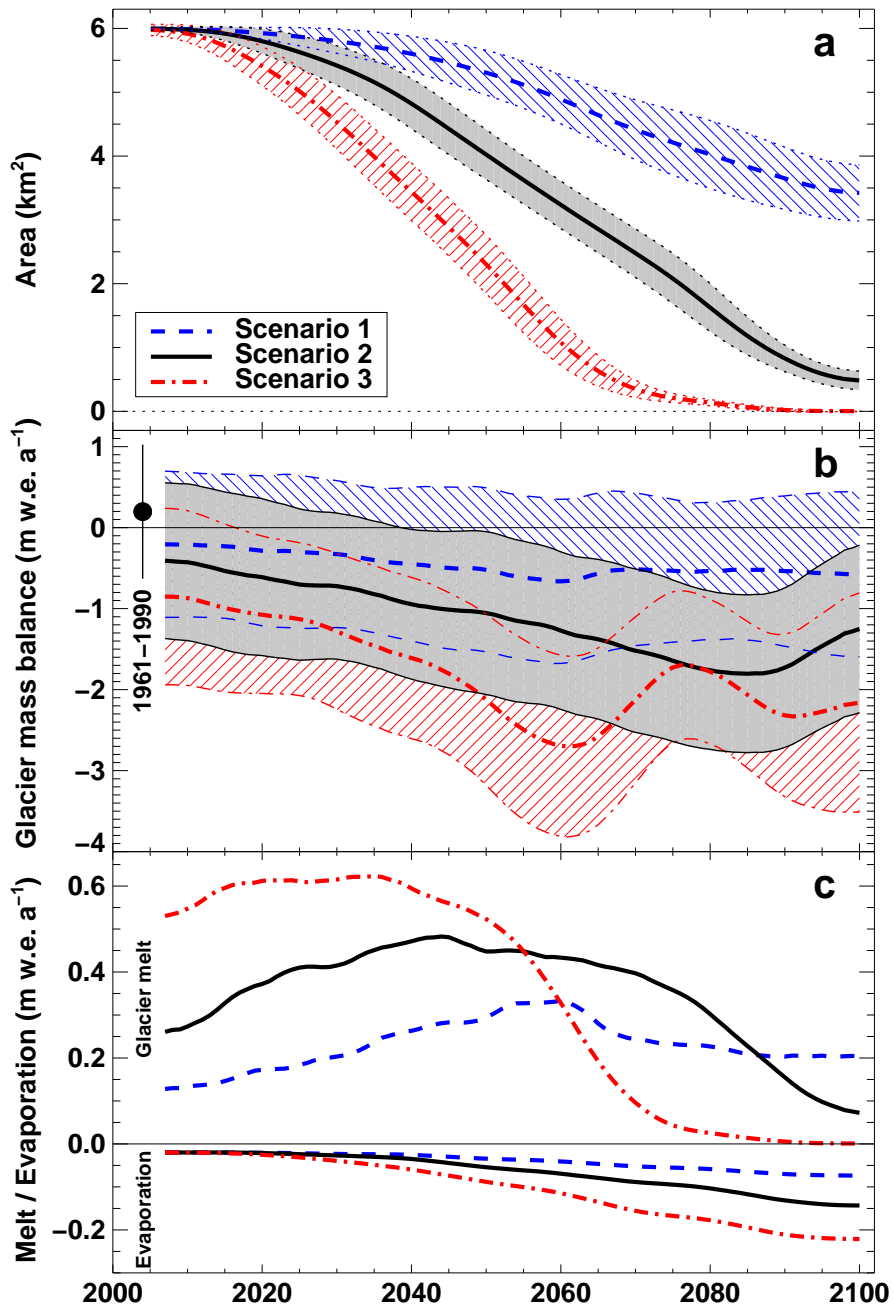


Figure 8.10: Evolution of (a) glacial area, (b) mean specific mass balance and (c) water balance components (glacier melt contribution ΔS , evaporation E) shown for Glacier de Moming using the Scenarios 1 to 3 (2007–2100). The shaded (Sc2) and hatched (Sc1, Sc3) ranges between the thin lines show a 95% confidence interval of the year-to-year fluctuations based on 20 multiple model runs using random offsets from the mean scenario changes. The variability range is not shown in (c) for better visibility. The symbol in (b) indicates the mean glacier mass balance during the climatic normal period ± 2 standard deviations (σ).

future (Fig. 8.10b). However, the effect of the year-to-year variability of climate is considerable. Positive mass balances may occur over the entire 21st century according to Scenario 1. Generally, the mass balance series reveal a trend towards more negative values. This implies that the glaciers are not able to adapt their size as fast as the climate changes and thus never reach a steady-state. After the year 2080 some stabilization of glacier mass balance is evident

Table 8.3: *Compilation of model results for the Scenarios (Sc) 1 to 3 (2050, 2100) for all three investigated catchments combined. Figures for glacier area and volume are relative to 2006. \bar{b}_n is the mean specific glacier surface mass balance and Q is the annual runoff volume.*

	2050			2100		
	Sc1	Sc2	Sc3	Sc1	Sc2	Sc3
Area (%)	85	65	37	49	6	0
Volume (%)	65	37	18	22	1	0
\bar{b}_n (m w.e.)	-0.69	-1.46	-2.52	-0.83	-1.47	-
Q ($10^6 \text{ m}^3 \text{ a}^{-1}$)	65.1	67.5	62.8	67.0	47.1	32.0

(Fig. 8.10b). This is due to the complete loss of low-lying glacier tongues.

The evolution of annual runoff volume shows a uniform pattern for the three drainage basins analyzed (Fig. 8.11). Discharge is increasing in the near future due to a reduction of the ice mass. In the median climate scenario, discharge reaches a culmination after three to four decades, depending on the glacierization of the catchment. The culmination of annual runoff is earlier and more pronounced in the warm-dry Scenario 3. No distinct culmination of annual runoff is attained according to the cold-wet Scenario 1 (Fig. 8.11).

In general, the greater the decrease in catchment glacierization, the more the runoff volume will be determined by precipitation. After several decades, the glaciers will have reduced their surface area considerably and retreated up to higher elevations. Thus, they cannot provide much additional meltwater. This implies that glaciermelt has an important impact on runoff during intermediate periods; however, it is low at the end of the 21st century (Fig. 8.10c). Compared to the climatic normal period, annual runoff by 2025 from the Glacier de Moming catchment is enhanced by +34% (Sc1), +48% (Sc2) and +57% (Sc3). By 2075 the figures change to +49% (Sc1), +39% (Sc2) and -13% (Sc3). However, during the period 1961-1990 glacier mass balances were positive, which led to reduced runoff at that time. During the last decade (1997-2006) the annual runoff was 18% higher compared to the climatic normal period.

Table 8.4 and Figure 8.10c show the evolution of water balance components. The mean inter-annual precipitation sums are virtually constant, whereas the variation in runoff is determined mainly by the change in the glaciermelt contribution ΔS . The contribution of glaciermelt to runoff is important during the first half of the 21st century and approaches zero towards its end due to the disappearance of glacier coverage, except for Scenario 1 (Fig. 8.10c). At present,

Table 8.4: *Specific water balance components according to Scenario 2. The values represent area-weighted means of the three catchments. Q : runoff, P : precipitation, E : evaporation. The importance of the glaciermelt contribution ΔS decreases as the glaciers shrink. Quantities contributing to runoff are positive, quantities reducing runoff negative.*

Year	Q	P	E	ΔS	Glac.	ELA
		mm a^{-1}			(%)	(m a.s.l.)
1961-1990	1307	1558	-27	-224	67	2994
2025	1983	1601	-51	433	53	3368
2050	1982	1535	-87	534	38	3585
2075	1721	1554	-132	299	16	3699
2100	1383	1500	-181	64	3	3742

evaporation is low due to the high glacierization of the catchment and the lack of vegetated surfaces. Because of deglaciation and a corresponding rise in the vegetation zones, an increasing water loss by evaporation and transpiration is predicted and becomes considerable in the second half of the 21st century (Table 8.4 and Fig. 8.10c). The ELA rises by nearly 800 m during the next century, compared to the period 1961-1990.

We evaluated the annual discharge cycle in the past and for four snapshots in the future (Fig. 8.12). At first, a substantial increase in runoff during the summer months is predicted. By 2025 the July-August discharge increases by +33% (Sc1), +42% (Sc2) and +47% (Sc3) compared to 1961-1990. Due to enhanced temperatures the exposed bare ice surfaces are melting rapidly and provide additional runoff. There is a significant increase in the length of the melting season. The peak runoff occurs slightly later in the year during a first phase of about two decades and then shifts from the end of July to June (Fig. 8.12). This shift is related to the shrinkage of the ice masses and corresponds to the transition from an icemelt to a snowmelt dominated regime.

By 2100 the results of Scenarios 2 and 3 show a significant decrease in July-August runoff to much lower values than during the climatic normal period: -55% (Sc2) and -92% (Sc3). In contrast, there is a significant increase in May-June runoff due to an earlier onset of the melting season: +190% (Sc2) and +66% (Sc3). The results also indicate a significant increase in autumn runoff because precipitation will mostly occur in liquid form in this season. When considering Scenario 1, however, runoff is much less affected. By 2100 even in summer an increase of +26% compared to 1961-1990 is calculated. Only a minor shift in the runoff peak towards early summer is observed (Fig. 8.12b).

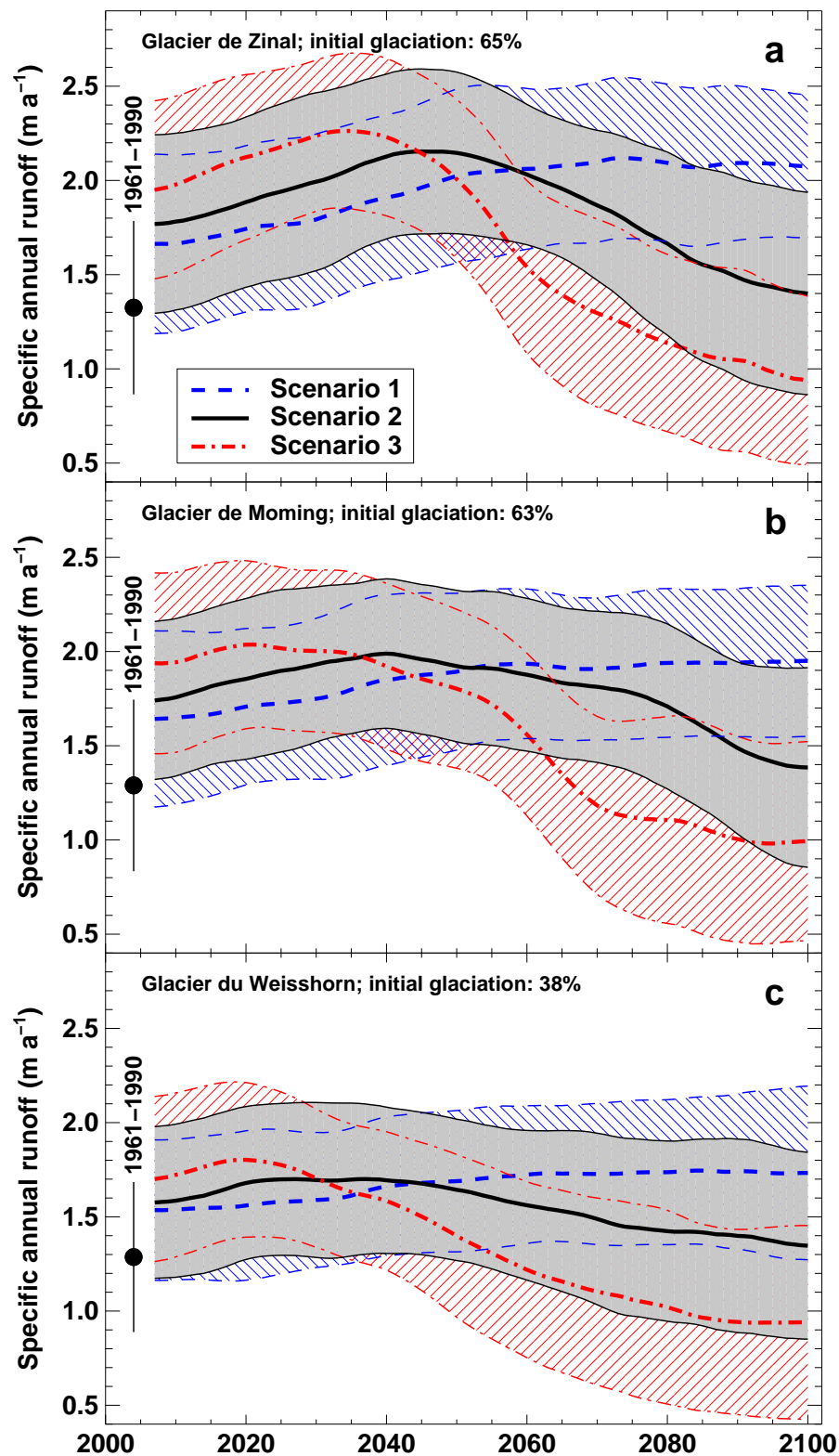


Figure 8.11: Evolution of annual runoff volume according to the climate change Scenarios 1 to 3 (2007–2100) shown for the (a) highly glacierized drainage basins of Glacier de Zinal and (b) Glacier de Moming and (c) the moderately glacierized catchment of Glacier du Weisshorn. Runoff is given normalized by the catchment area in order to allow comparison of the three basins. The symbol at the beginning of the time series shows the mean runoff during the climatic normal period $\pm 2\sigma$. The simulation results do not have the same origin because the climate change scenarios refer to the climate in 1990 and already differ by 2007 (see Fig. 8.8).

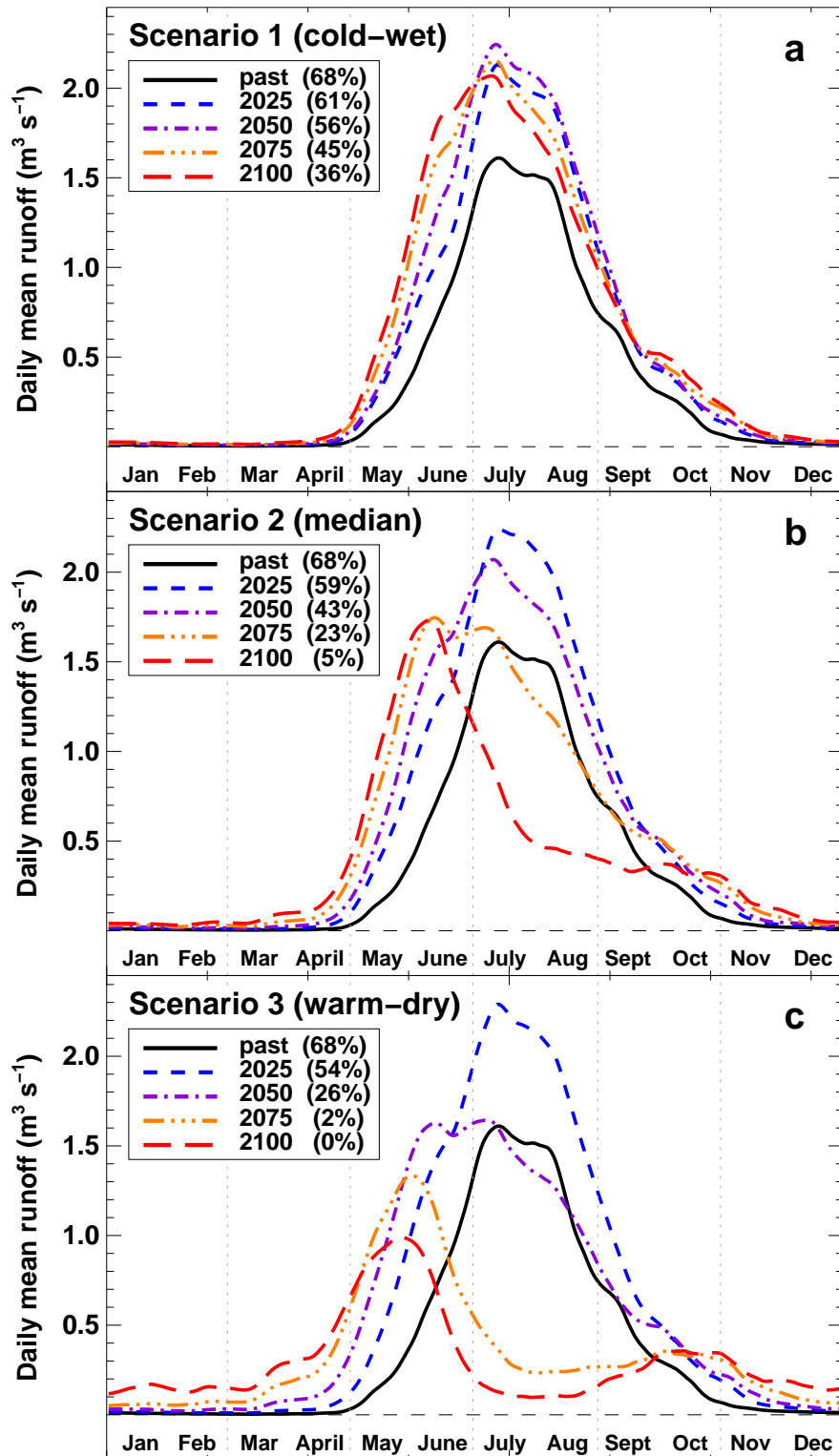


Figure 8.12: Annual cycle of runoff of Glacier de Moming shown for the past (1961-1990) and four snapshots in the future. The glacierization of the catchment at each evaluation year is given in brackets. (a) Scenario 1 (cold-wet), (b) Scenario 2 (median) and (c) Scenario 3 (warm-dry).

8.5 Discussion

Predictions of future runoff from glacierized drainage basins have significant uncertainties due to the modelling procedure and the unknown evolution of climate. In this section, these uncertainties are discussed in detail.

We propose a new method to determine the ice thickness distribution of glaciers not covered by field data. The initial ice volume is a sensitive input parameter in high-mountain catchment modelling and may have considerable impact on future runoff. A validation of our method with a comparison of calculated and measured ice thickness on different Alpine glaciers has shown that it produces plausible estimates of ice volume and ice thickness distribution (Fig. 8.3).

Temperature-index melt models are often used in hydrological studies to describe melt processes. They are easy to handle and require only temperature as climatic input. However, unambiguous calibration of the parameters of temperature-index models requires a variety of field measurements (Seibert, 2000; Huss and others, 2008a). Here, no direct observations of winter accumulation are available. Several sets of parameters may yield good agreement with the field data and this ambiguity could have an impact on the results for future periods. Furthermore, it is not yet clear how stable the model parameters are over time. Careful calibration using a variety of field data on different Swiss glaciers during the 20th century revealed decadal variations in the parameter values of up to 10% (Huss and others, 2008a). In this study, we assume the calibrated parameters to remain constant over time. Changing energy fluxes and a completely different climate regime may lead to changes in the statistical relation between air temperature and melt rate and, thus, in the parameter values. This assumption has therefore the potential to cause significant error in the prediction of future glacier extent and runoff.

The model results show that at present, evaporation is a negligible component in the water balance of high mountain catchments (Table 8.4). The increase in evaporational water loss is predicted to be rather large in future and needs to be taken into account. However, the uncertainty in modelling future evaporation and transpiration is considerable due to the effects of the changing surface - atmosphere interactions and unknown reaction of vegetation to climate change. The simulated values of evaporation represent best estimates given similar boundary conditions for evaporation as in the current situation.

The parameterization of glacier retreat is an important component of our model approach. It adapts the 3D glacier surface geometry annually in response to the calculated ice volume change. This approach makes it possible to compute the transient evolution of glacial runoff during the next decades as the change in ice volume contributing to discharge is included in the calculation. Two important feedback mechanisms are taken into account: (i) Glaciers retreat to higher elevations and get closer to steady-state because of the loss of their low-lying glacier tongues, and (ii) the decrease in glacier surface elevation associated with glacier retreat is a positive feedback, which causes higher melt rates. Our approach cannot reproduce time scales for the transfer of mass from the accumulation area to the ablation area. The ice volume change is distributed annually over the glacier surface according to a pattern which is theoretically and observationally founded (Jóhannesson and others, 1989; Bauder and others, 2007). We assume the same shape of the Δh -parameterization (Fig. 8.5b) for all glaciers as well as for retreat and advance. However, the distribution of elevation change over the glacier surface is influenced by ice dynamics and the geometry of the glacier. This may also explain the inferior ability of this approach to reproduce the surface elevation change in short periods of mass gain. However, we expect that glacier retreat will be far more important than glacier advance. When considering

decadal periods our simple parameterization yields good agreement with the observed surface elevation changes in the past although different glacier geometries are involved. The good performance of the Δh -parameterization to simulate glacier retreat could also be confirmed by testing the approach on other Alpine glaciers (Grosser Aletschgletscher, Rhonegletscher).

Although crude, the method copes well with complex topography and ensures conservation of mass. The ice thickness distribution is essential for the determination of the future glacier extent, but is not a sensitive variable for the calculation. It is difficult to apply full models of 3D ice dynamics to the investigated glaciers due to the scarcity of available field data and the complex terrain. Thus, our approach is well suited in hydrological studies for inferring the area and volume evolution of ice masses with a lack of field measurements.

In order to assess the impact of updating the glacier surface on the simulated future runoff, we performed two tests. In a first experiment, we keep the glacier surface area constant and compare the simulated discharge using the identical input parameters for the period 2007–2100 with the results presented above. According to Scenario 2 annual runoff differs by only 3% after two decades, but differences are greater in summer. By 2050 the differences in annual runoff volume when not accounting for a change in glacier extent are +25% (Sc2), +7% (Sc1) and +72% (Sc3) and increase to more than 100% by 2100. This implies that keeping the glacierization fixed is only justifiable for runoff forecasts in the next three decades, but leads to much higher runoff in a later stage compared with our approach. When not adapting the glacierized area the glaciers become an inexhaustible source of water.

In a second test, we implement a simple approach to update glacier surface – here referred to as the AAR-method – in GERM (AAR: Accumulation Area Ratio). This approach was recently proposed by several authors (Horton and others, 2006; Schaeffli and others, 2007; Paul and others, 2007b). These studies assume that the glacierized area A_{glacier} is proportional to the multi-year mean accumulation area A_{acc} , which is calculated based on climate variables. A_{glacier} is derived using the relation

$$A_{\text{glacier}} = A_{\text{acc}} / AAR_s, \quad (8.8)$$

where AAR_s is the accumulation area ratio required to yield a steady-state of the glacier (Schaeffli and others, 2007). We calculate the accumulation area A_{acc} as a mean value of 10 years in order to average out climate variability. At the end of each decade an updated glacier area A_{glacier} is determined using Equation 8.8. AAR_s is prescribed and equals 0.6 (Schaeffli and others, 2007). It is implicitly assumed that the glacier area is always in balance with the prevailing climate conditions. A major drawback of this method in modelling studies of future high mountain runoff is that mass conservation is not satisfied, i.e., ice volume may disappear without contributing to discharge. Furthermore, the effect of surface lowering on the melt rate is neglected.

The differences between the method to update glacier surface as proposed in this paper (reference) and the AAR-method are considerable. The glacier surface area is smaller by 30 to 55% (2025) using the AAR-method compared to the reference. Towards the end of the 21st century the difference in glacier area is smaller. Calculated annual runoff volumes are up to 30% lower than the reference using the AAR-method (Table 8.5). The differences are even more significant during the summer months. Moderate disagreement of the two methods is found for the cold-wet Scenario 1, however, lower runoff than for the reference results is predicted throughout the entire 21st century using the AAR-method (Table 8.5). For Scenario 3, by contrast, the differences in runoff volume are most pronounced in 2050. Runoff in summer is more than 50%

Table 8.5: Differences in annual runoff volumes Q_a and July-August runoff Q_{JA} between the reference model run using the Δh -parameterization to update glacier area and the test run where the glacier surface area is updated according to the AAR-method. Deviations are given in %. Negative values indicate that runoff is lower using the AAR-method.

Year	Scenario 1		Scenario 2		Scenario 3	
	ΔQ_a	ΔQ_{JA}	ΔQ_a	ΔQ_{JA}	ΔQ_a	ΔQ_{JA}
2025	-16	-18	-24	-30	-30	-39
2050	-17	-22	-26	-37	-31	-52
2075	-18	-23	-16	-29	-1	-6
2100	-11	-14	-2	-5	0	0

below the reference according to the AAR-method. Due to a complete wastage of the glaciers towards 2100 the disagreement gradually decreases to zero (Table 8.5). The results from the two methods differ more strongly for large glaciers (e.g. Glacier de Zinal) than for the small Glacier de Weisshorn, which is able to keep its extent closer to steady-state due to a shorter response time.

The comparison of the two methods for updating glacier surfaces implies that the AAR-method is not suited for modelling the transient evolution of runoff from glacierized catchments for the coming decades. We consider the approach proposed in this study to be more realistic because it is mass conserving and allows to calculate a transient evolution of the glacier geometry.

The uncertainty of climate change during the 21st century is considerable (IPCC, 2007; Christensen and Christensen, 2007) and determined by a wide range of possible evolutions of population, technology, emissions and, thus, CO_2 concentration. The predefined climate Scenarios 1 to 3 span a 95% confidence interval of climatic impact on glacier existence based on the evaluated RCM results (Frei, 2007; Fig. 8.7 and 8.8). In the case of Scenario 1, the runoff characteristics only show only minor changes compared to the past (Fig. 8.12b). This indicates that even moderate changes are possible within the range of uncertainty in future climate evolution. However, the climate change observed in the last two decades does not support this evolution. The scenarios for temperature and precipitation change (Frei, 2007) are relative to the climate in 1990. Until present Scenario 3 (warm-dry) corresponds best to the measured meteorological data (Fig. 8.8).

The two extreme scenarios predict significant changes in the annual precipitation (Fig. 8.8). However, results of individual RCMs within the PRUDENCE project show that temperature and precipitation change are related to each other. A substantial increase in air temperature may cause an intensification of the seasonal distribution of precipitation, namely a reduction in summer and an increase in winter precipitation (Christensen and Christensen, 2007). Scenarios 1 and 3 do not take this effect into account. We tested the impact of high winter precipitation associated with the 97.5% quantile temperature increase. The results of this experiment indicate that an intensified annual precipitation cycle slightly moderates the dramatic changes predicted for Scenario 3 (Fig. 8.12c). According to this climate projection, the differences in the annual runoff volumes (Fig. 8.11) between the two extreme scenarios are attenuated as well.

The range of expected variability due to the year-to-year fluctuations in climate is particularly illustrative for runoff (Fig. 8.11). Whereas in the first half of the 21st century low flow is not to be expected due to the compensating effect of icemelt, it may be abundant after 2070, especially for Scenario 3. In the next decades the hazard potential for flooding is increased. Floods could

occur when intense melt in the summer season is combined with heavy thunderstorms providing rain that contributes immediately to stream-flow runoff due to the low retention capacity of bare ice surfaces.

In this study we apply the conservative assumption that the internal variability of climate will be the same as in the past. However, RCM model results indicate that the year-to-year variability will increase, with an emphasis in summer (Christensen and others, 2002; Hingray and others, 2007). This may even amplify the expected extreme events of droughts and floodings (Seneviratne and others, 2002).

The use of seasonal climate scenarios is of crucial importance for impact studies with high spatial and temporal resolution (Horton and others, 2006; Huss and others, 2007b). Glacier retreat is decelerated by a general increase in winter precipitation, because it occurs frequently as snow at elevations higher than 3000 m a.s.l., even in a warmer climate. The expected decrease in summer precipitation, however, adds to the water scarcity in this season, which is predicted for the second half of the 21st century due to the almost complete disappearance of the glaciers.

Comparable studies of runoff from high mountain catchments in the same topographic region were performed by Horton and others (2006) and Schaeffli and others (2007) for the period 2070-2099. The results of our work are mostly consistent with the previous studies. Similar trends in the water balance components are simulated. Annual precipitation slightly decreases according to the Scenario 2 (median), evaporation increases significantly and the annual runoff drops below the current level by the end of the 21st century (Table 8.4 and Fig. 8.11). However, our results predict a more significant contribution of glaciermelt to discharge than do previous studies, because the present work does not assume that the glaciers are always in balance with the prevailing climate. This is a major advantage of the approach proposed in this study and allows a transient modelling of runoff from glacierized drainage basins.

8.6 Conclusion

A glacio-hydrological model is presented to calculate the daily runoff from highly glacierized alpine drainage basins. It includes an annual updating of the glacier surface and regional climate scenarios in seasonal resolution for the period 2007–2100. Glacier evolution and runoff are calculated using a median and two extreme scenarios assuming temperature trends of $+3.8 \pm 2.4^\circ\text{C}$ and precipitation changes of $-6 \pm 21\%$ per century. The mean changes in the meteorological time series are perturbed using random offsets in order to include the year-to-year fluctuations of the meteorological variables. Thus, a range of variability in future runoff is estimated that will have an important impact on the management of water resources. The proposed approach to updating the glacier surface geometry on an annual basis is mass conserving, easy to apply and thus well suited to simulate the transient evolution of runoff in hydrological studies of glacierized drainage basins.

Glacier retreat in the next decades will be considerable. The deglaciation of high alpine drainage basins causes a transition from an icemelt- to a snowmelt-dominated runoff regime. According to the median scenario, the annual runoff volume from highly glacierized drainage basins increases for two to four decades and then drops below the current level. When the glacier surface is kept constant, the annual runoff volumes at the end of the 21st century are more than two times greater than our values; significantly lower runoff volumes (up to -30%), however, result when using the AAR-method to derive glacier extent. Our glacio-hydrological model

predicts a significant decrease in runoff during the summer months, whereas water supply from mountainous regions increases in autumn and particularly in spring. The model results indicate that substantial changes will occur in the runoff regime of high alpine catchments linked with the shrinkage of the glaciers. These changes will have an impact on the management of water resources in future decades, on both a local and a regional scale.

Acknowledgments

The study was commissioned by the Forces Motrices de la Gougra SA hydropower company. R. Hock made an important contribution to the development of the mass balance model. C. Frei provided the climate scenario data. We thank all members of the radio-echo sounding field campaigns in 2006 and 2007. Photogrammetrie Perrinjaquet, Gümlingen and H. Bösch evaluated the aerial photographs. MeteoSwiss provided the weather data. S. Braun-Clarke proofread the English. We thank M. Truffer for helpful discussions. Constructive comments by an anonymous reviewer, B. Schaefli and the scientific editor R. Hock contributed to improving the clarity of the manuscript.

Chapter 9

Parameterizations for calculating future glacier retreat

ABSTRACT: The calculation of glacier extent in the future requires models for describing the climate forcing acting on the glacier and the dynamic response of the ice mass. Ice dynamics can be analyzed using flow models that often demand considerable computation power and field data input. Four different parameterizations for calculating the change in glacier surface elevation and extent as consequence of climate warming are proposed and validated against results of a 3D finite element ice flow model for Rhonegletscher over the period 2008-2100. Δh -parameterizations yield the best agreement with the ice flow model and can closely reproduce the distributed ice thickness change, as well as glacier area and length. Such empirical functions can be derived for individual glaciers from the observed pattern of glacier retreat in the past, but are also applicable to unmeasured ice masses. More simple parameterizations completely ignoring the effect of ice dynamics – the AAR-method and non-dynamic downwasting – perform significantly worse compared to Δh -parameterizations. The retreat of Rhonegletscher in the 21st century is analyzed using three climate scenarios enveloping a probabilistic range of changes in the climate system. According to the most likely evolution Rhonegletscher will be reduced to a small ice field by 2100.

9.1 Introduction

The assessment of the temporal change in glacier geometry requires the description of two main factors: (1) the climatic forcing acting on the glacier surface and (2) the ice flow dynamics (for which the initial ice thickness distribution is a basic boundary condition). In order to obtain well-founded forecasts of glacier change during the next decades both components must be adequately described by models taking into account the principal back-coupling mechanisms. In particular for applied problems related to glacier retreat, e.g. hydrological forecasts, there is a need for simple models. These should be easily applicable to larger catchments and require only a limited amount of readily available input data (obtained e.g. from remote sensing or

topographic maps). This chapter proposes methods to parameterize the distributed change in glacier surface elevation and ice thickness due to the wastage of the ice mass. Comparison with a 3D finite element ice flow model allows the validation of different parameterizations for Rhonegletscher over the period 2008 to 2100.

The climatic forcing that acts on the glacier can be described using mass balance models of varying complexity. They relate meteorological variables to accumulation and ablation rates at the glacier surface (e.g. Arnold and others, 1996; Klok and Oerlemans, 2002; Hock and Holmgren, 2005; Pellicciotti and others, 2005; Huss and others, 2008a). The ice dynamics of alpine glaciers have been assessed in many glaciological studies ranging from simple flowline models (e.g. Greuell, 1992; Oerlemans, 1997; Huss and others, 2007b) to complex 3D ice flow models (e.g. Hubbard and others, 1998; Gudmundsson, 1999; Jouvét and others, 2008). The change in glacier extent in the Alps in the next decades has been investigated using combined models of mass balance and ice dynamics of different levels of sophistication (Vielí and others, 1997; Wallinga and van de Wal, 1998; Schneeberger and others, 2003; Sugiyama and others, 2007a; Le Meur and others, 2007). Also less data intensive approaches were applied (Zemp and others, 2006; Schaeffli and others, 2007; Paul and others, 2007b; Huss and others, 2008b). The future evolution of Rhonegletscher has previously been addressed (Wallinga and van de Wal, 1998; Sugiyama and others, 2007a). Rhonegletscher is well suited for developing new models due to its large basis of field data and the simple geometry that is typical for alpine valley glaciers.

Four different parameterizations for the change in glacier surface elevation in response to mass balance are introduced: Two Δh -parameterizations, the **AAR-method** (proposed by Schaeffli and others (2007) and Paul and others (2007b)) and **non-dynamic downwasting**. The latter two parameterizations do completely neglect the effect of ice dynamics on glacier retreat. The so called Δh -parameterizations (Huss and others, 2008b, see Chapter 8) are based on a function relating the elevation of the glacier surface h to the elevation change Δh (equivalent

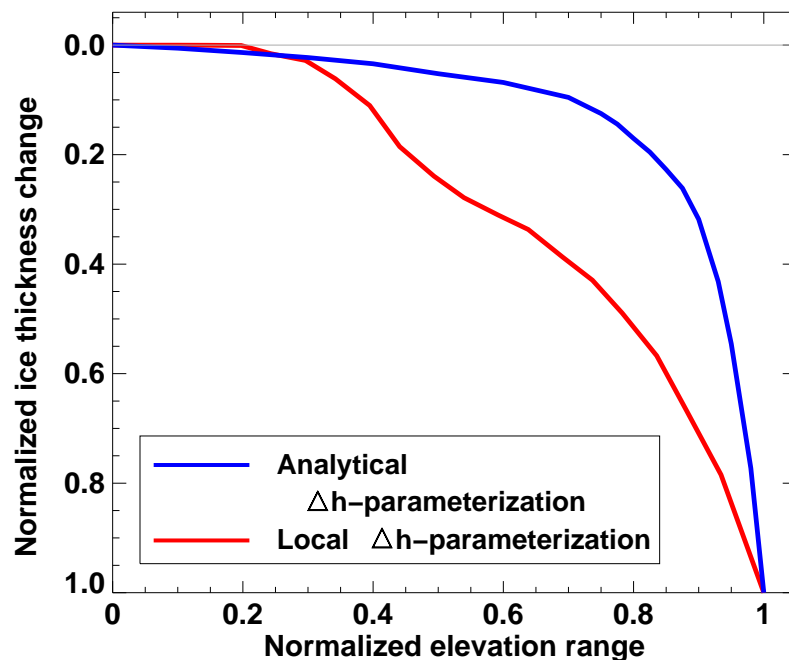


Figure 9.1: Δh -parameterizations for Rhonegletscher. The normalized elevation ranges from the highest point of the glacier (left) to the lowest glacier elevation (right). Ice thickness changes are small in the upper part of the glacier and largest near the glacier terminus.

to ice thickness change) occurring over a time interval of one or several years. Typically, elevation changes are small in the accumulation area and largest at the glacier terminus (Fig. 9.1) as could be shown by observations on alpine glaciers (e.g. Bauder and others, 2007) and using theoretical considerations (Jóhannesson and others, 1989). Jóhannesson and others (1989) analytically calculated the transient change in ice thickness between two steady-states for an ideally shaped glacier. They showed that the glacier rapidly approaches a steady-state geometry after a step like change in climate. Huss and others (2008b) parameterized h versus Δh using a function based on a model result by Jóhannesson and others (1989), see Figure 5 in their paper. Throughout this chapter this function is referred to as 'analytical Δh -parameterization'. A second function is proposed, here termed the 'local Δh -parameterization' (Fig. 9.1), which is determined for each glacier individually.

The rationale of this chapter is the comparison of different approaches for calculating the change in ice thickness and glacier extent in response to future climate warming. This chapter seeks to shed light on the question whether complex 3D ice flow modelling is indispensable to calculate glacier evolution in the 21st century or whether the ice flow dynamics can also be approximated using simple parameterizations. The future evolution of Rhonegletscher 2008 to 2100 is simulated based on different climate change scenarios. The calculations are performed using (1) a 3D finite element ice flow model (Jouvet and others, 2008, submitted) and (2) four different parameterizations for the change in ice thickness. This chapter proposes feasible methods for the annual updating of glacier surface elevation and extent. Input data requirements are limited to (1) a digital elevation model of the bedrock (obtained for any glacier applying the procedure described in Farinotti and others, in press) and (2) distributed surface mass balance for each year (obtained applying the methods described in Chapters 2 or 8).

9.2 Study site and field data

During the last Ice Age Rhonegletscher was the largest glacier in the Alpine mountain range. Nowadays, it has receded to a size of roughly 16 km² and a length of 10 km. From an accumulation basin below the summits of Dammastock (3633 m a.s.l.) and Rhonestock the glacier flows over an ice fall to the ablation area forming its tongue in a deeply incised valley. The glacier now ends above the second ice fall over which it spectacularly cascaded only 100 years ago. Particular for the geometry of Rhonegletscher are two large overdeepenings (Farinotti and others, in press). In front of the current glacier terminus a lake is now forming.

A variety of field data is available for Rhonegletscher covering different temporal and spatial scales. Between 1874 and 2007 seven digital elevation models (DEMs) derived either from topographic maps (before 1960) or from aerial photographs are available (Bauder and others, 2007). These allow ice volume changes to be calculated. A total of 19 radio-echo sounding profiles acquired in 2004 and 2008 provides information about the ice thickness distribution (Zahno, 2004; Farinotti and others, in press). Measurements of net balance at stakes were carried out at the end of the 19th century (Mercanton, 1916), by Funk (1985) during three years in the 1980s and from 2006 to 2008 (Huss, 2008). Additionally, distributed snow probings were performed in five accumulation seasons – in 2008 at more than 700 locations. They provide information about the snow distribution pattern over the glacier surface. The discharge records from the gauging station at Gletsch maintained by BAFU (catchment glacierization in 2007: 47%) cover more than 50 years. Meteorological data (daily mean air temperature and precipitation sums) are available for several nearby weather stations of MeteoSwiss, some of the time

series reaching back to 1864. For an overview of the methods used to obtain representative and continuous meteorological time series for Rhonegletscher refer to Chapter 2.

All data mentioned above were combined using a distributed mass balance model for the period 1865-2007 (Huss and others, 2008a). The calculated net balance for every grid cell and every year is used to drive the ice flow model for the past. Assumptions on future climate are based on Frei (2007), who statistically evaluated the results of 16 regional climate models within the PRUDENCE project (Christensen and others, 2002). Three scenarios for the seasonal change in air temperature and precipitation are defined according to Huss and others (2007b) and Huss and others (2008b). Scenario 2 represents the median (most probable), Scenario 1 a glacier friendly evolution (cold-wet) and Scenario 3 is the most adversary to glacier existence (warm-dry). The three scenarios envelope a 95% confidence interval of future climate change in the Alps (Fig. 8.8).

9.3 Methods

9.3.1 Model description

Three dimensional ice flow model

A three dimensional finite element ice flow model is used to calculate the dynamics of Rhonegletscher. The model is described in detail by Jouvét and others (2008) and is based on a Volume of Fluid (VOF) formulation (Scardovelli and Zaleski, 1999). The model has a high level of physical sophistication and solves the nonlinear Stokes equations. It has been successfully applied to different types of fluids (e.g. Maronnier and others, 2003) and was first employed by Jouvét and others (2008) to calculate glacier dynamics.

Mass conservation along the ice-air interface yields a transport equation which can be used to determine the evolution of glacier geometry. Given the initial shape of the glacier, the ice flow velocity \mathbf{u} is obtained by solving a 3D nonlinear Stokes problem with a nonlinear sliding law along the ice-bedrock interface. Then, glacier geometry is updated by computing the volume fraction of ice φ , which satisfies the transport equation

$$\frac{\partial \varphi}{\partial t} + \mathbf{u} \cdot \nabla \varphi = b \delta_{\Gamma_A}, \quad (9.1)$$

where $b \delta_{\Gamma_A}$ is a source term (i.e. mass balance) acting only on the ice-air interface Γ_A . A decoupling algorithm allows the equations to be solved using different numerical techniques (Jouvét and others, 2008). The nonlinear Stokes problem is solved on a fixed, unstructured finite element mesh consisting of tetrahedrons. The transport equation is solved using a fixed, regular grid of smaller cells. The 3D ice flow model was implemented for Rhonegletscher by Jouvét and others (submitted) in order to predict its transient evolution from 2008 to 2100.

Implementation of Δh -parameterizations

The framework of glacier surface updating based on different parameterizations is the glacio-hydrological model (GERM) described in Huss and others (2008b), see Chapter 8. The model

is designed to calculate the future runoff from highly glacierized drainage basins and includes a mass balance model, an evaporation model and a runoff routing module. For a description of these model components refer to Chapter 8. The 3D glacier geometry is updated annually. At the end of the hydrological year the lost or gained ice volume determined using the mass balance model is converted into a distributed ice thickness change. The method described hereafter is identical for both Δh -parameterizations (Fig. 9.1). For practical reasons the h - Δh -function is normalized with the elevation range of the glacier. Integration of the Δh -parameterization over the glacier surface, weighted with the relative area of elevation bands must be equal to the total annual change in glacier mass given by the mass balance computation. In order to satisfy this criterion, the magnitude of the h - Δh -function is adapted in an iterative procedure so that its curvature remains constant. Thus, for each elevation band of 10 m an annual surface elevation change is determined. Near the glacier terminus the annual surface lowering is restricted not to exceed that year's local surface mass balance in ice equivalent. This corresponds to non-dynamic downwasting of the glacier tongue, currently observed on several alpine valley glacier tongues. In this case the h - Δh -function is then rescaled in order to accommodate the entire annual volume change. The Δh -parameterization is not applied near the borders of the glacier (i.e. where the ice thickness is smaller than 10 m). It is assumed that in these regions thinning due to ice dynamics is small. Thus, in these regions ice thickness change is calculated only based on the local mass balance in ice equivalent. For all parameterizations the ice extent is determined by comparing the updated glacier surface elevation and the DEM of the glacier bedrock topography. The glacier disappears where the ice thickness drops to zero.

9.3.2 Further parameterizations

The AAR-method

In previous studies of future glacier retreat a simple method based on the accumulation area ratio (AAR) was applied to update the glacier surface area (e.g. Schaeffli and others, 2007; Paul and others, 2007b). It is assumed that the glacierized area A_{glacier} is proportional to the multi-year mean accumulation area $A_{\text{acc.}}$, which is calculated based on climate variables. A_{glacier} is derived using the relation

$$A_{\text{glacier}} = A_{\text{acc.}} / AAR_s, \quad (9.2)$$

where AAR_s is the accumulation area ratio required to yield a steady-state of the glacier. The accumulation area $A_{\text{acc.}}$ is calculated as the mean of the previous 10 years in order to average out the year to year fluctuations of climate. An updated glacier area A_{glacier} is determined annually using Equation 9.2. AAR_s is prescribed and equals 0.6 (Schaeffli and others, 2007). In this approach it is implicitly assumed that the glacier is always in balance with the prevailing climate conditions, which is not justified for large ice masses in a dynamically changing climate. A major draw-back of this parameterization is that it does not account for the conservation of mass. For transient hydrological modelling, in particular, this represents a serious problem as ice volume can disappear without contributing to discharge. The advantage of the AAR-method is that it requires no information about ice thickness distribution.

Non-dynamic downwasting

Given the mass balance and the ice thickness distribution the change in glacier extent can be calculated by rigorously assuming non-dynamic downwasting. Ice thickness change at each grid cell equals the annual mass balance in ice equivalent. This approach completely neglects a transport of mass from the accumulation to the ablation area. Thus, the lowering of the glacier tongue is expected to be too fast and surface elevation is supposed to increase at high elevations. This simple method might not seem realistic, however, in the case of a further acceleration of glacier wastage, downwasting of an entire glacier with rapidly stagnating ice flow could still be a reasonable approximation. An advantage of this approach compared to the AAR-method is that ice volume is transiently modelled, i.e. mass is conserved.

9.3.3 Deriving a local Δh -parameterization

The distribution of surface elevation change in response to a change in climate depends on (i) the geometry, (ii) the size, (iii) the ice flow regime and (iv) the mass balance distribution of each single glacier. A feasible option to derive a local Δh -parameterization for an individual ice mass is to retrieve information on the surface elevation change patterns from digital elevation models in the past. This requires at least two DEMs, preferably more, covering an adequate time span (more than five years). By comparing the elevation change between two DEMs in glacier elevation bands of 10 m a distribution of h versus Δh is obtained. If several DEMs are available h - Δh can be computed for all intervals. When deriving Δh -parameterizations from observations one has to be careful not to include noise, which would then be amplified in the modelling. Therefore, the h - Δh function needs to be smoothed, in particular in the uppermost parts of the accumulation area, where the uncertainty in the DEMs is relatively high and the area covered by individual elevation bands is small. In general, the quality of the h - Δh relation increases with the time span covered and the changes that occurred during this period. Furthermore, the observed distribution of elevation changes is disturbed by long periodic fluctuations in climate forcing (see e.g. Figure 3.8b). The distribution of Δh over the glacier surface is inherently different for periods of (1) 'stable' or accelerated glacier retreat (e.g. since the 1990s), (2) during time intervals of positive mass balances (e.g. the 1970s) or (3) following such a period (e.g. the 1980s). In future we expect mostly negative mass balances – this is what the current climate models imply. Thus, it is proposed to derive the Δh -parameterization, which will be applied for intense glacier retreat in the future, from observations in the past that mostly cover case (1), i.e. constantly negative mass balances. If DEMs embracing such periods are not available, it is advisable to consider elevation changes between the first and the last DEM (the longest period covered) in order to average out as much 'noise' as possible. If several well suited periods exist for the establishment of the h - Δh relation, the results can be stacked in a second step.

The local Δh -parameterization for Rhonegletscher (Fig. 9.1) was derived as follows: For the DEM periods 1929-1959 ($\overline{b_n} = -0.30$ m w.e. a⁻¹), 1991-2000 ($\overline{b_n} = -0.42$ m w.e. a⁻¹) and 2000-2007 ($\overline{b_n} = -0.89$ m w.e. a⁻¹) negative mass balances prevail. These time intervals do not include important subperiods of mass gain (see e.g. Fig. 2.6). For each of the periods the distribution of Δh with elevation was computed. The curves were normalized with the elevation range of the glacier (for h) and the maximum elevation change (for Δh). Finally, the three curves were stacked and smoothed.

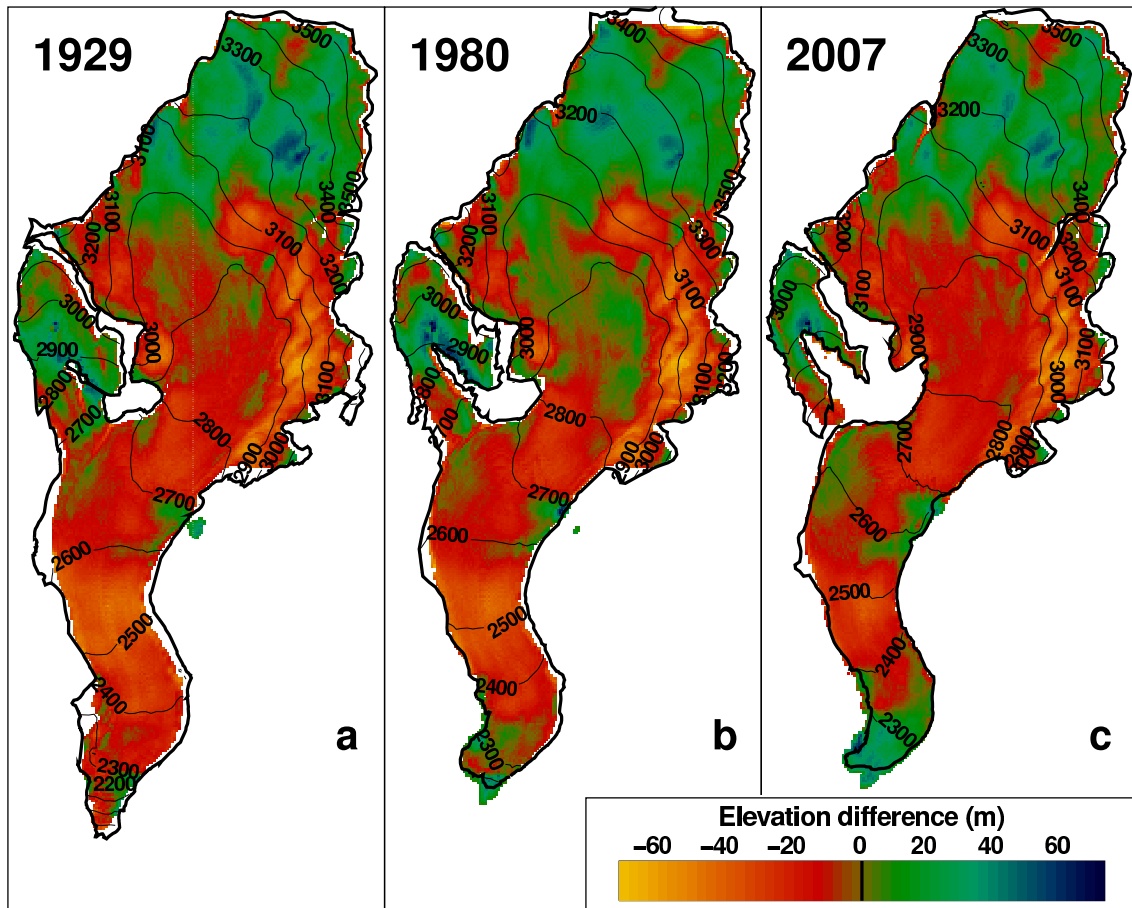


Figure 9.2: Difference in surface elevation and glacier extent obtained from comparison of DEMs and results of the 3D ice flow model in (a) 1929, (b) 1980 and (c) 2007 ($h_{\text{ice flow model}} - h_{\text{observation}}$). The model was initialized in 1874 and forced using the mass balance distribution of each year in the period 1874 to 2007.

9.3.4 Validation of the ice flow model in the past

The 3D ice flow model is validated against repeated observations of glacier geometry and ice flow velocities (Bauder and others, 2007; Nishimura, 2008). The model is forced using the mass balance distribution of each year in the period 1874 to 2007 (Huss and others, 2008a) and is initialized employing the glacier geometry of 1874. By tuning the flow rate factor A and the sliding coefficient (see Juvet and others, submitted) good agreement of calculated and measured surface flow speed is obtained (not shown). Comparison with DEMs is displayed in Figure 9.2. Glacier area and length are reproduced well. Differences in modelled and measured surface elevation in the accumulation area (with both signs) are mostly attributed to the uncertainty in the bedrock map. The deviations are largest in regions not covered by radio-echo sounding measurements. A method to exploit misfits of calculated and observed glacier surface in order to correct the bedrock map was successfully tested. The updated ice thickness distribution is, however, not yet used in this study. Towards 2007 the model evidently overestimates surface elevation near the terminus (Fig. 9.2c). Uncertainties in the distribution of surface mass balance might be partly responsible for this misfit. On average, a root-mean-square error of 21 m between observed and simulated glacier surface is found. This value is regarded as the a priori uncertainty in the 3D ice flow model in the present configuration. Generally, the accuracy

of the model results are affected by the uncertainty in (i) the bedrock elevation, (ii) the mass balance distribution and (iii) the description of ice dynamics.

9.4 Results

The 3D ice flow model and GERM, which is implemented with different parameterizations for the ice thickness change, are forced using the same climatic input for the period 2008 to 2100. Mass balance is calculated in daily resolution for every grid cell applying the parameters calibrated between 2000 and 2007. Methods and scenarios are described by Huss and others (2008b) and the anticipated changes in the meteorological variables are displayed in Figures 8.7 and 8.8. Model runs were performed for the Scenarios 1 to 3. GERM was run applying the analytical Δh -parameterization, the local Δh -parameterization, the AAR-method and non-dynamic downwasting. Because the identical mass balance input was used to drive the models, differences in simulated surface elevation and glacier extent are only attributable to ice flow dynamics. The ice flow model is assumed to reproduce these in an optimal way and is regarded as the reference result.

Comparison of 3D ice flow model results in the spatial domain and on a longitudinal flow line are shown for (1) the analytical Δh -parameterization and (2) the local Δh -parameterization (see Figs 9.3 to 9.6). The distribution of the ice covered area is reproduced well using these parameterizations. Furthermore, the distributed surface elevation change is captured accurately. In the second half of the 20th century the use of the analytical Δh -parameterization leads to an overestimation of the glacier surface in the central parts of the glacier, whereas surface elevation is too low close to the terminus (Fig. 9.5). The local Δh -parameterization slightly underestimates the rate of surface lowering near the terminus before 2050, however, in general, agrees very well with the ice flow model over the entire modelling period (Figs 9.4 and 9.6). The root-mean-square error of surface elevation obtained with the ice flow model and the local Δh -parameterization is smaller than 20 m throughout the entire modelling period (Table 9.1). This is within the uncertainty in the ice flow model results (Fig. 9.2). Note, that the uncertainty in future climate change is large. However, as the models are forced using the same climatic input, this factor does not have an impact on the comparison of the different methods to calculate glacier retreat.

The validation shows that the local Δh -parameterization performs slightly better, particularly towards the end of the modelling period, than the analytical Δh -parameterization (Table 9.1). This was expected, as the former was specifically designed for Rhonegletscher based on observations in the past. The full set of figures is only shown for the local Δh -parameterization – regarded as the the best solution – for Scenarios 1 and 3.

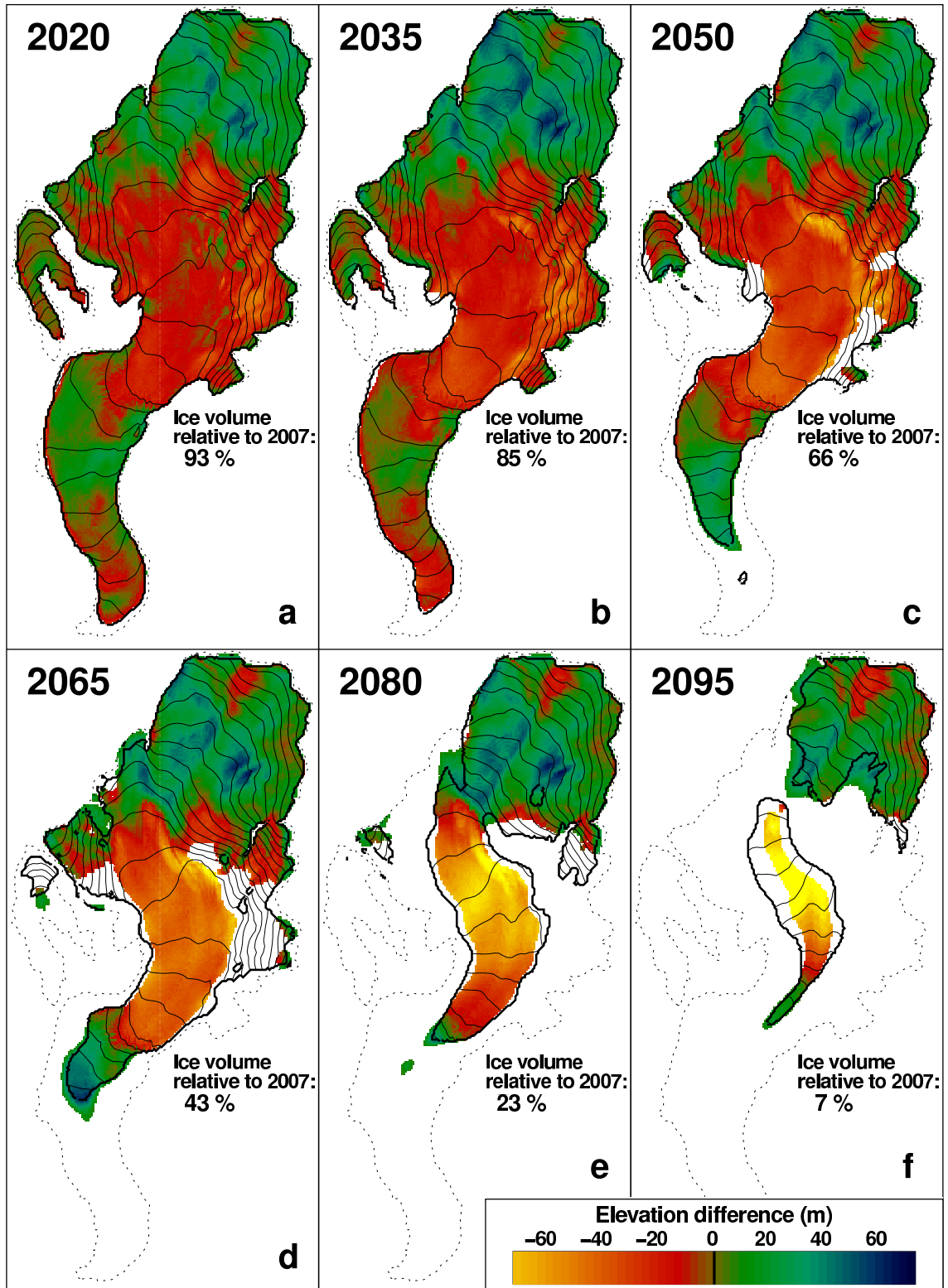


Figure 9.3: Comparison of surface elevation ($h_{\text{ice flow model}} - h_{\text{parameterization}}$) and glacier extent calculated for Scenario 2 (median) using the 3D ice flow model and the analytical Δh -parameterization. Coloured areas indicate glacier coverage as calculated by the ice flow model. The colours refer to the difference in elevation obtained from comparing the results of both models. Solid lines with contours show the glacier extent as calculated using the parameterization. The dotted line indicates the glacier outline in 2007.

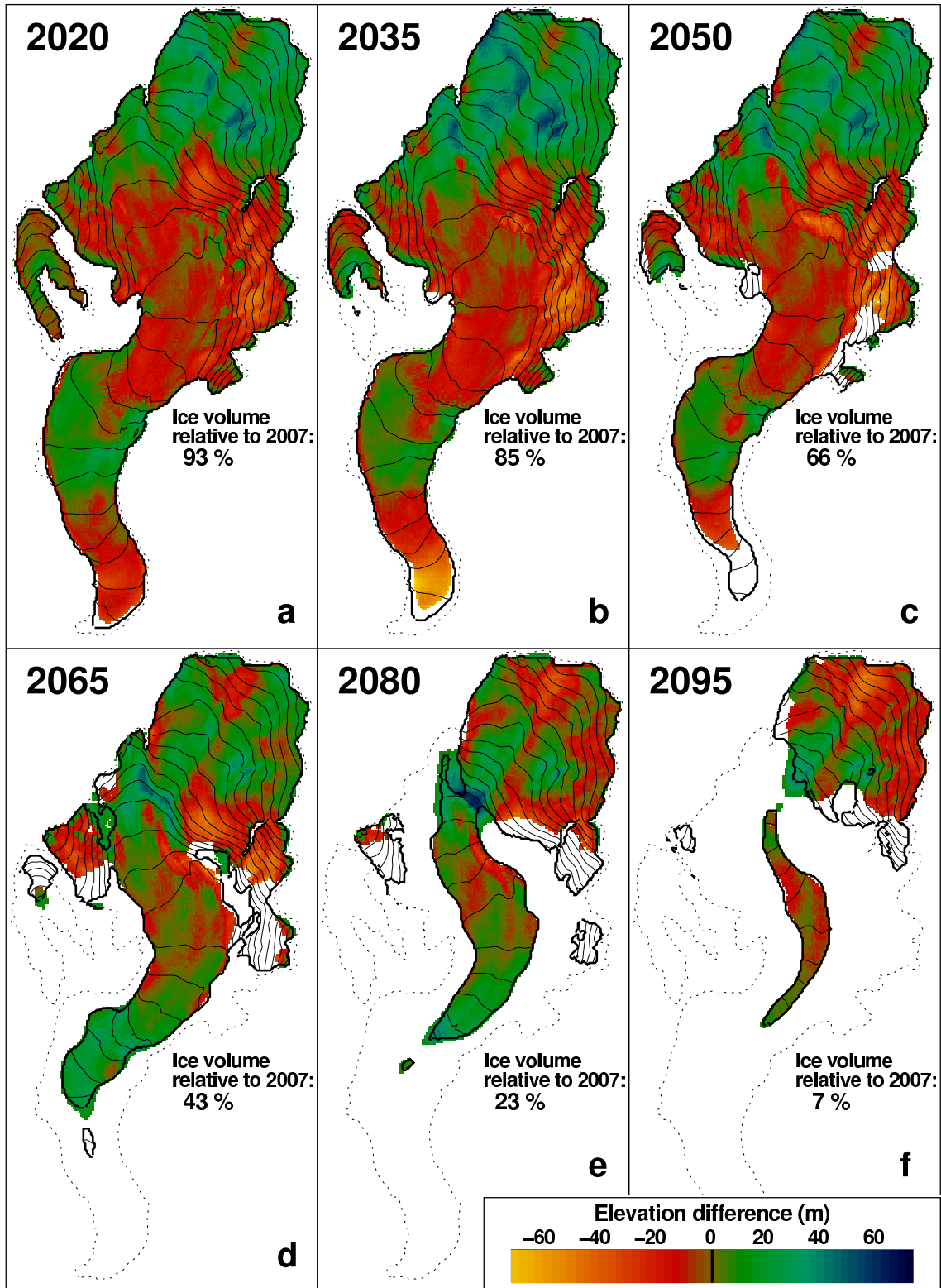


Figure 9.4: Comparison of surface elevation ($h_{\text{ice flow model}} - h_{\text{parameterization}}$) and glacier extent calculated for **Scenario 2 (median)** using the 3D ice flow model and the **local Δh -parameterization**. Coloured areas indicate glacier coverage as calculated by the ice flow model. The colours refer to the difference in elevation obtained from comparing the results of both models. Solid lines with contours show the glacier extent as calculated using the parameterization. The dotted line indicates the glacier outline in 2007.

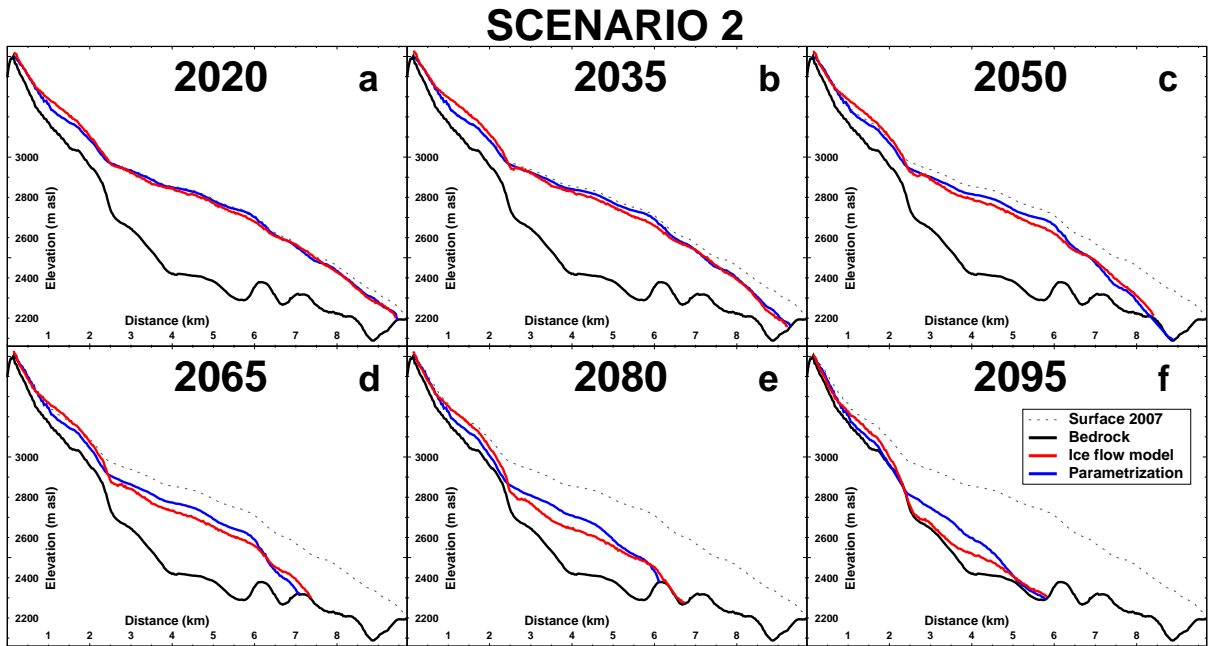


Figure 9.5: Glacier surface elevation calculated for Scenario 2 (median) using the 3D ice flow model and the analytical Δh -parameterization in a longitudinal glacier profile.

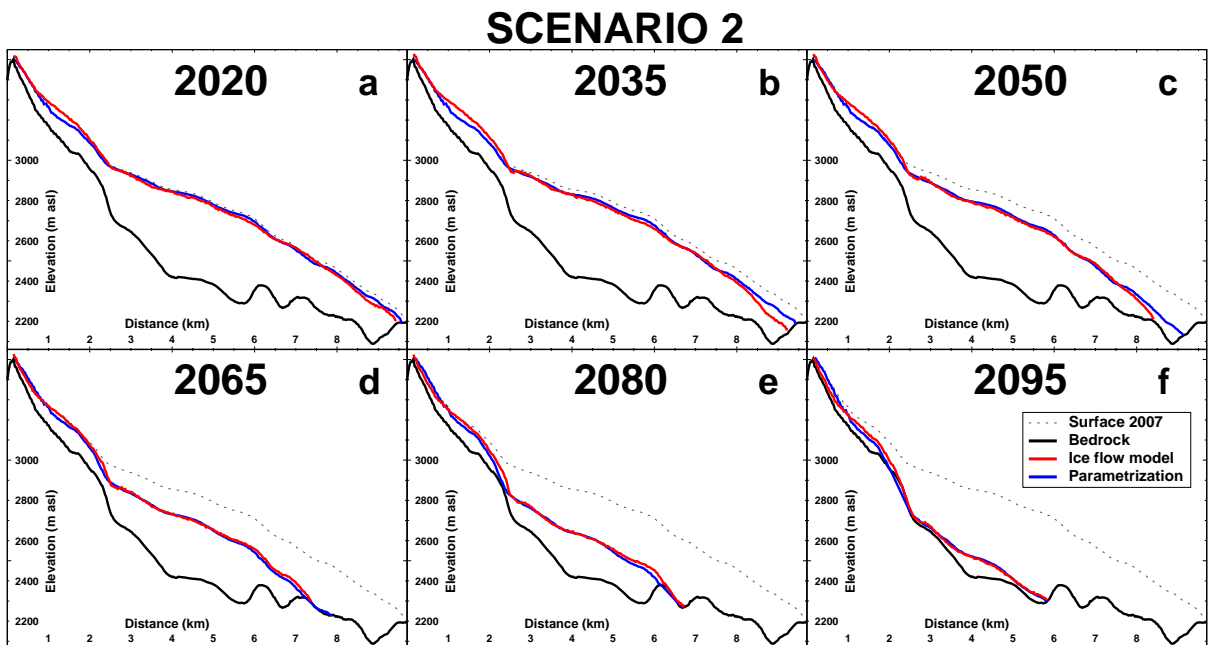


Figure 9.6: Glacier surface elevation calculated for Scenario 2 (median) using the 3D ice flow model and the local Δh -parameterization in a longitudinal glacier profile.

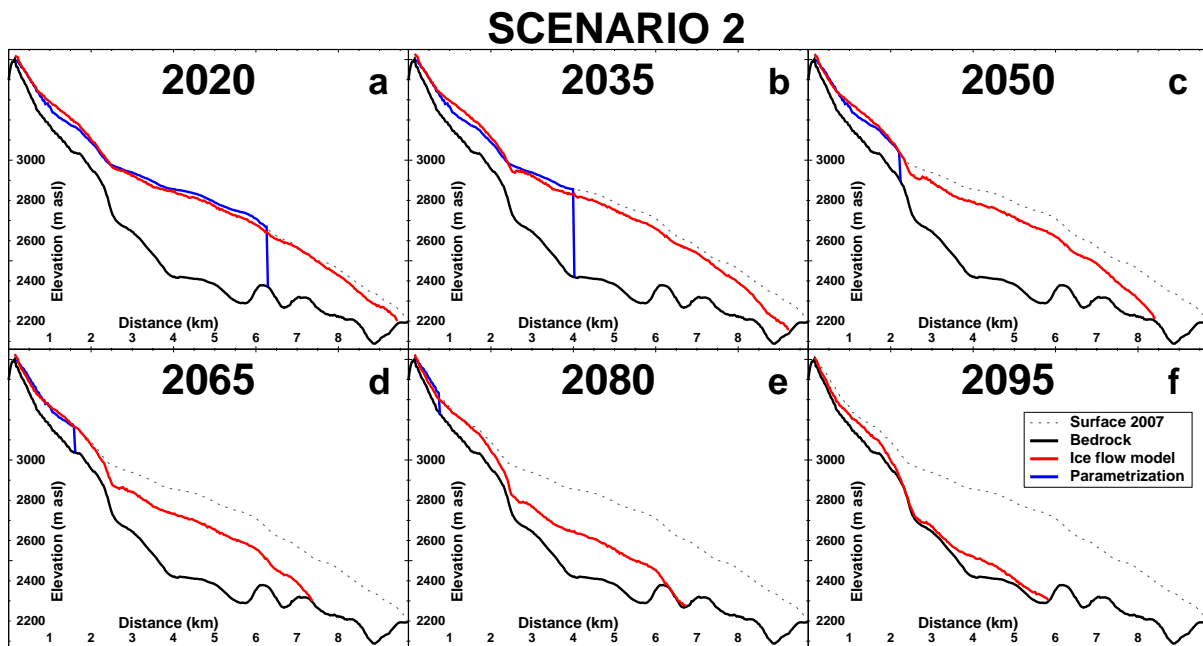


Figure 9.7: Glacier surface elevation calculated for Scenario 2 (median) according to the 3D ice flow model and the **AAR-method** in a longitudinal glacier profile.

Figure 9.7 shows that the AAR-method does a bad job in estimating glacier extent. According to this parameterization Rhonegletscher almost immediately loses its tongue. Most Alpine glaciers are presently out of equilibrium, i.e. their size is too large for the current climate conditions. The AAR-method does not account for the time scale glaciers need to get rid of their excess ice mass. Thus, the AAR-method predicts too fast glacier retreat (Fig. 9.9). The misfits are largest around 2050 when the glacier is far from equilibrium and become smaller as the glacier area decreases. To estimate glacier area change in a discrete time step of one century (as performed e.g. by Schaeffli and others, 2007) the AAR-method may yield reasonable results, especially for small glaciers. Huss and others (2008b) tested the effect of using the AAR-method on runoff forecasts in the 21st century. The AAR-method is not suitable in transient runoff modelling, because it is not mass conserving. Discharge volumes may be underestimated by up to 40%, depending on catchment characteristics.

Assuming non-dynamic downwasting of the ice mass results in surprisingly low misfits with the ice flow model (Fig. 9.8). The power of this crude approach in reproducing glacier area and length is significantly better than the AAR-method and is not much worse than the Δh -parameterizations (Fig. 9.9). However, the root-mean-square errors increase rapidly with the length of the modelling period (Table 9.1), which is explained by unhindered and continuous growth of the ice mass in the accumulation area.

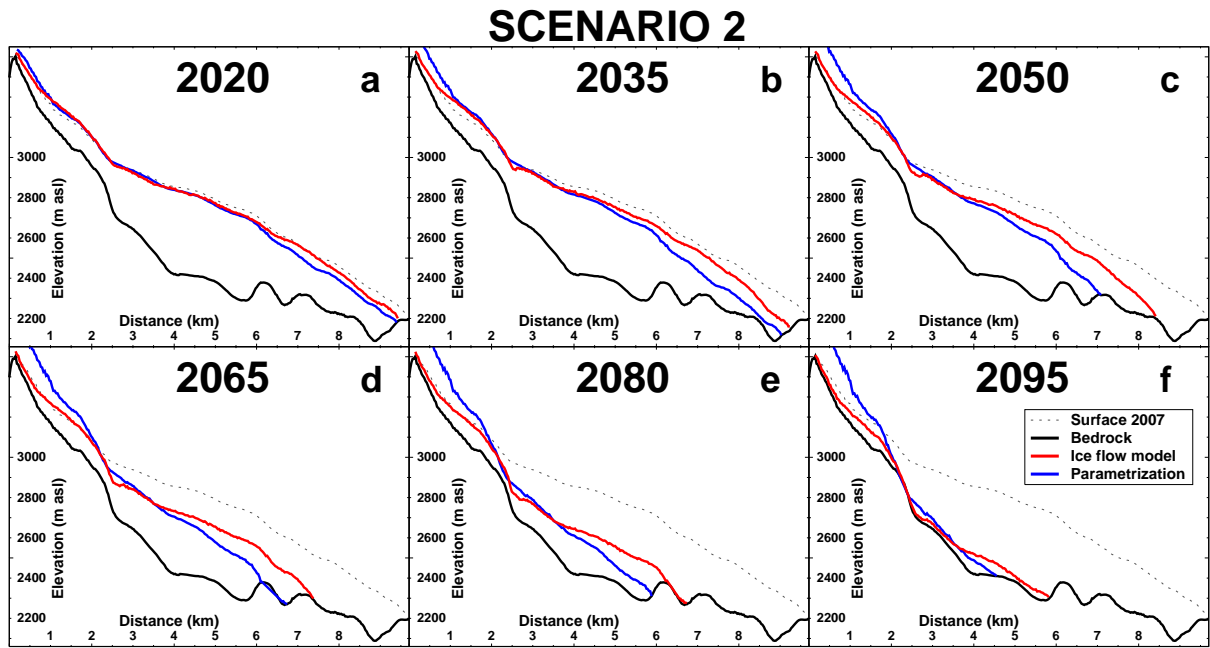


Figure 9.8: Glacier surface elevation calculated for Scenario 2 (median) according to the 3D ice flow model and assuming **non-dynamic downwasting** in a longitudinal glacier profile.

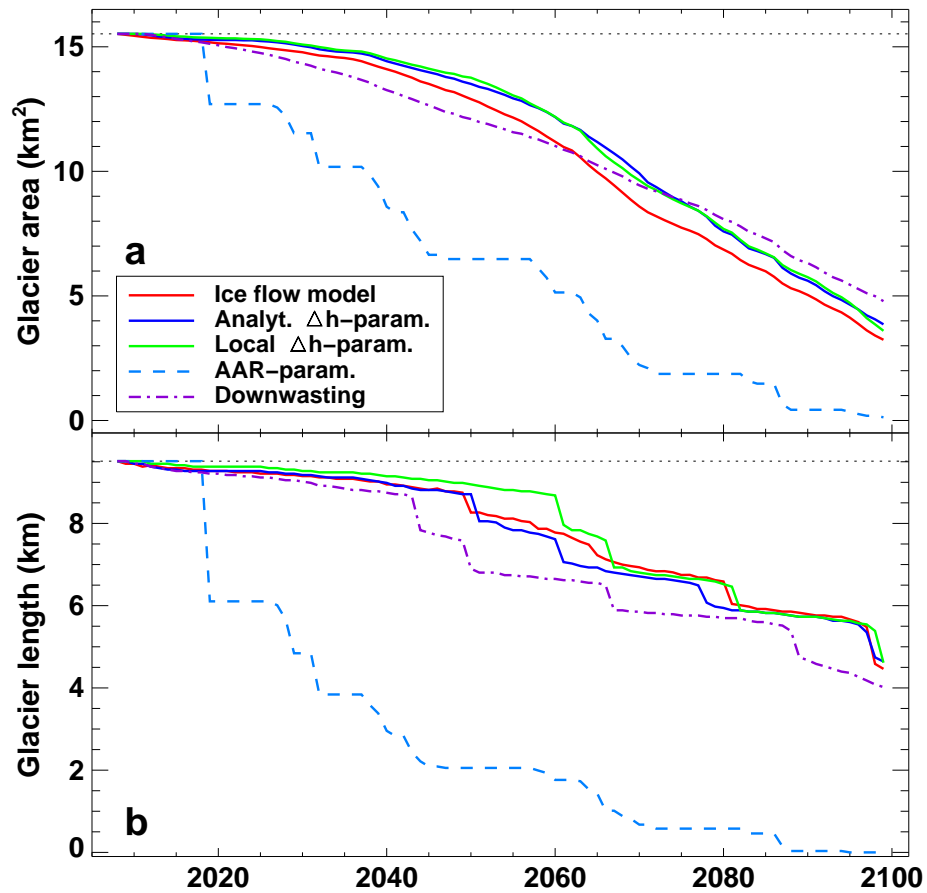


Figure 9.9: Glacier (a) length and (b) area calculated for Scenario 2 using different approaches.

Table 9.1: Validation of surface elevation calculated using different parameterizations against the ice flow model for three 30-year periods and scenarios in the future. $\overline{\text{rms}_d}$ represents root-mean-square errors of the difference in elevation ($h_{\text{ice flow model}} - h_{\text{parameterization}}$) at all grid cells averaged over the period considered.

Scenario	Period	$\overline{\text{rms}_d}$ (analytical Δh)	$\overline{\text{rms}_d}$ (Local Δh)	$\overline{\text{rms}_d}$ (AAR-method)	$\overline{\text{rms}_d}$ (Downwasting)
Scenario 2	2008-2040	17.2 m	16.5 m	67.7 m	30.4 m
	2041-2070	27.2 m	20.1 m	117.7 m	70.5 m
	2071-2100	37.4 m	20.7 m	68.6 m	115.0 m
Scenario 1	2008-2040	17.2 m	16.9 m	53.0 m	37.4 m
	2041-2070	22.1 m	22.3 m	98.1 m	97.3 m
	2071-2100	24.3 m	23.1 m	114.1 m	155.2 m
Scenario 3	2008-2040	20.2 m	15.3 m	90.0 m	27.8 m
	2041-2070	30.2 m	22.1 m	81.9 m	46.3 m
	2071-2100	9.0 m	11.4 m	9.7 m	42.0 m

Figures 9.10 and 9.11 illustrate the performance of the local Δh -parameterization according to the moderate climate change Scenario 1 (cold-wet). Also in this case this parameterization yields the best agreement with the ice flow model (Table 9.1). Both Δh -parameterizations capture glacier area and length well, whereas the AAR-method and non-dynamic downwasting significantly underestimate them (Fig. 9.12). The misfits of these two parameterizations are largest for Scenario 1, because ice dynamics, that are explicitly excluded in these approaches, are important (Table 9.1).

The local Δh -parameterization also performs well under the warm-dry Scenario 3 (Fig. 9.13 and 9.14). The misfit with surface elevation given by the ice flow model is mostly within its uncertainties (Table 9.1). According to the AAR-method Rhonegletscher is virtually gone in 30 years (Fig. 9.15). Considering the reaction time of a glacier and the conservation of mass this results is highly improbable. Under these climate conditions, non-dynamic downwasting yields acceptable results, since ice dynamics are almost negligible in this case (Table 9.1 and Fig. 9.15).

The validation shows that the change in glacier surface elevation and extent can be approximated reasonably well using Δh -parameterizations (Fig. 9.1) instead of complex 3D ice flow modelling. The use of a complex 3D ice flow model requiring considerable computational power and field data for calibration does not provide a significantly different result. Furthermore, the sensitivity of the parameterization to uncertainties in the bedrock elevation is by far smaller, which makes it very suitable for glaciers with little field data. The good performance of simple Δh -parameterizations is partly attributed to the fact that in future, ice flux plays a minor role compared to surface melting. The parameterizations used in this study could for instance not simulate the distributed change in ice thickness during glacier advance periods satisfyingly. However, the Δh -parameterizations account for some of the effects of ice dynamics and work well for periods of glacier retreat. Parameterizations explicitly ignoring ice dynamics – such as the AAR-method and non-dynamic downwasting – performed significantly worse in predicting future glacier retreat (Table 9.1). The use of these methods is discouraged as they are neither computationally less expensive nor require less input data.

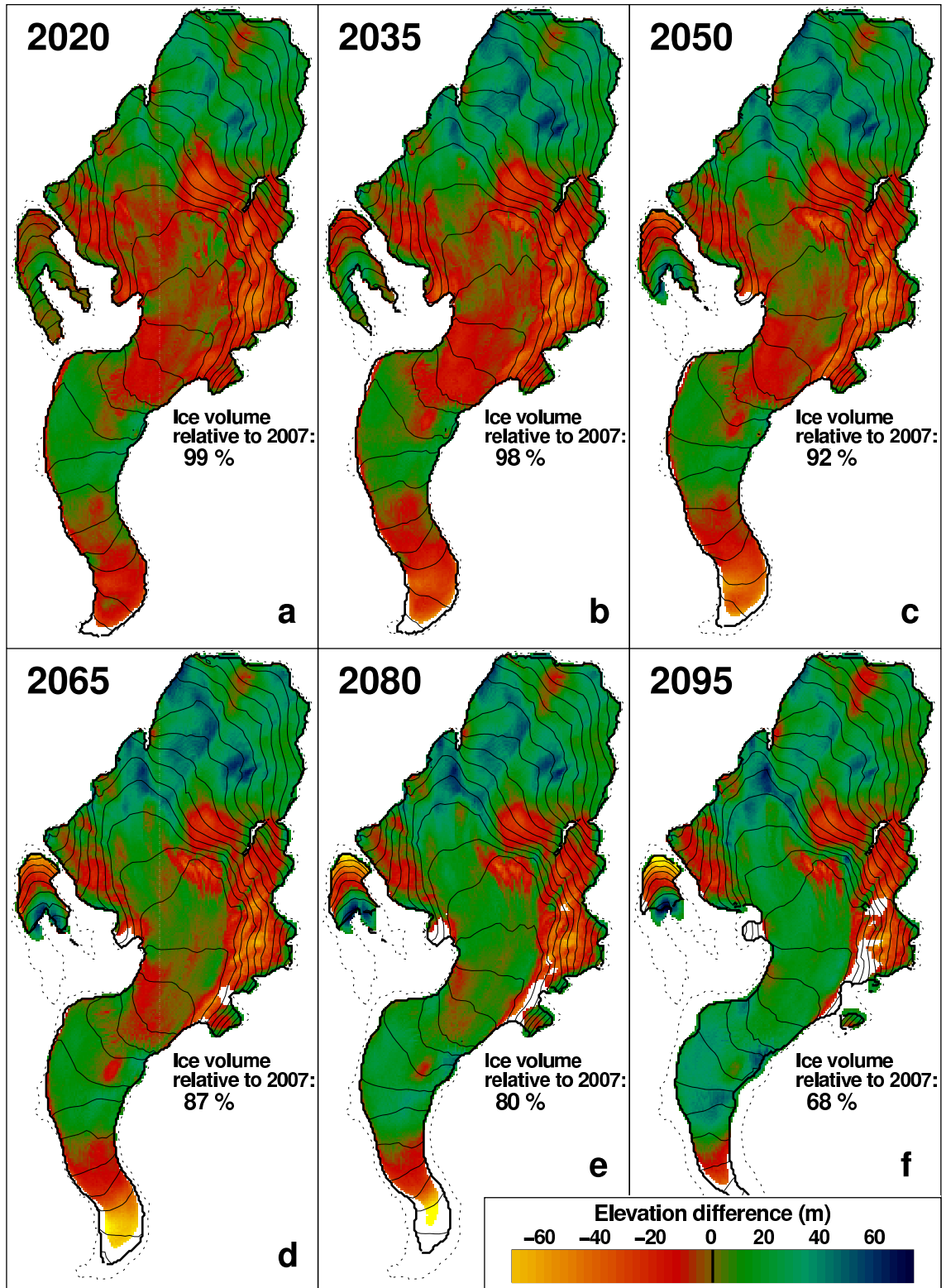


Figure 9.10: Comparison of surface elevation ($h_{\text{ice flow model}} - h_{\text{parameterization}}$) and glacier extent calculated for Scenario 1 (cold-wet) according to the 3D ice flow model and the local Δh -parameterization. Coloured areas indicate glacier coverage as calculated by the ice flow model. The colours refer to the difference in elevation obtained from comparing the results of both models. Solid lines with contours show the glacier extent as calculated using the parameterization. The dotted line indicates the glacier outline in 2007.

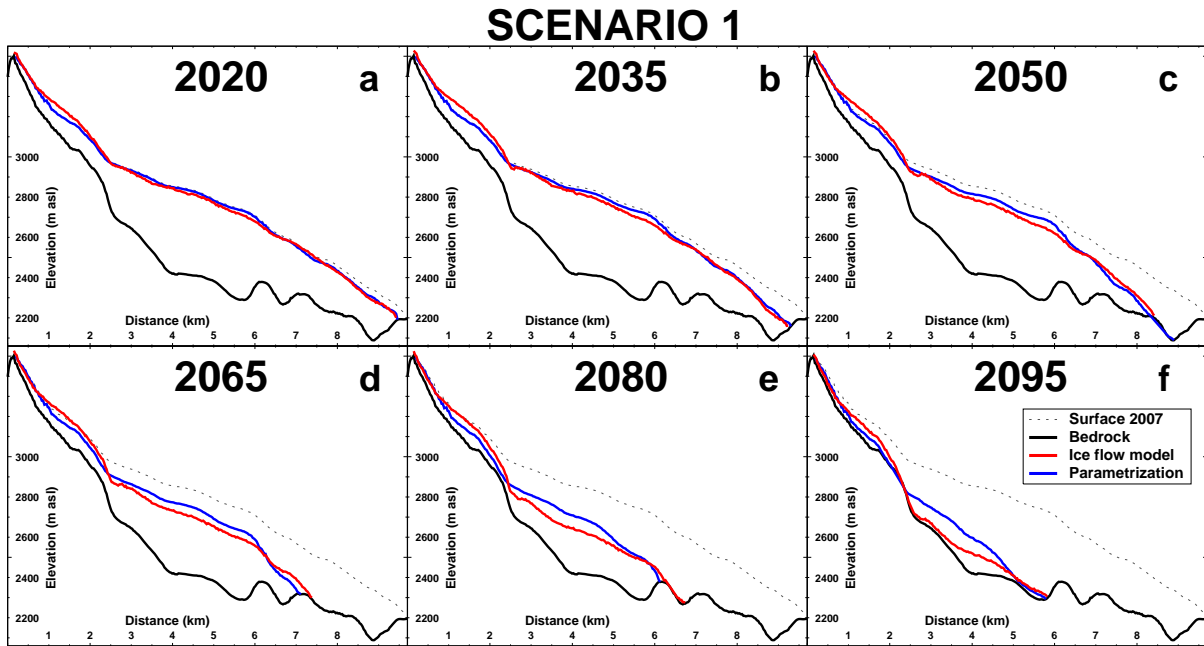


Figure 9.11: Glacier surface elevation calculated for Scenario 1 (cold-wet) using the 3D ice flow model and the local Δh -parameterization in a longitudinal glacier profile.

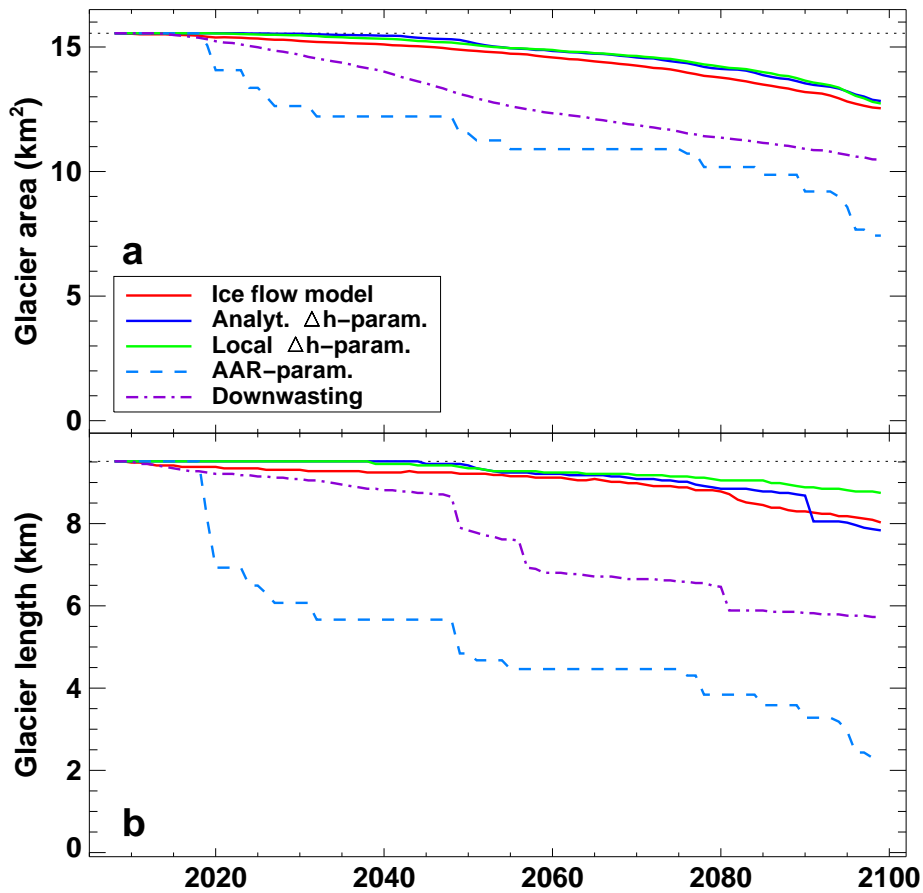


Figure 9.12: Glacier (a) length and (b) area calculated for Scenario 1 using different approaches.

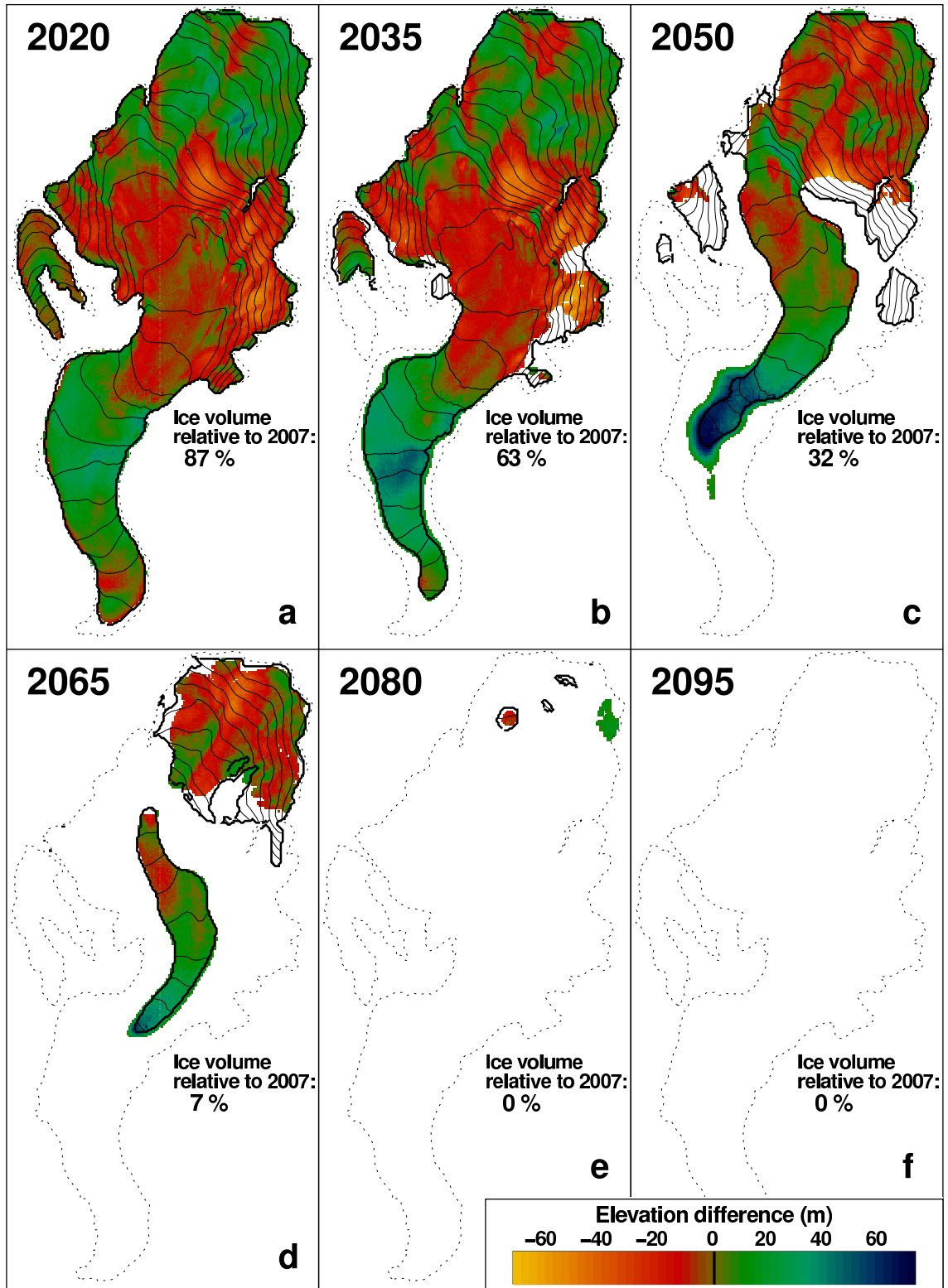


Figure 9.13: Comparison of surface elevation ($h_{\text{ice flow model}} - h_{\text{parameterization}}$) and glacier extent calculated for Scenario 3 (warm-dry) according to the 3D ice flow model and local Δh -parameterization. Coloured areas indicate glacier coverage as calculated by the ice flow model. The colours refer to the difference in elevation obtained from comparing the results of both models. Solid lines with contours show the glacier extent as calculated using the parameterization. The dotted line indicates the glacier outline in 2007.

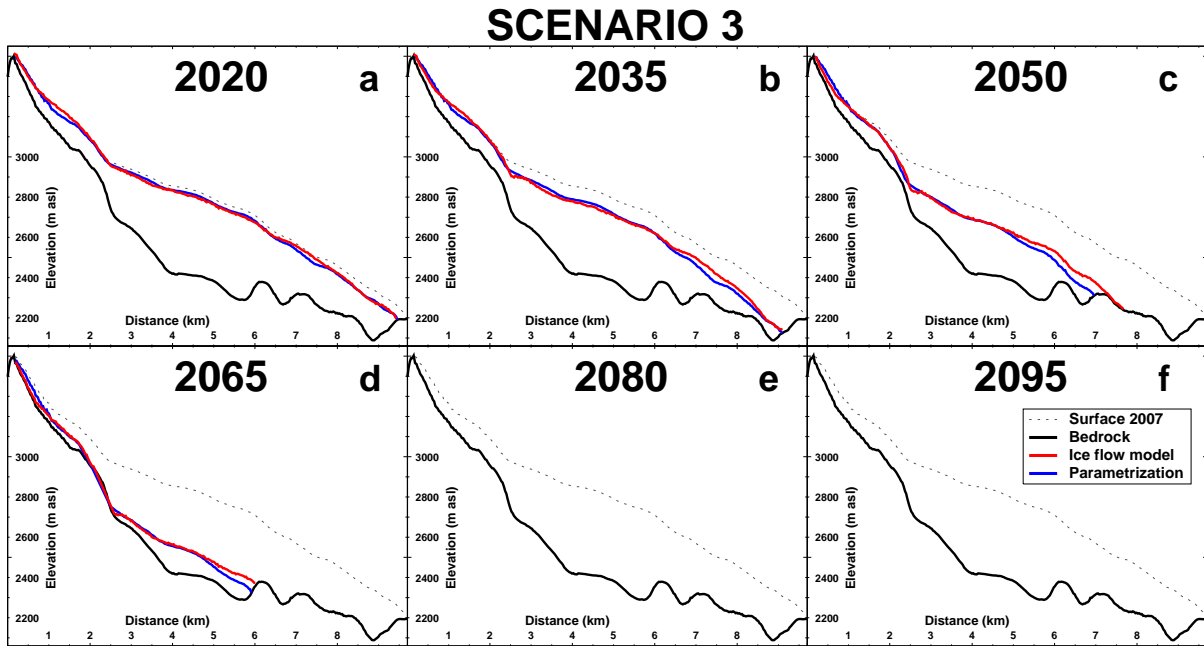


Figure 9.14: Glacier surface elevation calculated for Scenario 3 (warm-dry) using the 3D ice flow model and the local Δh -parameterization in a longitudinal glacier profile.

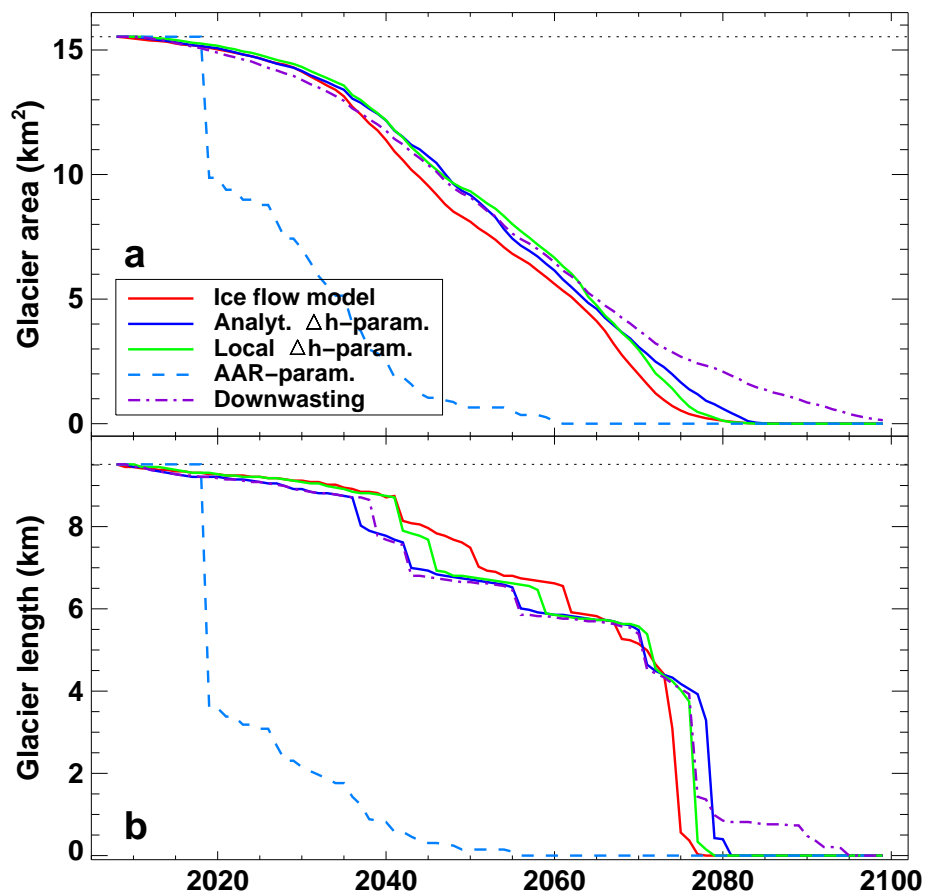


Figure 9.15: Glacier (a) length and (b) area calculated for Scenario 3 using different approaches.

9.5 Discussion

9.5.1 Uncertainties in modelling future glacier evolution

The major source of uncertainty for the prediction of future glacier extent are the changes in the climate system and how they act on the glacier surface. State-of-the-art climate models still indicate a wide range of possible climate trends in the future. This spread is mainly due to the unknown evolution of human technology and whether and when we are able to cope without energy provided by fossil fuels. However, different climate models also exhibit considerably diverging results when forcing them with the same CO₂ input (Christensen and others, 2002; Christensen and Christensen, 2007; Frei, 2007). The use of ensembles, allowing a probability distribution of the climate model results to be determined is, therefore, of benefit.

It is the task of the glacier impact modeller to translate the change in the climatic variables to an effect on the cryosphere. The most straight-forward approach is to develop relations between meteorological data and glacier change in the past and apply these to future conditions. This strategy is both simple and obvious and has been applied in many forecasts of the future evolution of Alpine glaciers (e.g. Wallinga and van de Wal, 1998; Schneeberger and others, 2003; Zemp and others, 2006; Sugiyama and others, 2007a; Le Meur and others, 2007; Huss and others, 2007b, 2008b).

Investigation of the changes in the climatic forcing at the elevation of the long-term equilibrium line has shown that the degree-day factors of temperature-index models may change systematically over long time periods (Huss and Bauder, in press). A decrease in the degree-day factor for snow of 14% since the 1960s was found (Fig. 3.8a). The relation between air temperature and melt is not constant over time (Braithwaite, 1995; Ohmura and others, 2007; Carezzo and others, in press). The entire energy balance is lumped into the degree-day factors. Changes in the relative importance of heat budget components directly influence the degree-day factors in empirical temperature-index modelling. Model parameters calibrated in the past under a given magnitude of the radiative heat fluxes may thus be subject to significant changes in the future. This requires a more physical description of the processes governing melt, considering the changes in (temperature dependent) longwave and shortwave heat fluxes separately. Such an approach should, however, not increase the field data requirements of the mass balance model in order to ensure a robust application to long time periods.

9.5.2 Deriving Δh -parameterizations for unmeasured glaciers

This chapter has shown that parameterizing glacier surface elevation change and, thus, glacier dynamics using a simple relation of h versus Δh is a well suited alternative to complex 3D ice flow modelling. As the h - Δh function is site dependent, best results are obtained when defining it for each investigated glacier individually. There are two possibilities for deriving local Δh -parameterizations: (1) An ice flow model (e.g. Jouvett and others, 2008) is applied to derive a local h - Δh function which then considerably facilitates the calculations, e.g. for hydrological modelling; (2) the h - Δh function is derived from observed surface elevation changes in the past (as described in Section 9.3.3 for the local Δh -parameterization of Rhonegletscher).

Option (1) is time- and resource-consuming and relies on the application of a complex model. Option (2) is only applicable, if several DEMs are available for the glacier under investigation.

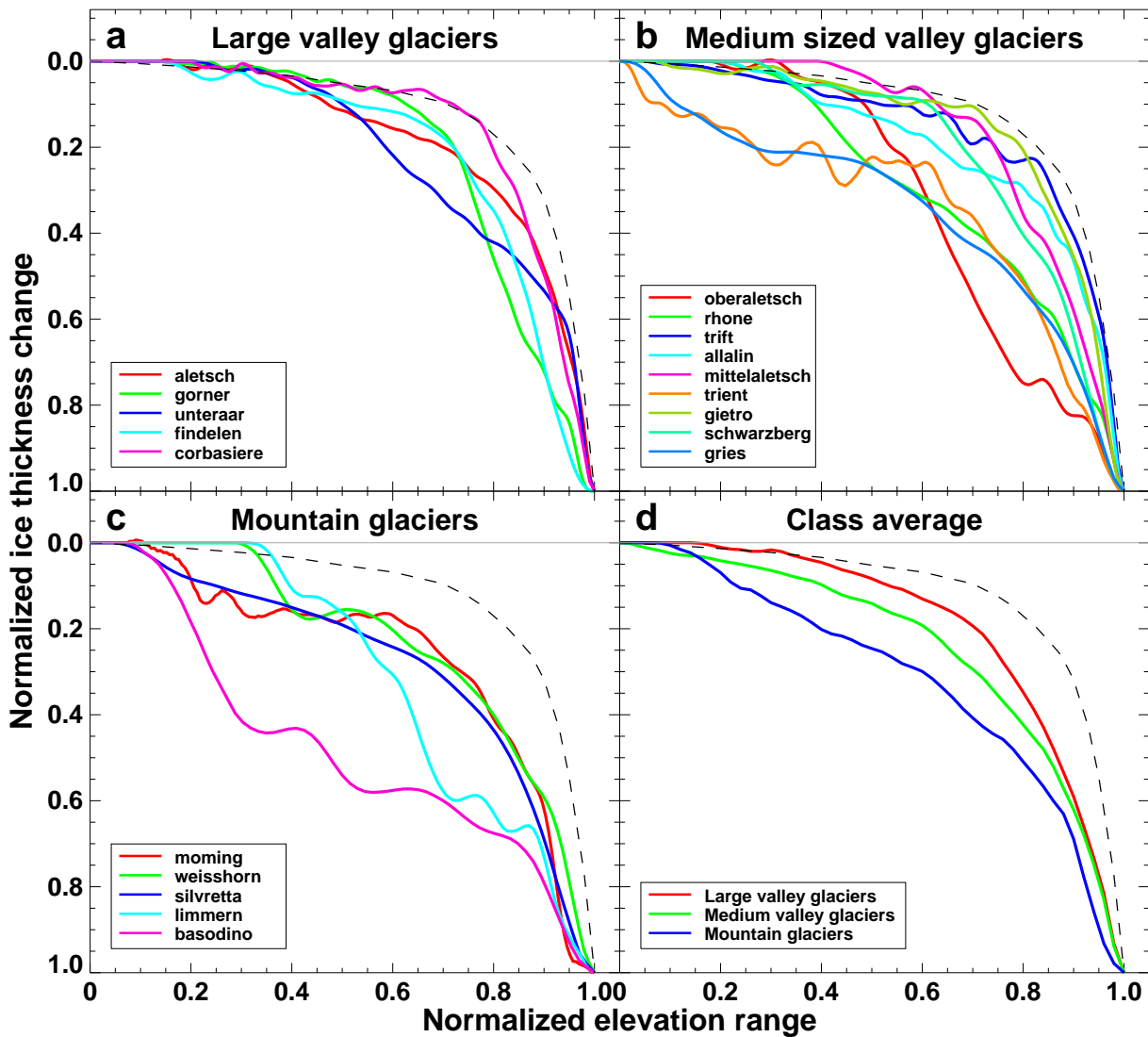


Figure 9.16: h versus Δh functions derived from digital elevation models for 19 glaciers in Switzerland. Δh -parameterizations for (a) large valley glaciers, (b) medium sized valley glaciers and (c) small mountain glaciers with no distinct canalisation of ice flow. The analytical Δh -parameterization is shown as comparison in each panel (dashed). (d) Average of all Δh -parameterizations in each glacier class.

To overcome this restriction, Δh -parameterizations for different glacier classes were computed (Fig. 9.16d). For 19 glaciers located in Switzerland for which repeated DEMs over the 20th century are available (Bauder and others, 2007) local Δh -parameterizations are derived (Fig. 9.16a to c). The averaging of these h - Δh functions in three classes (*large valley glaciers*, *medium sized valley glaciers*, *mountain glaciers*) yields Δh -parameterizations representing an applicable solution for glaciers covered with no field data in the past. The h - Δh function for valley glaciers with a well developed tongue (such as Grosser Aletschgletscher) are closest to the analytical Δh -parameterization and display small ice thickness changes over a large part of their elevation range (Fig. 9.16a). On mountain glaciers, in contrast, here defined as ice masses with no distinct canalisation of ice flow and a limited altitudinal extension (such as Silvrettagletscher) ice thickness changes are not restricted to regions near the glacier terminus, but extend to almost the entire elevation range (Fig. 9.16c). The parameterizations can be approximated using

empirical equations (see Table 9.2). These were fitted based on least squares and are of the form

$$\Delta h = -(h + a)^\gamma + (h + a) \cdot b + c. \quad (9.3)$$

γ , a , b and c are parameters that need to be determined empirically. The exponent γ decreases with glacier size and canalisation of flow, respectively. The analytical Δh -parameterization applied in Huss and others (2008b) causes too much concentration of mass loss near the glacier terminus and too little near the equilibrium line (Table 9.2 and Fig. 9.16).

Table 9.2: *Approximations of the Δh -parameterizations for different glacier classes (Fig. 9.16d). The equations are of the form $\Delta h = -(h + a)^\gamma - (h + a) \cdot b + c$. h is the normalized elevation range of the glacier surface, Δh is the normalized ice thickness change.*

Δh -parameterization	Parameters of approximation			
	γ	a	b	c
Analytical	11	-0.02	-0.12	0
Large valley glaciers	6	-0.02	-0.14	0
Medium valley glaciers	5	-0.04	-0.2	-0.02
Mountain glaciers	4	-0.10	-0.40	-0.04

9.5.3 Restrictions for applying Δh -parameterizations

Δh -parameterizations have been designed for the calculation of glacier retreat in response to future climate warming avoiding the application of complex ice flow models. They have proven to be well suited for this task. However, as Δh -parameterizations represent rigorous simplifications of three dimensional glacier geometry changes, some restrictions need to be discussed.

Δh -parameterizations do not perform well in simulating glacier advance. Generally speaking, the pattern of the altitudinal distribution of the ice thickness changes only differs by sign for glacier retreat and advance (Jóhannesson and others, 1989) – but only after reaching a steady state. Large alpine glaciers such as Rhonegletscher take several decades to reach a new equilibrium geometry after a step like change in climate. The Δh -parameterization is applied at the end of every year, assuming an immediate transformation of the local mass change into a distributed surface elevation change over the entire glacier. As the local Δh -parameterization was explicitly derived for periods of consistently negative mass balances (see Section 9.3.3) the surface elevation change in the case of glacier advance cannot be simulated accurately. The local Δh -parameterization for Rhonegletscher was tested against measurements during the last century. In the two decadal periods of substantial mass gain (1910s and 1970s, see Figure 2.6) the parameterization transports much ice mass down to the glacier terminus, resulting in a too slow glacier retreat. Thus, the transient evolution of glacier geometry is not reproduced well. By 2007, however, after 123 years of simulation the root-mean-square error of modelled (using the local Δh -parameterization) and observed surface elevation is 29 m, which is only 40% higher compared to the misfit of the ice flow model results for the same period. Δh -parameterizations perform well in the case of regular glacier retreat, however, they do not cope with a climate forcing displaying long-periodic fluctuations between positive and negative mass balances. For reproducing the transient change in glacier geometry in that case correctly, an ice flow model is required.

Furthermore, changes in the shape of the optimal Δh -parameterization over time are expected. With glacier shrinkage the exponent γ (Eq. 9.3) decreases. As the curvature of the h - Δh -function is basically given by ice dynamics, γ is also dependent on the rate of climate change. However, given the good performance of the Δh -parameterizations over a time interval of 100 years in the future (see e.g. Fig. 9.6) these factors are assumed to be of minor importance.

The question might arise, whether the Δh -parameterizations shown in Figure 9.16d (derived for glacier classes) are applicable to every alpine glacier. As the h - Δh -functions reflect the prevailing ice thickness change pattern of retreating alpine glaciers, an approximate geometrical change of every ice mass can be captured. However, for very small glaciers this statement must be put into perspective: When there are almost no ice dynamics the use of a Δh -parameterization derived from "dynamical" conditions in the past, might cause erroneous results. In the case of ice patches with negligible ice flow, non-dynamic downwasting is expected to yield more realistic forecasts of glacier change. Thus, it is proposed to define a lower limit of the glacier size, where the Δh -parameterization is applied.

Concluding remarks

In this chapter parameterizations for the future change in glacier surface elevation and extent were implemented and validated against results obtained from a 3D ice flow model. The future evolution of Rhonegletscher was simulated for the period 2008-2100 based on three different climate change scenarios. Simple Δh -parameterizations can reproduce the retreat of a valley glacier in the 21st century equally well as a complex ice flow model. Input data requirements are limited to (1) mass balance maps in annual resolution (see Huss and others, 2008a,b) and (2) the initial ice thickness distribution (see Farinotti and others, in press). All of these inputs can be calculated based on readily available data sets. Thus, Δh -parameterizations are applicable to any alpine glacier. The performance of two other parameterizations, explicitly ignoring the effect of ice dynamics, is inferior. As they do not require less input data than the Δh -parameterizations their application to glacier retreat modelling does not yield an advantage.

Δh -parameterizations are based on a relation of observed glacier surface elevation change (Δh) in the past versus normalized glacier elevation (h). Local h - Δh -functions can be derived for any glacier with several digital elevation models available in the 20th century. A local Δh -parameterization yields the best representation of glacier retreat for the particular geometry of the considered ice mass. Empirical functions derived for different glacier classes allow the application of the parameterization to unmeasured glaciers. Based on the excellent performance of Δh -parameterizations in reproducing (i) surface elevation, (ii) glacier extent and (iii) glacier length given by a state-of-the-art 3D ice flow, such functions are recommended for the simplified simulation of future glacier retreat, e.g. for hydrological purposes.

Acknowledgments

I am indebted to Guillaume Juvet (EPF Lausanne), who was responsible for running the ice flow model. Daniel Farinotti provided the bedrock topography as well as helpful comments on the manuscript. The wide variety of field data used in this study was acquired over several years by many colleagues of the VAW-ETHZ. The weather data were taken from the MeteoSwiss data base. Christoph Frei provided the climate scenarios. Hermann Böschi established digital elevation models from aerial photographs and Bruno Nedela digitized topographic maps. I thank Martin Funk for interesting discussions.

Chapter 10

Conclusion

10.1 Synthesis

This thesis combines a wide variety of data types acquired all over the last century with mass balance modelling. Different methods for calculating distributed glacier mass balance, long-term mass balance time series and for homogenizing existing field measurements are presented. With the lessons learned from the past, it is attempted to forecast the future of glaciers in the Alps.

Modelling is a powerful tool that allows to expand mass balance records in space and time. However, in-situ observations are required to tie these models to reality. The field measurement of mass balance carried out with an enormous input of manpower on almost a dozen Swiss glaciers over many decades, as well as the ice volume changes derived from digital elevation models for over 30 Swiss glaciers (Bauder and others, 2007) provide a unique data basis for glacier studies in Switzerland. The combination of measurements and modelling provides the key to understanding the consequences of past and present climate change on the glaciers. Long time series have an immense value for the analysis of climate variations in high mountain regions covered with no weather records. For these reasons, I would like to stress the importance of continuing the mass balance measurements on Swiss glaciers. Modelling will never be able to replace them – but to increase their value!

The investigations of the climate forcing acting on glacier surface were performed using an enhanced temperature-index model. The model has been shown to perform excellently when calibrated with field data. It is important to note that temperature-index models are statistical tools and not strictly physical models. This has an important advantage: The user of temperature-index models does not need to consider all relevant processes in glacier melt – they are often so complex that thorough local investigations would be required to describe each of them adequately. This makes temperature-index approaches easily applicable to many different problems. Their statistical nature allows a tuning, and thus an optimal fit of the field observations. And this is the basis for a successful temporal downscaling of measurements (e.g. seasonal to daily mass balance quantities) or their spatial extrapolation (e.g. point mass balance to the entire glacier). The advantage of simple mass balance models lies in their robustness due to little and readily available input data.

It could be shown that cumulative mass losses of glaciers located only several dozens of kilometres apart may differ by a factor of almost three over the last century. The differences can be

attributed both to the time for the dynamic reaction of the ice masses and significant changes in the local precipitation conditions. This implies that individual mass balance time series are not suitable for deriving overall mass changes of an entire mountain range. Note that the strong differences in the cumulative mass balance between individual glaciers could only be detected due to comprehensive data coverage for these ice masses.

On alpine glaciers more energy was consumed for melt in the 1940s than nowadays. This is revealed by time series of glacier-wide mass balances, as well as continuous in-situ measurements near the equilibrium line. The 1940s are characterized by low winter accumulation and significantly more solar irradiance than we face presently. These effects caused extremely negative glacier mass balances at that time, although the air temperatures were higher during the last decade. The fluctuations in climate forcing are similar for the entire Swiss Alps and show long-term oscillations with a period of about 65 years superimposed on a negative trend, which is, however, not highly significant according to statistical tests. Climate change in the 20th century was not a linear process – many glaciers reacted with advances to short favourable periods. With future climate warming, however, a substantial prolongation of the melting season, as well as a decrease in the fraction of solid precipitation is expected both favouring lower glacier albedo. These feedback mechanisms will contribute to enhanced glacier melt in the next decades.

Simulations of glacier retreat for the next 100 years using different methods show equivocal results. Alpine glaciers will almost completely disappear – with severe consequences for us: By 2100 a water shortage in summer is expected, the management of hydropower production will have to adapt to the new conditions and the tourism sector in Switzerland will no longer advertise with everlasting ice streams. However, glaciers will not have gone when we open our eyes tomorrow. Large ice masses, in particular, will most probably endure the entire 21st century. The substantial masses of fresh water stored at high elevations in the form of ice require many decades to be melted completely, even when no more accumulation occurs. This causes water supply in abundance during a first stage, also favouring flood events, when phases of intense icemelt are combined with heavy rainfalls. When the glaciers have shrunk to small ice patches, a scenario which is probable for many Alpine glacier for the second half of the 21st century, they can no longer supply melt water during summer. Glacier change during the next decades will be so fast that it is even impressive in one human lifetime. But glacier retreat is not immediate – glaciologists will still have research opportunities for many years.

10.2 Concluding discussion and outlook

Field measurements are the key to successfully setting up models of glacier surface mass balance and ice dynamics. A wealth of field data is available over many years in the past. However, there can never be enough! More field measurements of variables that are not simulated well by the models are required to understand the processes governing them. For example, snow probings of the winter balance in high resolution can be accomplished with manageable effort and provide important information on processes determining small-scale variations in the snow deposition. This is in turn a prerequisite for correctly reproducing the distribution of net balance. This variable was measured with a dense stake network in the 1970s on several glaciers. A repetition of these highly resolved mass balance measurements could provide important information about changes in the mass balance distribution pattern and help to set up better models for capturing this spatial variability.

Small glaciers are a dying species. Nevertheless, they matter: The vast majority of glaciers in Switzerland is small. This size class has not been investigated so far. The first results of the mass balance monitoring set up on Pizolgletscher connected to this thesis are promising. Processes governing the mass balance of small glaciers could be identified and investigated in high spatial and temporal resolution. The measurements on small glaciers should be continued in order to understand the reaction of these ice fields to climate change.

In the course of this dissertation an exhaustive digital data basis of mass balance measurements performed in the Swiss Alps during the last century was compiled. However, there is still doubt about its completeness. Every single measurement – also if isolated in space and time – has a value, which cannot be counterbalanced with any model. Thus, additional effort should be put into the tracing of forgotten field data and records. As many of these are only reported in manually written and dust loaded field books the quest for such data is laborious, but nevertheless rewarding.

The homogenization of mass balance time series is an important issue (see Chapter 4). The time series of mass balance monitoring programs have been established with a considerable effort over several decades. However, only homogeneous data sets are valuable for the interpretation past climate change. In Switzerland, there are four long-term time series (Limmern- and Plattalvagletscher, Glacier de Giéthro and Ghiacciaio del Basodino) that require a careful re-analysis. Normally, only the raw measurements at the stakes and in most cases the dates of the readings are reported. The previous researchers had a well founded knowledge about the spatial distribution of mass balance from observing melt out patterns over many years. This experience is often conveyed in the form of manually drawn mass balance maps. This meta-source of information could also be exploited in order to constrain distributed mass balance models.

The method to determine long-term mass balance time series (see Chapter 2) should be applied to a representative set of Swiss glaciers in order to obtain a comprehensive regional picture of climate forcing over the 20th century. Some selected glaciers were already analyzed, however the number of ice masses with a data basis that allows the model to be calibrated is exhaustive. Mass balance time series calibrated for the past are a prerequisite for simulating the future evolution of the glacier, including the changes in runoff. Forecasts of the glacier runoff for the next decades in several climatic regions of Switzerland and different catchment characteristics will be of high value for the future management of water resources in the Alps.

There is still a substantial potential for developing better models to calculate 21st century glacier change and its consequences. Modelling the future is fundamentally different from simulating – re-analyzing – the past: In the past the model serves as a tool for interpreting and best exploiting field measurements – and can be directly constrained by these. Models for the future must understand the back-coupling effects on a physical basis in order to be able to yield realistic forecasts. However, there is presently no way to tell, which model approach is the most appropriate. Almost all methodological steps in the modelling of future glacier extent or runoff are subject to possible enhancements, always bearing in mind that we will only know whether the effort led to an enhanced or even a worsened model performance, when we're old...

The largest uncertainty in future impact studies arises from ourselves. Nobody knows whether we will be able to control our releases of greenhouse gases during the next decades. Climate models try to translate changed CO₂ forcing into changes in the meteorological variables. The application of such results in local impact studies is often not trivial. The downscaling of climate parameters from a grid with several tens of kilometres grid spacing to the glacier scale requires a careful analysis of the local meteorological conditions. The models to forecast glacier change

proposed in this thesis (see Chapters 7 to 9) are based on the future climate forcing given by a probabilistic range of results from 16 regional climate models in seasonal resolution (Frei, 2007). There are several issues to be discussed:

- Linear trends in the mean seasonal changes in temperature and precipitation between time slices (1990, 2030, 2050, 2070) evaluated from the climate models (Frei, 2007) are assumed (see Chapter 8). First of all, climate change is not a linear process and for impact studies a temporal resolution much higher than seasonal values is required. This implies that a downscaling, superimposing a realistic synthetic variability in the meteorological variables, must be performed. These synthetic short-term fluctuations do not allow an assessment of future extreme events – which is a very important issue. However, as climate models run on a subdaily time scale it should be possible to use not only mean values as an output of these models, but results with high temporal resolution allowing an analysis of the effects of a changing climate variability on, for example, stream-flow runoff.
- The use of climate model ensembles is almost imperative for impact studies in order to provide meaningful results: As the spread in the climate model results is substantial, a measure for the uncertainty induced in glacier forecasts must be provided. The disadvantage of the ensembles used in the present work is that they include different emission scenarios. It would be more transparent for the judgement of the climate change impact to aggregate the range of possible results according to separate emission scenarios.
- Two extreme scenarios enveloping the 95% confidence interval of possible climate forcing on the glaciers were defined (see Chapter 7). They are based on a separate consideration of temperature and precipitation changes. However, changes in these variables are always linked together, thus, the extreme scenarios are unrealistic. It would be of benefit to perform a joint analysis of temperature and precipitation changes predicted by the climate models, in order to define extreme scenarios based on ensemble results that show combinations of these variables that really might occur.

Ice dynamics can not be neglected in future glacier modelling, although their importance decreases with the magnitude of climate warming. Simple and widely applicable parameterizations have been shown to be in excellent agreement with a complex 3D ice flow model for the case of a climate scenario following a linear trend (see Chapter 9). However, particularly for a moderate climate change in particular with long-periodic fluctuations in climatic forcing (as observed in the last century) these simple parameterizations are likely to yield unsatisfying results. The full 3D finite element code used to simulate Rhonegletscher in the 21st century represents a promising alternative. The application of this state-of-the-art ice flow model to other glaciers with sufficient field data coverage might permit a more physically based modelling of future glacier evolution.

Accurate knowledge of the glacier bed is a precondition for the use of ice flow models and for all studies focussing on future glacier retreat. The method proposed by Farinotti and others (in press) is a step towards a determination of the glacier bed geometry from topographical information only. If radio-echo soundings are available the method is also well suited to assimilate them. However, ice thickness estimation in unmeasured regions is still highly uncertain. An ice flow model can reveal regions where ice flux calculated based on the estimated glacier bed is not in balance with surface topography. Assuming that the errors in the ice flow model are

small compared to the estimated bedrock topography, it can be used as a tool for correcting estimated ice thicknesses in a distributed manner. This control process could provide bias-corrected bedrock maps. This technique should be further refined in the future and has a substantial potential for the estimation of ice volumes.

Temperature-index models for the calculation of snow- and icemelt are widely used (Hock, 2003). They are applicable to large areas with no in-situ weather data, because temperature as the only input variable is widely measured and can be extrapolated well in space. Also for simulating future glacier melt temperature-index models are handy; climate model results, e.g. temperature trends, can easily be implemented. There is evidence, however, that the parameters of temperature-index models change significantly both at daily or subdaily time scales related to changes in the heat fluxes (Braithwaite, 1995; Carenzo and others, in press) and over decadal time periods (Huss and Bauder, in press). This is due to the fact that melt is not determined by temperature alone (being a good indicator for the incoming longwave heat flux), but also by the temperature independent shortwave radiation. Assuming constant degree-day factors of temperature-index models for the future implies that the relative contributions of shortwave and longwave radiation to the surface heat flux determining the melt rate remain constant over time. This assumption is probably not justified as temperature – and therefore longwave irradiance – increases in the future, whereas climate change does not enhance shortwave radiation. This variable might even decrease due to a higher percentage of cloud coverage. These changes would lead to a decreasing trend in the degree-day factors, which indeed could be shown based on direct field data in the 20th century (see Chapter 3).

This obviously encourages the use of models that explicitly solve the energy balance, when simulating the future. Energy balance models have been shown to perform very well in modelling melt for discrete points where many parameters were measured (e.g. Klok and Oerlemans, 2002; Pellicciotti and others, 2008). For the assessment of melt in entire drainage basins the problem of extrapolating the input variables of energy balance models arises. Furthermore, for future model runs, several partly highly sensitive variables need to be downscaled from climate models. For these reasons, the application of full energy balance models for the future induce a substantial uncertainty. Many error sources are possible and are difficult to control. Therefore, a statistical approach such as temperature-index modelling still seems to be more promising. However, we must find ways to combine the advantages of physical energy balance models with those of simple temperature-index models that require a small number of input parameters. Approaches of the Pellicciotti and others (2005)-type seem to a feasible alternative, which, however, first needs to be validated with long-term data in the past.

Evaporation in the high Alps is still an unresolved issue. Currently, this term is probably almost negligible for mass balance studies above elevations of 2500 m.a.s.l. However, it might become a major moisture sink in the future. Whereas evaporation is relatively well studied over vegetated areas, this term was only rarely measured over snow and ice and is even more difficult to estimate over rocky areas. Physical evaporation models exist, but require a considerable field data input which is not readily available. The empirical evaporation model proposed in Chapter 8 incorporates the major processes, such as interception, transpiration and highly variable evaporation rates over snow in the course of the year. However, there is presently no way to validate the results. The development of an evaporation model for high mountain areas that is driven by meteorological input provided by the climate models would require a substantial amount of work, including field measurements.

In summary: There is still a lot of work to be done. Calculating glacier change from climate

variables both in the past and in the future remains an interesting field to explore. A lot of mysteries are yet unresolved – and this is how it should be: This is science.

Appendix A

The mass balance of Pizolgletscher

A.1 Mass balance measurements on Pizolgletscher

Introduction

Very small glaciers ($<0.5 \text{ km}^2$) are rarely subject of glaciological studies. Although these ice masses only cover a small fraction of the glacierized area of the Alpine mountain range, their number is considerable. In the Swiss Glacier Inventory 1973, Müller and others (1976) estimated the number of glaciers smaller than 0.5 km^2 as 1695, which corresponds to 82% of all glaciers in Switzerland at that time (Table A.1). The vast majority of ice fields in the Alps is small! This makes them a relevant object for glaciological investigations.

The mass balance of very small glaciers was never studied in Switzerland until present. As ice masses in this size class exhibit almost no ice dynamics they may react differently to ongoing climate change (see Figure A.3). With future climate warming many glaciers will pass into a state of downwasting. Mass balance monitoring of small glaciers can provide important insights into processes governing glacier wastage. Small scale processes, also dominating the mass balance of larger glaciers allow a detailed investigation. The shape and the location of small ice fields is importantly determined by wind deposition and redistribution of snow (Dadic and others, submitted). Thus, mass balance measurements on small glaciers, also represent a key to understanding processes of snow deposition in alpine terrain. The hydrological properties of drainage basins are significantly altered already with a minor fraction of ice covered surfaces (Braun and others, 2000). The mass balance of small glaciers is therefore assumed to be relevant for the assessment of water resources at present and in the future.

Table A.1: *Small glaciers in the Swiss Alps. Selected numbers from the Swiss Glacier Inventory 1973 (Müller and others, 1976). The values are compared to the total number of glaciers and their area in the Swiss Alps.*

Size class	Number	Area
0–0.1 km ²	1022	40.1 km ²
% of total	50%	3%
0–0.5 km ²	1695	194.0 km ²
% of total	82%	15%

This chapter summarizes the first results of the mass balance monitoring program set up on Pizolgletscher, eastern Switzerland, in 2006. A method to determine the glacier-wide mass balance based on seasonal point measurements is presented. Extensive snow probings in early spring are the key element. Whereas distributed models for calculating ablation are relatively advanced, the spatial variation in accumulation is still poorly understood and no models satisfyingly reproducing small scale features of snow distribution have yet been achieved. This gap needs to be bridged with field measurements. The approach described hereafter has also been applied to Rhonegletscher, Griesgletscher and Silvrettagletscher for all years with sufficient field data coverage (Huss, 2008).

For Pizolgletscher a detailed evaluation of the two mass balance years 2006/2007 and 2007/2008 is presented. The benefit of using the method for mass balance determination proposed in this chapter is illustrated with results generally unavailable within conventional mass balance monitoring programs. Additionally, a long-term time series of the seasonal mass balance since 1961 based on ice volume changes is provided.

Study site and field data

Pizolgletscher is a very small ice field in eastern Switzerland with an area of presently less than 0.1 km² (Fig. A.1b). It is a steep cirque glacier protected on three sides by rocky walls culminating in the peak of Pizol (2856 m a.s.l.). The glacier currently covers an elevation range from 2630 to 2780 m a.s.l. Processes of snowdrift have a major importance for Pizolgletscher. Snow is deposited mainly over the central part. The glacier is structured into (i) a steep lower section characterized by solid glacier ice, (ii) a flat central section, where accumulation is concentrated – the surface type is firn – and (iii) a steep upper section that did not obtain any accumulation in the last three years and is about to be split off from the main ice body (Fig. A.1). In front of the current glacier terminus dead ice patches are found below a layer of fine debris with a thickness of 20-50 cm. Pizolgletscher is too small for developing a subglacial drainage system in all years. Moulins are rare; most of the meltwater runs off at the surface.

The mass balance observations on Pizolgletscher were started in 2006 connected to this PhD thesis. The monitoring program includes two field surveys per year, one in April and one in September. During the winter survey probings of the snow depth are performed all over the glacier and the snow density is determined in a snow pit. For measuring net balance aluminum stakes are drilled into the ice. On 15 April, 2006 – the first glaciological field visit of Pizolgletscher – 61 snow probings were performed covering all regions of the glacier surface as well as the glacier forefield (the data of this survey are not discussed here). The same survey was carried out in April 2007 (86 probings) and 2008 (43 probings). In September 2006 two stakes of 4 m length were drilled into the ice (stake 1 and 2, see Fig. A.1c). In fall 2007 a stake near the upper end of the glacier was added (stake 3), and in fall 2008 the number of stakes was increased to six.

Changes in glacier area and volume in the 20th century

Seven aerial photographs acquired during the last four decades are available for Pizolgletscher (1968, 1973, 1979, 1985, 1990, 1997, 2006). Glacier outlines were digitized from rectified orthophotographs which were evaluated using photogrammetry (Fig. A.2). The resulting Digital

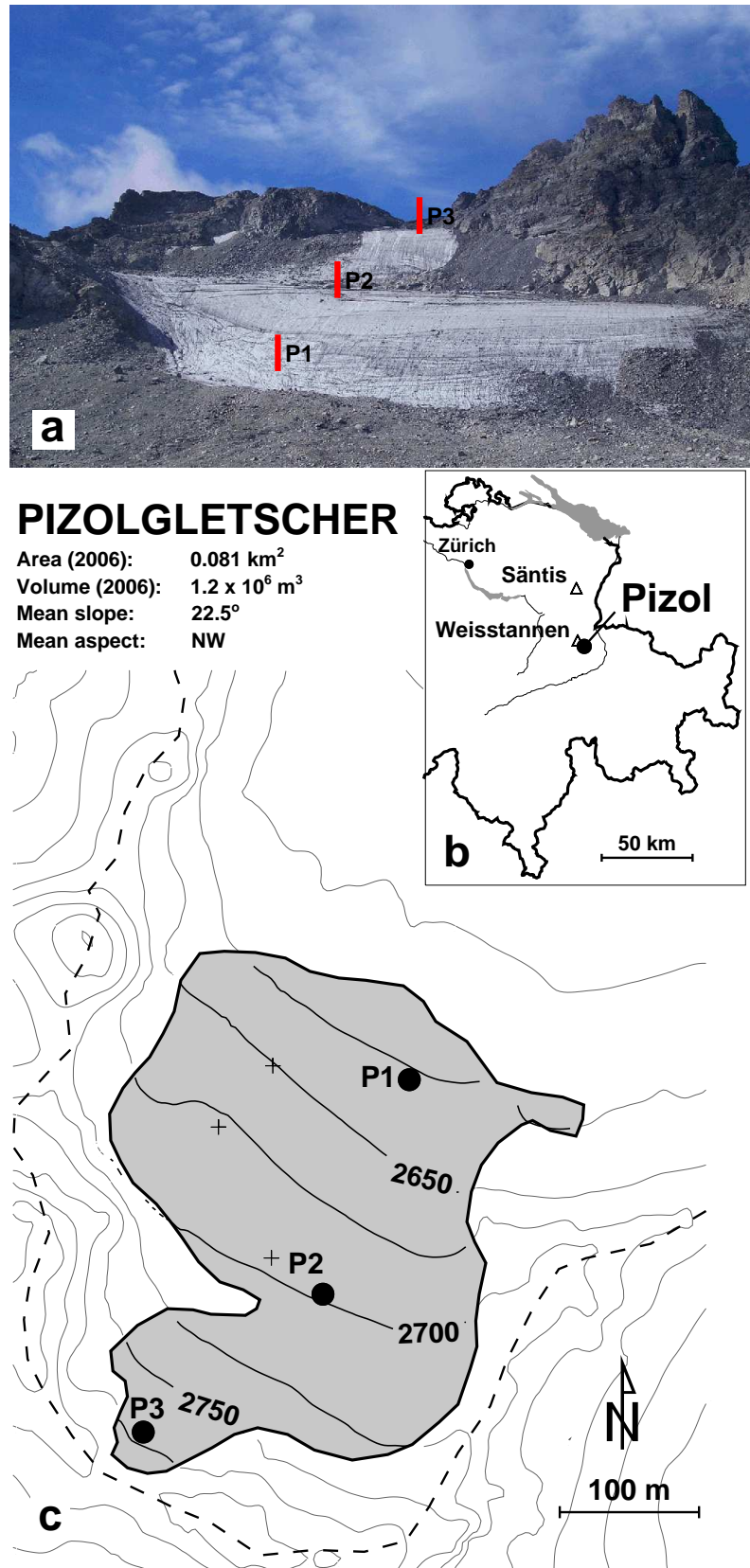


Figure A.1: Overview of the study site. (a) Front view of Pizolgletscher taken in September 2007. The position of the mass balance stakes is shown. (b) Location of Pizolgletscher in Switzerland. Relevant weather stations are marked with triangles. (c) Study site map. The glacier outlines refer to 2006. Dots show the position of mass balance measurements. New stakes (late summer field survey 2008) are indicated with crosses. The contour interval is 25 m. The dashed line marks the hydrological catchment of Pizolgletscher.

Elevation Models (DEMs) have a spatial resolution of 5 m. A DEM for 1961 was established based on a topographic map. The date of this map is, unfortunately, not exactly known; it might have been acquired some years earlier than 1961. This data basis allows an assessment of the changes in glacier area and ice volume over the last five decades and also provides information on the spatial distribution of mass balance.

The ice volume of Pizolgletscher in 2006 was determined based on the Farinotti-method (Farinotti and others, in press) and some manually applied corrections as $1.2 \times 10^6 \text{ m}^3$. According to this rough estimate the maximum ice thickness is slightly more than 30 m. Relative to the year 1968 the volume of Pizolgletscher has decreased by more than 60% (inset in Fig. A.2). During the last decade (1997-2006) Pizolgletscher has lost 40% of its ice volume! Over the last 40 years glacier area has decreased by two thirds – from 0.24 km^2 in 1968 to 0.08 km^2 by 2006 (inset in Fig. A.2).

The orthophotograph in Figure A.2 illustrates the characteristics of the mass balance distribution of Pizolgletscher for the fall 1973. This pattern seems to prevail in most years and is principally

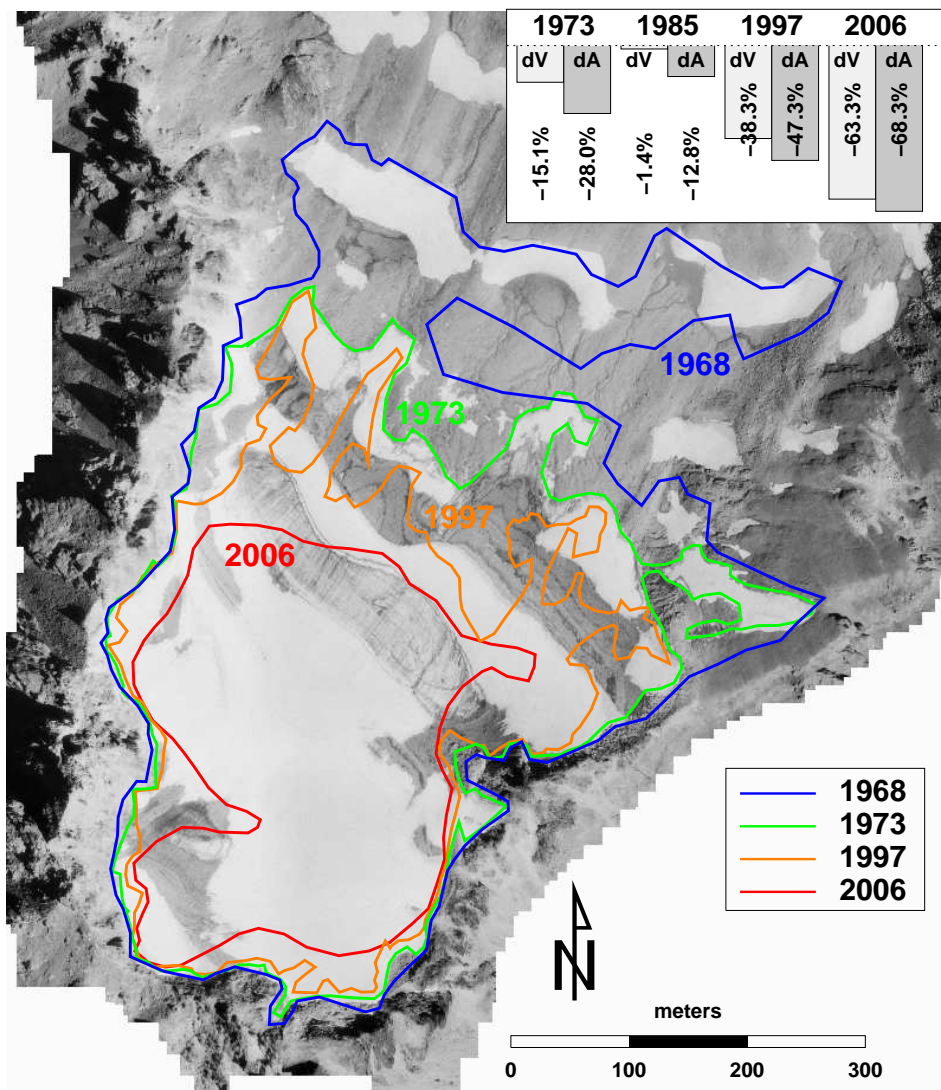


Figure A.2: Orthophotograph of Pizolgletscher taken in September 1973. Lines indicate the glacier extent in 1968, 1973, 1997 and 2006. The inset shows the change in glacier area (dA) and volume (dV) relative to the year 1968.

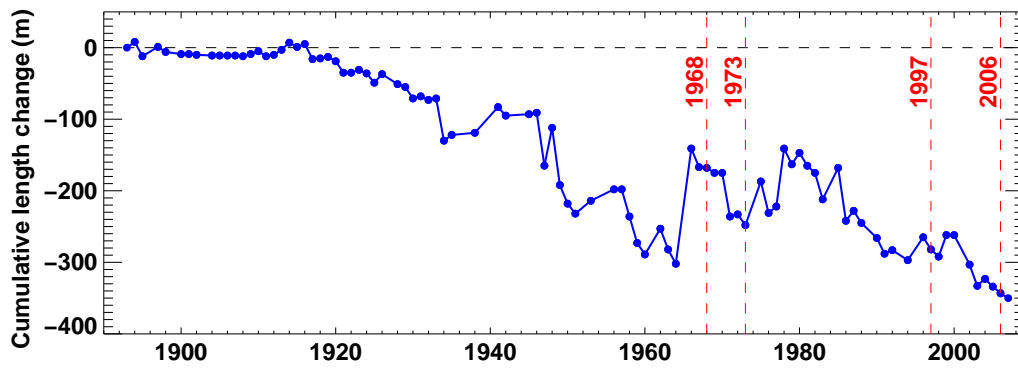


Figure A.3: Measured cumulative length variations of Pizolgletscher since 1893. Vertical lines indicate the dates of the glacier outlines shown in Figure A.2.

determined by wind-driven deposition of snow. Where the surface slope is small, snow is left at the end of the summer: that is in the central regions of the glacier and several parallel linear structures near the glacier terminus (Fig. A.2). Due to reduced accumulation in winter the uppermost part and the steep section in the lower part are snow free. This pattern appears to be similar in all years judging from the aerial photographs and is also confirmed by the direct measurements. Thus, the spatial variation in mass balance of Pizolgletscher (and probably many glaciers of that size class) strongly differs from a common mass balance distribution that can be described with altitudinal gradients. Pizolgletscher gains most of its mass in positive years in an elevation band around its mean altitude as well as at the glacier terminus.

This implies that an advance of the small glacier does at first not take place due to a dynamic reaction of the ice mass (as for larger glaciers), but due to so called 'apposition' of firn in front of the glacier terminus. Thus, small glaciers can potentially 'advance' several 100 meters in some years. However, they may lose this length gain equally fast in a succession of only a few warm years, because the frontal glacier section only consisted of a shallow multi-year firn field connected with the main ice body. The effects of this process often observable on small glaciers is well recognizable in the shape of the glacier margins (Fig. A.2). All glacier outlines excluding 2006 are highly irregular and mainly shaped by the extent of multi-year firn in front of the dynamic ice mass (Fig. A.2). During the last decade, in contrast, all shallow appositions of firn have melted and the glacier outline of 2006 is given by the body of solid and old glacier ice. This is also reflected in the measurements of length change (Fig. A.3). Variations in glacier length are monitored since 1893 almost annually. Length change is determined by measuring the distance from fixed points installed in the glacier forefield to the glacier terminus along several parallel lines. The data show high rates of retreat and advance in individual years (e.g. in the 1940s or 1960s, respectively). In these periods the length of Pizolgletscher is determined by appositions of firn. There are also more stable periods of relatively slow glacier retreat (e.g. 1920s or the last decade) when no snow was accumulated at the glacier terminus in several consecutive years. Then, the length change is given by the retreat of the main ice body.

Determination of distributed mass balance in daily resolution

The principle of the method to determine mass balance presented here is the constraining of a distributed model with seasonal field data for each year. The model, as well as certain methodological steps, are described in detail in several chapters of this thesis (see e.g. Chapters 2 and 4). Only the most important features of the procedure are discussed.

Required input data are

- net balance measurements at some stakes over an arbitrary period of about one year,
- snow probings and a snow density profile in early spring,
- a digital elevation model and glacier outlines, and
- daily air temperature and precipitation measured at nearby weather stations (not necessarily the same).

Preferably, precipitation records should be taken from a station close to the study site, temperature data are still appropriate if measured more distantly from the glacier, but at a similar elevation. In this study, time series of daily mean air temperature recorded at Säntis (2490 m a.s.l., 32 km from study site) and daily precipitation sums from Weisstannen (998 m a.s.l., 5 km from study site) are used. The data are provided by the network of MeteoSwiss.

The mass balance model calibrated with the seasonal field data provides daily time series of accumulation and ablation for every grid cell of the glacier. This allows (i) an extrapolation of measured point mass balance based on an algorithm including the main processes governing mass balance distribution, (ii) the determination of glacier-wide mass balance over arbitrary time periods (e.g. the hydrological year), and (iii) the separation of the components of mass balance –accumulation and ablation. This comprehensive set of variables is much better suited for further analysis in the context of water resources or climate change than results provided by a conventional evaluation of mass balance. The method is schematized in Figure A.4 and the major steps are shortly described hereafter.

1. Snow depth (in water equivalent) measured during the winter survey is interpolated spatially over the entire glacier surface. Due to the highly variable distribution of snow it is desirable that the probings cover as much of the glacier surface as possible and are more or less homogeneously distributed. From the interpolated snow depth a dimensionless spatial accumulation map $D_{\text{snow}}(x, y)$ is derived, which is used to spatially distribute precipitation of each individual event in the course of the year. $D_{\text{snow}}(x, y)$ is normalized to an average of 1 over the glacier surface and varies between 0 (no deposition of snow) and about 2 (twice as much snow as in the glacier-wide average). Thus, processes of preferential deposition of snow, as well as snow drift are included in the model via field measurements integrating the entire accumulation season.
2. The mass balance model is run over the winter period with an initial set of melt parameters f_M , r_{ice} and r_{snow} and a guess for the accumulation parameter c_{prec} . As melt is of minor importance in winter, this run is used to calibrate the precipitation correction factor c_{prec} that scales the accumulation distribution map $D_{\text{snow}}(x, y)$ for every snow fall event (Fig. A.4).

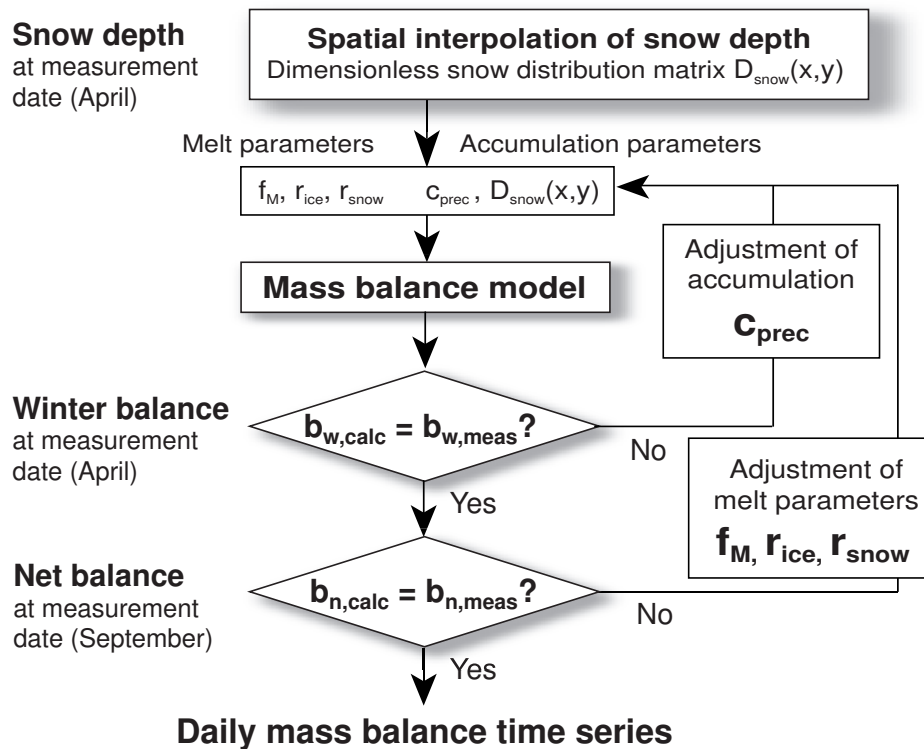


Figure A.4: Schematization of the mass balance determination method.

3. As soon as a good agreement of measured and calculated winter accumulation is obtained the model is run over the entire year and the melt parameters are calibrated so that the model matches the observed point net balances (Fig. A.4).
4. A recalibration of both the melt and accumulation parameters is required in a final step, since the accumulation period is rarely free of melt and solid precipitation occurs also in summer.

Applying this procedure a close match of both the distributed winter measurements and the net balance at stakes is achieved. The mass balance model applied here is not regarded as physical model, but as a statistical tool for temporal downscaling of seasonal mass balance data and spatial interpolation of point measurements.

A.2 Results

Mass balance of Pizolgletscher in 2007 and 2008

The method described above is applied to determine the mass balance of Pizolgletscher in high spatial and temporal resolution for the hydrological years 2006/2007 and 2007/2008. Tables A.2 and A.3 show a compilation of the seasonal mass balance measurements. In April 2007 there was significantly less snow on Pizolgletscher than in 2008 and net balance at the stakes was

Table A.2: *Compilation of winter balance measurements (snow probing) at the locations of the stakes on Pizolgletscher for 2007 and 2008. The stake identifier is specified with the year in which the stake was drilled. The starting day of the period covered by winter balance measurements is defined as the absolute minimum of glacier mass in the previous fall. This date can only be obtained from modelling (or continuous field observations) and normally does not equal the date of the late summer field survey (Table A.3).*

Stake	Date of late summer minimum	Date of winter survey	x (m)	y (m)	z (m a.s.l.)	b_w (m w.e.)
1 (2006)	27.10.2006	02.04.2007	748537	202906	2629	1.03
2 (2006)	27.10.2006	02.04.2007	748475	202752	2700	1.16
1 (2007)	17.10.2007	02.04.2008	748532	202911	2629	1.15
2 (2006)	17.10.2007	02.04.2008	748475	202752	2700	1.55
2 (2007)	17.10.2007	02.04.2008	748438	202778	2698	1.55
3 (2007)	17.10.2007	02.04.2008	748336	202647	2777	1.46

more negative by about 1 m w.e. in the first year. The raw data already show that the variability of mass balance on Pizolgletscher is high. The difference in net balance at the stakes 1 and 2 would translate into an altitudinal mass balance gradient of -2.5 m w.e. per 100 m, which is higher by a factor of more than three compared to values reported for larger alpine glaciers (Huss and others, 2008a). Mass balance quantities are evaluated according to the measurement period and the fixed date system (Table A.4). Fixed date net balance refers to the hydrological year (Oct. 1 - Sept. 30) and fixed date winter balance to the period October 1 to April 30.

Table A.3: *Compilation of net balance measurements at all stakes on Pizolgletscher for 2007 and 2008. The stake identifier is specified with the year in which the stake was drilled.*

Stake	Date of previous late summer survey	Date of that year's late summer survey	x (m)	y (m)	z (m a.s.l.)	b_n (m w.e.)
1 (2006)	13.09.2006	03.09.2007	748537	202906	2629	-2.90
2 (2006)	13.09.2006	03.09.2007	748475	202752	2700	-1.29
1 (2007)	03.09.2007	25.09.2008	748532	202911	2629	-2.09
2 (2006)	03.09.2007	25.09.2008	748475	202752	2700	-0.10
2 (2007)	03.09.2007	25.09.2008	748438	202778	2698	-0.14
3 (2007)	03.09.2007	25.09.2008	748336	202647	2777	-0.66

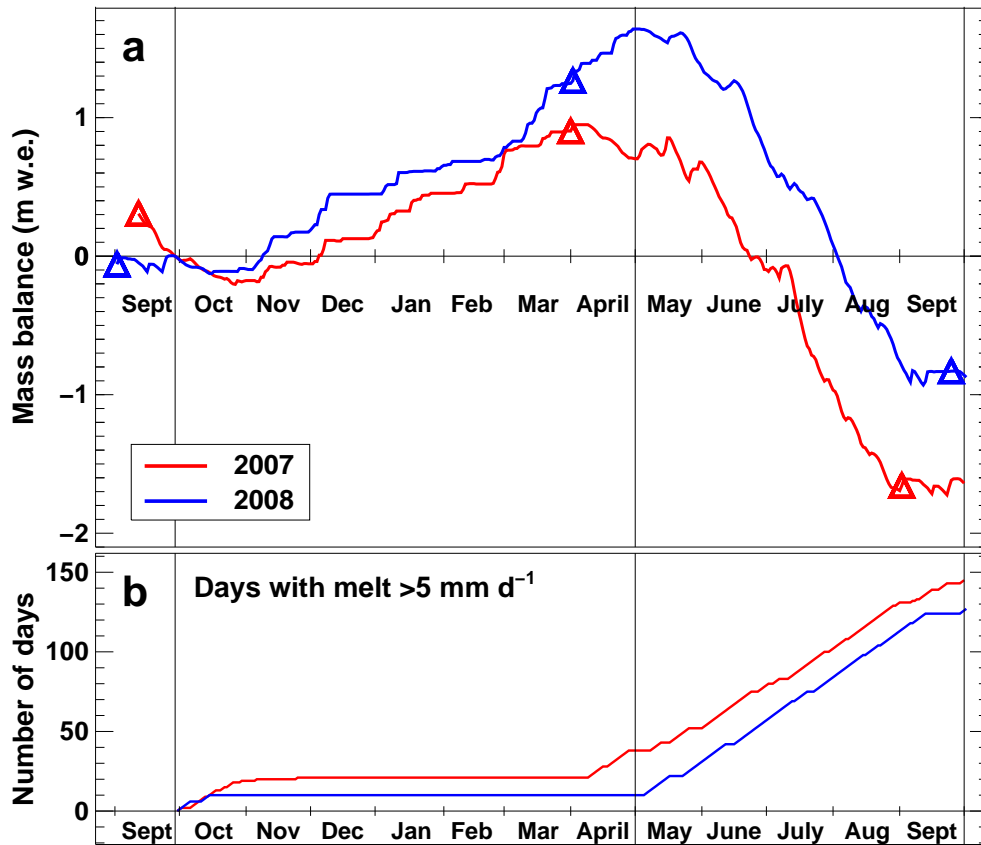


Figure A.5: (a) Cumulative daily mass balance in 2006/2007 and 2007/2008. Symbols indicate the dates of field surveys and vertical lines refer to fixed date periods. (b) Cumulative number of days exceeding 5 mm w.e. of melt per day.

The evolution of mass balance over the years 2007 and 2008 shows significant differences (Fig. A.5a). Winter balance in 2007 was significantly lower (Table A.4) and the melt season

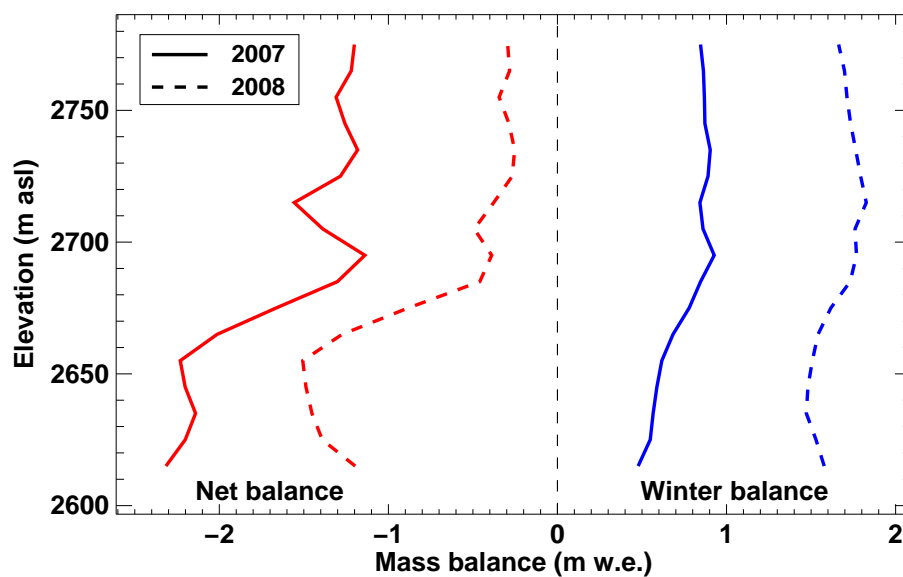


Figure A.6: Altitudinal distribution of fixed date winter balance (blue) and net balance (red) in 2006/2007 and 2007/2008, respectively.

started early in that year (Fig. A.5b). Melt rates were almost the same in both summers; in total between 3 and 4 m w.e. of snow- and icemelt averaged over the glacier occurred. Net balance in the hydrological year 2006/2007 was -1.61 m w.e. and in 2007/2008 -0.83 m w.e. (Table A.4). These differences are mainly due to much higher winter precipitation in 2008. Figure A.5 and Table A.4 illustrate the importance of homogenizing mass balance quantities to common periods if one intends to compare different years. After the field survey in late summer 2006 a significant amount of ablation has occurred. The accumulation maximum in the winter 2008 would have been missed as well without the use of weather data for the temporal downscaling of the seasonal mass balance data.

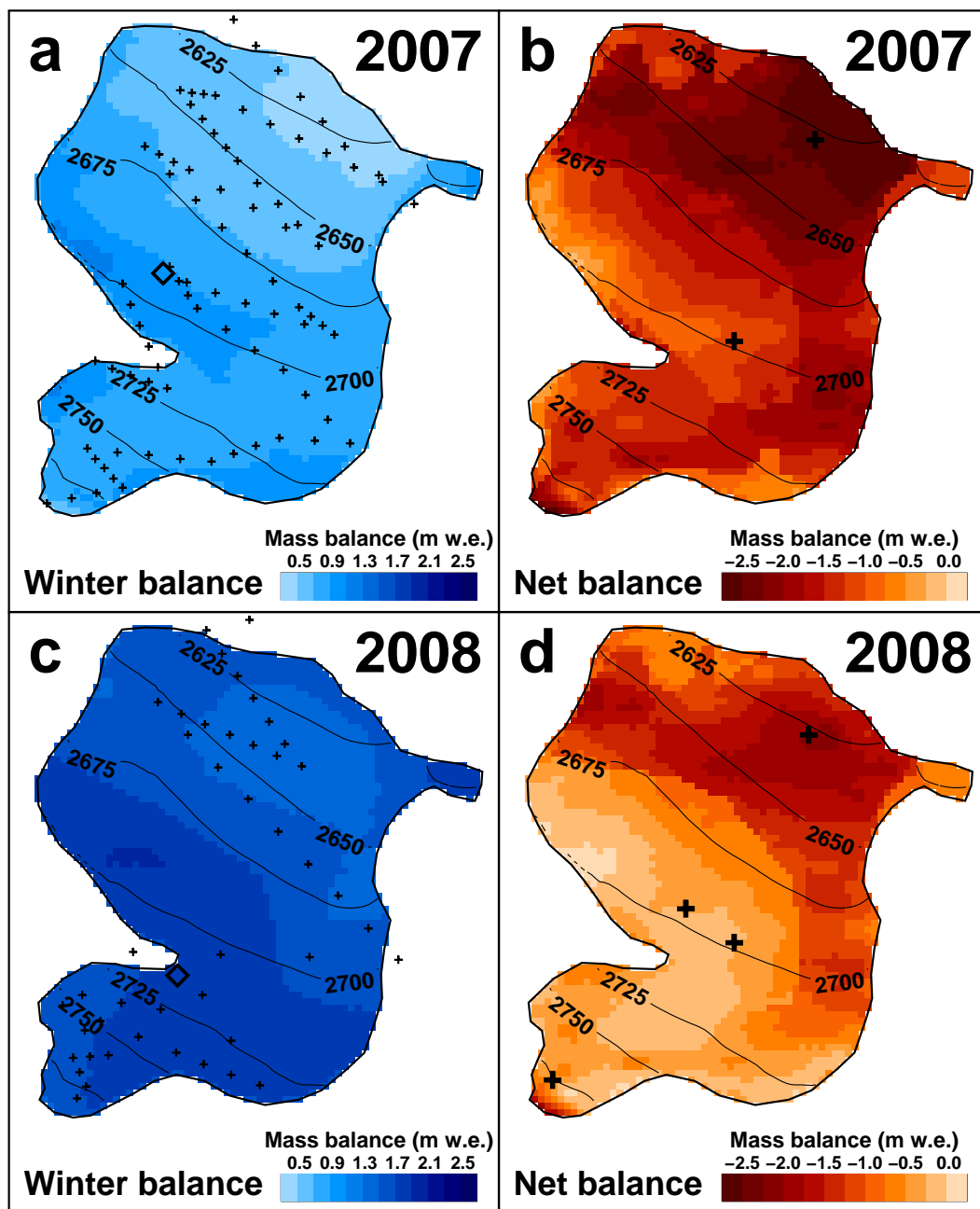


Figure A.7: Spatial distribution of (a,c) winter balance and (b,d) net balance in 2007 and 2008 (fixed date periods), respectively. Symbols indicate the location of snow probes (a,c) and stakes (b,d). Squares refer to snow pits.

Table A.4: *Compilation of mass balance variables for the years 2006/2007 and 2007/2008. Results are given for the measurement period (meas) and the fixed date period (fix) for both annual and seasonal time scales. The mass balance components (accumulation c and ablation a) are reported separately. For the dates of the measurement period refer to Tables A.2 and A.3. Fixed date quantities are determined from October 1 to September 30 for the annual period, from October 1 to April 30 for the winter period and from May 1 to September 30 for the summer period.*

Mass balance	Annual period		Winter period		Summer period		Unit
	$\overline{b_n^{\text{meas}}}$	$\overline{b_n^{\text{fix}}}$	$\overline{b_w^{\text{meas}}}$	$\overline{b_w^{\text{fix}}}$	$\overline{b_s^{\text{meas}}}$	$\overline{b_s^{\text{fix}}}$	
2007	-1.89	-1.60	1.14	0.73	-3.03	-2.33	m w.e.
2008	-0.82	-0.83	1.45	1.66	-2.25	-2.41	m w.e.
Accumulation	$\overline{c_a^{\text{meas}}}$	$\overline{c_a^{\text{fix}}}$	$\overline{c_w^{\text{meas}}}$	$\overline{c_w^{\text{fix}}}$	$\overline{c_s^{\text{meas}}}$	$\overline{c_s^{\text{fix}}}$	Unit
	2007	1.92	2.09	1.19	1.23	0.73	0.86
2008	2.49	2.31	1.46	1.79	1.03	0.61	m w.e.
Ablation	$\overline{a_a^{\text{meas}}}$	$\overline{a_a^{\text{fix}}}$	$\overline{a_w^{\text{meas}}}$	$\overline{a_w^{\text{fix}}}$	$\overline{a_s^{\text{meas}}}$	$\overline{a_s^{\text{fix}}}$	Unit
	2007	-3.81	-3.69	-0.05	-0.50	-3.76	-3.19
2008	-3.30	-3.14	-0.02	-0.12	-3.28	-3.02	m w.e.

The mass balance distribution of Pizolgletscher is complex and strongly determined by the accumulation pattern of winter snow (Fig. A.7). However, also the melting conditions in summer display a considerable variability. At stake 2 (Fig. A.1c) significantly less melt occurs than at stake 3 located in the uppermost part of the glacier. This can only partly be attributed to less snow in winter. Probably, also an albedo effect is involved: The center of the glacier – where stake 2 is located – was the only place Pizolgletscher has received net accumulation during the last six years. Thus, this is the only region, where a shallow firn coverage protects the bare ice surfaces that are characterized by a lower albedo. By prescribing lower melt factors for firn than for bare ice this effect could be captured in the modelling. Reduced rates of ablation over debris covered ice are taken into account by reducing melt with a constant factor ($f_{\text{debris}}=0.6$, see Chapter 7).

The altitudinal distribution of net and winter balance is similar in 2007 and 2008 (Fig. A.6). In both mass balance years Pizolgletscher did not exhibit any accumulation at all, however, in 2008 some sections of the glacier were almost in equilibrium. The distribution patterns of winter accumulation are amplified in the course of the melting season due to an albedo feedback effect (Fig. A.6).

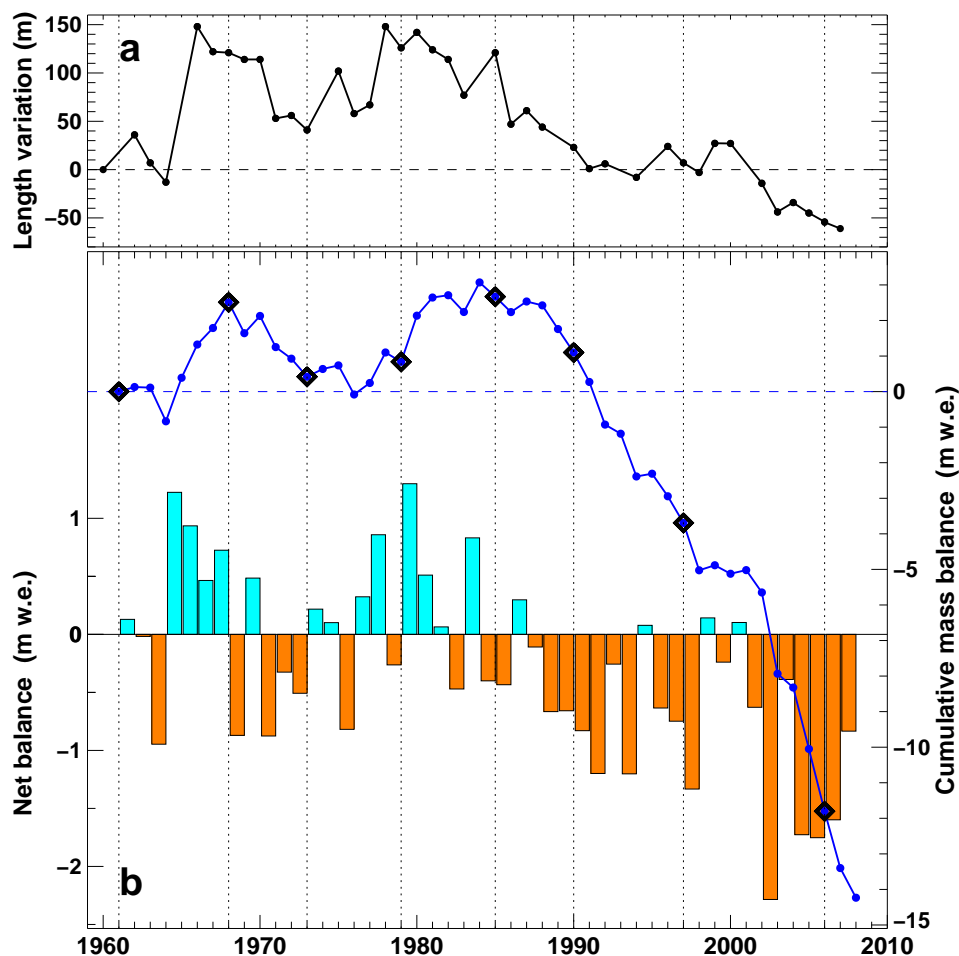


Figure A.8: (a) Measured cumulative length change of Pizolgletscher since 1961. (b) Calculated time series of net balance and cumulative mass balance based on ice volume changes. Symbols and vertical lines indicate the timing of DEMs.

Seasonal mass balance series since 1961

The seasonal mass balance of Pizolgletscher was reconstructed for the period 1961 to 2008 applying the method described in Chapter 2 (Huss and others, 2008a). Based on daily weather data the mass change calculated by the distributed model is tuned so that the observed ice volume changes are matched. The eight DEMs available during the study period constrain the long-term course of the mass balance evolution in subdecadal intervals. The field data from 2007 and 2008 have a crucial importance in providing information on the mass balance distribution over the glacier surface, which is assumed remain similar over time.

A cumulative mass balance of -14 m w.e. is inferred for the period 1961-2008. The mass loss of Pizolgletscher is in line with the (homogenized) long-term mass balance series of Silvrettagletscher (-12 m w.e.) and Griesgletscher (-29 m w.e.) over the same time interval (see Chapter 4). Pizolgletscher experienced mass gains in the 1960s and 1970s (Fig. A.8b). This is mainly due to reduced melt in summer (Fig. A.9). Accelerated mass losses of Pizolgletscher are evident in the last decade. The average mean specific net balance since 1998 is -0.93 m w.e. a^{-1} and since 2003 even -1.43 m w.e. a^{-1} . The low winter balances in the years 2005-2007 are eye-catching (Fig. A.9). As Pizolgletscher basically lives on substantial snow accumulation, this reduction has severe consequences for the "health" of the glacier and has resulted in some

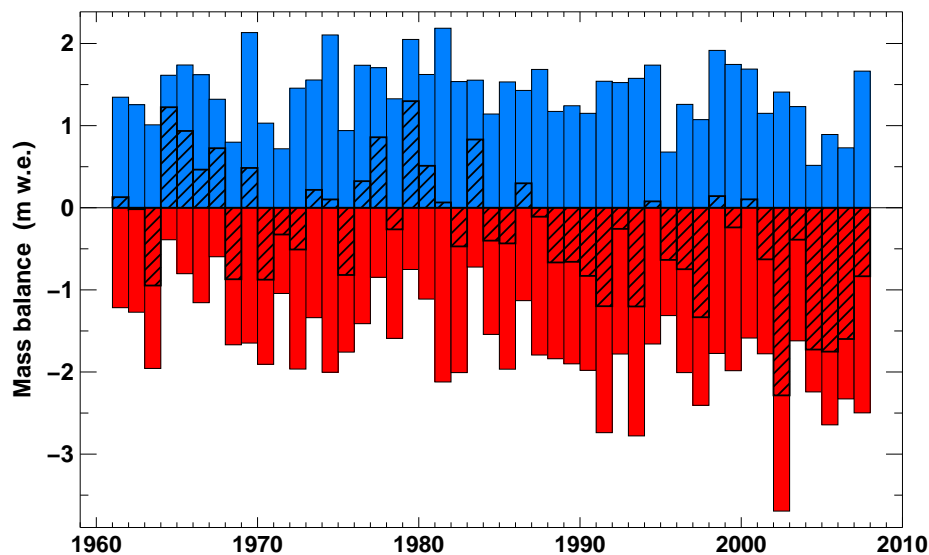


Figure A.9: Fixed date seasonal mass balance time series of Pizolgletscher. Winter balance (blue), summer balance (red) and net balance (hatched) are shown.

of the most negative mass budget years since 1961. Figure A.8 shows the length change measurements in comparison to the cumulative mass balance. The correlation between the two variables is low on an annual basis ($r^2=0.19$). Although small glaciers are assumed to react very fast to changes in climate forcing by increasing or decreasing their size, the length change measurements of Pizolgletscher are not well suited as indicators for its short-term mass budget. However, the general course of the cumulative mass change of Pizolgletscher is reproduced by glacier length variations (Fig. A.8).

Concluding remarks

Direct mass balance measurements on Pizolgletscher have been performed over two years. The first results are promising and a continuation of the "youngest" mass balance monitoring program in Switzerland is recommended. The mass balance time series of Pizolgletscher provide an example for the response of very small mountain glaciers to climate change. The number of glaciers in this size class represents the overwhelming majority in the Swiss Alps. Nevertheless, these ice masses have not been studied so far.

The seasonal field surveys have already provided insights into some important processes governing the mass balance of small glaciers: for example (i) the high small scale variability in accumulation and melting conditions, (ii) the importance of snow drift and (iii) the impact of albedo feedback mechanisms on glacier mass balance. These processes can be studied in detail on Pizolgletscher. It is well accessible and due to its limited extent it is possible to be grasped in its entirety. Understanding small scale variability in mass balance is the key to correctly reproducing the mass balance distribution of larger glaciers in numerical models.

The method to determine mass balance based on seasonal in-situ measurements achieves a considerable advantage for the evaluation of glacier-wide mass balance in glacier monitoring programs. The spatial extrapolation of point measurements is performed based on a description of the most important processes determining the distribution of mass balance components in space. Furthermore, the incorporation of weather data for the temporal downscaling allows

the projection of mass balance quantities to common periods, as well as a separation of the two major components of mass balance – accumulation and ablation – from one another. This allows an unbiased comparison of different years and different glaciers. A separate analysis of trends in the components of mass balance is of crucial importance for understanding the current changes in climate forcing acting on glaciers. Thus, the method to determine glacier-wide mass balance presented in this chapter is recommended for the current evaluation of mass balance in monitoring programs of alpine glaciers. It ensures both the best possible exploitation of information contained in the field measurements and standardized results for the analysis of mass balance under the aspect of changing climatic conditions.

Acknowledgements

Andreas Bauder, Daniel Farinotti and Mauro Werder are acknowledged for their support in the field and helpful discussions. H. Bösch established DEMs from aerial photographs and Stephanie Usselman digitized the topographic map of 1961. Swisstopo was responsible for the aerial photograph surveys. I thank Arnold Hartmann for performing the length change measurements of Pizolgletscher for many years. The weather data were recorded by MeteoSchweiz.

Appendix B

New evidence for strong glacier melt around 1950

MATTHIAS HUSS AND MARTIN FUNK

Analysis of the world's longest glacier mass balance time series reveals a stronger glacier melt around 1950 than in recent years.

ABSTRACT: A new 94-year time series of annual glacier melt rates at high elevations of the Swiss Alps has been inferred from measurements of seasonal glacier surface mass balance. These continuous data from four high altitude sites represent the world's longest mass balance records. Analysis of these data shows that the average surface energy flux was higher around 1950 than it is at present despite lower air temperature. This is attributed to changes in the relative magnitude of heat budget components. A decrease in the solid precipitation fraction and a prolongation of the melting season are evident from the data.

Changes in climate forcing at high elevations are directly reflected by the surface mass balance of alpine glaciers. Seasonal mass balance has been measured since 1914 at four locations in the Swiss Alps at elevations of between 2700 and 3350 m a.s.l. ¹ (Huss and Bauder, in press). These measurements have been carried out up to present and provide the longest direct observations of glacier mass balance worldwide.

The data were homogenized systematically using a statistical mass balance model (Hock, 1999) relating air temperature and precipitation to mass balance ². The model is constrained in each seasonal period by the field data (Huss and Bauder, in press). It thus allows the calculation of absolute quantities of solid precipitation and melt for each year. Over temperate snow and ice surfaces any energy excess is consumed for melting. Based on the total melt during one year, the surface energy flux (SEF) is inferred from the latent heat of fusion.

The fluctuations in SEF are similar for all time series (Fig. B.2) and are therefore averaged. Figure B.1A shows the relative deviations of SEF from the long-term mean. Three decadal periods are highlighted: During 1942–1952 and 1998–2008 SEF was significantly above average, while it was lower in 1971–1981 (see inset in Fig. B.1A). The year 1947 had the most dramatic impact on the glaciers; SEF was higher than in the extreme summer of 2003 (Schär and others, 2004). Snow- and icemelt around 1950 exceeded the last decade by 4%. This is intriguing because air temperatures during the 20th century never were as high as today (dashed line in Fig. B.1A). Long-term observations at stations in the Swiss Alps show that in summer air humidity was significantly lower around 1950 than at present. Measured global radiation has decreased by 10% since the onset of the records² (Fig. B.1A), which is attributed to a dimming effect caused by aerosols (Wild and others, 2005; Ohmura and others, 2007). These changes in the radiative heat budget alter the relation between air temperatures and melt. It is essential to understand the

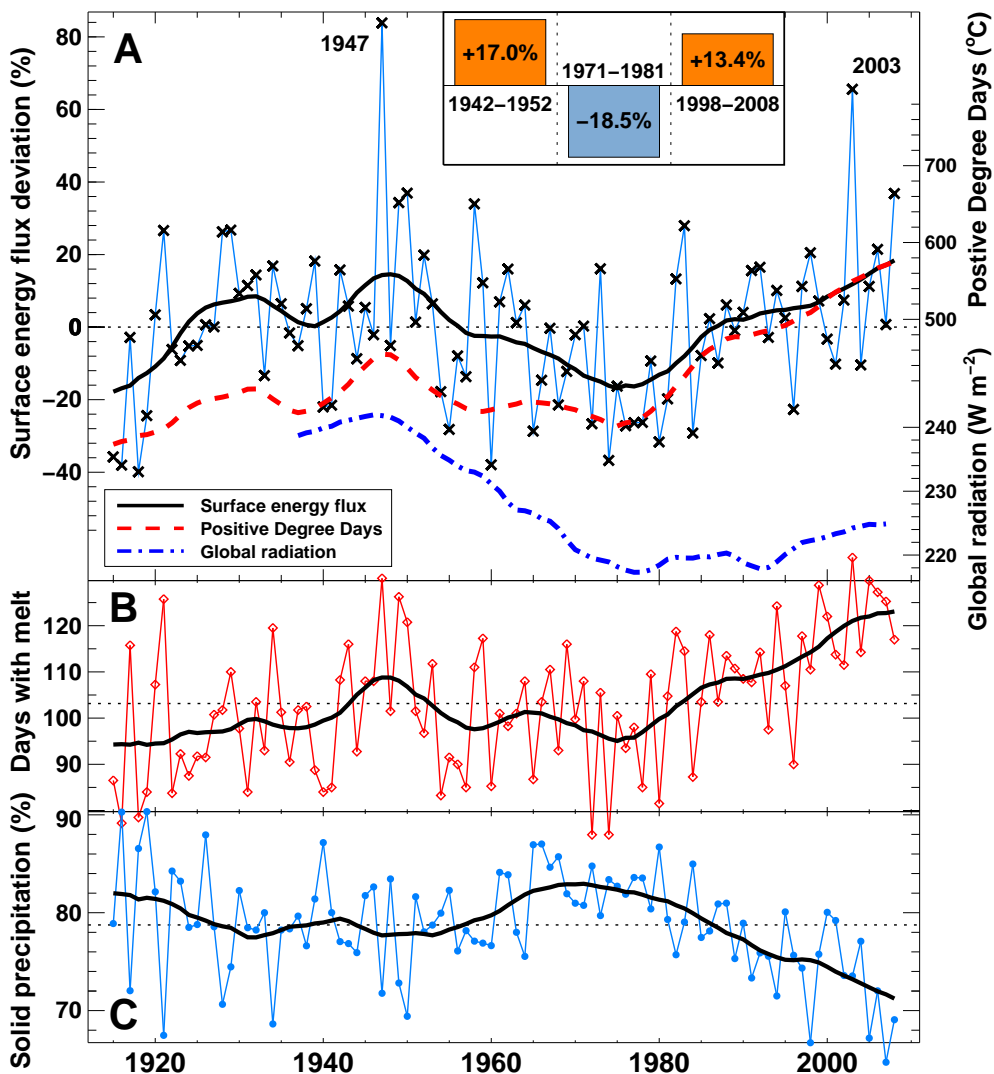


Figure B.1: (A) Annual deviation of the surface energy flux (SEF) from the long-term mean. Sum of daily air temperatures above 0°C over the year (Positive Degree Days) and measured global radiation in the summer months (annual data not shown). Bold lines represent 10-year running means. Offsets in climate forcing for selected periods are shown in the inset. (B) Length of the melting season. (C) Fraction of solid precipitation at the elevation of the study sites.

processes governing the changes in climate forcing in the past to predict the impact of future climate warming on mountain glaciers.

Our results indicate a prolongation of the melting season by almost one month since the 1970s (Fig. B.1B). Simultaneously, the fraction of snow fall relative to the total annual precipitation has decreased by 12% (Fig. B.1C). Precipitation in form of rain instead of snow can not be retained by a temperate glacier. These processes have the potential to considerably accelerate future glacier wastage.

¹ Glacier surface mass balance of alpine glaciers is given by the sum of solid precipitation and melt throughout one year. In spring and late summer of every year the winter accumulation of snow and the summer ablation, respectively, are determined at stakes drilled into the ice.

² See supporting text and figures

Supporting text and figures

The four 94-year glacier mass balance time series investigated in this study originate from three glaciers in the Swiss Alps – Claridenfirn (two sites at 2680 and 2900 m a.s.l., resp.), Grosser Aletschgletscher (one site at 3340 m a.s.l.) and Silvrettagletscher (one site at 2730 m a.s.l.) (Huss and Bauder, in press). The measurement program consists of two field surveys per year: one in spring (maximum of winter accumulation) and one in late summer at the end of the melting season. Accumulation and ablation is measured at a stake placed at the same location over the entire study period (Müller and Kappenberger, 1991). The snow density is determined in snow pits.

A homogenization of the time series is required in order to correct for the effects of the varying lengths of the annual measurement periods and to fill the data gaps in a consistent way (before homogenization 9% of the late summer and 26% of the winter measurements are missing). A temperature-index model is applied to calculate melt based on a relation with positive air temperature. The model includes the effect of potential radiation on the melting cycle and accounts for different albedo over snow and bare ice surfaces (Hock, 1999). Daily mean air temperature and total precipitation, measured at the weather stations Jungfraujoch, Säntis and Davos, were used to tune two parameters, one for accumulation and one for melt, respectively. This procedure is performed for each year individually so that the field data are matched by the calculated daily mass balance curve (Huss and Bauder, in press). Thus, the two components of glacier surface mass balance – accumulation and melt – are separated. Note that the mass balance quantities are determined by the direct field measurements; the climate data are used for temporal downscaling of the seasonal measurements.

The mean surface energy flux (SEF) varies between 10 and 30 W m^{-2} , depending on the site elevation. The percental fluctuations around the long-term mean are, however, similar for all study sites (Fig. B.2). Regional differences in SEF over the Alps are small throughout the 20th century (Vincent and others, 2004). The time series are thus regarded as representative for the high elevation of the Alps and were averaged for further analysis.

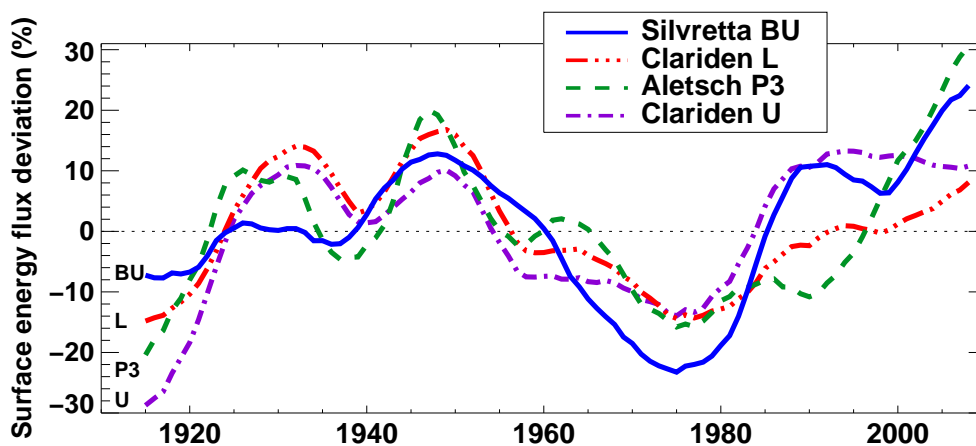


Figure B.2: Deviations of the surface energy flux from the long-term mean. The lines represent 10-year running means of the four time series separately. Annual data points are not displayed.

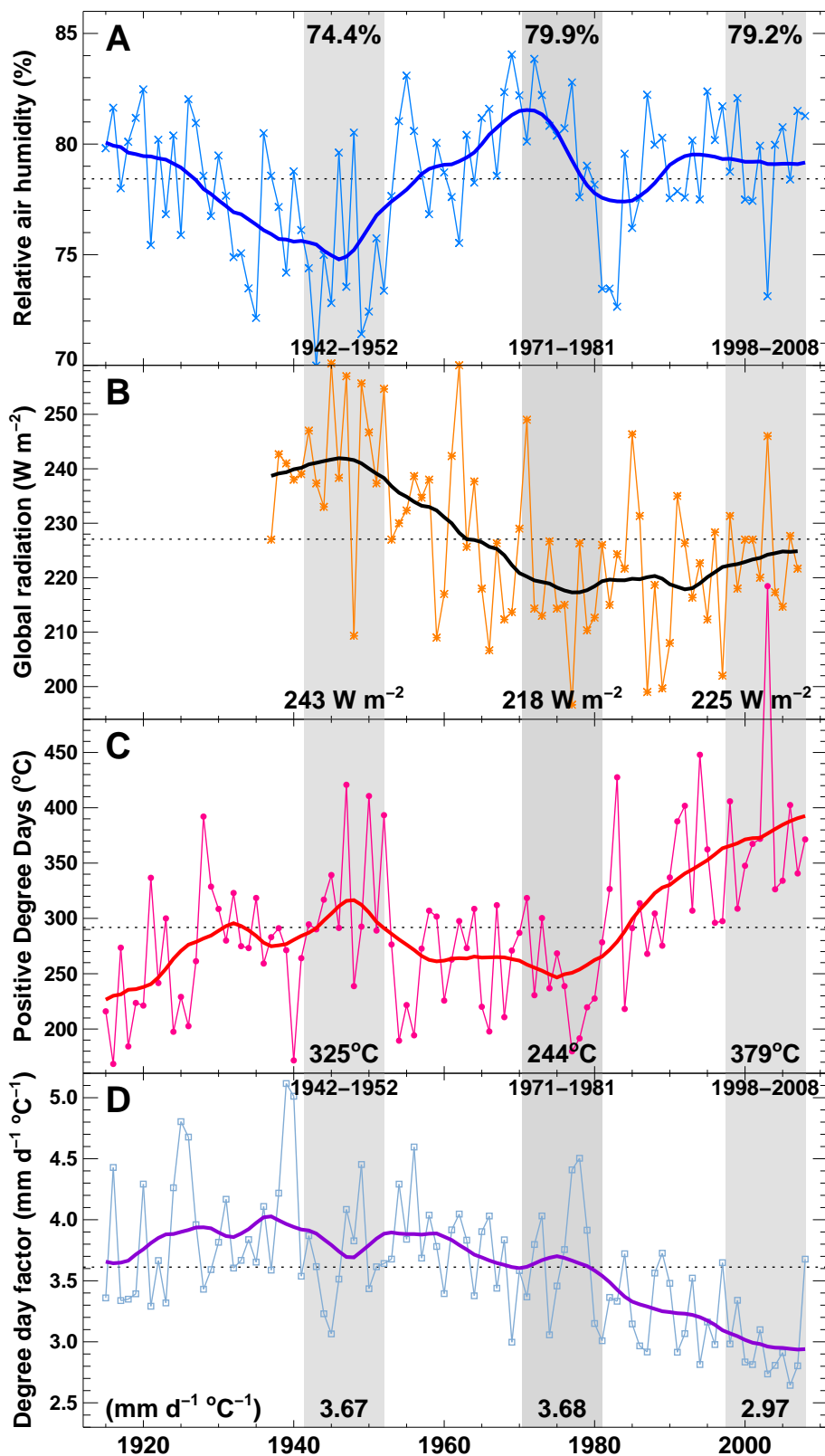


Figure B.3: Measured (A) relative humidity and (B) incoming global radiation in June to August. Solid lines represent 10-year running means. Mean values in three highlighted periods are given. (C) Sum of daily air temperatures above $0^{\circ}C$ in June to August (average of the four study sites). (D) Degree-day factors for snow, calibrated for each year individually based on the seasonal field data.

As fluctuations in climate forcing over the Alps are not only driven by temperature changes (Ohmura and others, 2007), additional meteorological variables were analyzed. Records of air temperature and relative air humidity at Davos and Säntis were obtained from the network of MeteoSwiss. Monthly means of global radiation at Davos were provided by the World Radiation Centre, PMOD, Switzerland. We only consider these variables in the summer months June to August, being the most important for melting. Three decadal periods are highlighted: 1942–1952, 1971–1981 and 1998–2008. Relative air humidity is significantly lower around 1950 than it is at present (Fig. B.3 A). Measurements of global radiation indicate that solar irradiance around 1950 was higher by 8% compared to the first decade of the 21st century (Fig. B.3 B). This is attributed to a brightening of solar radiation in the 1940s and '50s, followed by a dimming trend until the 1980s related to the aerosol content of the atmosphere (Wild and others, 2005; Ohmura and others, 2007). Summer air temperatures only weakly reflect these fluctuations and show a significant step-like increase since 1982 (Fig. B.3 C). Temperature-index models are widely used in glaciological and hydrological sciences for the calculation of snow- and icemelt (Hock, 2003). Our results show that considerable changes in the degree-day factors, obtained from tuning to the seasonal field data, occurred during the 20th century (Fig. B.3 D). The downward trend in the statistical relation between air temperature and melt since the 1960s is due to a decrease in energy provided by shortwave radiation and an increase in (temperature dependent) incoming longwave radiation. This demonstrates the limitations of using constant degree-day factors for melt modelling.

Acknowledgments

This study was funded by ETH Research Grant TH-17 06-1. We are indebted to A. Bauder, H. Müller, G. Kappenberger and many previous researchers carrying out field surveys.

Appendix C

Co-authored publications

- Bauder, A., M. Funk and **M. Huss** (2007). Ice volume changes of selected glaciers in the Swiss Alps since the end of the 19th century. *Annals of Glaciology*, 46:145–149.
- Bauder, A., M. Funk, **M. Huss**, P. Riesen and S. Sugiyama (2008). Triggering and drainage mechanisms of the 2004 glacier-dammed lake outburst in Gornergletscher, Switzerland. *Journal of Geophysical Research*, 113, F04019, doi:10.1029/2007JF000920.
- Farinotti, D., **M. Huss**, A. Bauder, M. Funk and M. Truffer (in press). A method to estimate ice volume and ice thickness distribution of alpine glaciers. *Journal of Glaciology*.
- Jouvet, G., **M. Huss**, H. Blatter, M. Picasso and J. Rappaz (submitted). Numerical simulation of Rhonegletscher from 1874 to 2100. *Journal of Computational Physics*.
- Farinotti, D., **M. Huss**, A. Bauder and M. Funk (submitted). An estimate of the glacier ice volume in the the Swiss Alps. *Global and Planetary Change*.

Bibliography

- Abdalati, W., W. Krabill, E. Frederick, S. Manizade, C. Martin, J. Sonntag, R. Swift, R. Thomas, J. Yungel and R. Koerner, 2005. Elevation changes of ice caps in the Canadian Arctic Archipelago, *Journal of Geophysical Research*, **109**, F04007.
- Adalgeirsdóttir, G., T. Jóhannesson, H. Björnson, F. Pálsson and O. Sigurdsson, 2006. Response of Hofsjökull and southern Vatnajökull, Iceland, to climate change, *Journal of Geophysical Research*, **111**, F03001, doi:10.1029/2005JF000388.
- Adams, W. P., J. G. Cogley, M. A. Ecclestone and M. N. Demuth, 1998. A small glacier as an index of regional mass balance: Baby Glacier, Axel Heiberg Island, 1959-1992, *Geografiska Annaler*, **80**(1), 37–50.
- Aellen, M., 1996. Glacier mass balance studies in the Swiss Alps, *Zeitschrift für Gletscherkunde und Glazialgeologie*, **31**, 159–168.
- Agassiz, L., 1840. Etudes sur les glaciers, vol. 1, Jent & Gassmann, Neuchâtel.
- Anderson, R.S., J.S. Walder, S.P. Anderson, D.C. Trabant and A.G. Fountain, 2005. The dynamic response of Kennicott Glacier, Alaska, USA, to the Hidden Creek Lake outburst event, *Annals of Glaciology*, **40**, 237–242.
- Anderson, R. S., 2000. A model of ablation-dominated medial moraines and the generation of debris-mantled glacier snouts, *Journal of Glaciology*, **46**(154), 459–469.
- Anderson, S. P., J. S. Walder, R. S. Anderson, E. R. Kraal, M. Cunico, A. G. Fountain and D. C. Trabant, 2003. Integrated hydrologic and hydrochemical observations of Hidden Creek Lake jökulhlaups, Kennicott Glacier, Alaska, *Journal of Geophysical Research*, **108**(F1), 6003.
- Anonymous, 1969. Mass-balance Terms, *Journal of Glaciology*, **8**(52), 3–7.
- Arendt, A. and M. Sharp, 1999. Energy balance measurements on a Canadian high arctic glacier and their implications for mass balance modelling, *Interactions between the Cryosphere, Climate and Greenhouse Gases*, IAHS, vol. 256, 165–172.
- Arnold, N. S., I. C. Willis, M. J. Sharp, K. S. Richards and W. J. Lawson, 1996. A distributed surface energy–balance model for a small valley glacier. I. Development and testing for Haut Glacier d’Arolla, Valais, Switzerland, *Journal of Glaciology*, **42**(140), 77–89.
- Aschwanden, H. and C. Leibundgut, 1982. Die Markierung der Wasser des Gornerseesausbruchs mit drei Fluoreszenztracern, Leibundgut, C. and R. Weingartner, eds., *Tracermethoden in der Hydrologie*, Beiträge zur Geologie der Schweiz, vol. 28, 535–549.

- Auer, I. and others, 2007. HISTALP - historical instrumental climatological surface time series of the Greater Alpine Region, *International Journal of Climatology*, **27**(1), 17–46.
- Bader, H., 1954. Sorge's law of densification of snow on high polar glaciers, *Journal of Glaciology*, **2**(15), 319–323.
- Baker, D., H. Escher-Vetter, H. Moser, H. Oerter and O. Reinwarth, 1982. A glacier discharge model based on results from field studies of energy balance, water storage and flow, Hydrological aspects of alpine and high mountain areas, Exeter 1982, IAHS, vol. 138, 103–112.
- Bamber, J., W. Krabill, V. Raper and J. Dowdeswell, 2004. Anomalous recent growth of part of a large Arctic ice cap: Austfonna, Svalbard, *Geophysical Research Letters*, **31**, L12402.
- Barber, D. G., J. M. Hanesiak, W. Chan and J. Piwowar, 2001. Sea-ice and meteorological conditions in northern Baffin Bay and the North Water polynya between 1979 and 1996, *Atmosphere-Ocean*, **39**(3), 343–359.
- Barnett, T. P., J. C. Adam and D. P. Lettenmaier, 2005. Potential impacts of a warming climate on water availability in snow-dominated regions, *Nature*, **438**, 303–309.
- Bauder, A., 2001. Bestimmung der Massenbilanz von Gletschern mit Fernerkundungsmethoden und Fließmodellierungen, Dissertation No 14110, ETH Zürich.
- Bauder, A., M. Funk and G. H. Gudmundsson, 2003. The ice thickness distribution of Unteraargletscher (Switzerland), *Annals of Glaciology*, **37**, 331–336.
- Bauder, A., M. Funk and M. Huss, 2007. Ice volume changes of selected glaciers in the Swiss Alps since the end of the 19th century, *Annals of Glaciology*, **46**, 145–149.
- Begert, M., T. Schlegel and W. Kirchhofer, 2005. Homogeneous temperature and precipitation series of Switzerland from 1864 to 2000, *International Journal of Climatology*, **25**(1), 65–80.
- Bergström, S., 1995. The HBV model, Singh, V.P., ed., *Computer Models of Watershed Hydrology*, Water Resources Publications, 443–476.
- Bernath, A., 1991. Zum Wasserhaushalt im Einzugsgebiet der Rhône bis Gletsch. Untersuchungen zu Niederschlag, Verdunstung und Abfluss in einem teilweise vergletscherten Einzugsgebiet, *Zürcher Geographische Schriften* 43, Zürich.
- Bezinge, A., J. Perreten and F. Schafer, 1973. Phénomènes du lac glaciaire du Gorner, Symposium on the Hydrology of Glaciers, Cambridge 1969, IAHS, vol. 95, 65–78.
- Birsan, V.-M., P. Molnar, P. Burlando and M. Pfaundler, 2005. Streamflow trends in Switzerland, *Journal of Hydrology*, **314**, 312–329.
- Björnsson, H., 1988. Hydrology of ice caps in volcanic regions, **45**, *Societas Scientiarum Islandica*, Reykjavik.
- Björnsson, H., 1992. Jökulhlaups in Island: Prediction, characteristics and simulation, *Annals of Glaciology*, **16**, 95–106.
- Björnsson, H., 1998. Hydrological characteristics of the drainage system beneath a surging glacier, *Nature*, **395**, 771–774.

- Björnsson, H., 2002. Subglacial lakes and jökulhlaups in Iceland, *Global and Planetary Change*, **35**(3-4), 255–271.
- Blatter, H. and G. Kappenberger, 1988. Mass balance and thermal regime of Laika ice cap, Coburg Island, N.W.T., Canada, *Journal of Glaciology*, **34**(116), 102–110.
- Blöschl, G., R. Kirnbauer and D. Gutknecht, 1991. Distributed snowmelt simulations in an Alpine catchment, I: Model evaluation on the basis of snow cover patterns, *Water Resour. Res.*, **12**(27), 3171–3179.
- Bradley, R. S., 2006. Threats to water supplies in the Tropical Andes, *Science*, **312**, 1755–1756.
- Braithwaite, R. J., 1995. Positive degree-day factors for ablation on the Greenland ice sheet studied by energy-balance modeling, *Journal of Glaciology*, **41**(137), 153–160.
- Braithwaite, R. J. and Y. Zhang, 1999. Modelling Changes in Glacier Mass Balance that may Occur as a Result of Climate Changes, *Geografiska Annaler*, **81A**(4), 489–496.
- Braithwaite, R. J. and Y. Zhang, 2000. Sensitivity of mass balance of five Swiss glaciers to temperature changes assessed by tuning a degree-day model, *Journal of Glaciology*, **46**(152), 7–14.
- Braun, L.N., M. Weber and M. Schulz, 2000. Consequences of climate change for runoff from Alpine regions, *Annals of Glaciology*, **31**(1), 19–25.
- Braun, L. N., M. Aellen, M. Funk, R. Hock, M. B. Rohrer, U. Steinegger, G. Kappenberger and H. Müller-Lemans, 1995. Measurement and simulation of high alpine water balance components in the Linth-Limmern head watershed (north-eastern Switzerland), *Zeitschrift für Gletscherkunde und Glazialgeologie*, **30**, 161–185.
- Burgess, D. O. and M. J. Sharp, 2004. Recent changes in areal extent of the Devon Ice Cap, Nunavut, Canada, *Arctic, Antarctic and Alpine Research*, **36**(4), 261–271.
- Burlando, P., F. Pellicciotti and U. Strasser, 2002. Modelling mountainous water system between learning and speculating, looking for challenges, *Nordic Hydrology*, **33**(1), 47–74.
- Carenzo, M., F. Pellicciotti, S. Rimkus and P. Burlando, in press. Assessing the transferability and robustness of an enhanced temperature-index glacier melt model, *Journal of Glaciology*.
- Christensen, J. H., T. Carter and F. Giorgi, 2002. PRUDENCE employs new methods to assess European climate change, *EOS*, **83**(147).
- Christensen, J. H. and O. B. Christensen, 2007. A summary of the PRUDENCE model projections of changes in European climate by the end of this century, *Climatic Change*, **81**, 7–30.
- Clague, J. J. and W. H. Mathews, 1973. The magnitude of jökulhlaups, *Journal of Glaciology*, **12**(66), 501–504.
- Clarke, G. K. C., 1982. Glacier outburst floods from “Hazard Lake”, Yukon Territory, and the problem of flood magnitude prediction, *Journal of Glaciology*, **28**(98), 3–21.
- Clarke, G. K. C., 2003. Hydraulics of subglacial outburst floods: new insights from the Spring-Hutter formulation, *Journal of Glaciology*, **49**(165), 299–313.

- Cogley, J. G. and W. P. Adams, 1998. Mass balance of glaciers other than the ice sheets, *Journal of Glaciology*, **44**(147), 315–325.
- Colgan, W. and M. J. Sharp, 2008. Combined oceanic and atmospheric influences on net accumulation on Devon Ice Cap, Nunavut, Canada, *Journal of Glaciology*, **54**(184), 28–40.
- Collins, D. N., 1979. Quantitative determination of the subglacial hydrology of two Alpine glaciers, *Journal of Glaciology*, **23**(89), 347–362.
- Collins, D. N., 1986. Characteristics of meltwaters draining from the portal of an Alpine glacier during the emptying of a marginal ice-dammed lake., *Materialy Glyatsiolokikh*, **58**, 114–122 (Russian), 224–232 (English).
- Collins, D. N., 2006. Climatic variation and runoff in mountain basins with differing proportions of glacier cover, *Nordic Hydrology*, **37**(4-5), 315–326.
- Copland, L., J. Harbor, S. Gordon and M. Sharp, 1997. The use of borehole video investigating the hydrology of a temperate glacier, *Hydrological Processes*, **11**, 211–224.
- Costa, J.E., 1988. Floods from dam failure, John Wiley and Sons.
- Cox, L. H. and L. S. March, 2004. Comparison of geodetic and glaciological mass-balance techniques, Gulkana Glacier, Alaska, USA, *Journal of Glaciology*, **50**(170), 63–70.
- Dadic, R., R. Mott, M. Lehning and P. Burlando, submitted. Wind influence on snow depth distribution and accumulation over glaciers, *Geophysical Research Letters*.
- Desloges, J.R., D.P. Jones and K.E. Rickner, 1989. Estimates of peak discharge from the drainage of ice-dammed Ape Lake, British Columbia, Canada, *Journal of Glaciology*, **35**(121), 349–354.
- Dowdeswell, J., J. Hagen, H. Björnsson, A. Glazovsky, W. Harrison, P. Holmlund, J. Jania, R. Koerner, B. Lefauconnier, C. Ommanney and R. Thomas, 1997. The mass balance of circum-Arctic glaciers and recent climate change, *Quaternary Research*, **48**, 1–14.
- Dyurgerov, M., 2003. Mountain and subpolar glaciers show an increase in sensitivity to climate warming and intensification of the water cycle, *Journal of Hydrology*, **282**, 164–176.
- Dyurgerov, M. B. and M. F. Meier, 2005. Glaciers and the Changing Earth System: a 2004 Snapshot, *Occasional Paper 58*, Institute of Arctic and Alpine Research, University of Colorado, pp. 117.
- Dyurgerov, M. B. and M. F. Meier, 1999. Analysis of winter and summer glacier mass balances, *Geografiska Annaler*, **81**(4), 541–554.
- Dyurgerov, M. B. and M. F. Meier, 2002. Glacier Mass Balance and Regime: Data of Measurements and Analysis, *Occasional Paper 55*, Institute of Arctic and Alpine Research, University of Colorado, pp. 89.
- Elliston, G. R., 1973. Water movement through the Gornergletscher, Symposium on the Hydrology of Glaciers, Cambridge 1969, IAHS, vol. 95, 79–84.

- Elsberg, D. H., W. D. Harrison, K. A. Echelmeyer and R. M. Krimmel, 2001. Quantifying the effects of climate and surface change on glacier mass balance, *Journal of Glaciology*, **47**(159), 649–658.
- Farinotti, D., M. Huss, A. Bauder, M. Funk and M. Truffer, in press. A method for estimating the ice volume and ice thickness distribution of alpine glaciers, *Journal of Glaciology*.
- Firnberichte, 1914–1978. Der Firnzuwachs 1913/14–1976/77 in einigen schweizerischen Firngebieten, no. 1-64 in Vierteljahrsschrift der Naturforschenden Gesellschaft in Zürich, Jahresberichte herausgegeben von der Gletscher-Kommission der Physikalischen Gesellschaft Zürich, später Schweizerische Meteorologische Zentralanstalt und ab 1973 durch A. Lemans.
- Fischer, U. H., A. Braun, A. Bauder and G. E. Flowers, 2005. Changes in geometry and subglacial drainage derived from digital elevation models: Unteraargletscher, Switzerland, 1927–1997, *Annals of Glaciology*, **40**, 20–24.
- Fischer, U. H., P. R. Porter, T. Schuler, A. J. Evans and G. H. Gudmundsson, 2001. Hydraulic and mechanical properties of glacial sediments beneath Unteraargletscher, Switzerland: implications for glacier basal motion, *Hydrological Processes*, **15**, 3525–3540.
- Flotron, 1924–2007. Vermessung der Aaregletscher, Berichte im Auftrag der Kraftwerke Oberhasli (unpublished).
- Flowers, G., H. Björnsson, F. Pálsson and G. Clarke, 2004. A coupled sheet-conduit mechanism for jökulhlaup propagation, *Geophysical Research Letters*, **31**, L05401, doi:10.1029/2003GL019088.
- Flowers, G. E., S. J. Marshall, H. Björnson and G. K. C. Clarke, 2005. Sensitivity of Vatnajökull ice cap hydrology and dynamics to climate warming over the next 2 centuries, *Journal of Geophysical Research*, **110**, F02011, doi:10.1029/2004JF000200.
- Fountain, A. G. and J. S. Walder, 1998. Water flow through temperate glaciers, *Reviews of Geophysics*, **36**(3), 299–328.
- Fowler, A. C., 1999. Breaking the seal at Grímsvötn, *Journal of Glaciology*, **45**(151), 506–516.
- Frei, C., 2007. Die Klimazukunft der Schweiz, Klimaänderung und die Schweiz 2050 – Erwartete Auswirkungen auf Umwelt, Gesellschaft und Wirtschaft, Beratendes Organ für Fragen der Klimaänderung (OcCC), 12–16, <http://www.occc.ch>.
- Frei, C. and C. Schär, 1998. A precipitation climatology of the Alps from high-resolution rain-gauge observations, *International Journal of Climatology*, **18**(8), 873–900.
- Frei, C., R. Schöll, S. Fukutome, J. Schmidli and P. L. Vidale, 2006. Future change of precipitation extremes in Europe: Intercomparison of scenarios from regional climate models, *Journal of Geophysical Research*, **111**(D6), D06105.
- Funk, M., 1985. Räumliche Verteilung der Massenbilanz auf dem Rhonegletscher und Ihre Beziehung zu Klimatelementen, Zürcher Geographische Schriften 24, Geographisches Institut der ETH Zürich, pp. 183.

- Funk, M., G. H. Gudmundsson and F. Hermann, 1994. Geometry of the glacier bed of the Unteraarglacier, Bernese Alps, Switzerland, *Zeitschrift für Gletscherkunde und Glazialgeologie*, **30**, 187–194.
- Funk, M., R. Morelli and W. Stahel, 1997. Mass balance of Griesgletscher 1961–1994: different methods of determination, *Zeitschrift für Gletscherkunde und Glazialgeologie*, **33**(1), 41–55.
- Gerbaux, M., C. Genthon, P. Etchevers, C. Vincent and J. P. Dedieu, 2005. Surface mass balance of glaciers in the French Alps: distributed modeling and sensitivity to climate change, *Journal of Glaciology*, **51**(175), 561–572.
- Glaciological reports, 1881–2008. The Swiss Glaciers, 1880–2002/03, No. 1–124, Yearbooks of the Cryospheric Commission of the Swiss Academy of Sciences (SCNAT), published since 1964 by Laboratory of Hydraulics, Hydrology and Glaciology (VAW) of ETH Zürich.
- Glen, J. W., 1955. The creep of polycrystalline ice, *Proceedings of the Royal Society of London, Ser. A*, **228**(1175), 519–538.
- Greuell, J. and J. Oerlemans, 1989. The evolution of the englacial temperature distribution in the superimposed ice zone of a polar ice cap during a summer season, Oerlemans, J., ed., *Proceedings of the Symposium on glacier fluctuations and climatic change*, Kluwer Academic Publishers, Dordrecht, 289–304.
- Greuell, W., 1992. Hintereisferner, Austria: mass-balance reconstruction and numerical modelling of the historical length variations, *Journal of Glaciology*, **38**(129), 233–244.
- Gudmundsson, G. H., 1999. A three-dimensional numerical model of the confluence area of Unteraargletscher, Bernese Alps, Switzerland, *Journal of Glaciology*, **45**(150), 219–230.
- Gudmundsson, G. H., A. Bassi, M. Vonmoos, A. Bauder, U. H. Fischer and M. Funk, 2000. High-resolution measurements of spatial and temporal variations in surface velocities of Unteraargletscher, Bernese Alps, Switzerland, *Annals of Glaciology*, **31**, 63–68.
- Gudmundsson, G. H., A. Bauder, M. Lüthi, U. H. Fischer and M. Funk, 1999. Estimating rates of basal motion and internal ice deformation from continuous tilt measurements, *Annals of Glaciology*, **28**, 247–252.
- Gurtz, J., A. Baltensweiler and H. Lang, 1999. Spatially distributed hydrotope-based modelling of evapotranspiration and runoff in mountainous basins, *Hydrological Processes*, **13**, 2751–2768.
- Haerberli, W., 1976. Eistemperaturen in den Alpen, *Zeitschrift für Gletscherkunde und Glazialgeologie*, **11**(2), 203–220.
- Haerberli, W., 1983. Frequency and characteristics of glacier floods in the Swiss Alps, *Annals of Glaciology*, **4**, 85–90.
- Haerberli, W., 1995. Glacier fluctuations and climate change detection – operational elements of a worldwide monitoring strategy, *WMO - Bulletin*, **44**(1), 23–31.
- Hagen, J. O., K. Melvold, F. Pinglot and J. A. Dowdeswell, 2003. On the net mass balance of the glaciers and ice caps in Svalbard, Norwegian Arctic, *Arctic, Antarctic and Alpine Research*, **35**, 264–270.

- Hagg, W., L. Braun, M. Kuhn and T. Nesgaard, 2007. Modelling of hydrological response to climate change in glacierized Central Asian catchments, *Journal of Hydrology*, **332**, 40–53.
- Hagg, W., L. Braun, M. Weber and M. Becht, 2006. Runoff modelling in glacierized Central Asian catchments for present-day and future climate, *Nordic Hydrology*, **37**(2), 93–105.
- Hamon, W. R., 1961. Estimating Potential Evapotranspiration, *Journal of the Hydraulics Division*, **87**(HY3), 107–120.
- Harrison, W. D., D. H. Elsberg, L. H. Cox and R. S. March, 2005. Different mass balances for climatic and hydrologic applications, *Journal of Glaciology*, **51**(172), 176.
- Helbing, J., 2005. Glacier dynamics of Unteraargletscher: Verifying theoretical concepts through flow modeling, Dissertation No 16303, ETH Zürich.
- Helsel, D. R. and R. M. Hirsch, 1992. *Statistical Methods in Water Resources*, Elsevier.
- Hingray, B., N. Mouhous, A. Mezghani, K. Bogner, B. Schaefli and A. Musy, 2007. Accounting for global-mean warming and scaling uncertainties in climate change impact studies: application to a regulated lake system, *Hydrology and Earth System Sciences*, **11**(3), 1207–1226.
- Hock, R., 1999. A distributed temperature-index ice- and snowmelt model including potential direct solar radiation, *Journal of Glaciology*, **45**(149), 101–111.
- Hock, R., 2003. Temperature index melt modelling in mountain areas, *Journal of Hydrology*, **282**(1-4), 104–115.
- Hock, R., 2005. Glacier melt: a review of processes and their modelling, *Progress in Physical Geography*, **29**(3), 362–391.
- Hock, R. and B. Holmgren, 2005. A distributed surface energy balance model for complex topography and its application to Storglaciären, Sweden, *Journal of Glaciology*, **51**(172), 25–26.
- Hock, Regine, Peter Jansson and Ludwig Braun, 2005. Modelling the response of mountain glacier discharge to climate warming, Huber, Uli M., Mel A. Reasoner and Harald Bugmann, eds., *Global Change and Mountain Regions - A State of Knowledge Overview*, Springer, Dordrecht, 243–252.
- Hock, R. and C. Noetzi, 1997. Areal melt and discharge modelling of Storglaciären, Sweden, *Annals of Glaciology*, **24**, 211–217.
- Hoinkes, H., 1970. Methoden und Möglichkeiten von Massenhaushaltsstudien auf Gletschern, *Zeitschrift für Gletscherkunde und Glazialgeologie*, **6**(2), 37–90.
- Holmlund, P., P. Jansson and R. Pettersson, 2005. A re-analysis of the 58 year mass-balance record of Storglaciären, Sweden, *Annals of Glaciology*, **42**, 489–495.
- Horton, P., B. Schaefli, A. Mezghani, B. Hingray and A. Musy, 2006. Assessment of climate-change impacts on alpine discharge regimes with climate model uncertainty, *Hydrological Processes*, **20**(10), 2091–2109.

- Hubbard, A., H. Blatter, P. Nienow, D. Mair and B. Hubbard, 1998. Comparison of three-dimensional model for glacier flow with field data from Haut Glacier d'Arolla, Switzerland, *Journal of Glaciology*, **44**(147), 368–378.
- Hubbard, B., M. Sharp, I. C. Willis, M. K. Nielsen and C. C. Smart, 1995. Borehole water-level variations and the structure of the subglacial hydrological system of Haut Glacier d'Arolla, Valais, Switzerland, *Journal of Glaciology*, **41**(139), 572–583.
- Huss, M., 2005. Gornergletscher – Gletscherseeausbrüche und Massenbilanzabschätzungen, Diploma Thesis, VAW-ETH Zürich, unpublished.
- Huss, M., 2008. Massenbilanz-Berichte, interne Publikation, VAW-ETHZ.
- Huss, M. and A. Bauder, in press. Twentieth century climate change inferred from four long-term point observations of seasonal mass balance, *Annals of Glaciology*, **50**.
- Huss, M., A. Bauder and M. Funk, in press. Homogenization of long-term mass balance time series, *Annals of Glaciology*, **50**.
- Huss, M., A. Bauder, M. Funk and R. Hock, 2008a. Determination of the seasonal mass balance of four Alpine glaciers since 1865, *Journal of Geophysical Research*, **113**, F01015.
- Huss, M., A. Bauder, M. Werder, M. Funk and R. Hock, 2007a. Glacier-dammed lake outburst events of Gornersee, Switzerland, *Journal of Glaciology*, **53**(181), 189–200.
- Huss, M., D. Farinotti, A. Bauder and M. Funk, 2008b. Modelling runoff from highly glacierized alpine drainage basins in a changing climate, *Hydrological Processes*, **22**(19), 3888–3902.
- Huss, M., R. Stöckli, G. Kappenberger and H. Blatter, 2008c. Temporal and spatial changes of Laika Glacier, Canadian Arctic, since 1959 inferred from satellite remote sensing and mass balance modelling, *Journal of Glaciology*, **54**(188).
- Huss, M., S. Sugiyama, A. Bauder and M. Funk, 2007b. Retreat scenarios of Unteraargletscher, Switzerland, using a combined ice-flow mass-balance model, *Arctic, Antarctic and Alpine Research*, **39**(3), 422–431.
- Iken, A., K. Fabri and M. Funk, 1996. Water storage and subglacial drainage conditions inferred from borehole measurements on Gornergletscher, Valais, Switzerland, *Journal of Glaciology*, **42**(141), 233–248.
- IPCC, 2001. Climate Change 2001. The scientific basis. Contributions of Working Group I to the Third Assessment Report of the Intergovernmental Panel on Climate Change, *Tech. rep.*, WMO/UNEP, Cambridge University Press.
- IPCC, 2007. Climate Change 2007. The scientific basis. Contributions of Working Group I to the Forth Assessment Report of the Intergovernmental Panel on Climate Change, *Tech. rep.*, WMO/UNEP, Cambridge University Press.
- Jansson, P., R. Hock and T. Schneider, 2003. The concept of glacier storage - a review, *Journal of Hydrology*, **282**(1–4), 116–129.
- Jóhannesson, T., C. Raymond and E. Waddington, 1989. Time-scale for adjustment of glaciers to changes in mass balance, *Journal of Glaciology*, **35**(121), 355–369.

- Jouvet, G., M. Huss, H. Blatter, M. Picasso and J. Rappaz, submitted. Numerical simulation of Rhonegletscher from 1874 to 2100, *Journal of Computational Physics*.
- Jouvet, G., M. Picasso, J. Rappaz and H. Blatter, 2008. A new algorithm to simulate the dynamics of a glacier: theory and applications, *Journal of Glaciology*, **54**(188), 801–811.
- Juen, I., G. Kaser and C. Georges, 2007. Modelling observed and future runoff from a glacierized tropical catchment (Cordillera Blanca, Perú), *Global and Planetary Change*, **59**, 37–48.
- Kääb, A., C. Huggel, F. Paul, R. Wessels, B. Raup, H. Kieffer and J. Kargel, 2003. Glacier monitoring from ASTER imagery: accuracy and applications, *EARSeL eProceedings*, **2**(1), 47–53.
- Kane, D. L. and R. E. Gieck, 1997. Snowmelt modeling at small Alaskan Arctic watershed, *Journal of Hydrologic Engineering*, **2**(4), 204–210.
- Kappenberger, G., 1976. Massenhaushalt und Bewegung des Laika Gletschers, Coburg Island, N.W.T., 1973/1974, Diploma Thesis, ETH Zürich.
- Kaser, G., J. G. Cogley, M. B. Dyurgerov, M. F. Meier and A. Ohmura, 2006. Mass balance of glaciers and ice caps: Consensus estimates for 1961–2004, *Geophysical Research Letters*, **33**(19), L19501.
- Kayastha, R. B., Y. Takeuchi, M. Nakawo and Y. Ageta, 2000. Practical prediction of ice melting beneath various thickness of debris cover on Khumbu Glacier, Nepal, using a positive degree-day factor, *Debris-Covered Glaciers*, IAHS, vol. 264, 71–82.
- Klok, E. J., K. Japser, K. P. Roelofsma, J. Gurtz and A. Badoux, 2001. Distributed hydrological modelling of a heavily glaciated Alpine river basin, *Hydrological Sciences Journal*, **46**(4), 234–240.
- Klok, E. J. and J. Oerlemans, 2002. Model study of the spatial distribution of the energy and mass balance of Morteratschgletscher, Switzerland, *Journal of Glaciology*, **48**(163), 505–518.
- Koerner, R. M., 1970. The mass balance of Devon Island Ice Cap Northwest Territories, Canada, 1961–1966, *Journal of Glaciology*, **9**(57), 325–336.
- Koerner, R. M., 2005. Mass balance of glaciers in the Queen Elizabeth Islands, Nunavut, Canada, *Annals of Glaciology*, **42**, 417–423.
- Krabill, W., W. Abdalati, E. Frederick, S. Manizade, C. Martin, J. Sonntag, R. Swift, R. Thomas, W. Wright and J. Yungel, 2000. Greenland Ice Sheet: High-elevation balance and peripheral thinning, *Science*, **289**(5478), 428–430.
- Krimmel, R. M., 1999. Analysis of difference between direct and geodetic mass balance measurements at South Cascade Glacier, Washington, *Geografiska Annaler*, **81A**(4), 653–658.
- Kuhn, M., G. Markel, G. Kaser, U. Nickus, F. Obleitner and H. Schneider, 1985. Fluctuations of climate and mass balances: different responses of two adjacent glaciers, *Zeitschrift für Gletscherkunde und Glazialgeologie*, **21**(1), 409–416.
- Lang, H. and L. N. Braun, 1990. On the information content of air temperature in the context of snow melt estimation, *Hydrology of mountainous areas*, IAHS, vol. 190, 347–354.

- Lang, H., B. Schädler and G. Davidson, 1977. Hydroglaciological investigations on the Ewigschneefeld – Grosser Aletschgletscher, *Zeitschrift für Gletscherkunde und Glazialgeologie*, **12**, 109–124.
- Le Meur, E., M. Gerbaux, M. Schäfer and C. Vincent, 2007. Disappearance of an Alpine glacier over the 21st Century simulated from modeling its future surface mass balance, *Earth and Planetary Science Letters*, **261**, 367–374.
- Lehning, M., H. Loewe, M. Ryser and N. Raderschall, 2008. Inhomogeneous precipitation distribution and snow transport in steep terrain, *Water Resources Research*, **44**(7).
- Lehning, M., I. Völksch, D. Gustavson, T. A. Nguyen, M. Stähli and M. Zappa, 2006. ALPINE3D: a detailed model of mountain surface processes and its application to snow hydrology, *Hydrological Processes*, **20**, 2111–2128.
- Lukas, S., L.I. Nicholson, F.H. Ross and O. Humulum, 2005. Formation, meltout processes and landscape alteration of high-arctic ice-cored moraines, *Polar Geography*, **29**(3), 157–187.
- Lundstrom, S.C., A.E. McCafferty and J.A. Coe, 1993. Photogrammetric analysis of 1984–1989 surface altitude change of the partially debris-covered Eliot Glacier, Mt. Hood, Oregon, U.S.A., *Annals of Glaciology*, **17**, 167–170.
- Machguth, H., F. Paul, M. Hoelzle and W. Haeberli, 2006. Distributed glacier mass balance modelling as an important component of modern multi-level glacier monitoring, *Annals of Glaciology*, **43**(1), 335–343.
- Mair, D., D. O. Burgess and M. J. Sharp, 2005. Thirty-seven year mass balance of Devon Ice Cap, Nunavut, Canada, determined by shallow ice coring and melt modeling, *Journal of Geophysical Research*, **110**, F01011.
- Maronnier, V., M. Picasso and J. Rappaz, 2003. Numerical simulation of three-dimensional free surface flows, *International Journal for Numerical Methods in Fluids*, **42**(7), 697–716.
- Marshall, S. J., M. J. Sharp, D. O. Burgess and F. S. Anslow, 2007. Near-surface-temperature lapse rates on the Prince of Wales Icefield, Ellesmere Island, Canada: implications for regional downscaling of temperature, *International Journal of Climatology*, **27**(3), 385–398.
- Mayo, L. R., M. F. Meier and W. V. Tangborn, 1972. A system to combine stratigraphic and annual mass-balance systems: A contribution to the International Hydrological Decade, *Journal of Glaciology*, **11**(61), 3–14.
- McGlone, Chris, Edward Mikhail and James Bethel, eds., 2004. Manual of Photogrammetry, American Society for Photogrammetry and Remote Sensing, 5 ed., 1151 p.
- Meier, M. F., 1962. Proposed definitions for glacier mass budget terms, *Journal of Glaciology*, **4**(33), 252–263.
- Meier, M. F., M. B. Dyurgerov, U. K. Rick, S. O’Neel, W. T. Pfeffer, R. S. Anderson, S. P. Anderson and A. F. Glazovsky, 2007. Glaciers Dominate Eustatic Sea-Level Rise in the 21st Century, *Science*, **317**(5841), 1064–1067.
- Mercanton, P. L., 1916. Vermessungen am Rhonegletscher, Mensurations au Glacier du Rhône, 1874–1915, *Neue Denkschriften der Schweizerischen Naturforschenden Gesellschaft*, **52**.

- Mesinger, F. and others, 2006. North American regional reanalysis, *Bulletin of the American Meteorological Society*, **87**(3), 343–360.
- Moritz, R. E., C. M. Bitz and E. J. Steig, 2002. Dynamics of recent climate change in the Arctic, *Science*, **297**, 1497–1502.
- Müller, F., T. Cafilisch and G. Müller, 1976. Firn und Eis der Schweizer Alpen: Gletscherinventar, Geographisches Institut der ETH Zürich 57, Zürich.
- Müller, Hans and Giovanni Kappenberger, 1991. Claridenfirn-Messungen 1914-1984, *Zürcher Geographische Schriften* 40, Geographisches Institut der ETH Zürich, pp. 79.
- Müller-Lemans, H., M. Funk, M. Aellen and G. Kappenberger, 1995. Langjährige Massenbilanzreihen von Gletschern in der Schweiz, *Zeitschrift für Gletscherkunde und Glazialgeologie*, **30**, 141–160.
- Nash, J.E. and J.V. Sutcliffe, 1970. River flow forecasting through conceptual models, *Journal of Hydrology*, **10**(3), 282–290.
- Ng, F. S. L. and H. Björnsson, 2003. On the Clague-Mathews relation for jökulhlaups, *Journal of Glaciology*, **49**(165), 161–172.
- Nishimura, D., 2008. Changes in surface flow speed over the past 100 years (Rhonegletscher, SwissAlps), Master thesis, Graduate School of Environmental Science, Hokkaido University.
- Nye, J. F., 1965. The flow of a glacier in a channel of rectangular, elliptic or parabolic cross-section, *Journal of Glaciology*, **5**(41), 661–690.
- Nye, J. F., 1976. Water flow in glaciers: jökulhlaups, tunnels and veins, *Journal of Glaciology*, **17**(76), 181–207.
- Oerlemans, J., 1994. Quantifying Global Warming from the Retreat of Glaciers, *Science*, **264**(5156), 243–245.
- Oerlemans, J., 1997. A flowline model for Nigardsbreen, Norway: projection of future glacier length based on dynamic calibration with the historic record, *Annals of Glaciology*, **24**, 382–389.
- Oerlemans, J., B. Anderson, A. Hubbard, Ph. Huybrechts, T. Jóhannesson and W.H. Knap, 1998. Modelling the response of glaciers to climate warming, *Climate Dynamics*, **14**(4), 267–274.
- Oerlemans, J., R. Bassford, W. Chapman, J. Dowdeswell, A. Glazovsky, J. Hagen, K. Melvold, M. de Ruyter de Wildt and R. van de Wal, 2005. Estimating the contribution from Arctic glaciers to sea-level change in the next hundred years, *Annals of Glaciology*, **42**, 230–236.
- Oerlemans, J. and J. P. F. Fortuin, 1992. Sensitivity of glaciers and small ice caps to greenhouse warming, *Science*, **258**(5079), 115–117.
- Ohmura, A., 2001. Physical basis for the temperature-based melt-index method, *Journal of Applied Meteorology*, **40**(4), 753–761.
- Ohmura, A., A. Bauder, H. Müller and G. Kappenberger, 2007. Long-term change of mass balance and the role of radiation, *Annals of Glaciology*, **46**, 367–374.

- Paterson, W. S. B., 1994. *The Physics of Glaciers*, Pergamon, New York, third ed., pp. 480.
- Paul, F. and A. Kääb, 2005. Perspectives on the production of a glacier inventory from multi-spectral satellite data in Arctic Canada: Cumberland Peninsula, Baffin Island, *Annals of Glaciology*, **42**, 59–66.
- Paul, F., A. Kääb and W. Haeberli, 2007a. Recent glacier changes in the Alps observed by satellite: Consequences for future monitoring strategies, *Global and Planetary Change*, **56**(1–2), 111–122.
- Paul, F., H. Machguth and A. Kääb, 2005. On the impact of glacier albedo under conditions of extreme glacier melt: the summer of 2003 in the Alps, *EARSeL eProceedings*, **4**(2), 139–149.
- Paul, F., M. Maisch, C. Rothenbuehler, M. Hoelzle and W. Haeberli, 2007b. Calculation and visualisation of future glacier extent in the Swiss Alps by means of hypsographic modelling, *Global and Planetary Change*, **55**(4), 343–357.
- Pellicciotti, F., M. Carenzo, J. Helbing, S. Rimkus and P. Burlando, 2008. On the role of subsurface heat conduction in glacier energy-balance modelling, *Annals of Glaciology*, **50**, 16–24.
- Pellicciotti, F., B. Brock, U. Strasser, P. Burlando, M. Funk and J. Corripio, 2005. An enhanced temperature-index glacier melt model including the shortwave radiation balance: development and testing for Haut Glacier d'Arolla, Switzerland, *Journal of Glaciology*, **51**(175), 573–587.
- Raymond, M., M. Wegmann and M. Funk, 2003. Inventar gefährlicher Gletscher in der Schweiz, *Mitteilungen 182*, Versuchsanstalt für Wasserbau, Hydrologie und Glaziologie der ETH Zürich, pp. 368.
- Reeh, N., 1991. Parameterization of melt rate and surface temperature on the Greenland ice sheet, *Polarforschung*, **59**(3), 113–128.
- Richardson, S.D. and J.M. Reynolds, 2000. An overview of glacial hazards in the Himalayas, *Quaternary international*, **66**(1), 31–47.
- Rignot, E. and R. H. Thomas, 2002. Mass Balance of Polar Ice Sheets, *Science*, **297**(5586), 1502–1506.
- Röthlisberger, H., 1972. Water pressure in intra- and subglacial channels, *Journal of Glaciology*, **11**(62), 177–203.
- Röthlisberger, H. and H. Lang, 1987. *Glacial Hydrology*, A.M. Gurnell and M.J. Clark (Ed.), *Glacio-Fluvial Sediment Transfer - An Alpine Perspective*, John Wiley and Sons, Chichester, New York, Toronto, Singapore, 207–284.
- Rousselot, Marie, 2006. A combined field and laboratory study of clast ploughing, *Mitteilungen 195*, Versuchsanstalt für Wasserbau, Hydrologie und Glaziologie der ETH Zürich, pp. 116.
- Sapiano, J., W. D. Harrison and K. A. Echelmeyer, 1998. Elevation, volume and terminus changes of nine glaciers in North America, *Journal of Glaciology*, **44**(146), 119–135.
- Scardovelli, R. and S. Zaleski, 1999. Direct numerical simulation of free-surface and interfacial flow, *Ann. Rev. Fluid Mech.*, **31**(7), 567–603.

- Schaepli, B., 2005. Quantification of Modelling Uncertainties in Climate Change Impact Studies on Water Ressources, Ph.D. thesis, EPFL–Lausanne, no. 3225.
- Schaepli, B., B. Hingray and A. Musy, 2007. Climate change and hydropower production in the Swiss Alps: quantification of potential impacts and related modelling uncertainties, *Hydrology and Earth System Sciences*, **11**(3), 1191–1205.
- Schaepli, B., B. Hingray, M. Niggli and A. Musy, 2005. A conceptual glacio-hydrological model for high mountainous catchments, *Hydrology and Earth System Sciences*, **9**(1), 95–109.
- Schär, C., P. L. Vidale, D. Lüthi, C. Frei, C. Häberli, M. A. Liniger and C. Appenzeller, 2004. The role of increasing temperature variability in European summer heatwaves, *Nature*, **427**, 332–336.
- Schmidli, J., C. Frei and P. L. Vidale, 2006. Downscaling from GCM precipitation: a benchmark for dynamical and statistical downscaling methods, *International Journal of Climatology*, **26**(5), 679–689.
- Schneeberger, C., O. Albrecht, H. Blatter, M. Wild and R. Hock, 2001. Modelling the response of glaciers to a doubling in atmospheric CO₂: a case study of Storglaciären, northern Sweden, *Climate Dynamics*, **17**(11), 825–834.
- Schneeberger, C., H. Blatter, A. Abe-Ouchi and M. Wild, 2003. Modelling changes in the mass balance of glaciers of the northern hemisphere for a transient 2×CO₂ scenario, *Journal of Hydrology*, **282**(1–4), 145–163.
- Schneider, T. and P. Jansson, 2004. Internal accumulation in firn and its significance for the mass balance of Storglaciären, Sweden, *Journal of Glaciology*, **50**(168), 25–34.
- Schöner, W. and R. Böhm, 2007. A statistical mass-balance model for reconstruction of LIA ice mass of glaciers in the European Alps, *Annals of Glaciology*, **46**, 161–169.
- Schuler, T., 2002. Investigation of water drainage through an alpine glacier by tracer experiments and numerical modeling, *Mitteilungen 177*, Versuchsanstalt für Wasserbau, Hydrologie und Glaziologie der ETH Zürich, pp. 146.
- Schuler, T., U. H. Fischer, R. Sterr, R. Hock and G. H. Gudmundsson, 2002. Comparison of modeled water input and measured discharge prior to a release event: Unteraargletscher, Bernese Alps, Switzerland, *Nordic Hydrology*, **33**(1), 27–46.
- Schulla, J. and K. Jasper, 2000. Model Description WaSiM-ETH, IAC ETH Zürich, Zürich.
- Schwarb, M., 2000. The Alpine Precipitation Climate, Ph.D. thesis, ETH–Zürich, no. 13911.
- Schwarb, M., C. Daly, C. Frei and C. Schaer, 2001. Mean annual and seasonal precipitation throughout the European Alps 1971-1990, Hydrological Atlas of Switzerland, plates 2.6, 2.7.
- Seibert, J., 2000. Multi-criteria calibration of a conceptual runoff model using a genetic algorithm, *Hydrology and Earth System Sciences*, **4**(2), 215–224.
- Semadeni-Davies, A., D. Maréchal, O. Bruland, Y. Kodama and K. Sand, 2004. Estimating latent heat over a melting arctic snow cover, *Nordic Hydrology*, **35**(3), 175–190.

- Seneviratne, S., J. Pal, E. Eltahir and C. Schär, 2002. Summer dryness in a warmer climate: a process study with a regional climate model, *Climate Dynamics*, **20**(1), 69–85.
- Sevruk, B., 1985. Correction of precipitation measurements, Workshop on the Correction of Precipitation Measurements, Zürich, Switzerland, WMO/IAHS/ETH, 13–23.
- Shuman, C. A., H. J. Zwally, B. E. Schutz, A. C. Brenner, J. P. DiMarzio, V. P. Suchdeo and H. A. Fricker, 2006. ICESat Antarctic elevation data: Preliminary precision and accuracy assessment, *Geophysical Research Letters*, **33**, L07501.
- Singh, P. and N. Kumar, 1997. Impact assessment of climate change on the hydrological response of a snow and glacier melt runoff dominated Himalayan river, *Journal of Hydrology*, **193**, 316–350.
- Spring, U. and K. Hutter, 1981. Numerical studies of Jökulhlaups, *Cold Regions Science and Technology*, **4**, 221–244.
- Stearns, L. A. and G. S. Hamilton, 2007. Rapid volume loss from two East Greenland outlet glaciers quantified using repeat stereo satellite imagery, *Geophysical Research Letters*, **34**, L05503.
- Steiner, D., A. Walter and H. J. Zumbühl, 2005. The application of a nonlinear backpropagation neural network to study the mass balance of the Great Aletsch Glacier, *Journal of Glaciology*, **51**(173), 313–323.
- Sugiyama, S., 2003. Influence of surface debris on summer ablation in Unteraar- and Lauteraargletscher, Switzerland, *Bulletin of Glaciological Research*, **20**, 41–47, iSSN : 1345-3807.
- Sugiyama, S., A. Bauder, M. Funk and C. Zahno, 2007a. Evolution of Rhonegletscher, Switzerland, over the past 125 years and in the future: application of an improved flowline model, *Annals of Glaciology*, **46**, 268–274.
- Sugiyama, S., A. Bauder, P. Weiss and M. Funk, 2007b. Reversal ice motion during the outburst of a glacier-dammed lake on Gornergletscher, Switzerland, *Journal of Glaciology*, **53**(181), 172–180.
- Sugiyama, S. and G. H. Gudmundsson, 2004. Short-term variations in glacier flow controlled by subglacial water pressure at Lauteraargletscher, Bernese Alps, Switzerland, *Journal of Glaciology*, **50**(170), 353–362.
- Suter, S., 2002. Cold Firn and Ice in the Monte Rosa and Mont Blanc Areas: Spatial Occurrence, Surface Energy Balance and Climatic Evidence, *Mitteilung 172*, Versuchsanstalt für Wasserbau, Hydrologie und Glaziologie der ETH Zürich, pp. 188.
- Thibert, E., R. Blanc, C. Vincent and N. Eckert, in press. Glaciological and volumetric mass balance measurements error analysis over 51 years for the Sarennes glacier, French Alps, *Journal of Glaciology*, **54**(186), 522–532.
- Torinesi, O., A. Letréguilly and F. Valla, 2002. A century reconstruction of the mass balance of Glacier de Sarennes, French Alps, *Journal of Glaciology*, **48**(160), 142–148.
- Uppala, S. M. and others, 2005. The ERA-40 re-analysis, *Quarterly Journal of the Royal Meteorological Society*, **131**(612), 2961–3012.

- Van de Wal, R. S. W. and M. Wild, 2001. Modelling the response of glaciers to climate change by applying volume-area scaling in combination with high resolution GCM, *Climate Dynamics*, **18**(3-4), 359–366.
- Verbunt, M., J. Gurtz, K. Jasper, H. Lang, P. Warmerdam and M. Zappa, 2003. The hydrological role of snow and glaciers in alpine river basins and their distributed modeling, *Journal of Hydrology*, **282**(1-4), 36–55.
- Vieli, A., M. Funk and H. Blatter, 1997. Griesgletscher: Berechnungen des Gletscherfließens und Perspektiven für die Zukunft, *Wasser Energie Luft*, **89**(5/6), 107–114.
- Vincent, C., 2002. Influence of climate change over the 20th Century on four French glacier mass balances, *Journal of Geophysical Research*, **107**(4375), D19.
- Vincent, C., G. Kappenberger, F. Valla, A. Bauder, M. Funk and E. Le Meur, 2004. Ice ablation as evidence of climate change in the Alps over the 20th century, *Journal of Geophysical Research*, **109**(D10), D10104.
- Vincent, C., E. Le Meur, D. Six, M. Funk, M. Hoelzle and S. Preukert, 2007. Very high-elevation Mont Blanc glaciated areas not affected by the 20th century climate change, *Journal of Geophysical Research*, **112**(9), D09120.
- Walder, J.S. and J.E. Costa, 1996. Outburst floods from glacier-dammed lakes: the effect of mode of lake drainage on flood magnitude, *Earth Surface Processes and Landforms*, **21**(8), 701–723.
- Walder, J.S., D.C. Trabant, M. Cunico, S.P. Anderson, R.S. Anderson, A.G. Fountain and A. Malm, 2005. Fault-dominated deformation in an ice dam during annual filling and drainage of a marginal lake, *Annals of Glaciology*, **40**, 174–178.
- Walder, J. S., D. C. Trabant, M. Cunico, A. G. Fountain, S. P. Anderson, R. S. Anderson and A. Malm, 2006. Local response of a glacier to annual filling and drainage of an ice-marginal lake, *Journal of Glaciology*, **52**(178), 440–450.
- Wallinga, J. and R. S. W. van de Wal, 1998. Sensitivity of Rhonegletscher, Switzerland, to climate change: experiments with a one-dimensional flowline model, *Journal of Glaciology*, **44**(147), 383–393.
- Weiss, P., 2005. Gletscherdynamik vor und nach der Entleerung des Gornersees im Sommer 2004, Diploma Thesis, VAW-ETH Zürich, unpublished.
- WGMS, 2000. Fluctuations of Glaciers, 1995–2000, Vol. VIII, *Tech. rep.*, IAHS(ICSII)–UNEP–UNESCO.
- Wigley, T.M.L. and S.C.B. Raper, 2001. Interpretation of high projections for global-mean warming, *Science*, **293**(5529), 451–454.
- Wild, M., H. Gilgen, A. Roesch, A. Ohmura, C. N. Long, E. G. Dutton, B. Forgan, A. Kallis, V. Russak and A. Tsvetkov, 2005. From Dimming to Brightening: Decadal Changes in Solar Radiation at Earth's Surface, *Science*, **308**(5723), 847–850.
- Wilhelm, G., 1967. Gornersee, rapport interne Grande Dixence (unpublished).

- Woodward, J., M. Sharp and A. Arendt, 1997. The influence of superimposed ice formation on the sensitivity of glacier mass balance to climate change., *Annals of Glaciology*, **24**, 186–190.
- Zahno, C., 2004. Rhonegletscher in Raum und Zeit: Neue geometrische und klimatische Einsichten, Diplomarbeit an der VAW/ETH-Zürich, (unpublished).
- Zemp, Michael, Wilfried Haeberli, Martin Hoelzle and Frank Paul, 2006. Alpine glaciers to disappear within decades?, *Geophysical Research Letters*, **33**(13), L13504.
- Zuo, Z. and J. Oerlemans, 1997. Contribution of glacier melt to sea-level rise since AD 1865: a regionally differentiated calculation, *Climate Dynamics*, **13**(12), 835–845.

Acknowledgements

Numerous people have contributed to the completion of this thesis in many different ways. Without their help this dissertation would not have been possible in this form. I would like to express my sincere gratitude to all of them.

Andreas Bauder has guided me through all the facets of glaciological science from the beginning. He showed me how fast one must run over the glacier to deserve a good beer in the evening. His codes have smoothed my ways into programming and in long discussions about the important and minor problems of our science I have obtained an immensity of useful advices. I thank Andreas for his dedication supervising me and the excellent collaboration we had during the last four years.

I am indebted to Martin Funk for his continuous support with fruitful discussions that have importantly contributed to many outcomes of this thesis. Martin has been a sincere "Doktorvater" to me during the last years, always encouraging me to go ahead.

Outside VAW there is one person, who was crucially important to many different aspect of my dissertation. Regine Hock has kindly provided the code of her melt model, and has, thus, made possible my start into glaciology. Her approaches have accompanied me throughout all the years of my work at VAW. But Regine did much more: She taught me how to write scientific paper, first as a co-author, then as an editor – I knew there is no way to ever escape her critic comments. But, as stern as they may have seemed in the beginning, they were always very helpful and I am grateful for all the effort Regine took for improving my papers.

My dissertation was funded by ETH Research grant TH-17 06-1. Martin Funk found means to employ me at VAW also for the 10 months before the actual take-off of the PhD-project.

Live at VAW was always pleasant! I would like to thank all my colleagues and friends that accompanied me during my thesis. There were good discussions in the Arvenstübli, but also many unforgettable days of field work or other spare-time activities. My thanks go to my PhD-colleagues Jed Brown, Pierre Dalban, Daniel Farinotti, Jakob Helbing, Arne Keller, Mélanie Raymond, Patrick Riesen, Marie Rousselot, Aurel Schwerzmann, Fabian Walter and Mauro Werder; and also to many other people I was happy to spend time with during the last years, like Andy Aschwanden, Hermann Bösch, Ruzica Dadic, Olaf Eisen, Jerome Failletaz, Albin Kretz, Alexandre Loye, Martin Lüthi, Horst Machguth, Bruno Nedela, Francesca Pellicciotti, Roger Rüegg, Claudia Ryser, Stefan Spichtig, Tetsuo Sueyoshi, Shin Sugiyama, Martin Truffer, Giuliana Turi, Stephanie Usselmann, Patrik Weiss and Tommy Wyder (in alphabetical order).

Of all my colleagues at VAW I would like to particularly thank Daniel Farinotti for the partly endless, but nevertheless productive discussions about our common scientific interests.

I am also especially grateful to Shin Sugiyama for his support during the beginning of my thesis. I will always remember well the day on Unteraargletscher, now almost six years ago, when he has convinced me that glaciology would be the right direction for me to go – he was right!

During my dissertation I had the opportunity to be part of interesting collaborations with scientists from other institutes, which was a valuable experience for me. I would like to acknowledge Guillaume Juvet and Reto Stöckli. They have made it possible to enter areas of research previously unfamiliar to me.

I am indebted to the referees of my thesis Georg Kaser, Christoph Schär and Heinz Blatter. They have agreed to read through all the chapters of my thesis and have provided valuable comments for improving its content.

For my work I could make use of an immense amount of field data. Dozens of people have contributed with days and days of work to compiling this data basis. Hermann Bösch evaluated numerous digital elevation models from aerial photographs and Bruno Nedela and Stephanie Usselman digitized many old maps. I am also indebted to many previous glaciologists carrying out field measurements over many decades. Here, I would like to particularly mention Hans Müller, Giovanni Kappenberger and Urs Steinegger for their efforts on Claridenfirn. Many indispensable field data were provided by Swisstopo (topographical information), MeteoSchweiz (weather data) and BAFU (discharge data).

This is also the place to express the most sincere gratitude to my parents. They have supported me throughout all the years of my education in many different ways and have made it possible to do what I really wanted to.

Not everything is science! Salome has accompanied me throughout my thesis and has shown me how sunny life can be. She always had an ear to listen to my glaciological worries and has given me the motivation to carry on. Thank you, Salome, for the good time you gave me!

Curriculum Vitae

Matthias Huss

Stockenstr. 2
9552 Bronschhofen
mhuss@bluewin.ch

Born on 9 March 1980
in Winterthur (ZH)
Citizen of Wiesendangen (ZH), Switzerland

Education and Professional Training

June 2006 – February 2009 :

PhD Student, ETH Zurich (Switzerland)

Doctorate at the Laboratory of Hydraulics, Hydrology and Glaciology,
in the Section of Glaciology of Prof. Dr. M. Funk.

”Past and future changes in glacier mass balance”

August 2007 – February 2008 :

Part-time geography teacher, Kantonsschule Rämibüel, Zürich

July 2005 – May 2006 :

Research associate, ETH Zurich (Switzerland)

October 2000 – May 2005 :

Study of Earth Sciences at ETH Zurich (Switzerland)

Diploma thesis in Glaciology under the guidance of

Dr. A. Bauder.

”Gornergletscher - Gletscherseeausbrüche und Massenbilanzabschätzungen”
(awarded with the medal of the ETH Zürich)

Dipl. Natw. ETH

1993 – 2000 : Gymnasium in Wetzikon (ZH), Switzerland.

Matura Typus B (award for the best student of the age-group).

1987 – 1993 : Primary school in Hittnau (ZH), Switzerland.

Publications

- Huss, M. and A. Bauder (in press). Twentieth century climate change inferred from four long term point observations of seasonal mass balance. *Annals of Glaciology*, **50**.
- Huss, M., A. Bauder and M. Funk (in press). Homogenization of long-term mass balance time series. *Annals of Glaciology*, **50**.
- Huss, M., R. Stöckli, G. Kappenberger and H. Blatter, 2008. Temporal and spatial changes of Laika Glacier, Canadian Arctic, since 1959 inferred from satellite remote sensing and mass balance modelling. *Journal of Glaciology*, 54(188), 857–866.
- Huss, M., D. Farinotti, A. Bauder and M. Funk, 2008. Modelling runoff from highly glacierized alpine drainage basins in a changing climate. *Hydrological Processes*, **22**(19), 3888–3902., doi:10.1002/hyp.7055.
- Huss, M., A. Bauder, M. Funk and R. Hock (2008). Determination of the seasonal mass balance of four Alpine glaciers since 1865. *Journal of Geophysical Research*, 113, F01015, doi:10.1029/2007JF000803.
- Huss M., S. Sugiyama, A. Bauder and M. Funk (2007). Retreat scenarios of Unteraargletscher, Switzerland, using a combined ice-flow mass-balance model. *Arctic, Antarctic and Alpine Research*, 39(3), 422–431.
- Huss, M., A. Bauder, M. Werder, M. Funk and R. Hock (2007). Glacier-dammed lake outburst events of Gornersee, Switzerland *Journal of Glaciology*, 53(181), 189–200.